THE UNIVERSITY
of EDINBURGH

Bone Histopathology

The Effects of Pathology on Bone Microstructure and Implications for Histological Age Estimation

Caroline Elizabeth Lill Ruchonnet

PhD

University of Edinburgh

2019

Dedication

To my grandfather, Edward Lill, who believed me when I told him at 10-years-old that I would be a PhD, and for making it possible.

To my husband, Antoine, for your support.

Acknowledgements

First, my supervisor, Elena Kranioti, the wizard behind the curtain. Without her, none of this would have been possible.

Julieta Garcia-Donas, for her research which intertwined with mine, and for providing the healthy controls for this study.

The Edinburgh City Morgue and the Pathology lab at Western General Hospital, for the use of their space.

Andrea Bonicelli and Efi Michopoulou, who helped set up the histology lab and keep it running.

The enthusiastic MSc students who volunteered to come to the lab and macerate bone.

Dr Robert Paine, for introducing me to histopathology, and for the insight and advice along the way.

Meaghan Dyer, for keeping me sane through all the setbacks.

My family, Mom, Dad, Charley and Maddie, for always supporting, and believing in me, even when I didn't think I could do it.

My husband, Antoine, for being anything and everything I needed, throughout this entire process.

Abstract

Age estimation is a vital part of the creation of a biological profile for the purposes of identifying unknown individuals. Numerous macroscopic methods of analysing bone have been developed for this purpose. In some cases, however, fragmentation of the bone, poor preservation, and taphonomic damage will not allow for the implementation of these methodologies. For these cases, microscopic analytical methods have become the standard, and in the past several decades methodologies using different parts of the skeleton have been developed, most notably those using the rib for age estimation. These histological age estimation methods rely upon the measurements for cortical area and osteon population density (OPD) for an accurate age estimation. While these population specific methods have proven accurate and useful for the purposes of age estimation, they do not consider the health of the individual whose age they are attempting to estimate. Chronic pathology can change the microstructure of osseous tissue, which in turn could influence the accuracy of histological age estimation methods. The purpose of this study is twofold. First, to examine the microstructure of chronically ill individuals and provide detailed descriptions of microstructural changes for visual identification of pathology. Second, to quantitatively evaluate pathological samples using both standard measurements used in most age estimation calculations, as well as detailed osteon specific histomorphometrics to measure the specific changes to Haversian systems in cases of chronic pathology. By considering both the qualitative and quantitative characteristics of pathological bone in comparison with healthy controls it will be possible to determine what the effects of pathologically affected bone on methods of age estimation could be.

Pathological ribs (N=40) were obtained via autopsy from two populations (Albania and Crete), and from a modern skeletal collection (Crete). These were then compared with healthy ribs (N=40) obtained from autopsy (Crete) and from two modern skeletal collections (Crete and Cyprus). The mid-shafts were then prepared using standard protocols for histological methods. First, samples were assessed qualitatively. Samples were visually evaluated for abnormal microstructural features, and these features were then categorised. Samples were then divided and tested, using these pathological feature categories, by disease class and by age group. Second, samples were assessed quantitatively. Thin sections were first measured using the standard histological metrics of cortical area, OPD, number of complete osteons, number of fragmented osteons, and total number of osteons. Thin sections were then evaluated using a sampling method for ten osteon specific metrics (osteon maximum length, osteon minimum length, osteon circumference, osteon total area, osteon area, osteon circularity, canal area, canal maximum diameter, canal minimum diameter, and canal circularity).

Assessment for qualitative features was done by identifying abnormal features of the bone microstructure and dividing them into three defined categories. Samples were then sorted into seven different disease classes and healthy controls, and the presence or absence of these pathological features was noted. The samples were then evaluated using a chi squared test. Inter and intra-observer errors were carried out for both quantitative sections

using the Technical error of measurement (TEM), rTEM and the coefficient of reliability (R). Statistical analysis was carried out using RStudio.

Next comparative statistics, including correlations and regressions, were run between the complete data set, the pathological set, and the healthy set, specifically testing the relationship between actual age and cortical area, and actual age and OPD. This demonstrated that while the complete set did show a significant relationship between age and the two standard variables (R^2 0.24 for cortical area and age, R^2 0.21 for OPD and age), this relationship was stronger in the healthy data set (R^2 0.32 for cortical area and age, R^2 0.46 for OPD and age), and much weaker within the pathological data set (R^2 0.09 for cortical area and age, R^2 0.01 for OPD and age). Next the measurements for osteon specific metrics were evaluated for their relationship to age as a complete data set, then as a set including the metric means of each sample, and finally as forty age matched pairs. This was done using t-tests, correlations, and regression analysis. Correlation analysis for metric means found significant relationships between osteon area, osteon total area, osteon minimum length, osteon perimeter, osteon maximum length, and age in the healthy group. All these variables had *p*-values of <0.004. In the pathological group, correlations between the metric variables and age were much weaker, with only three variables, osteon maximum length, osteon area, and osteon minimum length yielding statistically significant relationships, and the *p*-values for these three relationships were all greater than 0.02, significantly weaker than the healthy group.

This research helps define visually identifiable pathological changes to the bone microstructure, and proves that there is a significant difference between the microstructure of pathological and healthy bone. It goes on to show that, while there is a strong relationship between certain microstructural elements and age which would be beneficial for creating population specific age estimation techniques, microstructural elements of pathological samples have much weaker relationships to age, and that their inclusion in data sets used to create population specific formulae would influence the method's accuracy. Further, if a sample is known to be pathological and shows pathological microstructural features, any histological age estimation technique would be less effective, and that if applied. It is recommended that more research is carried out focusing on specific pathologies, and that more population specific studies should be undertaken.

Lay Summary

Age estimation is an important part of the process to identify unknown individuals. Many techniques have been developed for this purpose using observational methods, however in cases where the bone is fragmented or poorly preserved, these methods are not able to be used effectively. In these cases, histology, or microscopic analysis of thin sections, can be helpful, and several population specific methods have been developed for this purpose. While these methods have proven accurate and useful for the purposes of age estimation, they generally do not consider the health of the individual whose age they are attempting to estimate. Long-term pathology can often impact the microstructure of bone, which in turn can influence the accuracy of histological age estimation. The purpose of this study is to first examine the microstructure of bone from chronically ill individuals, and second, to attempt to quantify these microstructural changes and their potential effect on histological age estimation techniques.

For this study, 80 rib samples, 40 from individuals with a history of chronic illness, and 40 from healthy individuals as controls, were examined. The mid-shafts of the ribs were then prepared using standard histological preparation methods. Samples were visually evaluated for abnormal microstructural features, and these features were then categorised and significance of relationships between pathology and features were assessed. After the samples were visually assessed, each thin section was measured using standard histological techniques, as well as new more specific metrics of osteons, the building blocks of bone microstructure. Once the relevant measurements had been taken, statistical analysis was done to assess the relationship between the various microstructural elements and age, and whether the health status of the individual affected said relationships.

This research helps to define visually identifiable changes to the bone microstructure related to health, and proves that there is a significant difference between the bone microstructure of healthy and chronically ill individuals. Further, while there are strong relationships between certain microstructural elements and age in healthy individuals, these relationships are much weaker in chronically ill individuals. This means that age estimation techniques would be better served taking an individual's health status into account when creating population specific methods, and that histological age estimation techniques should not be used on identifiably pathological individuals. The results of this research have the potential of being used as a stepping stone to create diagnostic standards for pathological conditions using bone histomorphometry. It is recommended that there should be further research into specific illnesses and their effects, and more population specific research should be undertaken.

Declaration of own work

I hereby declare that this thesis has been composed by me; the work presented here is my own and has not been submitted for any other degree or any professional qualification except as specified. Any previous own publication relevant to this work has been referenced in this work when appropriate.

Signed

.....

DEDICATION **3**

ACKNOWLEDGEMENTS **4**

ABSTRACT **5**

LAY SUMMARY **7**

DECLARATION OF OWN WORK **9**

TABLE OF FIGURES **17**

TABLE OF TABLES **21**

GLOSSARY OF ACRONYMS **25**

1. INTRODUCTION **27**

2. LITERATURE REVIEW **33**

2.1 BONE HISTOLOGY **33**
2.1.1 INTRODUCTION TO BONE BIOLOGY 33
2.1.1.1 Introduction to Osseous Tissue 33
2.1.1.2 Bone Composition 34
2.1.1.3 Haversian Systems 36
2.1.1.4 Bone Metabolism 39
2.1.1.5 Bone Pathology 42
Lesions and Periostitis 43
Osteoporosis 44
2.1.2 INTRODUCTION TO BONE HISTOLOGY 47
2.1.2.1 Introduction to Bone Histology Methods and Uses 47
2.1.2.2 Bone Histology and Age Estimation Using Ribs 50
2.2 CHRONIC DISEASE AND COMORBIDITIES INVOLVING BONE **55**
2.2.1 INTRODUCTION TO METABOLISM 55
2.2.1.1 Different metabolic rates of tissues 56
2.2.1.2 How different systems interact 56
2.2.2 PATHOLOGICAL CATEGORIES AND THEIR INTERACTIONS WITH BONE 57
2.2.2.1 Cancer 57
Metastatic Cancer 58
Cancer Therapies 59
2.2.2.2 Cardiovascular Disease 60
Coronary Artery Disease (CAD) 61
Atherosclerosis 61
Myocardial Infarction 62
Comorbidities Involving Bone 62
2.2.2.3 Diabetes 63
Comorbidities Involving Bone 64
2.2.2.4 Hepatic Disease 66
Alcoholic Liver Disease 66
Comorbidities Involving Bone 68
2.2.2.5 Pulmonary Disease 69
Chronic Obstructive Pulmonary Disease (COPD) 69
Bronchopneumonia 70

Comorbidities Involving Bone 71
2.2.2.6 Renal Disease 72
Chronic Kidney Disease (CKD) 72
Comorbidities Involving Bone 73

3. AIMS AND OBJECTIVES 75

4. MATERIALS AND METHODOLOGY 79

4.1 MATERIALS 79
4.1.1 SAMPLE COLLECTION 79
4.1.1.1 The Cretan Collection 79
4.1.1.2 Forensic Autopsy Samples 80
4.1.1.3 The Cypriot Collection 81
4.1.2 SAMPLE DISTRIBUTION 81
4.1.2.1 Pathological Samples 82
4.1.2.2 Control Samples 83
4.2 METHODOLOGY 84
4.2.1 SLIDE PREPARATION 85
4.2.1.1: Sample Selection 85
4.2.1.2 Cleaning 86
4.2.1.3 Embedding 87
4.1.2.4 Markings and Assignment of Identification Numbers 89
4.1.2.5 Preparing Samples for Mounting 90
4.1.2.6 Mounting Slides 91
4.1.2.7 Cutting 91
4.1.2.8 Grinding 92
4.2.2 SLIDE READING 92
4.2.2.1 Microscopes and Photographic Equipment 92
4.2.3 ANALYSIS 93
4.2.3.1 Qualitative Analysis 94
4.2.3.2 Quantitative and Metric Analysis 97
4.2.3 STATISTICS 101
4.2.3.1 Standard Histology Statistics 102
4.2.3.1.1 Inter-observer Error Analysis 102
4.2.3.1.2 Correlations 103
4.2.3.1.3 Regression analysis 104
4.2.3.1.4 Standard Errors 104
4.2.3.1.5 Bootstrapping 105
4.2.3.2 Osteon Specific Metrics 105
4.2.3.2.1. Inter and Inter-observer Error 106
4.2.3.2.1.1 Intra-observer Error 106
4.2.3.2.1.2 Inter-observer Error 107
4.2.3.2.2 Independent T-tests 108
4.2.3.2.3 Paired Independent T-tests 108
4.2.3.2.4 Metric Means 109
4.2.3.2.4.1 Correlations 109
4.2.3.2.4.2 Regressions 110

5. RESULTS 111

5.1 QUALITATIVE ANALYSIS 112
5.1.1 QUALITATIVE FEATURES 113

5.1.1.1 Category 1: Abnormally Shaped Osteons and Canals 113
5.1.1.2 Category 2: Deranged Haversian Systems (Swiss Cheese Effect) 116
5.1.1.3 Category 3: Striations of Rapid Bone Deposits 119
5.1.2 DISTRIBUTION AND ANALYSIS OF QUALITATIVE FEATURES 122
5.1.2.1 Distribution and Analysis by Pathology 123
5.1.2.1.1 Pathological features in the Healthy Control group 125
5.1.2.1.2 Pathological features in the Cancer class 127
5.1.2.1.3 Pathological features in the Cardiovascular class 128
5.1.2.1.4 Pathological features in the Diabetes class 129
5.1.2.1.5 Pathological features in the Hepatic class 131
5.1.2.1.6 Pathological features in the Pulmonary class 133
5.1.2.1.7 Pathological features in the Renal class 134
5.1.2.1.8 Pathological features in the Multiple class group 135
5.1.2.1.9 Analysis of Pathological Categories 136
5.2 QUANTITATIVE ANALYSIS 138
5.2.1 STANDARD BONE HISTOLOGY 139
5.2.1.1 Inter-observer Error 139
5.2.1.2 Correlations 141
5.2.1.3 Regression Analysis 144
5.2.1.4 Standard Errors 150
5.2.1.5 Bootstrapping 150
5.2.2: OSTEON SPECIFIC METRICS 156
5.2.2.1 Inter and Intra-observer Error 157
5.2.2.1.1 Inter-observer Error 157
5.2.2.1.2 Intra-observer Error 158
5.2.2.2 Independent T-tests (Full Sample) 159
5.2.2.3 Paired Independent T-tests (40 pairs, sex and age matched) 160
Age Group 1: Under 30 161
Pair 1: A14 and CC53 161
Pair 2: B1 and FC3 161
Age Group 2: 31-40 162
Pair 3: B12 and CC7 162
Pair 4: B20 and CC152 162
Pair 5: A11 and CC7 163
Pair 6: B31 and CC100 164
Pair 7: B7 and CC7 164
Pair 8: FC14 and CC100 165
Pair 9: A2 and FC6 165
Age Group 3: 41-50 166
Pair 10: B16 and CC184 166
Pair 11: A1 and CC184 166
Pair 12: B40 and CC184 167
Pair 13: A10 and CC194 168
Pair 14: A15 and CY191 168
Pair 15: B28 and CY191 169
Age Group 4: 51-60 169
Pair 16: FC13 and CC87 169
Pair 17: B29 and CC87 170
Pair 18: B41 and CC87 170
Pair 19: CC22 and CC202 171
Pair 20: B33 and CY121 172

Pair 21: FC18 and CY190 172
Pair 22: A13 and CY190 173
Pair 23: B27 and CC89 173
Pair 24: FC15 and CC89 174
Pair 25: FC16 and CC173 175
Pair 26: B24 and CC173 175
Pair 27: CC17 and CC173 176
Pair 28: CC6 and CY121 176
Age Group 5: Over 60 177
Pair 29: CC193 and CC173 177
Pair 30: FC9 and CC173 178
Pair 31: CC15 and CY202 178
Pair 32: CC45 and CC86 179
Pair 33: FC2 and CY202 179
Pair 34: CC27 and CY39 180
Pair 35: CC196 and CY39 180
Pair 36: CC169 and CY39 181
Pair 37: CC23 and CC187 182
Pair 38: CC203 and CC12 182
Pair 39: CC189 and CC195 183
Pair 40: CC45 and CY194 183
5.2.2.4 Metric Mean Values vs Age 184
5.2.2.4.1 Correlations 184
5.2.2.4.2 Regression Analysis 187

6. LIMITATIONS 195

6.1. RESEARCH LIMITATIONS 195
6.2 PRACTICAL LIMITATIONS 198
6.2.1 SLIDE ANALYSIS 199
6.3 PROBLEMS IN INFRASTRUCTURE 201

7. DISCUSSION 205

7.1 QUALITATIVE INTERPRETATIONS AND EXPLANATIONS 206
7.1.1 CATEGORY 1 FEATURES 206
7.1.2 CATEGORY 2 FEATURES 211
7.1.3 CATEGORY 3 FEATURES 214
7.2 QUANTITATIVE INTERPRETATIONS AND EXPLANATIONS 216
7.2.1 STANDARD BONE HISTOLOGY 217
7.2.1.1 Inter-observer Error 218
7.2.1.3 Correlations 220
7.2.1.4 Regression Analysis 222
7.2.1.5 Standard Errors 226
7.2.1.6 Bootstrapping 227
7.2.2 OSTEON SPECIFIC METRICS 230
7.2.2.1 Inter-observer Error 230
7.2.2.2 Intra-observer Error 231
7.2.2.3 Independent T-Tests (Full Sample) 233
7.2.2.4 Paired Independent T-Tests 234
Age Group 1: Under 30 235
Age Group 2: 31-40 236
Age Group 3: 41-50 236

Age Group 4: 51-60 238
Age Group 5: Over 60 239
7.2.2.5 Metric Mean Values vs. Age 241
7.2.2.5.1 Correlations 241
7.2.2.5.2 Regression Analysis 244

8: CONCLUSIONS 249

BIBLIOGRAPHY 255

APPENDIX 269

A. 1: SPEARMAN'S R AND CONVERTED *P*-VALUES FOR STANDARD HISTOLOGY 269
A.1.1 COMPLETE SAMPLE 269
A.1.2 PATHOLOGICAL SAMPLE 269
A.1.3. HEALTHY SAMPLE 270
A.2 REGRESSION OUTPUTS FOR STANDARD HISTOLOGY 271
A.2.1 COMPLETE SAMPLE REGRESSION MODEL OUTPUT: CORTICAL AREA AND AGE 271
A.2.2 PATHOLOGICAL SAMPLE REGRESSION MODEL OUTPUT: CORTICAL AREA AND AGE 271
A.2.3 HEALTHY SAMPLE REGRESSION MODEL OUTPUT: CORTICAL AREA AND AGE 271
A.2.4 COMPLETE SAMPLE REGRESSION MODEL OUTPUT: OPD AND AGE 272
A.2.5 PATHOLOGICAL SAMPLE REGRESSION MODEL OUTPUT: OPD AND AGE 272
A.2.6 HEALTHY SAMPLE REGRESSION MODEL OUTPUT: OPD AND AGE 272
A.3 OSTEON SPECIFIC METRICS CORRELATIONS 274
A.3.1 SPEARMAN'S R HEALTHY OSTEON SPECIFIC METRICS CORRELATIONS 274
A.3.2 CONVERTED *P*-VALUE HEALTHY OSTEON SPECIFIC METRICS CORRELATIONS 275
A.3.3 SPEARMAN'S R PATHOLOGICAL OSTEON SPECIFIC METRICS CORRELATIONS 276
A.3.4 CONVERTED *P*-VALUES PATHOLOGICAL OSTEON SPECIFIC METRICS CORRELATIONS 277
A.4 OSTEON SPECIFIC METRICS REGRESSION OUTPUTS 278
A.4.1 HEALTHY REGRESSION MODEL OSTEON AREA 278
A.4.2 PATHOLOGICAL REGRESSION MODEL OSTEON AREA 278
A.4.3 HEALTHY REGRESSION MODEL OSTEON TOTAL AREA 278
A.4.4 PATHOLOGICAL REGRESSION MODEL OSTEON TOTAL AREA 279
A.4.5 HEALTHY REGRESSION MODEL OSTEON MINIMUM LENGTH 279
A.4.6 PATHOLOGICAL REGRESSION MODEL OSTEON MINIMUM LENGTH 279
A.4.7 HEALTHY REGRESSION MODEL OSTEON PERIMETER 280
A.4.8 PATHOLOGICAL REGRESSION MODEL OSTEON PERIMETER 280
A.4.9 HEALTHY REGRESSION MODEL OSTEON MAXIMUM LENGTH 281
A.4.10 PATHOLOGICAL REGRESSION MODEL OSTEON MAXIMUM LENGTH 281
A.5 CONFERENCES AND CONTRIBUTIONS 282

Table of Figures

Figure 4.1: Dremel Saw, pp 88

Figure 4.2: Coloured labelling of samples (Garcia-Donas, 2017), pp 90

Figure 4.3: Left - Buehler MetaServ™ 250 Grinder-Polisher; Right - Buehler IsoMet™ 1000 precision saw, pp 90

Figure 4.4: Left – Close-up of an abnormal osteon from Sample CC169; Right – Close-up of a normal healthy osteon from Sample CC100 (courtesy of Julieta Garcia-Donas), pp 95

Figure 4.5: Left – Example of deranged Haversian systems from Sample CC203 (Courtesy of Julieta Garcia-Donas); Right – Example of normal, healthy Haversian systems from Sample FC6, pp 96

Figure 4.6: A hyperostotic lesion showing linear rapid bone deposits on a cross-section of a metatarsal, sample 1MT2 (100x magnification) (Lill, 2013), pp 96

Figure 4.7: Left – Close-up image of sample CC193 showing possible category 3 deposits near the periosteum (100x magnification), Right – Close-up image of sample CC77 showing no evidence of rapid bone deposits and a healthy periosteum (100x magnification) (Garcia-Donas, 2017), pp 97

Figure 4.8: Illustration of measurements taken for micrometrics. Included are osteon maximum and minimum diameter, canal maximum and minimum diameter, osteon area, canal area, and osteon perimeter. Not pictured are osteon total area, osteon circularity, and canal circularity, pp 100

Figure 5.1: Left - Close-up of sample CC169, a 78-year-old male who suffered from coronary disease, diabetes, and COPD showing Category 1 pathological features (exterior surface, 100x magnification) Right - close-up of sample number CY39. The sample comes from a 75-year-old male in the healthy control group. (interior surface, 100x magnification) (courtesy of Julieta Garcia-Donas), pp 113

Figure 5.2: Left - Close-up of sample FC2 showing Category 1 pathological Features (interior surface, 100x magnification); Right – Close-up of sample CY198, healthy control (interior surface, 100x magnification), pp 115

Figure 5.3: Left - Close-up of the interior surface of sample B28, showing category 1 features (100x magnification); Right–Close-up of sample CY191, healthy control (exterior surface, 100x magnification) (image of sample CY191 courtesy of Julieta Garcia-Donas), pp 115

Figure 5.4: Top – Stitched full cross-section of sample CC203 showing Category 2 pathological features; Bottom Left – Close-up of the exterior surface of sample CC203 showing Category 2 pathological features, 100x magnification; Bottom right – Close-up of the interior surface of sample CC187, healthy control, 100x magnification. (All images courtesy of Julieta Garcia-Donas), pp 117

Figure 5.5: Left - Close-up of interior surface of sample FC16, (59 years old) showing signs of category 2 features (100x magnification): Right - Close-up of interior surface of sample CY190 (57 years old), healthy control (100x magnification), pp 119

Figure 5.6: Close-up of exterior surface of sample CC193, showing possible Category 3 pathological features, arrow pointing to striations, 100x magnification, pp 121

Figure 5.7: Close-up of interior surface of sample CY198 (65-year-old, F), a healthy control, 100x magnification, pp 122

Figure 5.8: Top – Cross-section of sample CC26 from the healthy control group, belonging to a healthy 90-year-old female; Bottom –Cross-section of sample CC53 from the healthy control group, belonging to a healthy 19-year-old female. (Both images courtesy of Julieta Garcia-Donas), pp 127

Figure 5.9: Left – Close-up of the interior surface of sample CC45, from a 64-year-old female suffering from lung cancer (image of sample CC45 courtesy of Julieta Garcia-Donas); Right – Close-up of the interior surface of sample CY198, from a 65-year old healthy female, 100x magnification, pp 128

Figure 5.10: Left – Close-up of the exterior surface of sample FC18, a 57-year-old male with a myocardial infarction, CAD, and generalised atherosclerosis, 100x magnification; Right – Close-up of the interior surface of sample CY190, a healthy 57-year-old male, 100x magnification, pp 129

Figure 5.11: Top – Full cross-section of sample CC189, a 94-year-old male with diabetes; Middle Left – Close-up of sample CC189 exterior surface, 100x magnification; Middle Right – Close-up of sample CC83 exterior surface, a healthy 90-year-old female, 100x magnification; Bottom – full cross-section of sample CC83. (Pictures of CC83 courtesy of Julieta Garcia-Donas), pp 131

Figure 5.12: Left – Close-up of the exterior surface of sample B41 exterior surface, a 53-year-old male with generalised fatty liver; Right – Close-up of the interior surface of sample CY61 interior surface, a healthy 51-year-old female, 100x magnification. (image of sample CY61 courtesy of Julieta Garcia-Donas), pp 133

Figure 5.13: Left – Close-up of the exterior surface of sample CC203, an 85-year-old male with COPD, 100x magnification; Right – Close-up of the interior surface of sample CC187, a healthy 81-year-old male, 100x magnification. (Both images courtesy of Julieta Garcia-Donas), pp 134

Figure 5.14: Left – Close-up of the exterior surface of sample CC6, a 58-year-old female with uraemia, 100x magnification; Right – Close-up of the interior surface of sample CY190, a 57-year-old healthy male, 100x magnification, pp 135

Figure 5.15: Left - Close-up of the interior surface of sample FC13 (52-year-old male), from an individual suffering from hypertension, coronary disease, and pulmonary complications of chronic heavy smoking, showing signs of category 2 features. (100x magnification); Right - Close-up of the interior surface of sample CY191, (48-year-old male) healthy control. (100x magnification) (image of sample CY191 courtesy of Julieta Garcia-Donas) pp 136

Figure 5.16: Heat map of Spearman's correlations using the entire sample, and the converted p-values, pp 142

Figure 5.17: Heat map showing Spearman's correlations for only pathological samples, and converted p-values, pp 143

Figure 5.18: Heat map showing Spearman's correlations using only Healthy Samples, and converted p-values, pp 144

Figure 5.19: Scatterplot of Age compared to Cortical Area for the entire sample with the line of regression, pp 145

Figure 5.20: Scatterplot of Age compared to Cortical Area, separated by health status, with lines of regression, pp 146

Figure 5.21: Scatterplot of Age compared to OPD for the entire sample with the line of regression, pp 148

Figure 5.22: Scatterplot of Age compared to OPD, separated by health status, with lines of regression, pp 149

Figure 5.23: Plot of R-squared of Age and Cortical Area regression bootstrapping using All Samples, pp 151

Figure 5.24: Plot of R-squared of Age and Cortical Area regression bootstrapping using only pathological samples, pp 151

Figure 5.25: Plot of R-squared of Age and Cortical Area regression bootstrapping using only healthy control samples, pp 153

Figure 5.26: Plot of R-squared of Age and OPD regression bootstrapping using All Samples, pp 154

Figure 5.27: Plot of R-squared of Age and OPD regression bootstrapping using only pathological samples, pp 155

Figure 5.28: Plot of R-squared of Age and OPD regression bootstrapping using only healthy control samples, pp 156

Figure 5.29: Heat map showing p-value correlations between Age and osteon metric means for healthy control samples, pp 185

Figure 5.30: Heat map showing p-value correlations between Age and osteon metric means for pathological samples, pp 186

Figure 5.31: Scatterplot showing the distribution and lines of regression of osteon area metric means compared with Age, pp 187

Figure 5.32: Scatterplot showing the distribution and lines of regression of osteon total area metric means compared with Age, pp 189

Figure 5.33: Scatterplot showing the distribution and lines of regression of osteon minimum length metric means compared with Age, pp 190

Figure 5.34: Scatterplot showing the distribution and lines of regression of osteon perimeter metric means compared with Age, pp 192

Figure 5.35: Scatterplot showing the distribution and lines of regression of osteon maximum length metric means compared with Age, pp 193

All images, unless otherwise specified, belong to the author.

Table of Tables

Table 4.1: Sample Age Distribution, pp 82

Table 4.2: Table showing distribution of pathologies across the entire sample, pp 83

Table 4.3: Table of standard histological elements and their definitions; as defined by Stout and Crowder (Stout & Crowder, 2012), pp 98

Table 4.4: Table of the osteon specific metrics, pp 99

Table 5.1: Distribution of feature categories by disease class, pp 124

Table 5.2: Distribution of pathological features across age groups in the pathological sample, pp 125

Table 5.3: Table showing the distribution of pathological features in the Healthy Control group, separated by age group, pp 126

Table 5.4: Table of chi squared test results comparing categories of pathological features between the pathological and healthy control groups, further separated by age group, pp 137

Table 5.5: Table of chi squared test results comparing categories of pathological features with disease classes, pp 138

Table 5.6: Table of SEE calculations for linear regression comparing cortical area and age, and OPD and age, pp 150

Table 5.7: Table showing results of independent t-test comparing two observers, pp 158

Table 5.8: Showing p-values results from the t-tests for intra-observer error, pp 159

Table 5.9: Welch two sample t-test results comparing the complete healthy set with the complete pathological set, pp 160

Table 5.10: Pair 1 independent t-test results, pp 161

Table 5.11: Pair 2 independent t-test results, pp 162

Table 5.12: Pair 3 independent t-test results, pp 162

Table 5.13: Pair 4 independent t-test results, pp 163

Table 5.14: Pair 5 independent t-test results, pp 163

Table 5.15: Pair 6 independent t-test results, pp 164

Table 5.16: Pair 7 independent t-test results, pp 164

Table 5.17: Pair 8 independent t-test results, pp 165

Table 5.18: Pair 9 independent t-test results, pp 166

Table 5.19: Pair 10 independent t-test results, pp 166

Table 5.20: Pair 11 independent t-test results, pp 167

Table 5.21: Pair 12 independent t-test results, pp 167

Table 5.22: Pair 13 independent t-test results, pp 168

Table 5.23: Pair 14 independent t-test results, pp 168

Table 5.24: Pair 15 independent t-test results, pp 169

Table 5.25: Pair 16 independent t-test results, pp 170

Table 5.26: Pair 17 independent t-test results, pp 170

Table 5.27: Pair 18 independent t-test results, pp 171

Table 5.28: Pair 19 independent t-test results, pp 171

Table 5.29: Pair 20 independent t-test results, pp 172

Table 5.30: Pair 21 independent t-test results, pp 172

Table 5.31: Pair 22 independent t-test results, pp 173

Table 5.32: Pair 23 independent t-test results, pp 174

Table 5.33: Pair 24 independent t-test results, pp 174

Table 5.34: Pair 25 independent t-test results, pp 175

Table 5.35: Pair 26 independent t-test results, pp 175

Table 5.36: Pair 27 independent t-test results, pp 176

Table 5.37: Pair 28 independent t-test results, pp 177

Table 5.38: Pair 29 independent t-test results, pp 177

Table 5.39: Pair 30 independent t-test results, pp 178

Table 5.40: Pair 31 independent t-test results, pp 178

Table 5.41: Pair 32 independent t-test results, pp 179

Table 5.42: Pair 33 independent t-test results, pp 180

Table 5.43: Pair 34 independent t-test results, pp 180

Table 5.44: Pair 35 independent t-test results, pp 181

Table 5.45: Pair 36 independent t-test results, pp 181

Table 5.46: Pair 37 independent t-test results, pp 182

Table 5.47: Pair 38 independent t-test results, pp 182

Table 5.48: Pair 39 independent t-test results, pp 183

Table 5.49: Pair 40 independent t-test results, pp 184

Glossary of Acronyms

ALD – alcoholic liver disease

ALP – alkaline phosphatase

BCa – bias-corrected and accelerated bootstrap interval

BMD – bone mineral density

BMI – body mass index

BMP – bone morphogenic protein

BMU – basic multicellular unit

CAD – coronary artery disease

CArea – canal area

CCirc – canal circularity

CHD – coronary heart disease

CKD – chronic kidney disease

CMaxL – canal maximum length

CMinL – canal minimum length

COPD – chronic obstructive pulmonary disease(s)

CVD – cardiovascular disease(s)

DISH – diffuse idiopathic skeletal hyperostosis

DXA – dual-energy X-ray absorptiometry

GnRH – Gonadotropin-releasing hormone

GFR – glomerular filtration rate

IDDM – insulin-dependent diabetes mellitus

IHD – ischemic heart disease

HTA – Human Tissue Authority

MI – myocardial infarction

NCD – non-communicable disease(s)

NCP – noncollagenous proteins

NIDDM – non-insulin-dependent diabetes mellitus

OArea – osteon area

OCirc – osteon circularity

OMaxL – osteon maximum length

OMinL – osteon minimum length

OPD – osteon population density

OPeri – osteon perimeter

OPN – osteopontin

OTArea – osteon total area

TEM – technical error of measurement

rTEM – relative technical error of measurement

SEE – standard error of the estimate

SWGANTH – Scientific Working Group for Forensic Anthropology

WHO – World Health Organization

1. Introduction

In God we trust. All others must have data.

- Bernard Fisher

It's easy to make perfect decisions with perfect information. Medicine asks you to make perfect decisions with imperfect information.

- Siddhartha Mukherjee

For as long as there have been living things, there have been diseases. Whether they were the consequences of microorganisms, viruses, or simply the cells of the body turned against itself, they have always existed, adapting to new environments, species, and defences. In terms of archaeology, infectious disease has dominated much of human history. While other diseases existed, they languished in the shadows, rarely wreaking as much havoc as their infectious brethren. Thing began to change, however, as modern science began to catch up with these microscopic monsters. Vaccines were developed, penicillin discovered, sanitation and hygiene improved. Diseases that had plagued humanity for thousands of years, like small pox, were eradicated by the coordinated efforts of the global community. After the infectious diseases were, in theory, under control, the other diseases that had been lurking in the background, have now come to the fore. The killers of today are generally not infections, but instead non-communicable diseases that have flourished from our modern lifestyles.

According to the World Health Organization, non-communicable diseases (NCD's) are responsible for 41 million deaths annually, approximately 71% of all deaths. This includes 15 million people between the ages of 30 and 70, approximately 80% of all premature deaths. There are four major players who fall under the category of NCD's. The highest death toll

belongs to cardiovascular diseases, killing 17.9 million people annually. These include infarctions, heart attacks and strokes, the number one killer in the world today. Next is cancer, responsible for the deaths of 9 million people annually, then respiratory diseases, responsible for killing 3.9 million people annually, and lastly diabetes, responsible for 1.9 million deaths annually. Each of these diseases has the capacity to make changes inside the body, altering metabolism, changing hormone levels, and affecting other bodily systems. Although these diseases have always existed, they have blown up to epidemic proportions, thanks in large part to the lifestyles, habits, behaviours, and commodities made available by modern living. The inhaling or ingesting of harmful substances, like smoking, drinking alcohol, and breathing in the toxic fumes of factories and cities, as well as unhealthy diets full of processed, nutrient poor foods, and inactivity, have all lead to the prevalence of these diseases. Although many of these lifestyle changes originated in the high-income countries of the western world, NCD's now disproportionately affect the populations of middle and low-income countries, with deaths in the developing world now making up three quarters of all NCD deaths (World Health Organization, 2018). Without meaningful and drastic changes, to our modern lifestyles, the death toll from NCD's will only increase.

What does the advent of the NCD mean for the osteologist? These diseases are chronic conditions, developing over the course of months and years. Unlike many infections of the past, the time and the systemic effects of these diseases allow them to penetrate the slow metabolism of bone. Many of these diseases set in motion a cascade of pathological effects, triggering responses in system after system, until it finally reaches the skeletal system. While in the past seeing the bone loss associated with osteoporosis was restricted to the elderly or the infirm, it is now possible to see its effects in much younger individuals, thanks in large

part to the influence of NCD's. What we know about the human skeleton is being fundamentally changed by these diseases. The methodologies developed over the past one hundred years on past populations to create a biological profile, could no longer work on modern populations. These diseases have the potential to change not only what we see when we observe bone macroscopically, but microscopically as well.

At the microscopic level, changes in the metabolic process have the potential to derail the bone remodelling process. A change in hormone levels can trigger the destructive cells of bone, leaving them to outpace the constructive cells behind them, leading to a loss of bone. The presence of a neoplasm can have the opposite effect, stimulating the constructive cells, and creating proliferative lesions or rapid deposits of bone on the periosteum. Either effect will alter what is seen in cross-section, and potentially affect the methods developed for histological bone analysis, in particular age estimation.

Since the 1960's, when Jowsey (1960) discovered a possible connection between bone microstructure and age, biological anthropologists have been using these relationships for the creation of biological profiles. Kerley (1965) was the first to use the correlation between cortical area and age, and osteon population density (OPD) and age to develop a histological age estimation method for thin sections taken from the femur. Ever since, methods have continued to be developed and improved by a host of scientists, all attempting to predict the age at death of an individual from a small thin section or core of bone. In the 1970's Thompson (1979) improved upon Kerley's work by using core samples instead of thin cross-sections, making the method less destructive and time consuming. In the 1990's another significant improvement was made, with the introduction of the Stout and Paine method (1992) using

the rib and clavicle. Using the ribs, bones that are generally less significant in terms of other methodologies used to create biological profiles, was therefore a better choice than the long bones in terms of destructive techniques. As the next twenty years moved on, more studies appeared, improving on the past by accounting for differences in population (Cho & al., 2002), sexual dimorphism (Mulhern & Van Gerven, 1997), nutritional status (Paine & Brenton, 2006) and paleopathology (Schultz, 2001). Through each new development, these methods all relied upon the same fundamental principles first set out by Jowsey and Kerley, making the original idea more accurate, and better for forensic use. Each of these histological age estimation methods rely upon the microstructural elements of cortical area and OPD, and their relationship to age. While it has been acknowledged that individuals over the age of 50 yield less accurate results (Christensen, et al., 2014), due to the changes intrinsic in the aging process, considerations of these types of skeletal changes are rarely considered in the cases of younger individuals. If, however, these chronic metabolic diseases have a chance to affect the microstructure of the bone, especially in those individuals normally deemed young enough for worthwhile histological age estimation, it could potentially interfere with the ability of these techniques to accurately assess age.

While accuracy is appreciated in all forms of science, including biological anthropology in the archaeological context, it becomes absolutely vital in the context of forensics. There, the accuracy of the biological profile could mean the difference between identifying a victim or not. It has a real, and profound effect on the abilities of the justice system. In this day and age, with the realities of migration crises, regional conflicts, civil unrest, and increasing natural disasters caused by global warming, the forensic anthropologist's ability to create an accurate biological profile for the purposes of identification is only increasing in importance. While no

estimation method is perfect, as referenced in the second quotation at the beginning of this chapter, forensic scientists, like doctors, are forced to try to make perfect decisions with imperfect information. By increasing the knowledge base, and accounting for more variables, such as the increase in non-communicable diseases and their potential effects on the microstructure of the skeleton, it is possible for forensic anthropologists to and make better, more informed decisions, and create better, more informed biological profiles. The key is to understand these new variables to the best of our abilities.

This study hopes to delve deeper into the consequences of chronic disease on the skeletal system and its microstructure than previous studies have allowed. By making visual analyses of thin sections of both pathological and healthy ribs, and categorising the pathological features, it may be possible to simplify the identification of these features, making this kind of pathological assessment more accessible to other bone histologists. It further endeavours to quantify the changes made to the microstructure by the presence of pathology, and to assess the influence these changes have on the vital elements of cortical area and OPD. By quantifying these changes, they will not only provide support to the visual analyses of this and other studies, but also provide a platform for further studies make corrections to existing methods and formulae. In addition, these quantifications and analyses will be useful for forensic applications, as they will be able to enumerate the amount to which current forensic techniques can be seen to be affected by the presence of chronic, systemic pathology.

2. Literature Review

2.1 Bone Histology

2.1.1 Introduction to Bone Biology

Before beginning with the purpose of this study, it is first important to understand the fundamentals of bone biology. By understanding how bone is composed, its mechanical properties, its function in the human body, and how its microstructure is composed, it will be easier to understand what is happening when things go wrong in the presence of pathology. Once understood, it will be possible to discuss both the response of bone to pathology, and also its response to a pathology in other systems. Discussing the rudiments of bone biology will also lay the groundwork for understanding the fundamentals of bone histology, and how biological anthropologists use these microstructures to understand more about bone as a tissue, as well as the individual being studied.

2.1.1.1 Introduction to Osseous Tissue

Bone or osseous tissue is what makes up bones, the primary elements of the skeletal system (Gray, 2010) At its most fundamental level, bone is a multifunctional tissue. It provides support and protection for the body, is quintessential in mechanical function, as well as hematopoiesis and hormone production (Burr & Akkus, 2013). In essence, the skeletal system provides the scaffolding for the entire human body, and along with the muscular system, is what allows the body to move.

Bone can be observed on different microanatomical levels. The first level is the bone tissue itself. The second level is the microstructure and concerns the osteons and lamellae that make up the osseous tissue. The next level is the nanostructure and concerns the combination of

collagen and mineral deposits that come together to make the tissue. The final level is the molecular level and concerns the actual molecules that make up the crystal lattice of the osseous tissue (Burr & Akkus, 2013). While this study is primarily interested in the microstructural level, a basic understanding of the other microanatomical levels is necessary to understand why bone reacts to pathological stimuli the way it does.

2.1.1.2 Bone Composition

Bone is a unique tissue, in that it is made up of both organic and inorganic material, in this case, it is a mix of carbonated apatite and collagen. When weighed, approximately 65% of osseous tissue is made up of mineral materials, and between 20-25% collagen. The remainder is made up of water (Burr & Akkus, 2013). The nanostructure of bone is then made up of bundles of collagen fibrils, with crystals of hydroxyapatite embedded in the bundles of collagen. This structure is then what makes up the collagen matrix (Olszta, et al., 2007). It is during the mineralisation process that the mineral crystals are deposited in and around the collagen fibrils (Rey, et al., 2009). In addition to these materials, there is a small amount of noncollagenous proteins (NCP's) that help to regulate the construction and maintenance of the bone's nanostructure (Burr & Akkus, 2013). This combination of organic and inorganic materials is essential to providing bone with its unique properties; the mineral material provides strength and rigidity, while the collagen lends flexibility and elasticity to the material (Clarke, 2008).

Mineralisation is the process through which inorganic minerals are deposited within and around the collagen matrix. This takes place in two phases, primary and secondary mineralisation. During the initial primary phase of mineralisation, the crystals of

hydroxyapatite that are deposited within the framework of the collagen make up about 65-70% of the osseous tissue's total mineralisation. This occurs within three weeks of the first deposition of collagen. The next phase of mineralisation takes longer, with the crystals slowly accumulating more mineral deposits, growing to the physiologic limit. This can take anywhere from months to years (Burr & Akkus, 2013). This enlargement of the crystals occurs both as crystal growth and aggregation of mineral materials (Clarke, 2008). Vitamin D also plays a role in stimulating the mineralisation of bone, although indirectly. After being synthesised by the liver, the kidney is then triggered to produce serum 1,25-dihydroxyvitamin D. This serum then helps to maintain calcium and phosphorus to allow for passive mineralization of unmineralised matrix (Clarke, 2008). The arrangements of these collagen fibrils and mineral crystals within bone tissue varies slightly, adapting to the type of bone it will become, either trabecular or cortical bone (Burr & Akkus, 2013; Clarke, 2008; Augat & Schorlemmer, 2006).

Moving up from the nanostructure of bone, the collagen fibrils and mineral crystals can be arranged into one of two forms; woven, or lamellar bone. Another form of bone, plexiform bone, does exist, however this form is rarely, if ever, found in humans (Burr & Akkus, 2013). Woven bone is quickly deposited and disorganised in nature (Burr & Akkus, 2013). The orientation of the collagen fibrils is loose and random, making it less structurally sound than lamellar bone (Currey, 2003). Woven bone, as a rapidly deposited scaffolding for lamellar bone, can appear at the site of a healing fracture and in proximity to pathology, such as hyperparathyroidism or Paget's disease (Clarke, 2008; Burr & Akkus, 2013). In contrast, lamellar bone is deposited slowly, and usually in organised sheets of fibrils and crystals, forming Haversian systems in the cortical bone, and trabeculae in the trabecular bone (Burr & Akkus, 2013). Due to its organised and slow growing nature, lamellar bone is known to be

stronger than woven bone (Clarke, 2008). Of interest to this study is the lamellar bone found in the cortical bone, especially as it relates to the formation of secondary Haversian systems.

Bone tissue usually exists in one of two forms: trabecular or cancellous bone, and cortical or compact bone. While these two different organisations of osseous tissue fulfil different purposes, they are essential to the proper function of the skeletal system. Trabecular bone is sometimes referred to as spongy bone, is organised in a honeycomb-like structure, and is found on the interior of vertebrae, ribs, the iliac crest, and in the metaphyses of the long bones. It provides structural support for the skeletal system, but its spongy, porous nature prevents it from adding too much weight. Overall, it makes up only about 25-30% of bone tissue by weight (Burr & Akkus, 2013). In contrast, cortical bone is the dense, hard, outer layer of most bone. It is what makes up the diaphyses and shafts of the long bones, and provides a hard, protective covering for the trabeculae of the vertebra, ribs, iliac crest, and skull. Unlike the porous trabecular bone, cortical bone is only has about 3-5% porosity (Burr & Akkus, 2013). While trabecular bone in general has a higher turnover rate than cortical bone, it lacks the secondary osteons used in most histological age estimation methods. For this reason, this study will focus on the microstructure of cortical bone, as this is where the secondary osteons used in age estimation are found.

2.1.1.3 Haversian Systems

Haversian systems are the formations within the cortical bone that allow for the blood supply to reach the osseous tissue. These systems exist primarily in the intracortical area of the bone. The cortical bone has three distinct areas to observe in cross-section, the endosteal surface, the intracortical bone, and the periosteal surface. These refer the interior surface adjacent to

the medullary cavity, the cortical bone between the surfaces home to the osteonal lamellar bone, and the exterior protective surface of the bone, respectively (Currey, 2003). Lamellar bone exists in two morphological types; circumferential and osteonal lamellar bone. Circumferential lamellar bone is a part of the modelling process and occurs during bone growth. It can be found most often near the endosteal and periosteal surfaces. These are distinctive in that they do not follow the same patterns as osteonal lamellar bone. Osteonal lamellar bone is the production of the remodelling process and occurs as a part of bone maintenance. It is most often found in the intracortical bone (Reznikov, et al., 2014). According to Giraud-Guille, osteonal lamellar bone can be described as a series of nested arcs of "twisted plywood" structured collagen fibrils. This arrangement of fibrils creates the concentric circular formations seen in cross-section (Giraud-Guille, 1988). These layers are made up of fibrils arranged in both organised and disorganised motifs. The organised motif is usually around 2-3 μm thick, while the disorganised motifs are thinner, usually only about 0.25-1 μm thick (Reznikov, et al., 2014). These formations of osteonal lamellar bone then create both the primary and secondary osteons observed in cross-section (Reznikov, et al., 2014).

These formations often appear in cross-section as concentric circles of lamellar bone arranged around a central canal that houses a blood vessel. These systems usually form in one of two ways, either as primary or secondary cortical bone (Burr & Akkus, 2013). Primary bone is formed during the modelling process, and generally is more common in juveniles, as they are still generating new bone, rather than remodelling old bone. In this case, the lamellar bone does not completely form concentrically around a canal for a blood vessel, as the bone is growing too fast to fully envelop the vessels. These are referred to as primary because they

tend to form during the first phase of lamellar bone growth, and therefore are a part of the bone modelling, rather than remodelling, process. These are known as primary osteons (Kerley, 1965). On average, primary osteons are smaller than those found in secondary bone, usually between 50-100 μm in diameter (Burr & Akkus, 2013).

Secondary bone forms after primary bone and is a part of the remodelling process, essentially the maintenance of the osseous tissue. Like most bodily tissues, it is required for osseous tissue to turn over and be replaced. This occurs when previously existing bone is resorbed, and new bone tissue is created in its place. This results in the full concentric formation of lamellae around the central Haversian canal known as a secondary osteon (Burr & Akkus, 2013). These concentric formations are then bounded by a reversal or cement line, marking the edge of tissue resorption and recreation (Kerley, 1965). In addition to the presence of a cement line, and the complete nature of the concentric circle of lamellar bone surrounding the Haversian canal, secondary osteons are also larger than primary osteons, on average measuring 100-250 μm (Burr & Akkus, 2013). It is these secondary osteon formations that are of concern to this study, both as an indication of health, and as a tool for histological age estimation. Secondary bone is common in adults, and the number of secondary osteons seen in the bone cross-section often increases and becomes more crowded with age (Kerley, 1965).

Secondary osteons, sometimes referred to simply as osteons, are the building blocks of bone microstructure, and represent the mature network of Haversian systems and canals that flow through the dense cortical bone. The concentric formations of lamellae surrounding the canal are what make up the osteon (Burr & Akkus, 2013). While these appear circular when viewed in cross-section, in the actual bone they are more like tubes, branching out and connecting

with other canals (Maggiano, 2012). Osteons are formed during the remodelling process, when osseous tissue replaces itself, which is a function of the bone's metabolism. Due to the angle of the cross-section, osteons can appear in different shapes than the standard concentric circles. If the thin section is cut along a branch of the canal, the canal can appear elongated. If the thin section is cut not perfectly perpendicular to the canal shaft, the lamellar bone can appear elongated on one side, this is referred to as a drifting osteon. As the individual ages, as a consequence of remodelling, new osteons form on top of old osteons, sometimes obscuring the old canals and cement lines (Maggiano, 2012; Kerley, 1965). It is this phenomenon of bone remodelling and replacement of Haversian systems that this the subject of this study.

2.1.1.4 Bone Metabolism

Bone metabolism refers to the growth and maintenance of osseous tissue. As mentioned earlier, like any other bodily tissue, bone tissue is dynamic. It grows, gets worn out, and needs to be replaced. While this generally happens much slower in bone than in other bodily tissues, it still requires a certain amount of turnover. In the case of osseous tissue, the cells turnover about every three months. This occurs throughout the person's life (Gray, 2010; Maggiano, 2012).

Bone growth and maintenance is usually divided into two categories; modelling and remodelling. Modelling refers to the growth of bone tissue, and is usually seen in juveniles, and near the endosteal and periosteal surfaces. It determines the size and the shape of the bone (Frost, 1969). In the initial stages of bone growth in embryonic tissue, growth is divided into two categories of formation; endochondral and intramembranous. Endochondral bone

formation involves bone that is created from a scaffold of avascular hyaline cartilage. Intramembranous bone formation involves the formation of bone within a highly-vascularised membrane (Scheuer & Black, 2004). These sites of ossification usually begin as woven bone, often seen in foetal bones. As the child ages, this woven bone then develops into lamellar bone. This lamellar bone is characterised as primary bone and is studded with primary osteons formed around the early Haversian systems. During the remodelling process, this primary bone changes again, this time developing into the more complex secondary bone (Scheuer & Black, 2004).

Remodelling refers to the maintenance of osseous tissue. By destroying and replacing the old bone cells, the body is able to maintain the homeostasis of the tissue. This is done by the coordinated efforts of two types of cells, osteoblasts and osteoclasts. These cells together are referred to as a basic multicellular unit (BMU) (Frost, 1966). Together, these BMU's break down the lamellar bone, and rebuild new Haversian systems. When new osteons are built by the BMU's, they rarely create the new Haversian system in the exact same place, leaving partial or fragmented osteons behind. Over the course of an individual's lifetime, their bone will shift from mostly primary bone, to creating more and more secondary osteons, until finally a cross-section of their bone would be completely covered in complete and fragmented osteons, leaving no primary lamellar bone visible. Due to the fact that bone continuously remodels throughout an individual's life, and because it creates visually distinct micro-features such as osteons, it is possible to use these features to estimate the age of the individual at death (Stout & Crowder, 2012; Kerley, 1965; Frost, 2001).

In order for either modelling or remodelling to occur, two types of cells must be present. These are osteoblasts and osteoclasts. The first of these cells, osteoblasts, are the building cells. They are responsible for bone mineral secretion and mineralisation of bone, and are the creators of the bony matrix. Osteoblasts originate from mesenchymal progenitors, which also produce other types of cells, including muscle cells, chondrocytes, and adipocytes (Bellido, et al., 2013). In the case of bone modelling, osteoblasts act first, laying down new bony matrix, and allowing from the growth of bone in foetuses, infants, and juveniles. In in the case of remodelling, osteoblasts act as a part of the BMU. They act second, following the destruction of the osteoclasts and remaking the bone that was destroyed in the same place, thereby maintaining the osseous tissue that was already there (Seeman, 2008). Once their task has been completed, the cells either die by apoptosis, remain trapped in the matrix as osteocytes, or coat the bone as bone lining cells (Bellido, et al., 2013).

The other half of the BMU is the osteoclasts. These work in tandem with the osteoblasts during remodelling, destroying old bone to make way for the new bony matrix created by the osteoblasts. Different to osteoblasts, osteoclasts come from hematopoietic progenitors, from which macrophages also originate. It is the function of these cells to resorb the existing bony matrix, by excreting a variety of enzymes, which in turn break down the bone (Jähn & Bonewald, 2012). During the bone resorption process, osteoclasts become polarised and create three distinct membrane zones; a sealing zone to seal off the area from bone that is not to be resorbed, a secretory zone for secreting of bone resorbing enzymes, and a ruffled edge. This ruffled edge, referred to as a Howship's Lacuna, appears within the sealing zone and can be seen in cross-section (Väänänen, et al., 2000). Unlike osteoblasts, which are quite plentiful, osteoclasts are rare, with only two or three existing in each μm^3 of bone tissue. They

are also much larger in size than osteoblasts (Jähn & Bonewald, 2012). The resorption cycle of the osteoclasts ends with the cells either dying by apoptosis, or returning to an inactive, dormant state (Väänänen, et al., 2000).

There is a third type of cell involved in bone that should be mentioned. These are the osteocytes. They are the most populous cells in bone and make up about 90% of the cells within the bony matrix. Osteocytes are made up of osteoblasts that have become trapped in the lamellar bone. These can be seen in cross-section, as each cell is entrapped within a lacuna. They can be connected and communicate within the bone through narrow canaliculi between the layers of the bony matrix. These canaliculi also reach from the endosteal surface to the periosteal surface. It is thought that these cells act in a mechano-sensory function, controlling the modelling and remodelling processes, and helping the bone to adapt to stress and environmental factors (Bellido, et al., 2013). In addition, osteocytes appear to be instrumental in the regulation of mineral homeostasis, as well as the availability of calcium and phosphates (Jähn & Bonewald, 2012).

2.1.1.5 Bone Pathology

The above explanation of bone metabolism assumes that the process is uninhibited and that the systems of the body are healthy. When everything is working as it should, the activities of osteoblasts and osteoclasts are perfectly in balance, and remodelling works as it should, maintaining the same amount of bone. If, however, this balance is interfered with in the form of pathology, either a primary pathology originating in the bone, or a secondary pathology originating in another of the bodily systems and affecting the bone, this system can break down. In this case, bone generally behaves in one of two ways; either the osteoblasts outpace

the osteoclasts and bone is produced faster than it can be destroyed causing an excess, or the osteoclasts outpace the osteoblasts and bone is destroyed faster than it can be regenerated causing the bone to become diminished and porous (Väänänen, et al., 2000; Ortner, 2003). This can happen either in a localised area, often on the periosteum, the exterior surface of the bone, causing a lesion, or it can occur throughout the bone, such as in the case of osteoporosis (Burr & Akkus, 2013). In either instance, the metabolism of the bone is thrown out of balance, causing changes to the foundations of the bony matrix and affecting the microstructure of both the cortical and trabecular bone (Schultz, 2012). For the purposes of this study, the focus will be on the changes to the microstructure of the cortical bone, as this is the area of primary interest for age estimation techniques (Kerley, 1965).

Lesions and Periostitis

In general, localised reaction of the bone to disease is referred to as a lesion. As mentioned above, this can either be a lytic lesion, which is destructive, or a prolific lesion, which is constructive. Lytic lesions tend to be the result of slow, chronic, progressive disease, and often form on the bone adjacent to the lytic focus, or source of disease. These are most often caused by an imbalance in the BMU favouring the destructive osteoclasts. (Ortner, 2003). In most of these cases, the lesion will be sharply defined, and the surrounding bone will appear generally unaffected. The lytic focus can either be a primary bone disease, or the effects on the bone can be related to a disease of the soft tissue adjacent to the bone, for example, metastatic neoplasms (Ortner, 2003).

In contrast, prolific lesions, are often caused by an imbalance of the BMU favouring the constructive osteoblasts. Generally, this results in bone hypertrophy, which can occur

throughout the skeleton, or localised, and can occur in any part of the skeletal system. Proliferative lesions are often further broken down categorically depending on the area of the bone they predominantly affect. Lesions that occur on the outer surface of the bone are classed as periostitis, referring to the inflammation of the periosteum. Osteitis or endostosis refer to inflammation of the inner compact bone and Haversian systems, as well as the bone surface adjacent to the medullary cavity (Ortner, 2003). Again, periostitis is often the result of chronic conditions, some originating in the bone, and others adjacent to the bone. An example of disease originating in the bone that might cause dramatic periostitis is osteosarcoma. Most often, however, periostitis arises secondary to an infection (Ortner, 2003). Another kind of proliferative lesion that may occur is hyperostosis, or excessive production of the outer layer of bone (periosteum) (Martin, 2010). Hyperostosis often affects the bones of the skull, but can also affect other areas in relation to other skeletal diseases such as diffuse idiopathic skeletal hyperostosis (DISH) (Ortner, 2003; Ortner, 2003; Lill, 2013).

Osteoporosis

Bone is a metabolically sensitive tissue, meaning it is susceptible to changes in metabolism throughout the body. These metabolic changes can cause an imbalance in the metabolism and mineralisation of bone, with the potential to cause several skeletal diseases, including osteopenia and osteoporosis (Imel, et al., 2014). Osteopenia and osteoporosis are common disorders related to an unusual loss of bone, osteopenia being the general term for bone loss of any kind, and osteoporosis referring to increased porosity of osseous tissue that results in lower bone mass (Rosenberg, 1999; Ortner, 2003). They can also be defined by the degree of bone loss, with osteopenia being defined as 1.0-2.5 standard deviations below the young adult reference mean when measured by dual-energy X-ray absorptiometry (DXA), and

osteoporosis as greater than 2.5 standard deviations below the young adult reference mean when measured with DXA (Imel, et al., 2014). Osteoporosis can occur either generally, affecting the entire skeleton, or it can affect specific bones, due to disuse (Rosenberg, 1999). In either case, the diminishing bone mass is important, as it can, and often does, lead to fracture (Rosenberg, 1999; Imel, et al., 2014).

The most common forms of osteoporosis are senile, and postmenopausal osteoporosis. This is due to the imperfect remodelling sequence that maintains the osseous tissue. The maximum skeletal bone mass is achieved in early adulthood, and subsequently a deficit begins to accumulate with each cycle of remodelling, eventually adding up to a noticeable loss of bone mass (Rosenberg, 1999). While there are many contributing factors to osteoporosis and bone mass, often it is linked to physical activity, diet, hormone balances, muscle strength or atrophy, as well as vitamin D absorption (Rosenberg, 1999). In addition to the reduction in bone mass observed in individuals as they age, females are also more likely to lose additional bone mass in the decades after menopause, likely due to the change in hormonal balance, specifically an oestrogen deficiency. Females can lose up to 35% of their cortical bone, and up to 50% of their trabecular bone in the three or four decades after menopause. Age related osteoporosis and postmenopausal osteoporosis results from slightly different imbalances; senile osteoporosis results from a decrease in bone formation involving osteoblasts, while postmenopausal osteoporosis is marked by an increase in destructive osteoclast activity. Ultimately the result in either case is bone loss (Horvai, 2015). Although senile and postmenopausal osteoporosis are the most common forms of osteoporosis, osteoporosis is a known comorbidity of many conditions, and also may be connected to other diseases due to treatments or resultant inactivity. Of particular note are several thyroid

conditions (hyperparathyroidism, and hypo-hyperparathyroidism), type 1 diabetes, Addison's Disease, multiple myeloma, various conditions related to insufficient nutrition (malnutrition, malabsorption, vitamin C and D deficiencies, hepatic insufficiencies), chemotherapy, corticosteroid use, anticonvulsants, alcohol abuse, pulmonary disease, and anaemia, among others (Rosenberg, 1999).

While osteoporosis is often systemic, and does affect the entire skeleton, it does not usually affect all bones equally. Often the first bones to be affected, and the most severely affected, are the vertebrae, with the trabeculae of the vertebral bodies diminishing, and sometimes collapsing. This can force the vertebrae into a wedge shape and cause secondary kyphosis of the spine (Ortner, 2003). Another area where the trabeculae are often affected, causing collapse, is the femoral head and neck, which put the individual at risk for dangerous and painful hip fractures (Imel, et al., 2014). Both of these common problems are caused by the bone density loss in the trabecular scaffolding inside the bones. While these are the most common and often most dramatic consequences of osteoporosis, bone loss does eventually reach the cortical bone as well. This is because the remodelling process is slower within the denser cortical bone than the spongiform loose structure of the trabeculae (Ortner, 2003). One of the consequences for cortical bone in the development of osteoporosis is the 'trabecularisation' of the cortical bone, with the endosteal surface being transformed into a very porous, spongiform-like structure resembling the trabeculae. This in turn results in the thinning of the cortical bone (Parfitt, 1984). Another consequence involves the remodelling of Haversian systems, where osteoblasts are not able to replace the resorbed bone cleared by the osteoclasts, which results in a thinning of the osteon wall and larger canal sizes (Ortner, 2003). For the purposes of this study, the changes to the cortical bone in the ribs as a result

of systemic osteoporosis will be of particular interest, as these changes not only provide proof of skeletal involvement in disease originating in other systems, but also have the potential to affect the results of the histological age estimation techniques widely used today.

2.1.2 Introduction to Bone Histology

2.1.2.1 Introduction to Bone Histology Methods and Uses

Once the building blocks of bone biology and microstructure are understood, the next step is to observe these microstructures. How these microstructures are observed is through bone histology. This involves the cutting of thin cross-sections of bone, between 100 and 75 μm thick, to be observed through either transmitted light or polarised light microscopy (Kerley, 1965). It is also possible to observe bone histologically using a coring method, in addition to cross-sections, as this is more practical for certain bones and less destructive (Yoshino, et al., 1994; Thompson, 1979). While bone histology is, in essence, a destructive methodology, it is sometimes the best option for making observations. For example, if the bones have been broken, or if the skeleton is largely incomplete, making the use of macro analytical methods impossible, histology can be done on the fragments to assess certain aspects of the individual, such as age at death (Kerley, 1965). In the case of small fragments of bone where the species is not clear from macro observation, histology can also be used to distinguish between animal and human bone, an essential distinction in some forensic cases (Mulhern & Ubelaker, 2012).

Scientists have been observing the microstructures of cortical bone via thin sections since the 1960's, when Jowsey first published observations and analysis of a femoral cross-section (Jowsey, 1960). These early sections involved embedding a piece of a femur in methyl

methacrylate, and taking a thin section, approximately 100 μm thick, of a complete cross-section of the midshaft of femurs. From these thin sections, Jowsey observed changes to the Haversian systems dependant on the age of the individual (Jowsey, 1960). These initial observations have become the jumping off point for many studies making use of histological analysis of dry bone thin sections to estimate the age of individuals at death.

In 1965, Kerley took these observations of age-related changes to the cortical microstructure and created some of the first age estimation methods using thin sections of bone (Kerley, 1965). While there were problems with these early formulae, as discovered by Ahlqvist and Damsten in 1969, they provided a starting point for many more studies incorporating other bones and newer techniques (Ahlqvist & Damsten, 1969). Kerley later revisited the earlier femoral formula, changing the regressions and improving upon the original work (Kerley & Ubelaker, 1978). Studies continued to explore the histology of long bones, especially the femur. Several studies, including Stout and Gehlert (1982), and Lynnerup and colleagues (2006), explored Kerley's revised method from 1965 and 1978, discussing the effect of field size and subjectivity of the methods. From Jowsey and Kerley's research involving the femur, more studies appeared exploring the use of other bones for histological methods. Stout and Stanley explored the use of the radius, tibia, and fibula; Uytterschaut (1985), and Thompson and Galvin (1983) explored the tibia more in depth; and Yoshino and colleagues (1994) looked into the humerus. Pfeiffer and Zehr (Pfeiffer & Zehr, 1996) used research into the histology of the humerus to age a Neanderthal. Nor and colleagues (Nor, et al., 2014) considered the validity of all the long bones.

After the different long bones had all be explored, validation studies began appearing. These studies served to enhance and improve the methods. The most important of these were population specific studies, as it was found that the original methods, while affective for the populations used to develop them, needed to be adapted to accurately age other populations. Ericksen (1991) tested femoral methods on samples from North America, the Dominican Republic, and Chile. Ruff and colleagues (Ruff, et al., 1984) tested the method on a prehistoric Native American population from the coastal region of Georgia. Two other population studies involved a population from Sudanese Nubia (Martin, 1983; Mulhern & Van Gerven, 1997). Maat and colleagues (2006) then tested femoral methods on a Dutch population. Later, Han and colleagues (2009) study tested Maat's revised method on a Korean population. These studies implied that histological age estimation methods increased in accuracy when tailored to the observed population. In addition to the differences posed by different populations, there also appeared to be differences based on sexual dimorphism of the long bones (Mulhern & Van Gerven, 1997; Samson & Branigan, 1987). All of these studies moved the use of bone histology for age estimation forward, improving on previous methods, creating more and more accurate techniques for estimating age from histology of the long bones.

Of course, histological analysis for age estimation was not only tested on the long bones. As long bones are of use for macro analysis, it is rare that destructive methods are undertaken on these bones. In the early 1990's, several methods were developed using histology of the ribs and clavicles, solving several problems posed by the previous long bone methodologies. It is these methods that are explored further in this study.

2.1.2.2 Bone Histology and Age Estimation Using Ribs

In the 1990's a method for accurately aging skeletal materials using bone histology of rib thin sections was developed by Stout and Paine (1992). This method was developed using an American sample, including both white and African Americans. In their 1992 paper, they describe how by using thin sections of ribs or clavicles it was possible to take measurements and counting osteon density, which when inserted into their formula would yield the age of the individual (Stout & Paine, 1992). Stout and Paine then revisited the method and improved upon the original formulae in 1994 (Stout & Paine, 1994). These formulae were partially inspired by the case study Stout did using histology of the 6th rib for age estimation of the painter Pizarro in the late 1980's (Stout, 1986).

Methods using the ribs, such as the Stout and Paine method, while based on Kerley's method from 1965, had several benefits over previous methods involving histological age estimation. Firstly, it utilises ribs, which are much more likely to be available for thin sectioning than major long bones, as the long bones would most likely be kept intact for standard macro osteometric methods (Streeter, 2012). Secondly, as the bones being thin sectioned are much smaller, it is reasonably possible to count the true osteon population of the sample, rather than several sample population densities from different areas of the sample, as was done with thin sections or cores from the leg bones (Kerley, 1965; Thompson, 1979). In addition, although Stout and Paine's method specifies the sixth rib, further study has determined that non-sixth mid-thoracic ribs yield similar results (Crowder & Rosella, 2007). This is important as ribs are often broken when retrieved in skeletal form, and it is then difficult to determine the exact rib placement. By yielding accurate results with easily obtained bone samples, Stout and Paine's method has been found to be useful, especially in instances where other aging

methods could not be employed. Through the many validation studies undertaken, and the improvements made to the age estimation techniques using rib histology have made these methods the most accurate of the histological age estimation methods (Crowder, et al., 2012).

As with the methods utilising long bones, it emerged that population was an important factor in developing age estimation formulae. The most significant of these studies came in 2002, when Cho and colleagues tested the Stout and Paine formulae for inter-population variability. The study found that there was a statistically significant difference between the osteon population densities (OPD) of European-American and African-Americans. To remedy this oversight in the original study, Cho and colleagues supplied new formulae specific to European-Americans and African-Americans, as well as a general formula for samples of unknown ethnicity (Cho & al., 2002). Later, Cho and colleagues (2006) revisited these populations, this time also comparing for sex, revealing differences in age-related bone loss between the groups. Bednarek and colleagues (2009) tested the method on a Polish population, developing regressions specific to that population. According to the Polish team, uniformity of the methodological process was key to successfully using histology for age estimation. Another population study, undertaken by Lee and colleagues (Lee, et al., 2014), used a Korean population to test the clavicle formula from the Stout and Paine method. Like Cho, they found the Stout and Paine formula ineffective for the Korean population, and instead used the original method to develop a Korean population specific formula for the clavicle. Pfeiffer and colleagues (2016) tested Cho and colleagues 2002 formulae specific to European-American and African-American populations, and their general formula for individuals of unknown origin, on a diverse population from South Africa. They found that the population specific formulae did not improve the accuracy of the age estimations for the

South African population. While they tried creating a new formula specific to this population, it did not perform better than the Cho and colleagues' formulae. They found, rather, that the general formula for unknown ethnicity performed relatively well for all groups, reinforcing the validity of this formula for widespread use. Validation studies continue, including the one associated with this study (Garcia-Donas, 2017), exploring how far these methodologies can be pushed toward optimal accuracy.

Although these methods rely upon the changes to the bone microstructure as individuals age, certain age-related changes can decrease the reliability of the rib histology formulae. Goliath and colleagues (2016) found that advanced age decreased the size of osteons but increased the number of osteons per unit as well as the circularity of the osteons. This is likely due to age-related osteoporosis, one of the most common causes of osteoporosis (Rosenberg, 1999). These changes to the bone microstructure fundamentally change the microstructure of bone, as the balance of bone metabolism is disturbed. While it is unknown why exactly the balance of BMU's is undone as we age, most likely a combination of factors, up to 20-30% of bone can be lost (Brickley & Ives, 2008). Another common cause of changes to the bone microstructure is post-menopausal osteoporosis (Rosenberg, 1999). This is possibly due to an estrogen deficiency, which impacts extra-skeletal calcium homeostasis. This in turn causes an increase in bone resorption, throwing the normal BMU metabolism out of balance (Riggs, et al., 1998). These changes, which not only contribute to cortical bone loss, but also to changes in osteon shape and size, impact the fundamental building blocks of the age estimation formulae, decreasing their accuracy for individuals of advanced age (Parfitt, 1984; Goliath, et al., 2016).

Another consideration when implementing these age estimation formulae is degradation of the bone due to taphonomy or diagenesis. These changes can appear in both modern and archaeological samples exposed to time and the elements. While taphonomy is regularly acknowledged as a factor in macro analysis of bone, it also has the ability to make changes to the bone microstructure. If the microstructure is to be analysed, especially when estimating age for forensic purposes or for assessing pathology, it is essential to understand and differentiate the damage done by age, disease, and the environment. Once a body ceases to live, several different digenetic processes take place, including hydrolysis, dissolution, and microbial attack. These all have the ability to alter the microstructure of the bone as the body decomposes and comes to balance with its environment (Kontopoulos, et al., 2016). These changes are often centred around the Haversian canals, as the decomposition of the body is facilitated by bacteria and microorganisms travelling through the body's vasculature (Bell, 2012). These changes can also sometimes be misinterpreted as pathological in nature, called pseudopathology (Schultz, 2012). These processes often depend upon the exposure of the body, the air, the soil composition, and the temperature (Schultz, 2001). It is not only micro-organisms in the soil that can affect the bone, but also micro-organisms in the water (Bell, 2012). In general, the changes made by the environment, flora and fauna that invade the body and the skeleton after death during decomposition are discernible from the regular bone microstructure, as they often follow their own paths through the tissue. While they can enlarge canals, and cause micro-cracks in the cortical bone, these are differentiated from normal destructive processes and pathology by the tell-tale ruffles of the Howship's lacunae, and the flowing lamellar pattern of the bone (Bell, 2012; Schultz, 2012; Schultz, 2001).

While the above considerations are all common changes to bone that are encountered with relative frequency and should reasonably be expected to be incorporated into age estimation equations, another less common and more variable consideration is pathology. As the equation requires cortical area and osteon population, if there were a pathological or metabolic disturbance that had affected the cortical area of the bone or the osteon population density, the equation would be rendered inaccurate. This has been discussed in several previous studies, although more extensive research is necessary to better quantify the changes made to the bone. One such study was Paine and Brenton's (2006) study on pellagra in a South African population, which found sufferers of pellagra had higher instances of osteoporosis, impacting the results of age estimation techniques. There are several known connections between chronic metabolic diseases and metabolic bone disease, such as hyperparathyroidism (McCarthy, 2010; Stein, et al., 2011). As these diseases are the focus of this thesis, diseases belonging to each different system and their connections to metabolic bone disease will be discussed in the following section. Long-term infectious disease has also proven capable of making changes to the bone microstructure (Schultz, 2012; Schultz, 2001; Van der Merwe, et al., 2010). While the implications of these micromorphological changes have been discussed, more research and quantifications of these changes to the microstructure need to be made, and the exact effects of pathology on the efficacy of histological age estimation techniques needs to be quantified.

In the context of this study, Stout and Paine's method for histological aging will be discussed alongside the medical history of the subjects, containing known age at death. As Stout and Paine's equations were not created for this population, and therefore do not yield as accurate results (Garcia-Donas, 2017), the focus will instead be on the cortical area and OPD of the

samples, as these variables are the building blocks used by all histological age estimation techniques. By comparing the relationships between these two variables with the actual age at death of the individuals, it may be possible to determine the degree of inaccuracy in individuals with pathological microstructural changes related to chronic metabolic diseases. With respect to forensic methodology, this could help to more accurately assess age at death of individuals with disturbances in bone metabolism, regardless of the population.

2.2 Chronic Disease and Comorbidities Involving Bone

2.2.1 Introduction to Metabolism

In essence, metabolism is how the body maintains and sustains itself. While each system may have different metabolic rates and processes, these chemical reactions all interact together to keep the body growing and maintained. Some tissues may produce chemicals that are needed for the maintenance of another organ or system, creating an interconnected system in which the body is able to sustain itself (Kusinitz, 2014; Shulman & Peterson, 2017). Metabolism functions in one of two ways, anabolic processes (energy capture) during which energy is used to produce different substances, like proteins and nucleic acids, and catabolic processes (energy release) during which substances are broken down to create energy. These systems should be in balance to maintain the body. In terms of physics, the first law of thermodynamics is always maintained, with the energy input always equal to the energy output and storage (Shulman & Peterson, 2017). In the skeletal system, this can be seen in the functions of the BMU, building up and breaking down bone tissue to maintain the osseous tissue. If, however, the metabolism of one tissue or system is affected, either by environmental issues or pathology, this can cause cascading problems that end up affecting

other systems of the body. This is where pathology and bone most often interact. As different systems within the body are affected, these cascading consequences eventually find their way to the bone, if allowed to continue long enough (Ortner, 2003). This is where the different metabolic rates of tissues come in.

2.2.1.1 Different metabolic rates of tissues

Different tissues have different metabolic rates, with some tissues, such as bone, taking months to cycle through the destruction of old tissue and the creation of new replacement tissues (Burr & Akkus, 2013). Other tissues cycle through maintenance much faster, such as the liver, which is able to regenerate quickly after injury. Due to the liver's propensity for regeneration, most diseases of the liver up until the appearance of fibrosis (cirrhosis) can be completely reversed (Crawford, 1999). Due to the fact that bone tissue is the slowest of all the tissues to turnover, pathological conditions that affect other tissues do not often reach the point of affecting the bone. This is particularly true of acute infections of other tissues. If an infection, or disease, is present in the body for less time that it takes for the osseous tissue to metabolise, it will not affect the bone. If, however, there is chronic disease in another system, present over a period of months or years, it can have the ability to affect the bone metabolism (Ortner, 2003). For this reason, this study will focus only on chronic diseases that have the potential to negatively affect osseous tissue.

2.2.1.2 How different systems interact

As stated above, the metabolism of the different systems of the body are all interlinked, allowing disturbances in one system to have potentially catastrophic effects on the metabolism of another. As different chemicals and substances are produced in certain

systems and then used by another, this can create a potentially disastrous chain reaction if the metabolic processes are disturbed. One example of this is hyperparathyroidism, and its effects on bone. Hyperparathyroidism is usually caused by long periods of hypercalcemia resulting in hypersecretion of thyroid hormone. The increased amount of hormone in the system reach the osteoblasts, which then stimulate the osteoclasts to begin their activity. This causes increased, unbalanced resorption of osseous tissue, resulting in osteoporosis (Rosenberg, 1999). The chain reaction following the primary disease of the thyroid eventually makes its way to the skeletal system, causing secondary disease there. This is only one of many examples of secondary bone disease occurring as a comorbidity of primary disease elsewhere in the body. The following sections will discuss the different classes of disease found within this study and lay out the potential for each disease to affect the metabolism of the osseous tissue.

2.2.2 Pathological Categories and Their Interactions with Bone

2.2.2.1 Cancer

Cancer, or neoplasms, is one of the most common forms of disease found in the human body. It can manifest in any tissue and in any system. Neoplasm means 'new growth' and refers to the growth of tumours in the body. These include both benign and malignant tumours. The tumour, or neoplasm, refers to a mass of tissue whose growth exceeds that of the surrounding normal tissue, serving no purpose, and often weakening the host by competing with the surrounding tissue for energy and resources. These masses often divert blood supplies to the tumours, and can even produce substances, such as hormones, which can interfere with the regulation and maintenance of bodily systems. In terms of malignant

tumours, tumours that appear in the mesenchymal tissues are classed as sarcomas and tumours that appear in the epithelial cells are classed as carcinomas. (Cotran, et al., 1999). While there are primary malignant cancers of the bone, such as osteogenic sarcomas or osteosarcomas, bone is more often involved as a secondary to a primary tumour elsewhere. These are known as metastases (Ortner, 2003).

The effects of cancer are many and widespread, sometimes impeding the function of nearby tissues, sometimes synthesising substances, such as hormones, and unbalancing the body's natural production levels, causing bleeding in the area surround the tumour due to ulceration, as well as occasional rupture or infarction of the tumour or surrounding tissues. One example is hypercalcaemia, caused by paraneoplastic syndrome. This interruption has similar effects on bone to hyperparathyroidism (Guise & Mundy, 1998). Individuals with cancer can also experience cachexia, leading to loss of body fat and body mass, along with weaknesses, anorexia, and anaemia (Cotran, et al., 1999). All of these effects have consequences, not just for the affected systems, but for the body as a whole.

Metastatic Cancer

Metastatic cancer or metastases refer to tumours implanted in tissue away from the primary tumour. Metastases automatically classify the primary tumour as malignant, as benign tumours never metastasise to other tissues. Most cancers, with the exception of gliomas of the central nervous system and basal cell carcinomas of the skin can, and often do, metastasise. Often, the larger and more aggressive the primary tumour, the more likely it is that it will spread to other parts of the body and metastasise to other tissues (Cotran, et al., 1999). While bone is more likely to be involved in metastatic, rather than primary, cancer, it

is often difficult to tell the difference (Ortner, 2003). Using bone scintigraphy, it has been found that up to 85% of individuals with carcinomas will involve metastases to the skeleton (Dorfman & Czerniak, 1998). As reactions in bone tend to either imbalance the BMU system in favour of the osteoblasts or the osteoclasts, causing either prolific or lytic lesions, metastatic lesions are expected to be the same. In the case of metastatic lesions on bone, about 75% are lytic lesions, 15% are prolific, and about 10% are a mix of both lytic and prolific lesions (Greenspan & Remagen, 1998). Metastases often occur in the axial skeleton, as these bones are where hematopoietic marrow are found in adults. The tumour cells can then replace the marrow and grow from inside the marrow cavity outward towards the periosteum. Often these metastases remain within the marrow cavity and are only discovered upon autopsy, however some tumours do move further into the bone, first destroying the trabecular scaffolding, and eventually entering the cortical bone. The fastest growing of these tumours tend to be lytic in nature, while the slower growing tumours are often prolific. The ribs and sternum are the third most likely to be involved, behind the spine and the femur, with 25% of skeletal metastases involving the ribs or sternum (Ortner, 2003).

Cancer Therapies

Unfortunately for many patients, cancer therapies can damage the bone tissue as well as the disease they are fighting. Often individuals being treated for cancer are at risk for osteoporosis due to a combination of the activities of the cancer itself, as well as the effects of chemotherapy, corticosteroids, aromatase inhibitors, and androgen deprivation therapy (Drake, 2013). The effects of cancer treatment on bone can generally be divided into two categories; cytotoxic, which inhibits the activities of bone building osteoblasts, and hormonal where the interference of the therapy with the body's natural production of hormones can

stimulate osteoclast activity (Healey, 1999). One example is in therapies for breast cancer, treatments often target oestrogen production and receptors, as oestrogen receptors are expressed by about 70% of breast neoplasms. This, however, has a negative effect on BMD, similar to postmenopausal osteoporosis, as oestrogen is involved in the stimulation of osteoblasts (Hirbe, et al., 2006). In cases of prostate cancer, patients are often treated with hormone therapies with the potential to cause hypogonadism. Again, like oestrogen blocking treatments and postmenopausal osteoporosis, Gonadotropin-releasing hormone (GnRH) agonist treatments affect parathyroid hormone levels, again stimulating osteoclast activity (Smith, 2006). Cancer treatment can also have indirect effects on bone, such as mucositis caused anorexia, and malnutrition that can contribute to osteoporosis as well (Healey, 1999). In all, cancer patients are often at risk for osteoporosis, not only from potential metastatic bone involvement, or hormone secreting tumours, but also potentially from the treatments they are being prescribed. Often these hormone-related therapies cause chain reactions in the body's metabolism, resulting in marked bone loss for the patient.

2.2.2.2 Cardiovascular Disease

Cardiovascular diseases (CVD's) are now the number one cause of death worldwide. In 2015, approximately 17.7 million people died of CVD's, about 31% of all deaths worldwide that year. These diseases are on the rise, largely due to modern lifestyle changes including poor diet and inactivity. Major risk factors include obesity, diabetes, tobacco use, and alcohol abuse, all of which can be avoided by living a healthier lifestyle (World Health Organization, 2017). Of particular interest are coronary artery disease (CAD), in particular the manifestations of CAD as atherosclerosis and myocardial infarction (heart attack). CAD, in particular atherosclerosis and myocardial infarctions, are some of the most common forms of cardiovascular disease today. Each of these pathologies are chronic conditions, or,

in the case of myocardial infarction, the result of a chronic condition, and therefore have the ability to influence the metabolism of bone.

Coronary Artery Disease (CAD)

Coronary artery disease (CAD), sometimes referred to as coronary heart disease (CHD) or ischemic heart disease (IHD), refers to a group of conditions that result from myocardial ischemia, an imbalance in the perfusion and demand of oxygenated blood. This often results in an insufficiency of oxygen delivered to the body through the vessels, most of the time (90%) due to an obstruction in the arteries, also known as atherosclerosis, as well as other complicating factors such as intraluminal thrombosis and vasospasm. The end result of CAD is often a myocardial infarction, or heart attack, a potentially lethal consequence of years of plaque build -up and obstruction (Schoen, 1999).

Atherosclerosis

Atherosclerosis is characterised by the presence of atheromas or fibrous fatty plaques that line the walls of the arteries and protrude out into the lumen, obstructing blood flow (Schoen & Cotran, 1999). It is an incredibly common pathology and is one of the top contributors to CVD's place as number one cause of death in the world (World Health Organization, 2017). Atherosclerosis is a chronic condition, often beginning in the childhood years, and not becoming apparent until later in adulthood. It most often affects the elastic arteries, such as the aorta and carotid, as well as muscular arteries, like the coronary and popliteal arteries. As it involves the arteries and the blood supply for the entire body, it could potentially affect any area or organ, but the most commonly affected places are the heart, brain, kidneys, small intestine, and the legs. If the plaques are disrupted, they can precipitate a thrombosis (blood clot) obstructing blood flow even further. If untreated and allowed to continue unchecked,

atherosclerosis often results in myocardial infarction (heart attack), cerebral infarction (stroke), or aortic aneurism, depending on the site of the plaques (Schoen & Cotran, 1999).

Myocardial Infarction

While myocardial infarctions, otherwise known as heart attacks, are not in themselves a chronic disease, they are almost always the result of an underlying chronic cardiovascular condition, often CAD and atherosclerosis. Of the samples assessed in this study with a myocardial infarction listed as cause of death, most if not all, had CAD and/or atherosclerosis as well. A myocardial infarction can be deadly, and many patients die before they are able to be treated. A fast medical response is essential to the survival of the patient (Schoen, 1999). Of all deaths associated with CVD's 80% are attributed either to a heart attack or a stroke (cerebral infarction) (World Health Organization, 2017). Myocardial infarction refers to the cell death in the myocardium, or the heart muscle, usually limited to a specific area or ventricle. A myocardial response is triggered as a consequence of arterial obstruction, limiting the blood supply to the myocardium. Depending on the severity and the duration of blood flow deprivation, this can lead to localised necrosis. Myocardial infarctions (MI's) usually occur in one of two ways; a transmural MI, in which necrosis has affected the entire, or nearly entire, thickness of the ventricular wall, and a subendocardial MI, in which only the inner third to one half of the ventricular wall thickness is affected by necrosis (Schoen, 1999).

Comorbidities Involving Bone

Coronary artery disease and low bone mineral density (BMD) are known to have several common risk factors, although scientists are still trying to pinpoint exactly where the two interact, and whether the link is direct or indirect. It has been found that patients with low bone mass are at higher risk of a cardiac episode or death than patients with normal bone

mass (Sprini, et al., 2014; Bagger, et al., 2007; Magnus & Broussard, 2005; Farhat, et al., 2006). Marcovitz and colleagues (2005) were able to use low BMD as a predictor of CAD, connecting osteoporosis with heart disease predominantly in postmenopausal women. It has also been linked to cardiovascular death in men, where osteoporosis and low BMD were also used as a predictor (Mussolino, et al., 2003; Trivedi & Khaw, 2001; Van Der Klift, et al., 2002). Although previously thought to develop independently from different processes related to aging, it is now thought that cardiovascular disease and osteoporosis may develop from common pathophysiological risk factors. One possible connection may be the similarity between arterial calcification and bone mineralisation. It appears that both processes are relatively similar, and they share factors that are also used to stimulate osteogenesis, including bone morphogenetic protein (BMP), alkaline phosphatase (ALP), and osteopontin (OPN) (Sprini, et al., 2014). In terms of atherosclerosis, bone metabolism can also be affected locally, depending whether they are supplied by an obstructed artery (Bagger, et al., 2007). While the exact connection is not yet clear, the fact that a pathophysiological connection exists between CVD's and osteoporosis is generally agreed upon.

2.2.2.3 Diabetes

Diabetes mellitus, or diabetes as it is commonly known, is a disorder of the pancreas affecting carbohydrate, fat, and protein metabolism. This is the result of an inability or deficiency in the pancreas' ability to secrete insulin and therefore impairs the body's ability to manage glucose (Crawford & Cotran, 1999). As of 2014, 422 million people worldwide have been diagnosed with diabetes, and in the year 2015 an estimated 1.5 million deaths worldwide were attributed to the disease (World Health Organization, 2017). There are two main types of diabetes; type 1, previously known as insulin-dependent diabetes mellitus (IDDM), and type 2, previous known as non-insulin-dependent diabetes mellitus (NIDDM). Type 1,

sometimes also called juvenile-onset diabetes, is an autoimmune disease that accounts for about 10% of diabetes cases, and is the result of β-cell destruction, usually due to an autoimmune attack. This causes the pancreas to be unable to secrete enough insulin, leaving the patient dependent upon injected insulin for survival. Type 2 makes up the 80-90% of other patients with diabetes and had previously been known as adult-onset diabetes. Unlike type 1, type 2 diabetes does not appear to have any link to autoimmune reactions, but instead is highly associated with lifestyle, in particular obesity and diet. In type 2 diabetes, for example, obesity can contribute to deranged insulin secretion and insulin resistance in the surrounding tissue, leading to hyperglycaemia, ultimately resulting in β-cell exhaustion. For this manifestation of the disease, it is important to note that it is not necessarily a deficiency of insulin which is causing problems, although it can manifest in the later stages of the disease, but rather a resistance to insulin in the peripheral tissues, causing elevated serum levels of insulin to compensate (Crawford & Cotran, 1999). As diabetes intrinsically involves the body's metabolism it is known to cause a host of cascading effects and has a very long list of comorbidities (Crawford & Cotran, 1999; Bouillon, 1991).

Comorbidities Involving Bone

Osteoporosis is a known comorbidity of diabetes, specifically type 1 (Rosenberg, 1999). Diabetic bone disease, and especially its effects on juveniles, has long been documented (Morrison & Bogan, 1927). While osteoporosis can occur in both type 1 and type 2 diabetes, as type 2 is related to age and obesity the mechanism for bone loss is different than for type 1, and usually much less prevalent (Bouillon, 1991; Vestergaard, 2007; de Liefde, et al., 2005; Pérez-Castrillón, et al., 2004). The cascading effects of insulin deficiency from type 1 diabetes contribute to hormonal changes, in turn having an effect on the metabolism of bone, most

notably affecting vitamin D metabolism, which is vital to the synthesis of osteocalcin. In addition to insulin deficiency itself, diabetes also causes other problems associated with osteoporosis, including negative protein balance, reduced physical activity, and impaired gonadal function, inhibiting hormone production (Bouillon, 1991). In contrast to the effects of type 1 diabetes on bone, type 2 often has the opposite effect. Several studies have noted that type 2 diabetics actually have increased bone mass and a reduced risk of fracture (Van Daele, et al., 1995; Vestergaard, 2007; de Liefde, et al., 2005). While osteoporosis is a risk factor for both types of diabetes, BMI and obesity have an effect on the fracture risk of type 2 diabetics, with increased BMI ameliorating many of the risks associated with diabetic bone disease (Vestergaard, 2007). While type 2 diabetics often have higher BMD than average, this seems to be independent of their fracture risk, as despite the elevated BMD many type 2 diabetics show an increased incidence of fracture (Hofbauer, et al., 2007; de Liefde, et al., 2005; Pérez-Castrillón, et al., 2004). Most studies offer the hypothesis that increased fracture risk in type 2 diabetics may be due to complications of long term diabetes, however there is little proof thus far (Hofbauer, et al., 2007; de Liefde, et al., 2005). One possible long-term complication of diabetes that has the potential to change bone at the tissue level are the advanced glycation end products (AGEs). The glycation involved can affect not only turnover rates, but all the mechanical integrity of the matrix, leading to more brittle bone tissue, regardless of BMD (Viguet-Carrin, et al., 2006). The samples exhibiting diabetes in this study were not categorised as type 1 or 2, however as fracture incidence and decreased BMD is a possibility in both types, especially in those individuals of advanced age, an overarching view of diabetic bone disease was adopted.

2.2.2.4 Hepatic Disease

The liver has an amazing propensity for healing itself, and as such, recovers remarkably well from injury. If, however, the liver is repeatedly injured over a long period of time, it will eventually lose the ability to bounce back. While there are many diseases that can affect the liver, including infections, circulatory disorders, and congenital anomalies, the fact is that due to the function of the liver the pathologies that affect it the most are usually related to harmful lifestyle choices. The most common chronic condition encountered with the liver is related to chronic alcohol abuse, namely alcoholic liver disease (Crawford, 1999).

Alcoholic Liver Disease

Alcoholic Liver Disease (hereafter referred to as ALD) encompasses three types of liver disease related to alcohol abuse. These range from the relatively mild, reversible hepatic steatosis (or fatty liver) to the more serious and largely irreversible cirrhosis of the liver, all of which can be confirmed using histological samples of liver tissue (Crawford, 1999). Often the first liver disease to arise is hepatic steatosis. This is caused by micro-vesicular lipid droplets forming in the hepatocytes. These droplets can grow to form macro-vesicular globules, which in turn can displace or compress the nucleus of the hepatocytes. As the disease progresses, the liver becomes enlarged, yellow in colour, and greasy in appearance. At this stage, there is usually little to no fibrosis formed in the liver tissue. If changes in lifestyle are made, i.e. abstinence from alcohol, this stage of liver disease is completely reversible (Theise, 2015). The next disease to affect the liver is often alcoholic hepatitis. During this stage of liver disease there is often swelling of the hepatocytes and cell necrosis. The liver often undergoes a neutrophilic reaction and Mallory bodies are sometimes present. It is also possible at this stage for fibrous tissue to begin development. As with hepatic steatosis, it is possible to completely reverse

alcoholic hepatitis, with the exception of tissue fibrosis should it have begun to develop (Theise, 2015; Crawford, 1999).

The last, most serious, and irreversible stage of ALD is alcoholic cirrhosis. During the beginning stages of cirrhosis, the liver is often yellow, fatty and enlarged, similar to the appearance of hepatic steatosis. Over the years, however, the liver becomes brown, shrunken, and non-fatty. While cirrhosis can develop directly from hepatic steatosis, it can often develop more quickly from alcoholic hepatitis. In alcoholic cirrhosis, the most important feature of the disease is the development of fibrous tissue within the liver. Over time the liver develops from fine fibrous septa to full nodules. These nodules become more prominent, giving the liver a "hobnail" appearance (Crawford, 1999). As the fibrous tissue grows and extends into the liver, the organ loses fat and visibly shrinks in size. As the disease continues the liver is transformed into a combination of macro- and micro-nodules. Towards the end stages of the disease ischemic necrosis and fibrous tissue destroy the nodules, creating extensive areas of scar tissue. During this period, bile stasis often develops. Despite having a known cause, by its end stages alcoholic cirrhosis is not discernible, either macroscopically or microscopically, from other causes of cirrhosis, such as viral hepatitis (Crawford, 1999).

While short-term ingestion of alcohol in amounts up to 80 grams of ethanol can cause changes to the liver, such as fatty liver, these changes are reversible. Daily intake of 80 grams of ethanol or higher, however, can cause significant changes to the liver and pose a risk for serious hepatic injury. Ingestion of upwards of 160 grams of ethanol a day over the course of 10-20 years is consistently associated with severe hepatic injury. That being said, only about 10-15% of alcoholics develop cirrhosis of the liver, with females being more likely to have

severe hepatic injury. It is also possible for cirrhosis to develop independently of the other stages of ALD. For alcoholics with liver disease, the long-term outlook differs significantly based on the amount of time abusing alcohol. Alcoholics with liver disease see a 90% survival rate, but this percentage drops heavily to 50-60% in those who continue to abuse alcohol (Theise, 2015). In addition to disease and interference with hepatic functions, alcohol often becomes a major source of calories to the alcoholic, leading to malnutrition and subsequently other secondary metabolic disorders, such as osteoporosis (Feitelberg, et al., 1987; Bikle, et al., 1985).

Comorbidities Involving Bone

Chronic alcoholism has long been known to affect bone mineral density, and by extension bone microstructure (Rosenberg, 1999). Exactly how it affects the metabolism of bone is a matter of debate. Several studies have been done examining the connection between chronic alcohol abuse and decreased bone density (Bikle, et al., 1985; Feitelberg, et al., 1987). Diet, sun-exposure, 25 hydroxyvitamin D deficiency (Verbanck, et al., 1976; Arnaud, 1982; Herlong, et al., 1982; Mobarhan, et al., 1984; George, et al., 2009), as well as liver and renal disease have all been examined as possible causes for the increased incidence of osteoporosis and osteopenia in patients with chronic alcoholism (Long, et al., 1978; Spencer, et al., 1986; Labib, et al., 1989). Although there is a long list of conditions associated with chronic alcohol abuse, there have been cases of decreased bone density in patients without other ethanol-related diseases or deficiencies (Baran, et al., 1980; Lalor, et al., 1986; Turner, et al., 1987; Diamond, et al., 1990; Gonzalez-Calvin, et al., 1993). Several studies have implied that alcoholics with liver disease are more likely to also have decreased bone mineral density, though direct correlation has not yet been proven. Increased susceptibility to osteoporosis and osteopenia

in alcoholics could also explain the increased incidences of fractures in chronic alcoholics (Lindsell, et al., 1982; Diamond, et al., 1990; Peris, et al., 1992). As chronic alcoholism has been proven to cause a host of comorbidities, over 200 according to the World Health Organisation (2018), it is likely that these conditions, such as the vitamin d deficiency and hypogonadism often seen in ALD patients, contribute to cascading metabolic consequences that eventually affect the bone, resulting in suppression of the osteoblasts and stimulation of the osteoclasts (George, et al., 2009).

2.2.2.5 Pulmonary Disease

Pulmonary disease is incredibly common, from the common cold, to asthma. Worldwide, 235 million people suffer from asthma, and more than 3 million people die every year of chronic obstructive pulmonary diseases (COPD's), about 6% of all deaths (World Health Organisation, 2018). Of concern to this study are primarily obstructive pulmonary diseases, rather than restrictive. Many obstructive pulmonary diseases are chronic, and debilitating, even life threatening, to the patient. These diseases are characterised by a resistance to normal airflow caused by obstruction of the airway. This can be at any level of the respiratory tract, from the bronchi to the trachea (Kobzik, 1999).

Chronic Obstructive Pulmonary Disease (COPD)

Chronic obstructive pulmonary disease (COPD) is actually a term that applies to several conditions. All of these conditions share a common symptom, dyspnoea, meaning shortness of breath. These conditions are often caused or exacerbated by environmental factors such as tobacco smoke, airborne pollutants, and exposure to chemical fumes. While these conditions had formerly been categorized as different conditions, as many patients presented

with multiple symptoms falling under several different categories, they are now known under the umbrella term of COPD. These conditions include emphysema, meaning enlarged airspaces that can lead to the destruction of the walls of the airspaces, chronic bronchitis, meaning a persistent productive cough with sputum production often obstructing the airway, and lastly asthma, meaning an inflammatory disorder characterised by hyperactive episodic bronchoconstriction. COPD is a disease of middle to later life and does not usually manifest until the fourth or fifth decade (Kobzik, 1999). These three conditions often appear together in patients with COPD, and patients diagnosed with asthma as children may develop COPD later in life. Urbanisation, and airborne pollutants from industrialised nations, as well as smoking, have greatly contributed to the spike in COPD cases worldwide (World Health Organisation, 2017; Kobzik, 1999).

Bronchopneumonia

Like COPD, bronchopneumonia is a disease predominantly seen in later life, although it does sometimes appear in the very young as well. While often an acute condition, severe infections can linger for months, and in some cases is considered a chronic condition. It is characterised as a persistent, lower respiratory tract infection, resulting in patchy consolidation of the lung. These infections are most often caused by bacteria, and follow an earlier compromise to the immune system, such as bronchitis, chronic disease, or treatment with immunosuppressant's. It is often the case that bronchopneumonia is found at autopsy, especially following long periods of illness, such as progressive heart failure, and are often contracted while being treated in hospital (Kobzik, 1999).

Comorbidities Involving Bone

COPD and obstructive pulmonary conditions are incredibly debilitating and have a profound affect upon the patient's quality of life, making breathing and any kind of physical activity difficult. This leads to a largely sedentary lifestyle, bringing its own complications (Kobzik, 1999; Jørgensen, et al., 2007). Often, other conditions develop with the progression of the disease, including right ventricular heart failure, and osteoporosis (Jørgensen, et al., 2007). According to the World Health Organization, prevalence of osteoporosis in COPD patients is somewhere between 24-69% (Cavaillès, et al., 2013). Part of the explanation for why osteoporosis develops could be the use of gluco-corticosteroids in treatment, a known contributor to the development of osteoporosis and osteopenia (Jørgensen, et al., 2007; Rosenberg, 1999; Maggi, et al., 2009). Steroid use alone, however, is not sufficient explanation for the prevalence of osteoporosis in COPD patients, suggesting another factor may be at work (Jørgensen, et al., 2007; Fabbri, et al., 2008; Cavaillès, et al., 2013; Chatila, et al., 2008). It has also been found that COPD patients often present with metabolic syndrome as one of the many complex comorbidities associated with the disease, possibly contributing to the prevalence of osteoporosis in COPD patients, outside the factors of steroid treatment and sedentary lifestyle (Fabbri, et al., 2008; Cavaillès, et al., 2013). As time passes, COPD and osteoporosis also tend to feed into each other, with vertebral fractures contributing to further airway restriction, allowing the consequences of the COPD to worsen (Cavaillès, et al., 2013). In a study by Mineo and colleagues (2005), lung volume reduction surgery to improve the symptoms of emphysema also contributed to a marked improvement in bone density scores, despite the continued use of steroid therapies. Chronic bronchopneumonia, like myocardial infarctions, usually culminate following another chronic condition, and therefore has many of the same consequences of those conditions, such as CAD and COPD (Kobzik, 1999). It can

therefore be expected to also have many of the same complex comorbidities connecting it to bone metabolism.

2.2.2.6 Renal Disease

Renal disease refers to conditions of the kidney. For the purposes of this study, only chronic conditions of the kidney were examined. These are defined as decreased kidney function as measured by glomerular filtration rate (GFR) as well as markers of kidney structural damage (Webster, et al., 2017; Levey & Coresh, 2012). Kidney disease of this kind rarely occurs on its own, and often is the result of another chronic condition (Webster, et al., 2017). In many cases, the end stage of such a disease is kidney failure (Cotran, et al., 1999).

Chronic Kidney Disease (CKD)

Chronic kidney disease is an umbrella term that refers to a decrease in function and structure of the kidney for a duration of at least three months. It rarely occurs on its own, instead often being associated with the later stages of diabetes, which account for 30-50% of all CKD cases, as well as hypertension and heart disease. If it does originate in the kidney, it is often caused by glomerulonephritis, an inflammation of the glomeruli (Webster, et al., 2017; Cotran, et al., 1999; Levey & Coresh, 2012). To be clinically diagnosed, a GFR of less than about 60 mL/min per 1.73 m^2 is necessary (Levey & Coresh, 2012; Webster, et al., 2017). As the symptoms can be non-specific, diagnosis is often only picked up by routine blood or urine tests, or the disease can go undiagnosed until the symptoms become more severe. CKD can be incredibly dangerous, as patients with CKD are five to ten times more likely to die of it, rather than progress to the end stages of kidney disease and failure, requiring dialysis or transplantation (Webster, et al., 2017; Levey & Coresh, 2012). If the disease does reach its end stages, it is characterised by uraemia, or urea in the blood, a sign of final kidney failure as they are no

longer able to filter out the waste. The stage of uraemia signals not only the failure of the kidneys, but also major changes in metabolic and endocrine function, triggering responses in the gastrointestinal, neuromuscular, and cardiovascular systems (Cotran, et al., 1999). End stage CKD can also be noted by the development of fibrosis in the kidney as a response to chronic injury, characterised by glomerulosclerosis, tubular atrophy, and interstitial fibrosis (Webster, et al., 2017). Like many of the diseases discussed in this chapter, it is a disease primarily encountered in later life, with the countries reporting the most cases of end stage CKD being those with the highest number of elderly citizens, although age is not necessarily a prerequisite for disease (Webster, et al., 2017; Levey & Coresh, 2012).

Comorbidities Involving Bone

As CKD is known to cause major metabolic disturbances, it is likewise a known comorbidity of kidney disease. Known as renal bone disease, or renal osteodystrophy, it refers to the effects of renal failure on mineral metabolism, namely that renal disease triggers changes to phosphorus, calcium, and vitamin D metabolism, as well as parathyroid hormone, all leading to secondary hyperparathyroidism, a known factor in the development of osteoporosis (Malluche & Faugere, 1990; Williams, 2009; Ott, 2009). This can lead to several different bone disorders, including osteitis fibrosa cyctica (high bone turnover), adynamic bone disease (low bone turnover), or mixed bone disorder. In any case, the result is bone loss and an increased risk of fracture (Williams, 2009; Miller, 2005). To understand the specifics of renal osteodystrophy, previous studies have performed biopsies to measure bone turnover and resorption rates, mineralisation rates, and volume, as well as the standard dual-energy x-ray absorptiometry (DXA) used to diagnose osteoporosis (Ott, 2009; Leonard, 2009). In particular, the volume metric measures both mineralised and unmineralised bone, and is directly related

to porosity, a major consequence of osteoporosis (Ott, 2009). These metabolic abnormalities directly affect the microstructure of the bone, distorting the structure of the trabeculae, and thinning the cortical bone. In a study where full thickness biopsies of dialysis patients were taken, 45% bone loss was reported, largely due to cortical thinning (Leonard, 2009). An added complication is the medications usually prescribed to treat osteoporosis, bisphosphonates, are generally discouraged in patients with kidney function measuring less than 35 mL/min. As CKD has been described as a disease of advanced age, about 25% of patients of around 70 years of age have kidney function less than 25 m/min, excluding them from the standard treatment for osteoporosis, or putting them at risk for greater kidney injury, perpetuating the entire process (Miller, 2005). These multi-pronged factors make renal disease, and CKD in particular, a major contributor to not only pathological changes to bone microstructure, but to the metabolism of the body as a whole, often with catastrophic results.

3. Aims and Objectives

The broad aim of this study is to better understand pathology, especially secondary pathology, in the context of bone microstructure. While previous studies have observed changes to the microstructure in relation to pathological stimuli, there is a need for more specific terminology and definitions with regard to the presence and appearance of pathological bone micromorphology. The motive for this aim is twofold. First, to better understand the connections between diseases in other systems and their effect on bone microstructure, purely to improve anatomical knowledge and understanding. The second is related to the forensic context, as bone microstructure is an essential ingredient in histological age estimation techniques such as those developed by Stout and Paine (1992), and Cho and colleagues (2002). As pathology has the ability to change the microstructures these formulae rely upon, this study endeavours to quantify which features are most affected, and by how much.

To do this, analysis was split into two sections: qualitative and quantitative.

Qualitative analysis focused on observations of pathological and healthy thin sections from comparable populations. The focus was to:

- Define and quantify the pathological micromorphology. How does it differ from healthy micromorphology? How do the different categories of pathological micromorphology differ from each other?
- Analyse the results of these observations and compare with pathological data. Are any pathological micromorphology features associated with any particular disease class?

Which category of pathological micromorphology appears most often? Could this information be used for diagnostic purposes in an unknown sample?

Quantitative analysis focused on metrics taken from pathological and healthy thin sections from comparable populations. These metrics were again split into two sections: the standard histological metrics used in most age estimation formulae using the entire cross-section of the rib, and osteon specific measurements that were taken from four sampled areas of the rib cross-section.

For the standard histological analysis, the focus was to:

- Compare cortical area and osteon population density (OPD) variables with age, as a complete data set (to mimic the population used to create the original Stout and Paine (1992) method), and separately as pathological and healthy data.
- Did the relationships between cortical area and age, and OPD and age, seen in previous research, improve when the pathological samples were removed? By how much?

Finally, for the osteon specific analysis, the focus was to:

- Analyse the ten osteon specific metrics chosen for the study. Are any of them meaningful?
- How do the osteon specific metrics compare between the pathological and healthy samples? Do they support the observations made in the qualitative section?
- Are there any correlations or significant relationships between any of the metrics and age that might be useful for future age estimation formulae? Is there a difference in

the significance of these relationships between the pathological and healthy data sets? Could these results be used for diagnostic purposes on an unknown sample?

By carrying out the above objectives, it is hoped that the aims of this study pertaining to the better understanding of pathological bone microstructure and its effects on current histological age estimation techniques will be realised.

4. Materials and Methodology

4.1 Materials

4.1.1 Sample Collection

The materials for this study were selected from four separate sources from geographically similar regions, including Greece, Cyprus, and Albania. All samples were either selected and sent to the University by the forensic departments after being given the criteria of the study or were taken from the sampling of a simultaneous population study being done in the same lab that was excluding pathological samples. The healthy control samples were also collected from this same simultaneous study and work on said samples was done collaboratively. Depending on the origin of the sample, the condition upon arrival varied. While some arrived as clean dry bone, others arrived fresh, and maceration was required. In either case, once processed and prepared as slides, both types of bone were useable for histology.

4.1.1.1 The Cretan Collection

The first source is from the collection at the Department of Forensic Sciences at the University of Crete-Medical School. The samples from this collection come from the cemeteries of St Konstantinos and Pateles, both located in Heraklion, Crete. These individuals were born between 1867 and 1956 and died between 1968 and 1998. In the event that a living relative could not pay a rental fee for the individual's grave, the body would be removed and placed in a designated area by the city. Permission to use samples from these individuals for this study comes from the local district attorney. Background information, including age at death and cause of death were obtained from the Heraklion City Hall census archives, and sex was determined by the names recorded on the graves (Kranioti, et al., 2008). Both pathological

and healthy control samples were selected from this collection. Samples arrived as clean, dry bone and were immediately embedded without need for further cleaning.

4.1.1.2 Forensic Autopsy Samples

Additional pathological samples came from the Department of Forensic Sciences of the University of Crete, Greece and the division of Forensic Pathology of the Ministry of Justice in Tirana, Albania. The samples from Department of Forensic Sciences of the University of Crete were collected from autopsy with the consent of the families. The individuals included in this study died between October 2014 and February 2015 and ranged in age from 22 to 69. Any information on medical history, pathologies, and cause of death that were known to the forensic pathologists were included with the samples. Some samples also came with a corresponding liver sample, thin sectioned and prepared by the Forensic Department as part of the autopsy. Both pathological and healthy control samples were selected from this collection. Samples arrived both as chemically cleaned (boiled in a mild chemical solution to remove any remaining flesh) and as fresh samples requiring cleaning.

The samples from the division of Forensic Pathology of the Ministry of Justice in Tirana were also collected from autopsy, with the permission of the Proctor Fiscal, adhering to the ethical requirements of Albania. This study included individuals from this source that died between October 2014 and October 2015 and ranged in age from 19 to 59. Like the samples from the Forensic Department in Crete, the Albanian samples also included any medical histories, pathologies, and cause of death known to the forensic pathologists. Also like the forensic samples from Crete, some of the Albanian samples came with corresponding liver samples, again thin sectioned and prepared by the division of Forensic Pathology as part of the autopsy.

Due to time constraints and lab accessibility, only pathological samples were selected from this collection. These samples, like some of the samples from Crete, arrived fresh and required cleaning.

4.1.1.3 The Cypriot Collection

Samples were also selected from a Cypriot collection similar to the Cretan Collection. The Cyprus collection consists of about 200 individuals from the municipal ossuary of the St. Nicholas Cemetery in Limasol, Cyprus. According to Cypriot custom, each individual would have been buried for five years, exhumed, and then moved to the municipal ossuary. Permission to use the collection was given by the priest in charge of the municipal cemetery. The collection consists of individuals ranging in age from infants to 100 years old, who died between 1976 and 2003. Like the Cretan collection, sex was determined by name of the individual. (Kranioti, et al., 2017) As these samples were originally selected for a simultaneous population study of age estimation techniques, any obvious pathological conditions had been excluded through macro examination before being brought to the University of Edinburgh. (Garcia-Donas, 2017) As there were no confirmed pathological cases in this population available, samples were selected solely as healthy controls. Samples arrived as clean dry bone, ready to be embedded.

4.1.2 Sample Distribution

Table 4.1: Sample Age Distribution

Sample Category	19-30	30-40	40-50	50-60	60+
Controls	2	3	6	7	22
Pathological	2	7	6	13	12

This study included both males and females. Samples were limited to adult individuals. Through the Cretan collection and the autopsy samples collected from the Cretan Forensic Department, an attempt was made to control for ethnicity. Such control is important, as different populations have been shown to need different age estimation formulae. As different groups differ in their morphology, inconsistent populations could inadvertently insert additional bias into the study. (Stout & Paine, 1992; Stout & Paine, 1994; Cho & al., 2002). An effort was made to collect left rib midshafts of ribs 4, 5, or 6, however if a left was not available, a right midshaft was accepted. This was done for consistency, as most previous histological age estimation methods involving the rib have used these ribs. This is likely due to the original method by Stout and Paine (1992) using these particular ribs setting the standard, leading subsequent validation studies to also use left ribs 4-6.

4.1.2.1 Pathological Samples

For the purposes of this study, pathological samples were selected from medical histories and autopsy notes, as well as toxicology reports and histological samples of the liver, where available. Samples were collected from individuals suffering from chronic disease, including chronic alcoholism and other hepatic diseases, cancer (including brain and lung cancer), cardiovascular disease, pulmonary disease, renal disease, and/or diabetes, to guarantee an

effect on the osteological microstructure. In total, 40 pathological samples were used. Of those 40 samples, 20% (8 out of 40) had multiple pathologies falling into more than one category. These samples were separated out into their own disease class, as it is impossible to discern which condition affected the microstructure.

Table 4.2: Table showing distribution of pathologies across the entire sample

Cancer	Diabetes	Pulmonary	Hepatic	Cardiovascular	Renal	Multi
2	1	2	16	10	1	8

In addition to rib samples, corresponding liver histology samples were taken for the ribs collected from autopsies, where available. These slides were prepared as a part of the routine histological examination for each autopsy case and were sent along with the rib sections. The existence of microscopic evidence of pathology further confirms the suitability of the samples. (For example, one may have a history of alcoholism but if the liver is not seriously affected bone metabolism may still be normal.) Liver samples were only used to confirm cases of liver disease, and those samples with histories of other pathological conditions were confirmed by medical history and the findings of the forensic pathologist, when applicable.

4.1.2.2 Control Samples

For the purposes of this study, healthy control samples were required to be compared to the pathological samples. Health was confirmed using medical history and autopsy notes, specifically cause of death. If any signs of pathology were noticed upon histological examination, those healthy controls were excluded. Control samples were matched according to age and sex for better comparison. In total, 40 healthy control samples were used. The samples were selected from the Cretan collection and the Cyprus collection as these were

collected for another project conducted simultaneously in the lab and they were available at the time of this project. The healthy Albanian samples, as they arrived later than the other collections, and were then subjected to a six-month quarantine, could not be included. Although this might have a small effect on the outcomes, the populations are similar enough to warrant inclusion in the study.

4.2 Methodology

The methodology used for this study can be divided into four practical areas; slide preparation, slide reading, analysis, and statistics. The preparation, reading, and some of the slide analysis were based on previous methodologies created for observing bone histology, and developed within the collaborative environment of the University of Edinburgh's bone histology lab. The doctoral candidates and MSc students involved in the laboratory prepared their sample slides themselves after having been trained by Dr Elena Kranioti and Dr Robert Paine, and they worked together to develop new protocols and to improve on old ones. Details about the development of the slide preparation protocol can be found in Garcia-Donas et al (2017). The methods used to prepare and read the slides created for this study can also be seen in Garcia-Donas (2017) as both studies were done simultaneously in the same laboratory space. While certain aspects of the analysis were completed using previously defined protocols (Stout & Paine, 1992; Cho & al., 2002), others such as those used for analysing the micrometrics were developed independently for this study. The statistical analysis was based upon the aims and objectives of this study and informed by the data collected.

4.2.1 Slide Preparation

While certain aspects of Paine's method (2007) were used during the process of this study, amendments were made to account for availability of materials, equipment, and time. In addition, a new method of adhering samples was used, eliminating the need for removal of the sample from a grinding slide to later adhere to a reading slide (Garcia-Donas & al., 2017). These changes were made with the intention to save laboratory time and supplies while rendering a similarly clear result. Preparations made from 2014-2016 were done in the Histology Lab, located in the Anatomy department of the University of Edinburgh, and samples prepared in 2017 were prepared in the histology department of Western General Hospital in Edinburgh. Both laboratories were set up with the same equipment and supplies. Throughout the slide preparation process, care was taken to follow the health and safety protocols established by the Health and Safety Department of the University of Edinburgh and to follow the guidelines set out in the School of History, Classics and Archaeology's Laboratory User Handbook. All methods of preparation were done with the aim of preserving the osseous tissue. By cleaning and embedding the samples prior to slide preparation, the samples were able to be preserved and prevented any artefacts from being introduced to the samples.

4.2.1.1: Sample Selection

Samples were chosen using several sets of criteria. All samples were left ribs, preferably the 4^{th}, 5^{th}, or 6^{th} ribs. Medical history was also consulted, for the control samples to confirm general good health, or in the case of the pathological samples, to confirm chronic illness. In the case of the pathological samples of the alcoholics and those with hepatic disease, toxicology and histological liver samples were also consulted to confirm hepatic disease

and/or hepatic metabolic disturbance where available. The information on health and medical history was derived from the autopsy reports from Albania and Crete (for the autopsy samples) and from the Census office for the Cretan collection (Kranioti, et al., 2008). While this information had been passed on by the relevant forensic departments, exhaustive records were not available, therefore the records sent with the samples were assumed to be accurate. Samples selected as healthy controls were determined from autopsy reports (Crete), from the Census office (Cretan Collection), and from macro and histological examination (Cypriot Collection) (Garcia-Donas, 2017).

4.2.1.2 Cleaning

In the event that samples needed to be de-fleshed in order to be processed, two different processes were used. Earlier samples were cleaned using a boiling method based on previous methods, and then modified (R. Paine, *pers. comm.)* (Fenton, et al., 2003). Maceration of the bones using this method was done at the Edinburgh City Mortuary. Before boiling, as much of the flesh as possible was removed manually with a scalpel. The ribs were then individually wrapped in medical gauze, the ends secured with string. The wrapped ribs were then placed in boiling water for 30-40 minutes. After the allotted time, they were removed from the boiling water, unwrapped, and any remaining flesh could be easily removed with a scalpel. Boiling was the preferred method for preparing samples, as it has the added effect of destroying bacteria and other possible artefacts in the bone, ensuring clean slides.

For part of the samples, however, boiling was not an option, as the samples were also to be subjected to biomechanical analysis for another project, a process that requires the collagen of the bone to remain intact. Therefore, these samples were minimally defleshed, with only

a scalpel to remove excess soft tissue, so as to preserve the biomechanical properties of the bone. Once the bone had been cleaned, it was then cut in half with a Dremel saw. Half of the samples were used in this study for histological examination, and half were used in the biomechanical study. Cleaning of these samples was done in the laboratory at Western General Hospital. In the case of both cleaning methods, any remaining biological material that was removed from the bones was disposed of in accordance with the health and safety procedures of the University of Edinburgh (COSHH). Unlike boiling, this method of defleshing leaves a certain amount of residue. While not as effective as boiling, the samples were clean enough and by embedding in resin during the next stage of the process, any remaining bacteria were destroyed.

4.2.1.3 Embedding

First, the ribs were cut down to about 3.5-4 cm in length using a Dremel Saw (see figure 4.1), allowing the pieces of rib to fit more easily within Buehler moulds that were made to fit the Buehler MetaServ^{TM} 250 Grinder-Polisher.

Figure 4.1: Dremel Saw

Once the ribs had been cut down, the moulds were prepared. First, Buehler release agent was used to coat the inside of the moulds to make removal of the resin easier upon setting. This release agent was left to sit in the moulds for 5 minutes before adding epoxy resin, made by mixing Buehler Epothin resin and hardener. Small pieces of plain printer paper were placed in the bottom of the moulds with sample ID numbers that would then become embedded in the resin with the samples. The epoxy resin used was a Buehler Epothin resin and hardener where a ratio resin to hardener of 5:1.95 grams was used to prepare the resin. A new version of the Buehler Epothin resin and hardener were obtained partway through the processing, and this resin and hardener used a ratio of 2:1 resin to hardener. Once mixed, the epoxy was then put inside a vacuum impregnator to eliminate excess air bubbles. A thin layer of the epoxy resin was poured into the bottom of the moulds before inserting the samples. Once the samples were placed in the moulds, more epoxy resin was poured until the samples were covered. The samples were then left to cure for 24-48 hours inside an extractor fume hood.

4.1.2.4 Markings and Assignment of Identification Numbers

Each sample came to the department with an identification number. In the case of the Albanian autopsy samples, which did not come with numbers, a sample number was assigned to them. To ensure that medical records stayed connected to the correct samples, these numbers were kept and added to a database. From this point on, all analyses referred to the assigned numbers. By using numbers rather than patient names, the individuals in the study were allowed to remain anonymous, as dictated by the Human Tissue (Scotland) Act 2006, and the guidelines of the Human Tissue Authority (HTA). In the event that more than one slide was made with any one sample, the slides would be identified first by their sample number, and then a letter (e.g. slide CC196a). Sample numbers from the Cretan collection began with 'CC' and then their individual sample number. Sample numbers from the Cretan forensic department were marked 'FC', and samples numbers from the Cyprus collection were marked 'CY'. The Albanian samples arrived later and were assigned numbers based on the group they arrived with. Group A was marked as 'A' and then then their individual number, while Group B was marked as 'B'. While an overall unique numbering system would have been preferable, as the samples were shared between several projects, some predating this research, the above numbering system was implemented to ensure consistency across the laboratory.

Each rib from the Cretan collection was marked with a coloured marker to indicate orientation. Blue was used to indicate the cranial surface, Green was used to indicate the interior surface, and pink or red was used to indicate the exterior surface (See figure 4.2). This was done to make the cardinal surfaces of the cross-sections more easily identified, for example, the cranial edge and the caudal edge (White & Folkens, 2005).

Figure 4.2: Coloured labelling of samples (Garcia-Donas, 2017)

In the case of the samples that were not boiled, and therefore not completely dry, markings were not applied to the bones, for reasons of hygiene. As marking was not possible, the cardinal surfaces of these sections were identified by their morphology.

4.1.2.5 Preparing Samples for Mounting

After the allotted time, the samples were checked to see if the epoxy resin had cured. Once the samples were determined to have finished curing, they were removed from the moulds. A Buehler MetaServ™ 250 Grinder-Polisher (see figure 4.3) with coarse grinding paper was then used to remove the sloped edges of the resin from the tops of the samples.

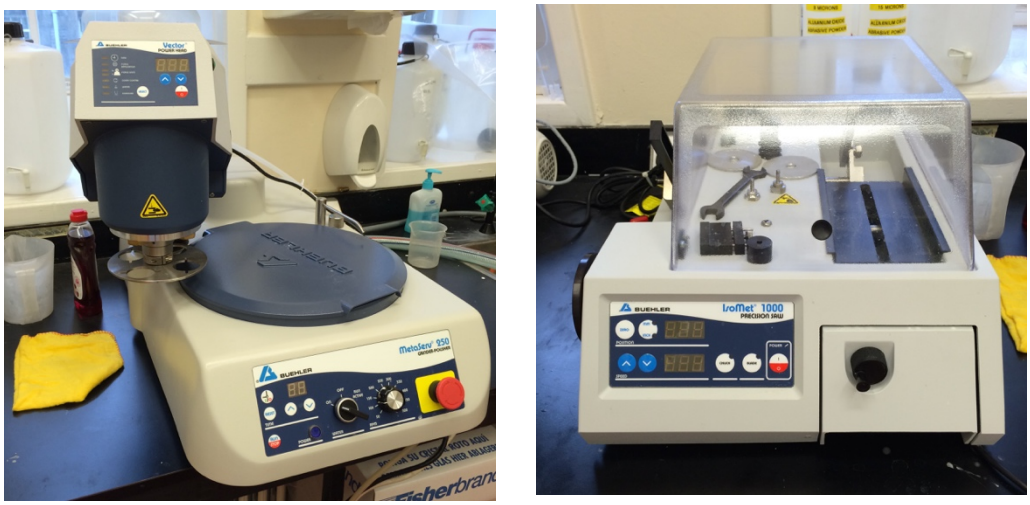

Figure 4.3: Left - Buehler MetaServ™ 250 Grinder-Polisher; Right - Buehler IsoMet™ 1000 precision saw

After the samples were levelled, a Buehler IsoMet™ 1000 precision saw (see figure 4.3) fitted with an Isocut wafering blade was used to trim excess resin from the samples, if needed. The samples were then cut in two. One half was put aside for possible use later, while the other half was prepared for mounting.

The Buehler MetaServ™ 250 Grinder-Polisher was fitted with fine grinding paper to remove any evidence of saw marks that might be visible under the microscope, as well as to even the surface for mounting. Glass slides were then prepared by using a 15 microns abrasive aluminium oxide powder and water on a glass plate. This created a frosted glass surface, which would allow the sample to adhere to the slide more easily and securely.

4.1.2.6 Mounting Slides

Once the slides were adequately frosted, the samples were adhered to the slides, once again using the same Buehler Epothin epoxy resin that was used for the embedding, with a ratio of resin to hardener 5:1.95, or in the case of the replacement resin, 2:1. A small amount of resin was placed on the slide and the samples were placed on top of the resin. The sample was moved around slightly on the slide to ensure total adherence as well as to get rid of any air bubbles that might be present. After this, the samples were placed on a hot plate at 60°C until warmed through. The samples were then placed in a weighted bonding jig inside a fume hood to cure overnight (Garcia-Donas & al., 2017; Garcia-Donas, 2017).

4.1.2.7 Cutting

Once the samples had cured, the excess was cut from the slide. A slide holder chuck was used to hold the slide in place on the arm of the IsoMet™ 1000 precision saw. The arm was then

moved towards the blade until the slide was flush with the blade surface. The measurement of the saw was then zeroed out, and the arm was moved exactly 1mm back from the blade, ensuring a 1mm thickness for the sample. Each sample was then cut on this setting. As the machine had been set to 1mm sample thickness, it was not necessary for the saw to be adjusted for subsequent samples.

4.1.2.8 Grinding

After the samples had been cut, the grinder was set up with first p800 grinding paper (coarser) and then p2500 grinding paper (finer). Slides were ground down using a petrographic slide holder, or a slide holding chuck, to approximately 75µm thickness, or until the osteons were clearly visible under a transmitted light microscope. Once the grinding was finished, the samples were polished with a Tex Met C polishing cloth. The slides were then ready for reading under both transmitted light and polarised light microscopes.

4.2.2 Slide Reading

4.2.2.1 Microscopes and Photographic Equipment

The earlier samples were read using a Leica DM750P microscope with Leica MC170 HD camera attachment, as it is capable of using both transmitted light and polarised light. Additionally, photographs were taken of each sample using the accompanying LAS Leica computer programme. After photographs were taken of each section of the sample, the photographs were then stitched together within the programme to allow a full view of the cross-section. After the move to the histology department at Western General Hospital, the

slides were read on an Olympus BX51 double eye-piece microscope, which allows for both transmitted and polarised light. The double eye-piece on the microscope also contributed to collaboration and inter-observer observations. The later slides were also photographed, using a slide scanner, eliminating the need to stitch multiple images together to view a complete cross-section, as well as the Leica set-up for close-up field of view photographs that would be used later for samples metrics.

4.2.3 Analysis

For the purposes of this study, the pathological samples were assessed both quantitatively and qualitatively in comparison with the healthy control samples.

Qualitative analysis allows the observer to identify specific features that indicate the presence of pathology. While these are subjective and rely on the observer's experience, they are nevertheless important. By observing signs of pathology in bone, it is then possible to quantify the rate of occurrence of these features throughout the sample, as well as helping to identify pathological samples for further study and analysis via metrics. The observation of abnormalities in the bony structure -that are not attributed to remodelling due to aging- can be considered as signs of pathology. These abnormalities can be changes in the shape and structure of the microscopic features of bone such as the Haversian systems and canals. Qualitative analysis is also essential for the differentiation between potential artefacts and actual pathology. For pathology research in particular, it is important to recognise what is pathological bone micro-formations, and what could be the result of artefacts in the bone. By

analysing each slide qualitatively, any abnormal formations not consistent with pathology could be excluded.

Quantitative analysis, on the other hand, allows for more precise analysis, by quantifying size differences that can allow for the generation of data that is easily compared and statistically analysed. While qualitative analysis requires more experience from the observer, the methods described for collecting and analysing quantitative data could be undertaken by anyone familiar with the basics of bone histology.

4.2.3.1 Qualitative Analysis

Qualitative aspects of the samples were assessed visually for microstructural differences between the pathological samples and the healthy controls. In terms of qualitative analysis, any features that occurred outside the range of normal for healthy samples were observed and noted. These differences usually fell into one of three categories.

1. Abnormally shaped osteons and/or canals: Complete Haversian systems that have an irregular shape outside the range of normal. This includes osteons and canals that are irregularly sized. What is not included are those shapes that are seen within the realm of normal, healthy Haversian systems. These would include drifting osteons, branching osteons,

and a balanced amount of Howship's lacunae. For an example of a category 1 osteon and a corresponding healthy osteon, see Figure 4.4.

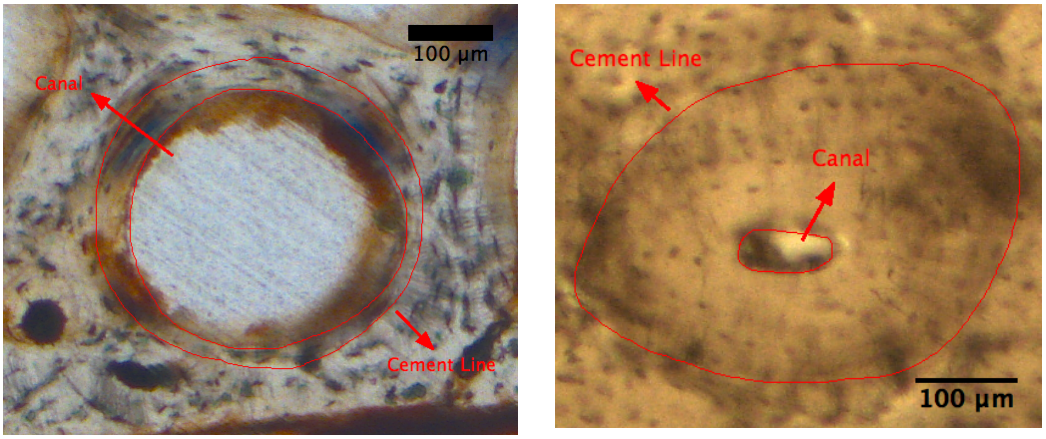

Figure 4.4: Left – Close-up of an abnormal osteon from Sample CC169; Right – Close-up of a normal healthy osteon from Sample CC100 (courtesy of Julieta Garcia-Donas)

2. Deranged Haversian systems: Haversian systems that fail to form completely or normally, resulting in large, irregularly sized canals, often merging with other nearby deranged systems (See figure 4.5). Often these deranged canals have the appearance of irregular, overactive Howship's lacunae. These pathological bone formations can be discerned from diagenesis by observing the cement lines and the direction of the lamellar bone. If the bone flows around the canal and there are cement lines present, that is how the bone grew. There may also be discernible destructive activity in the form of the rippled edges of a Howship's lacunae. This can also be called the 'Swiss Cheese Effect', as the canals in the cortical bone of the cross-section appear like the holes in Swiss cheese, or a sponge.

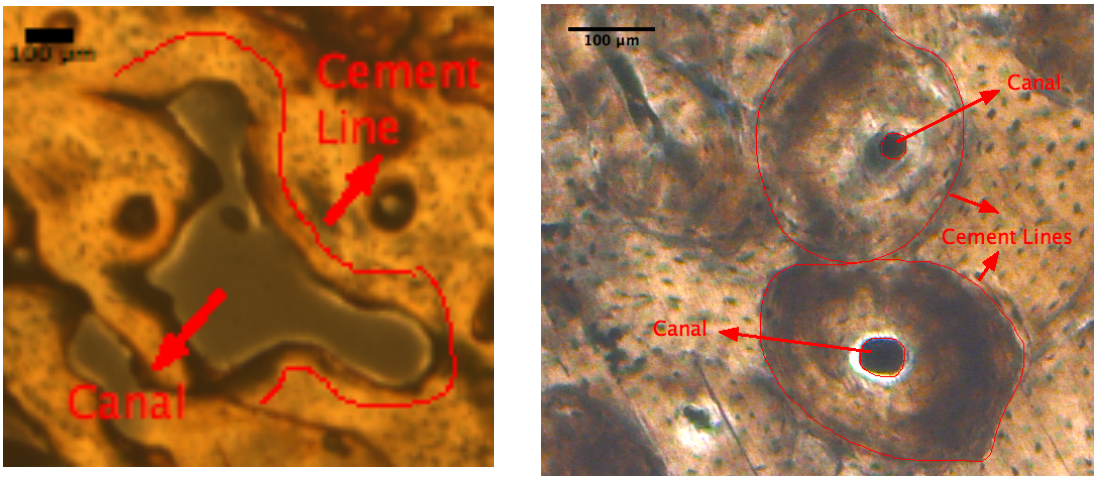

Figure 4.5: Left – Example of deranged Haversian systems from Sample CC203 (Courtesy of Julieta Garcia-Donas); Right – Example of normal, healthy Haversian systems from Sample FC6

3. Bone can also appear as rapid deposits, without forming a Haversian system at all. This has been observed before in a case of extra-spinal hyperostosis related to DISH. (Lill, 2013) In that case, the rapid linear deposits of bone were clearly visible at the site of the lesion on the periosteum (see figures 4.6 and 4.7). It is possible for this pathological formation to occur in other areas, related to other pathologies.

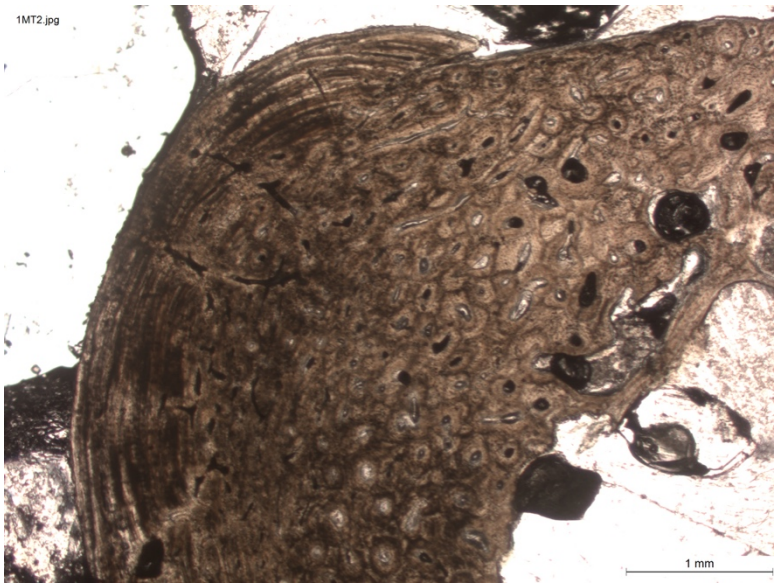

Figure 4.6: A hyperostotic lesion showing linear rapid bone deposits on a cross-section of a metatarsal, sample 1MT2 (100x magnification) (Lill, 2013).

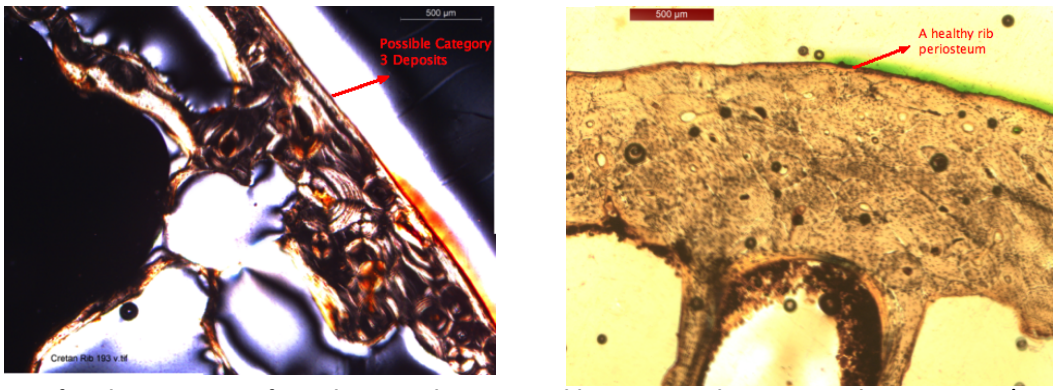

Figure 4.7: Left – Close-up image of sample CC193 showing possible category 3 deposits near the periosteum (100x magnification), Right – Close-up image of sample CC77 showing no evidence of rapid bone deposits and a healthy periosteum (100x magnification) (Garcia-Donas, 2017).

These three categories of pathological bone formation were then scored for each sample. Scoring involved being marked present or not present for each slide. Presence was determined differently for each category. In the case of category 1 features, as the presence of abnormal canals occasionally appears in healthy bone, it was determined that greater than 50% of the cross-section needed to show abnormal canals to be marked present. For category 2 features, as the deranged Haversian systems (Swiss Cheese Effect) usually only appear in pathological bone, only 20% needed to show the deranged systems to be marked present. As with category 2 features, category 3 features are rarer and less likely to appear on healthy bone, so they were also scored as present if 20% of the periosteum showed rapid linear deposits. This data could then be analysed for frequency chi^2 and statistical significance, as well as any patterns that might emerge involving pathological groups or specific pathologies.

4.2.3.2 Quantitative and Metric Analysis

The next section involved quantitative and metric analysis. This analysis was then divided into two sections, one involving standard histological analysis, the other involving osteon specific metrics.

First were the standard histological analyses, being the standard analyses used by most bone histologists. For this, the samples were measured, and important elements were quantified. For a list of each important element and their definitions, please see Table 4.3.

Table 4.3: Table of standard histological elements and their definitions; as defined by Stout and Crowder (Stout & Crowder, 2012)

Histological Element	Definition
Cortical Area	The amount of cortical bone in a cross-section, expressed in mm^2.
Complete Osteon	A secondary osteon with a canal that is at least 90% complete.
Fragmentary Osteon	A secondary osteon with a canal that is less than 90% complete.
Total Osteons	The sum of the number of complete and fragmentary osteons
Osteon Population Density (OPD)	A variable that is equal to the sum of the number of complete and fragmentary osteons, divided by the cortical area.

The number of complete osteons and fragmentary osteons were noted and used later to calculate osteon population density (OPD). These quantifications were done using a microscope, while a tally was kept of the complete and fragmentary osteons. Then the cortical area was measured, this time from a stitched photograph of the rib cross-section. This too was later used to calculate OPD.

The second section involved the osteon specific metrics. Measurements were taken from complete secondary osteons, as defined by Stout and Crowder (Stout & Crowder, 2012). (See table 4.4 for osteon specific metrics and their definitions)

Table 4.4: Table of the osteon specific metrics.

Metric	Definition
Osteon Maximum Diameter (OMaxL)	The maximum diameter of a complete, secondary osteon. Expressed in μm.
Osteon Minimum Diameter (OMinL)	The minimum diameter of a complete, secondary osteon. Expressed in μm.
Osteon Circumference (OPeri)	The circumference of a complete, secondary osteon. Expressed in μm.
Osteon Total Area (OTArea)	The total area of a complete, secondary osteon, including the canal. Expressed in μm^2.
Canal Area (CArea)	The area of the canal of a complete, secondary osteon. Expressed in μm^2.
Osteon Area (OArea)	The area of a complete, secondary osteon, minus the canal area. Expressed in μm^2.
Osteon Circularity (OCirc)	A measurement of complete, secondary osteon quantifying how close the osteon shape is to a perfect circle. Expressed as a number between 1 and 0, with 1 being perfectly circular.
Canal Maximum Diameter (CMaxL)	The maximum diameter of the canal of a complete, secondary osteon. Expressed in μm.
Canal Minimum Diameter (CMinL)	The minimum diameter of the canal of a complete, secondary osteon. Expressed in μm.
Canal Circularity (CCirc)	A measurement of the canal of a complete, secondary osteon quantifying how close the canal shape is to a perfect circle. Expressed as a number between 1 and 0, with 1 being perfectly circular.

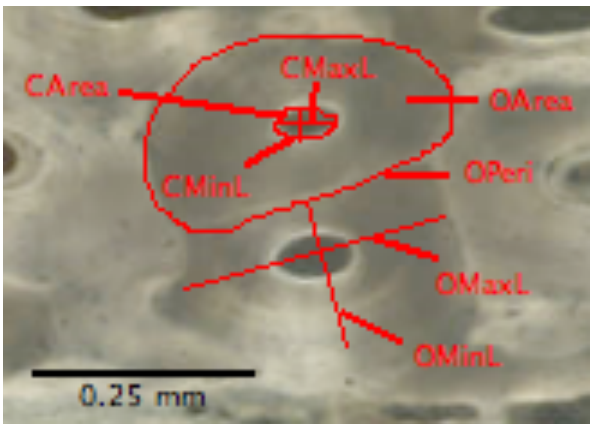

Figure 4.8: Illustration of measurements taken for micrometrics. Included are osteon maximum and minimum diameter, canal maximum and minimum diameter, osteon area, canal area, and osteon perimeter. Not pictured are osteon total area, osteon circularity, and canal circularity.

Measurements were taken using a sampling method, using four field of view photographs from each slide. Each field of view photograph was taken using 100x magnification. To create consistency in the sampling method, each of the four photographs was taken to represent each of the four cardinal edges of the rib cross-section, one each for the cranial surface, caudal surface, exterior surface, and interior surface. Metrics were then taken using the software ImageJ. The software was run using a 2009 MacBook Pro, and an iPad Air 2. The iPad was connected to the MacBook using the Astropad software, allowing the iPad to be used as a drawing tablet. As it is currently not possible to automate the process of measuring osteons, each osteon was measured individually. A stylus was used to draw around the cortical area, and around the osteons and canals, enabling more accurate measurements to be taken more quickly. Measurements were taken by following the cement line around the osteon, or around the border of the canal walls. All measurements could be recorded by measuring the border of the osteon and the canal. By drawing around the osteon, total osteon area, circumference (perimeter in ImageJ), max and min diameter (Feret and minFeret in ImageJ), and circularity could be measured. By drawing around the canal, area, max and min diameter, and circularity could be measured. True osteon area could then be calculated by subtracting

the canal area from the total osteon area. These measurements were taken from every complete osteon in each photograph.

Initially, metrics had been taken from every osteon in the complete cross-section of the sample, however this was determined to be impractical and prohibitively time-consuming. Five samples were compared, using two sets of data from each slide. The first set including all metrics from the complete cross-section, the second set included only those metrics present within four fields of view from the four edges of the rib. These data sets were then analysed using an independent student t-test, and it was determined that there was no statistically significant difference between the two sets of data. These results then allowed for the sampling method of the metrics to continue.

Once all of this data had been collected, an age at death was estimated using OPD and cortical area, for each individual, as defined in Stout and Paine's histological age estimation method, and then compared to the actual age at death (Stout & Paine, 1992).

4.2.3 Statistics

Once the raw data had been collected from the histological samples, statistical analysis was run to determine the significance of the various elements that had been quantified and measured. This analysis was then split into two sections; the analysis run on the standard quantitative data, including numbers of complete and fragmented secondary osteons, cortical area and OPD, and the more in-depth, osteon specific data (osteon metrics). Statistical models were then applied to these separate sets of data. In terms of analysis, both

qualitative and quantitative, of the samples it was important to account for both inter and intra-observer error. As the samples used for this study included pathological specimens that are often excluded or ignored by most research in histology, it was important to make observations that were repeatable and easily recognisable. All statistical analysis was done using the RStudio software package.

4.2.3.1 Standard Histology Statistics

For the standard bone histology data, statistics followed several lines of inquiry. As the age estimation formulae already in existence did not work for this population, age estimation was not prioritised in the statistical analysis. (Stout & Paine, 1992; Cho & al., 2002).

First, comparative statistics were run. The most important relationship to compare was the relationship between the various histological elements and true age at death (hereafter referred to as age). These comparisons would be run with the complete sample, to simulate previous studies that did not separate out pathological samples, and then the data would be split into the pathological and control groups with the same comparisons being run on each group individually.

4.2.3.1.1 Inter-observer Error Analysis

The standard histological data was also analysed for inter-observer error. One set of data was analysed by both the primary observer, and another observer. These analyses would allow for a measurement of the accuracy of the collected data, as well as the consistency. This follows previous research comparing age estimation methods used on the same population

incorporated in this study (Garcia-Donas, 2015). Statistical analyses of inter-observer error were calculated using RStudio.

The inter-observer error for the standard histology was done as a collaborative effort and the results were used in two studies. Due to the cooperative nature of the lab and the work, Julieta Garcia-Donas, another researcher in the department undertaking a population study on age estimation at the same time as this study, and the author of this study collaborated on the inter-observer error for the standard histology methods as a way to save time and resources (Garcia-Donas, 2017). This involved the analysis of 22 slides by both parties using standard histological methods to quantify complete and fragmentary secondary osteons. By cooperating on one inter-observer study, it was possible to use the results for both projects. The two sets of observations were then compared using a paired t-test to test statistical significance. In addition to the paired t-tests used to compare the quantifications, Garcia-Donas also carried out technical error of measurement analysis, yielding a technical error of measurement (TEM), a relative technical error of measurement (rTEM), and an R coefficient (R) to measure the precision of the observations (Garcia-Donas, 2017; Ulijaszek & Kerr, 1999).

4.2.3.1.2 Correlations

For correlation statistics, a Spearman's R test was performed on the data using the RStudio package. Spearman's R was chosen as the method for correlation calculations over the more standard Pearson's r due to the shape of the data distribution. While the complete data sample and the healthy group of data both had relatively normal distributions, the pathological group had a nonparametric distribution. As Pearson's assumes a parametric distribution, Spearman's rank correlation was chosen. As stated above, these correlations

were calculated for each variable three times, once for the complete data set, once for the pathological group, and once for the healthy control group. Once the correlations had been calculated for each group, this data was then converted into *p*-values, and charted in a heat map, illustrating significant positive and negative correlations between sets of data. The data for the correlation calculations are also available as matrices, two for each group, one with the Spearman's r calculations, and one with the corresponding *p*-value conversions.

4.2.3.1.3 Regression analysis

Next, regression analysis was performed on the data, once again using RStudio. From the correlation results and previous studies (Stout & Paine, 1992; Cho & al., 2002), it was determined that cortical area and OPD have the strongest relationships. Based on these relationships, linear models were created, comparing age as the independent variable, with cortical Area and OPD as the dependent variables. This was done to calculate the strength of the variables in their ability to predict age. Once again, the models were done in three groups, one for the complete data set to simulate past research, and one each for the pathological and healthy control groups. First, cortical area was compared with age, and then osteon population density (OPD) was also compared with age. The results for each linear model returned several values, including five residuals, four coefficients, residual standard error, multiple and adjusted R-squared, the F-statistic, and a *p*-value.

4.2.3.1.4 Standard Errors

After the regression analysis, standard errors were calculated for each of the linear regression models, using RStudio. The standard error used was the standard error of the estimate (SEE) that measures the accuracy of predictions made with the regression line. SEE was calculated

for the regression models comparing cortical area and age, and OPD and age, giving an indication of the accuracy of the standard histology regression models.

4.2.3.1.5 Bootstrapping

Finally bootstrapping was applied to the data as a resampling method, to evaluate the accuracy of sample estimates. This was done using RStudio. For the standard histology statistics, an ordinary nonparametric bootstrap was used to test the R-squared statistic from the regression models comparing age and cortical area and age and OPD. The bootstrap was set with 1000 replications. This yielded bootstrap statistics of original, bias, and standard error, as well as four confidence intervals; normal, basic, percentile, and bias-corrected and accelerated (BCa). Once these were calculated, the results were plotted into histograms.

4.2.3.2 Osteon Specific Metrics

After the standard histological data had been analysed according to established practices, the new data in the form of the osteon specific metrics needed to be evaluated. 5,270 osteons were measured, with each osteon having ten metrics taken, as described earlier in this chapter. In total, 52,700 measurements were taken. Once compiled, this data needed to be statistically evaluated. First, inter- and intra-observer errors were calculated using samples of the osteon specific metric data set, to evaluate the accuracy and consistency of the measurements taken. Once these assessments had been done, more descriptive statistical analyses were applied. As the variables were new in this context, the significance of each metric variable needed to be assessed. This was done in two ways; the first evaluating the complete data sets of all the samples, both divided into pathological and healthy control

groups and as sex and age matched pairs, the second was evaluating the metric means of all the variables.

4.2.3.2.1. Inter and Inter-observer Error

Inter and intra-observer errors for the osteon specific metrics were evaluated. The primary focus for this evaluation was the accuracy and consistency of the measurements taken for the osteon specific metrics. The repeatability of the new methodology required the measurements between one and two observers to remain consistent. For both the inter- and intra-observer error, the software ImageJ was used to take measurements, and the same photographs taken by the primary observer were available to all observers. To test intra-observer error, the primary observer read and measured five of the slides twice, with the above-mentioned sampling method using the four defined fields of view. To test inter-observer error, measurements taken by the primary observer were compared with a sample of nine slides. These sets of data, for both the inter- and intra-observer error, were compared using t-tests. The Welch's t-test was chosen as it is the appropriate test to use for data sets of unequal variances, and due to the variability in the number of osteons measured per sample, the data sets in question were of unequal variance.

4.2.3.2.1.1 Intra-observer Error

To test inter-observer error, five slides were measured twice by the primary observer. Measurements were taken using the sampling method described earlier in the chapter and involved all ten metric variables. These two sets of measurements were separated by several months, to decrease any chance of bias. Once the two sets of data were complete, they were compared using a Welch's independent two sample t-test as there was unequal variance

between the data sets. Each metric variable was tested for statistically significant difference between the data sets, returning a t value, df value, *p*-value, 95% confidence interval, and sample estimates for each data set.

4.2.3.2.1.2 Inter-observer Error

A student in Greece volunteered to undertake the inter-observer analysis for the osteon specific methods. He was given a detailed description of the methodology and the software used to take the metrics of the microstructural elements, as well as high resolution photographs of nine slides, including both pathological and healthy control samples. As the error comparison took place early in the assessment, the specifics of the methodology later changed to include two more variables (osteon and canal circularity) and the sampling method. As a result, the second observer measured the complete cross-section of the nine slides and evaluated seven of the metric variables including osteon maximum length (OMaxL), osteon minimum length (OMinL), osteon total area (OTArea), canal area (CArea), osteon area (OArea), canal maximum length (CMaxL), and canal minimum length (CMinL). The second observer did not measure osteon circumference. These were then compared to the data collected by the primary observer and analysed for error. As with previous data in this study, a Welch's independent two sample t-test had to be used to evaluate the inter-observer data as there was unequal variance between the two groups of data accumulated by the observers. Each metric variable measured by the second observer was compared with the data from the primary observer, returning a t value, df value, *p*-value, 95% confidence interval, and sample estimates for each observer.

4.2.3.2.2 Independent T-tests

The first set of t-tests involved comparing the complete set of osteon specific metric data from the pathological group with the complete set of data from the healthy control group. A Welch's two sample independent t-test was used to compare the measurements from each metric variable using RStudio to evaluate whether there was a statistically significant difference between the measurements taken in the pathological group versus the control group. Again, a Welch's t-test was used, due to unequal variance in the sample. Each t-test returned a t-value, a df value, a *p*-value with any value less than 0.05 being deemed as significant, a 95% confidence interval, as well as sample estimates for each group.

4.2.3.2.3 Paired Independent T-tests

After the t-tests comparing the complete sets of data between groups, individual pairs of samples were compared and assessed. In total, 40 pairs of samples, with each group containing the data from one pathological and one healthy control sample were assessed. These samples were first matched for age, and then matched for sex, if the data allowed. As the healthy controls had been selected for age match, as well as sex match wherever possible, it was possible to compare all the pathological samples to a relevant healthy control. Due to the need to match for age and sex, several controls were repeated in the comparison, as it was determined that an age and sex match was more important for comparison than having 40 sets of completely distinct pairs. Once again, each pair was evaluated using a Welch's two sample independent t-test. Like the tests comparing the complete sample, the pairs of data were of unequal variance, so an independent, rather than a paired t-test, was necessary. For each pair, a t-test was done to compare each metric variable, resulting in ten t-tests per pair, or 400 tests overall. As above, each test returned a t-value, a df value, a *p*-value, a 95%

confidence interval, and sample estimates for each sample in the pair. These values were then put into a table for each pair to allow for easier reading and comparison.

4.2.3.2.4 Metric Means

Once the complete sets of data had been evaluated, the data was broken down into the more easily managed means. This was done by taking the mean of each variable for each sample. The result of this was that each sample had one mean for each of the ten metric variables. This data could then be put into a table along with other relevant variables such as age, sex and health status. Once the data had been reorganised, it was possible to evaluate the metrics means using correlations and linear regression models. As with the standard histology data, the data was split into pathological and healthy control groups, and each variable was compared with age to evaluate if there was any significant relationship between the variable and age.

4.2.3.2.4.1 Correlations

The pathological group of the metric means data, similar to the standard histological data, did not have a normal distribution, so again a Spearman's rank correlation was chosen over Pearson's to accommodate the distribution. Correlations were run using RStudio, and matrices of Spearman's r and converted *p*-values were created for both the pathological group and the healthy control group. Once these matrices had been created, a heatmap showing the strength of the relationships between the variables and age were created for each group.

4.2.3.2.4.2 Regressions

To compare the metric means of the variables with age, linear regression models were created. Once again, the data for these models were separated into pathological and healthy control groups. Within each group, a linear regression model was created comparing age with each of the ten metric variables, with the metric variable serving as the predictive variable. Each regression model returned five residuals, four coefficients, residual standard error, multiple and adjusted R-squared, an F-statistic, and a *p*-value. The results of each metric variable could then be compared across the pathological and healthy control groups for predicative strength of the model. Once all of the models had been created, a scatterplot showing the sample distribution with lines of regression for the pathological and healthy groups were created for each model, to better illustrate the results of the models.

5. Results

This chapter will recount the results of the research undertaken during the course of this study. Osteology has long relied upon a mix of observational or qualitative methods, as well as quantitative techniques. Likewise, the data generated for this project has been considered using both qualitative and quantitative methods. For the purposes of this study, qualitative refers to observable features, and quantitative refers to the metric and statistical analysis of the cross-sections and Haversian systems.

Qualitative analysis allows the observer to identify specific features that indicate the presence of a pathology. By observing signs of pathology in bone, it is then possible to quantify the rate of occurrence of these features throughout the sample, as well as helping to identify pathological samples for further study and analysis via metrics. The observation of abnormalities in the bony structure, that are not attributed to remodelling due to aging, can be considered as signs of pathology. These abnormalities can be changes in the shape and structure of the microscopic features of bone such as the Haversian systems and canals.

Quantitative analysis, on the other hand, allows for more precise analysis, by measuring size differences that can be easily compared statistically. While qualitative analysis requires more experience from the observer, the methods described for collecting and analysing quantitative data could be undertaken by anyone familiar with the basics of bone histology.

For these reasons, both qualitative and quantitative data needed to be collected and analysed for the current study.

5.1 Qualitative Analysis

Having previously defined the types of features it is possible to see in samples effected by pathology, the features observed in the sample data will now be shown, as well as their distribution throughout the sample. This will include a description of the features observed in the sample, the quantity of features observed in each category, if any samples exhibited characteristics belonging to more than one category, and if there was any significant relationship between the pathology class or age group and the pathological features.

For the purposes of qualitative analysis, this section is only remarking upon observable changes in the cortical bone, and as such, primarily concerns the pathological samples, as all healthy controls were selected to represent healthy bone microstructure. Any controls that exhibited evidence of pathology inconsistent with age were excluded. These assessments are reliant upon the observations of the observer and are not to be confused with the metric analyses of the osteons and canals that are included further in this chapter under quantitative analysis. As changes to the bone microstructure can be quite subtle, these observations rely upon the expertise of the observer. By creating categories of pathological samples and defining criteria for each category, an attempt was made to standardise this observational method and limit its subjectivity.

In addition to the assessment of the pathological samples, the healthy control samples were also observed and assessed based on the same criteria as the pathological group. This was done to confirm the prevalence of the defined pathological features in the pathological group as opposed to the healthy control group. These groups were further split into six age groups

for assessment, as the age of the individual, regardless of health status, could influence the appearance of the cortical bone microstructure (Parfitt, 1984). Specifically, this was done to account for the possibility of age-related osteoporosis occurring in the older members of the healthy control sample. The consequences of these age-related effects are that the difference between the pathological group and the healthy control group becomes less pronounced in the older samples.

5.1.1 Qualitative Features

5.1.1.1 Category 1: Abnormally Shaped Osteons and Canals

Abnormally shaped osteons and canals were the most common features observed in this study. This includes osteons outside the norm of shape, including circularity of the osteon and the canal. An example of these features can be seen in Figure 5.1. These do not appear in the healthy control of similar age.

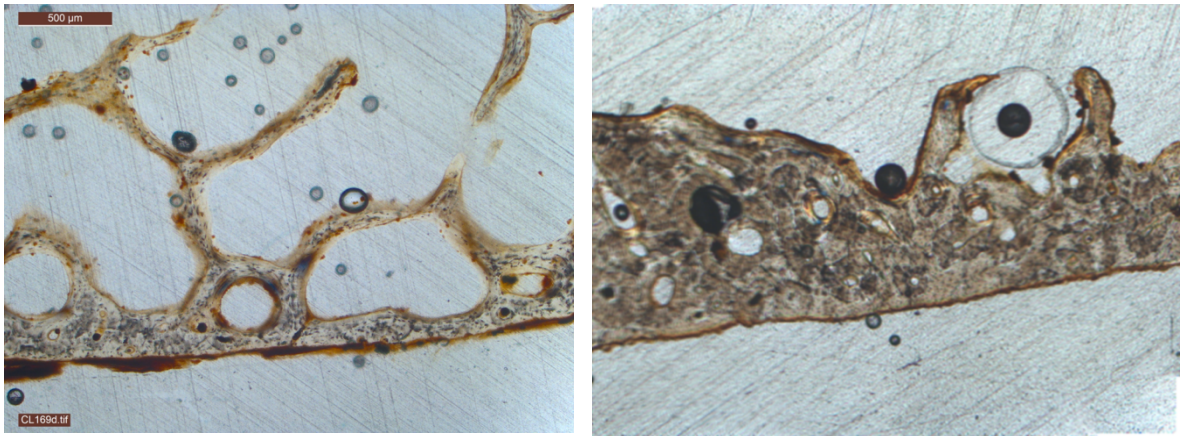

Figure 5.1: Left - Close-up of sample CC169, a 78-year-old male who suffered from coronary disease, diabetes, and COPD showing Category 1 pathological features (exterior surface, 100x magnification) Right - close-up of sample number CY39. The sample comes from a 75-year-old male in the healthy control group. (interior surface, 100x magnification) (courtesy of Julieta Garcia-Donas)

Changes to the size and shape of secondary osteons and canals have been previously connected to pathology before, for example in Paine and Brenton's 2006 study on pellagra (Paine & Brenton, 2006). These changes to the Haversian systems most often accompany a

noticeable thinning of the cortical bone, and may present a connection to osteoporosis or osteopenia (Parfitt, 1984; Ortner, 2003). It is also important to note that these features may appear in either the entire cross-section, or in more concentrated areas of the cross-section. If 50% or more of the cross-section was affected, it was counted as present. If less than 50%, or none, of the cross-section was affected, it was marked as absent. It is possible for cross-sections showing pathological features from category 1 to overlap with features from category 2 or 3, with all three categories occasionally occurring simultaneously in the same sample. Figure 5.1 is a close-up of pathological sample number CC169, and a healthy control. Sample CC169 belongs to a 78-year-old male, who suffered from coronary disease, diabetes, and COPD. These diseases fall into the cardiovascular, diabetes, and pulmonary classes of diseases, as defined for the purposes of this study. This picture illustrates not only the increase in porosity caused by the abnormally large canals, but also the thinning of the cortical bone that often accompanies the features seen in category 1. In addition, the size and shape of the osteons is quite variable, showing the imbalanced activity of the osteoclasts.

The following images are two sets of close-up photographs of samples showing visual evidence of category 1 pathological features. Though not all, many of the pathological samples observed also have a distinctive thinning of the cortical bone, in addition to the defined pathological features. Between the thinning of the cortical bone, and the increased porosity of the cortical bone caused by the category 1 features, these samples should be visually identifiable as pathological. Following each pathological image will be a close-up of an age and sex matched sample from the healthy control group. This will allow for better visualisation of the pathological features, when compared with the healthy control.

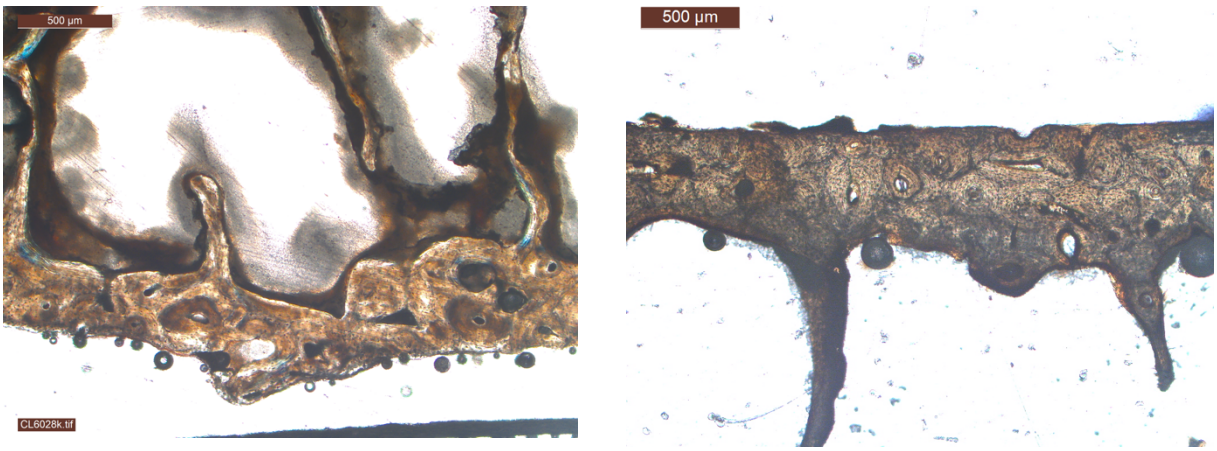

Figure 5.2: Left - Close-up of sample FC2 showing Category 1 pathological Features (interior surface, 100x magnification); Right – Close-up of sample CY198, healthy control (interior surface, 100x magnification)

Figure 5.2 shows a pathological sample belonging to a 68-year-old male with hypertension and CAD, and a healthy control sample from a 65-year-old female. The pathological sample shows a thinning of the cortical bone, as well as the category 1 pathological features, namely irregularly shaped and sized Haversian systems, compared to a normal, healthy sample. These changes are visually observable, and do not require histomorphometrics to be recognised.

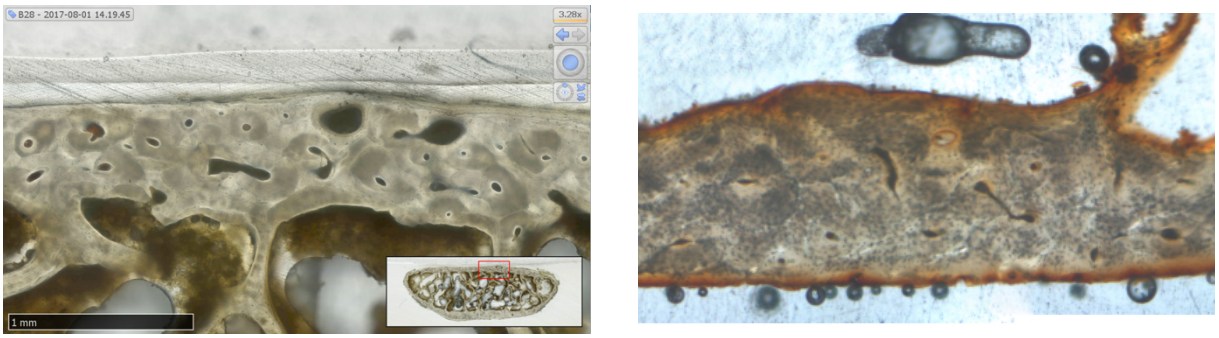

Figure 5.3: Left - Close-up of the interior surface of sample B28, showing category 1 features(100x magnification); Right– Close-up of sample CY191, healthy control (exterior surface, 100x magnification) (image of sample CY191 courtesy of Julieta Garcia-Donas)

Figure 5.3 shows another pathological sample, this one belonging to a 50-year-old male with fat deposits in the liver, and a healthy control sample belonging to a 48-year-old male. Again, the pathological sample, while perhaps having slightly thinner cortical bone than one would normally expect for a male this age, most certainly shows signs of category 1 pathological

features, the effect of which is that the cortical bone appears much more porous than the comparative healthy control.

5.1.1.2 Category 2: Deranged Haversian Systems (Swiss Cheese Effect)

The second most encountered category of pathological features were Deranged Haversian Systems. In addition to the increased porosity seen in the first category of pathological features, the Deranged Haversian Systems shows a sharp increase in osteoclast activity. The metabolism of the bony tissue has been disrupted, hindering the ability of the cortical bone to remodel in a normal way (Parfitt, 1984). This is then expressed as overly large canals, often connecting and branching to meet the canals of neighbouring osteons, and oddly shaped osteons and canals, to the point where the osteons are almost no longer identifiable. This can also be called the "Swiss Cheese Effect" as the cortical bone cross-section begins to resemble that of the eponymous cheese. Similar malformations of Haversian systems have been seen in other pathologies present in other bones, such as cribra orbitalia in the orbital roof, syphilis in the long bones, and extra-spinal hyperostosis related to DISH (Schultz, 2012; Lill, 2013). While some samples have the involvement of nearly the entire cross-section, samples were noted as having category 2 features if approximately 20% or more of the observed cross-section was involved.

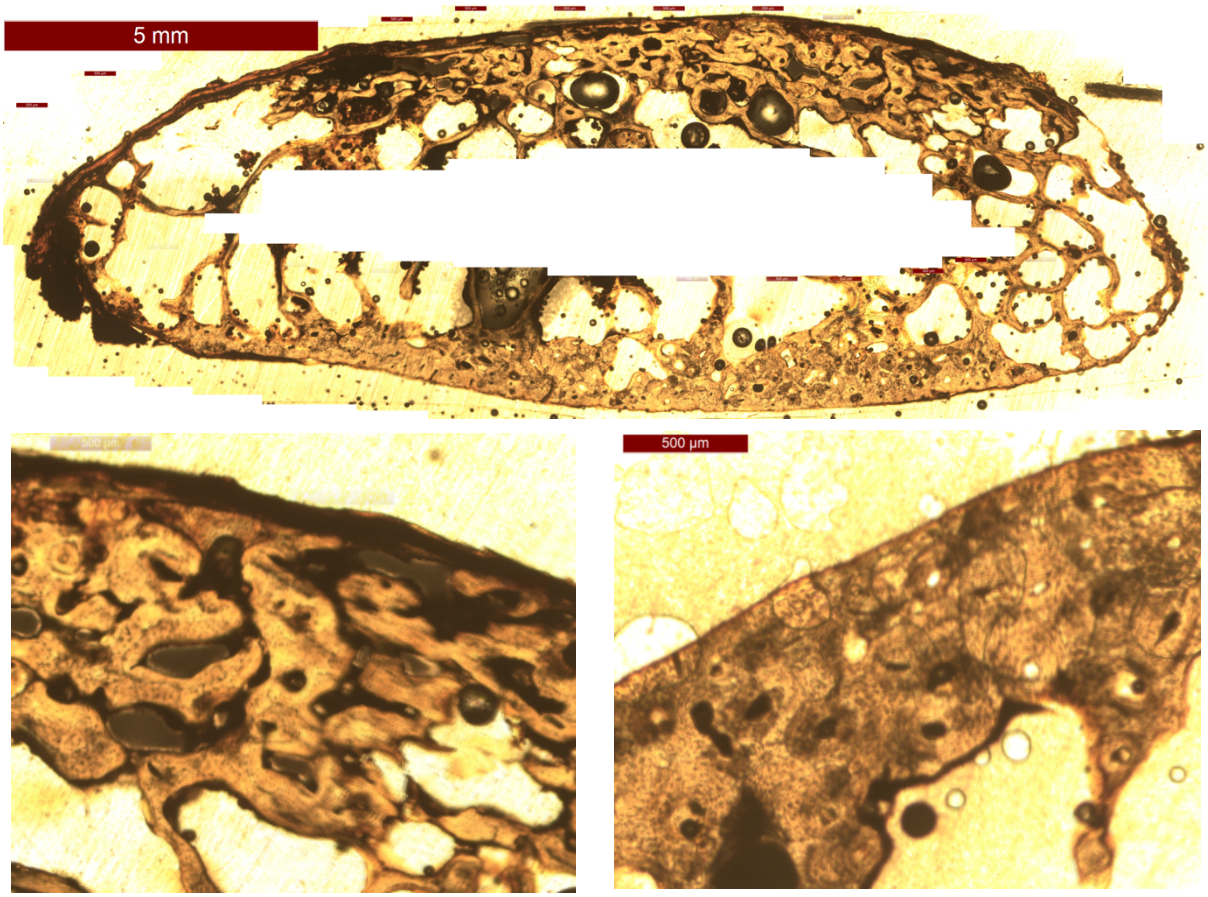

Figure 5.4: Top – Stitched full cross-section of sample CC203 showing Category 2 pathological features; Bottom Left – Close-up of the exterior surface of sample CC203 showing Category 2 pathological features, 100x magnification; Bottom right – Close-up of the interior surface of sample CC187, healthy control, 100x magnification. (All images courtesy of Julieta Garcia-Donas)

In figure 5.4 shows a full cross-section and a close-up of sample number CC203, as well as a close-up of a similarly aged healthy control for comparison. This pathological sample belonged to an 85-year-old male suffering from chronic obstructive pulmonary disease (COPD), placing this sample in the pulmonary class of pathologies. This sample is a good example of full cross-section involvement of category 2 pathological features, as seen in the first image. The disorganised canals have completely taken over the entre cross-section of the rib, showing the extreme extent of the inhibition of the metabolic function of the bone. This is even more visible in the close-up photograph, showing the extent of the abnormal osteoclast activity in the bone. While not necessarily thinning overall, with the exception of

the area to the right of the full cross-section, the bone is extremely porous, owing to the abnormal bone remodelling.

The features seen in this pathology category often only cover part of the cross-section and are concentrated in one or two areas. These features also sometimes occur near a lesion, particularly lytic lesions. Due to the deranged remodelling seen in this category of features, it is immediately obvious to the observer that something is wrong with the cortical bone, making this category of features easy to identify even by those observers less experienced in bone histology, unlike those features seen in category 1. It is also possible for features in category 2 to appears alongside features from category 1 or category 3, and occasionally all three categories are present at once.

The following images are two close-up photographs of samples showing visual evidence of category 2 pathological features. Unlike the category 1 features, category 2 features are much more difficult to quantify and measure, and for that reason are not comparable to the metric analysis in the Quantitative Analysis section of this chapter. As in the previous section, following each pathological image will be a close-up of an age matched sample from the healthy control group. This will allow for better visualisation of the pathological features, when compared with the healthy control.

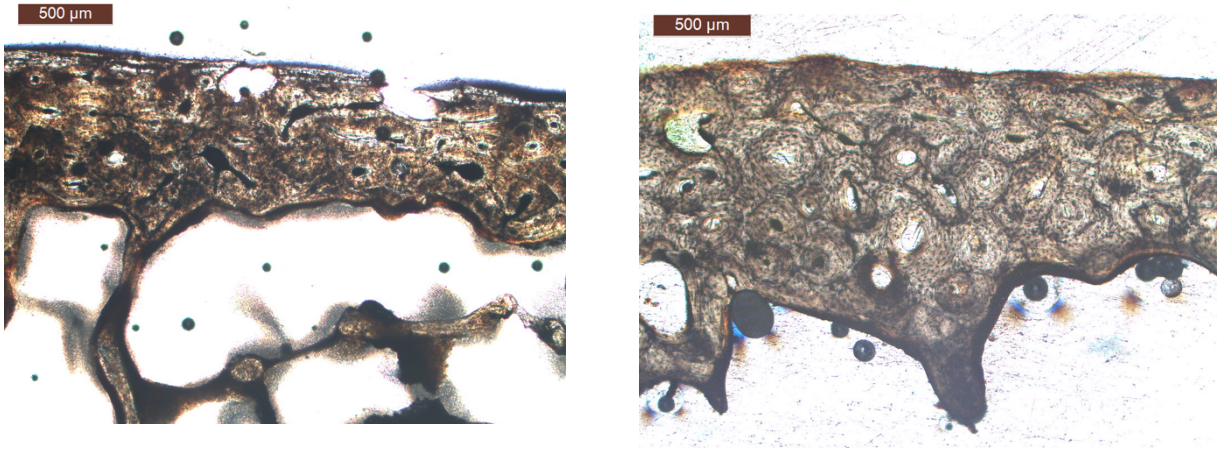

Figure 5.5: Left - Close-up of interior surface of sample FC16, (59 years old) showing signs of category 2 features (100x magnification): Right - Close-up of interior surface of sample CY190 (57 years old), healthy control (100x magnification).

Figure 5.5 shows a pathological sample with category 2 features, as well as a similarly aged healthy control. The pathological sample is from a 59-year-old male with a myocardial infarction and a history of CAD. The comparative sample is from a 57-year-old healthy male. Once again, the cortical bone of the pathological sample appears more porous, and the Haversian systems more irregular than the healthy control. It is also observable that the pathological sample has thinning cortical bone, when compared with the healthy control.

5.1.1.3 Category 3: Striations of Rapid Bone Deposits

The third category of pathological features is the least commonly observed in this study. This category does not involve the Haversian systems of the cortical bone, but rather refers to striations of bone. These striations are formed by overactive osteoclasts, once again interrupting the regular metabolic processes of cortical bone. This interruption of metabolic activity causes the osteoblasts to rapidly deposit bone in layers, usually near the periosteum, without following the pattern of the normal Haversian system, and therefore not creating osteons. Evidence of these striations of rapidly deposited bone have also been seen in relation to other pathologies in different bones, such as syphilis in the long bones, and extra-spinal

hyperostosis related to DISH (Schultz, 2012; Lill, 2013) These features are usually concentrated in only one or two areas of the cross-section, and are most often seen in proximity to prolific lesions. Like the features present in category 2, these striations very clearly fall outside the range of normal for cortical bone microstructure, making them easily identifiable. The features in category 3 can also occur simultaneously alongside features from categories 1 and 2. As in the previous category, samples were counted as having category 3 features if there was approximately 20% involvement, this time of the periosteum rather than the entire cross-section, as category 3 features occur primarily along the periosteum.

The following is an image of the only sample with possible Category 3 pathological features, compared with a sex and age matched healthy control sample. As the rarest category of pathological features, it would be beneficial in the future to increase sample size in order to have more samples with these features to be compared. Like the features in category 2, category 3 features should be easily identifiable, once the observer knows what to look for.

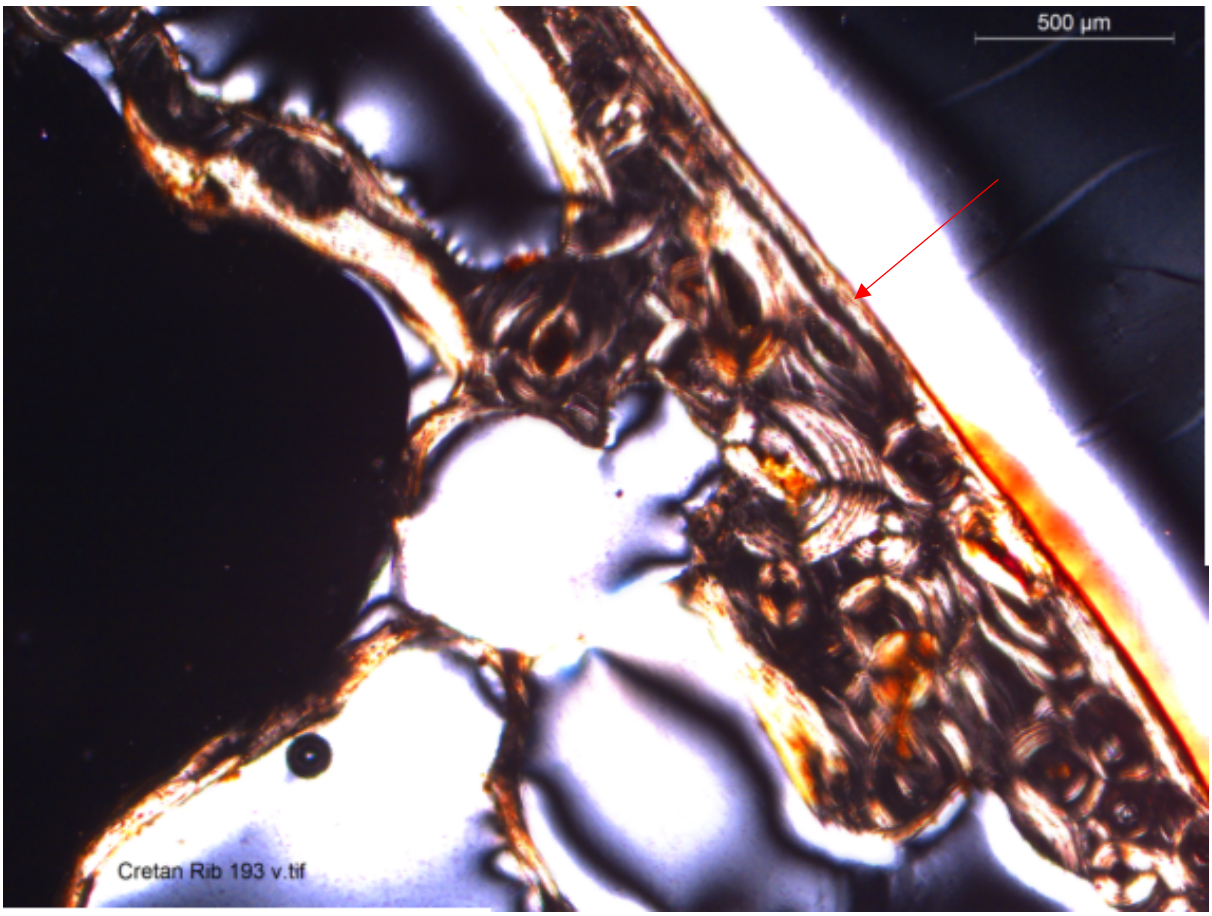

Figure 5.6: Close-up of exterior surface of sample CC193, showing possible Category 3 pathological features, arrow pointing to striations, 100x magnification

Figure 5.6 is a close-up of sample number CC193. This sample belonged to a 62-year-old male suffering from liver cirrhosis, placing this sample in the hepatic class of pathologies. This sample shows clear evidence of category 1 pathological features, and possible visual evidence of category 3 pathological features. In this close-up, there appears to be a thin layer of rapidly deposited bone. This occurs when the metabolic processes of the bone are disrupted, and the osteoblasts begin creating bone in the wrong place, usually along the periosteum, sometimes

near the site of a lesion. That does not appear to be the case with this sample. It may be that another study focusing more on infectious disease might encounter these features more.

Figure 5.7: Close-up of interior surface of sample CY198 (65-year-old, F), a healthy control, 100x magnification

Figure 5.7 is from sample number CY198. This sample belonged to a 65-year-old female in the healthy control group. Again, this sample is a good example of healthy bone for this age group. Compared with the previous pathological sample, this sample shows relative consistent osteon size and shape, and shows no signs of any of the 3 categories of bone pathological features. While the periosteum is slightly irregular, there is no evidence of rapidly deposited bone. Furthermore, unlike the matched pathological sample, the cortical bone is a normal thickness, and does not show any signs of unusual bone thinning.

5.1.2 Distribution and Analysis of Qualitative Features

5.1.2.1 Distribution and Analysis by Pathology

To measure the distribution of the three categories of qualitative features, the pathological samples were separated into six classes of pathology based on the specific conditions noted in their medical records. These classes are cancer cardiovascular, diabetes, hepatic, pulmonary, and renal. Some individuals had multiple pathologies in two or more classes, and these were also noted. Once separated into classes of pathology, observations of each sample were counted and recorded.

The following table (see table 5.1) illustrates the results of these observations. As some samples had multiple pathologies in two or more classes, they were counted in the Multiple Classes row, instead of being counted multiple times in the other disease classes. This was to see if having conditions in multiple classes had any bearing on the manifestation of pathological features in any particular category. It was also noted if any samples had features falling into more than one category. While it is possible for a single cross-section to have features that fall into all three categories, none of the pathological samples in this study had features that fell into more than two categories. Lastly, the healthy control samples were also counted, to see how many of them showed evidence of pathological bone in any category. While some may show small amounts of pathological bone, this is most likely due to age, as any obvious signs of pathology not related to age would have excluded them from the control sample.

Table 5.1: Distribution of feature categories by disease class

Class	Number of Cases	Category 1	Category 2	Category 3	2 Categories	3 Categories
Cancer	2	2 (100%)	1 (50%)	0 (0%)	1 (50%)	0 (0%)
Cardiovascular	10	9 (90%)	4 (40%)	0 (0%)	3 (30%)	0 (0%)
Diabetes	1	1 (100%)	1 (100%)	0 (0%)	1 (100%)	0 (0%)
Hepatic	16	13 (81.25%)	3 (18.75%)	1 (6.25%)	3 (18.75%)	0 (0%)
Pulmonary	2	2 (100%)	2 (100%)	0 (0%)	2 (100%)	0 (0%)
Renal	1	1 (100%)	0 (0%)	0 (0%)	0 (0%)	0 (0%)
Multiple Classes	8	8 (100%)	2 (25%)	0 (0%)	2 (25%)	0 (0%)
Healthy Controls	37	4 (10.81%)	0 (0%)	0 (0%)	0 (0%)	0 (0%)

Overall, category 1 features were the most widespread across all classes of pathology. In four of the six individual classes, category 1 features were present in 100% of cases, while in the remaining two classes, category 1 features were present in greater than 81.25% of cases. In samples with multiple classes category 1 features were present in 100% (8 of 8) of cases. Category 2 features were the second most common in the pathological group. These features were present in five of the six classes of pathology. In samples with multiple classes, category 2 features were present in 25% (2 of 8) of cases. Finally, category 3 features were the rarest of three types of features seen in the Pathological group. They were present in only the hepatic class of the six pathology classes. Of the sixteen samples in the hepatic class, category 3 features were present in only 6.25% (1 of 16) of cases.

In some of the cases, features in more than one category were present in the sample. While there were cases with features in two categories, there were no samples exhibiting features in all three categories. In all but one of these cases, the features exhibited were category 1 and category 2 features. A single case in the hepatic class showed evidence of category 1 and category 3 features. Multiple categories of features were present in five of the six classes of pathology, as well as in the multiple class category.

Table 5.2: Distribution of pathological features across age groups in the pathological sample

Age Group	No. Samples	Category 1	Category 2	Category3
<20	1	1 (100.00%)	1 (100.00%)	0 (0.00%)
21-30	1	1 (100.00%)	0 (0.00%)	0 (0.00%)
31-40	7	4 (57.14%)	3 (42.86%)	0 (0.00%)
41-50	7	7 (100.00%)	1 (14.29%)	0 (0.00%)
51-60	13	12 (92.31%)	4 (30.77%)	0 (0.00%)
>60	11	11 (100.00%)	4 (36.36%)	1 (9.09%)

In addition to analysing the samples by class of pathology, the pathological samples were also separated into age groups (see table 5.2). This was done to better compare with the healthy control group. Although the healthy control was selected specifically to not show any observable signs of pathology, this was done with the caveat that normal age-related changes would not be discounted. While several samples in the older age groups of the healthy control sample were found to show pathological features, these were much more restrained in their prevalence when compared with the pathological group.

5.1.2.1.1 Pathological features in the Healthy Control group

As well as the pathological samples, the healthy control samples were also observed, and presence of any of the categories of pathological features was noted (see table 5.3). High

prevalence of these features was not expected, as they had been pre-screened by another researcher for use in another project. It is possible, however, that some of the older samples might be expected to have some pathological features, due to an age-related decrease in bone density (see figure 5.8). All controls were selected from the databases of two osteological collections. Controls were selected from those individuals with no record of pathology at the time of their death, however it is possible some individuals may have had undiagnosed conditions that were never recorded.

Table 5.3: Table showing the distribution of pathological features in the Healthy Control group, separated by age group

Age Group	No. Samples	Category 1	Category 2	Category3
<20	1	0 (0.00%)	0 (0.00%)	0 (0.00%)
21-30	1	0 (0.00%)	0 (0.00%)	0 (0.00%)
31-40	4	0 (0.00%)	0 (0.00%)	0 (0.00%)
41-50	4	1 (25.00%)	0 (0.00%)	0 (0.00%)
51-60	8	1 (12.50%)	0 (0.00%)	0 (0.00%)
>60	19	2 (10.53%)	0 (0.00%)	0 (0.00%)
Total	37	4 (10.81%)	0 (0.00%)	0 (0.00%)

The results of this analysis were overall concurrent with expectations. There were no cases of pathological features in individuals under 46 years of age, and those samples that did show signs of pathological features were limited to the first category of features, the most common category. Category 1 features most notably imply an increase in bone porosity due to the larger area of the canals 3observed and are often found in conjunction with thinning cortical bone. That said, there were cases in the older age groups of the healthy control group that had thinning cortical bone, but seemingly normal sized and shaped osteons (see figure 5.9). Overall, only 10.81% (4 of 37) of the control samples showed signs of pathological features, compared with 95% (38 of 40) pathological samples. It may also be worth mentioning that three of the four samples with observed pathological features in the healthy control group were female, a demographic more likely to suffer from age-related and/or postmenopausal

osteoporosis and osteopenia, a possible contributing factor to the appearance of said pathological features.

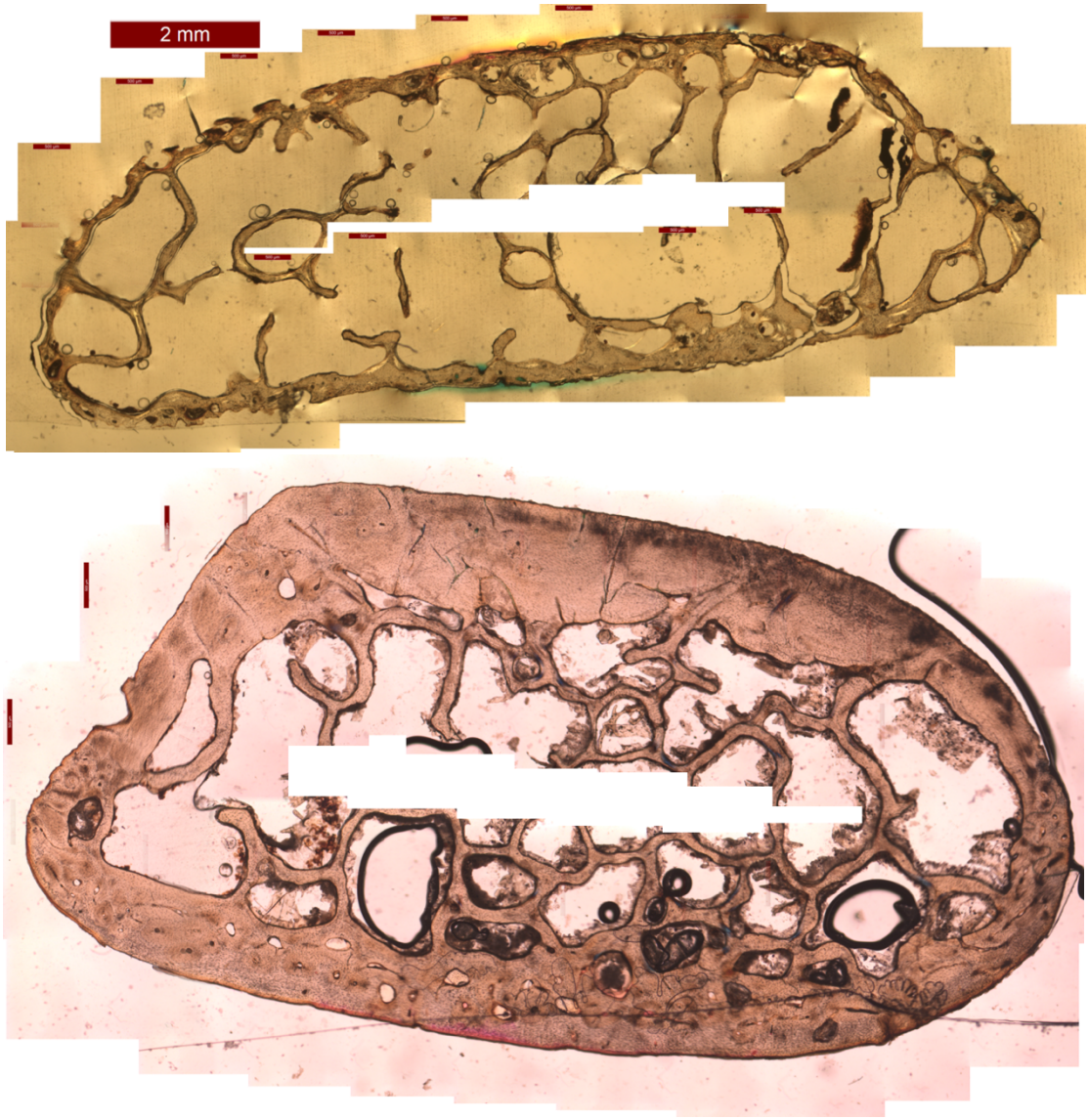

Figure 5.8: Top – Cross-section of sample CC26 from the healthy control group, belonging to a healthy 90-year-old female; Bottom –Cross-section of sample CC53 from the healthy control group, belonging to a healthy 19-year-old female. (Both images courtesy of Julieta Garcia-Donas)

5.1.2.1.2 Pathological features in the Cancer class

The cancer class consisted of two samples, one with cancer of the brain, and one with cancer of the lungs. It is unknown from the available medical history what stage of cancer or if the cancer had metastasised anywhere outside the sample. Neither sample in the cancer class

had metastatic lesions present on the ribs, although this could be a possibility in other cancer samples, as skeletal involvement is common in most malignant neoplasms (Ortner, 2003).

While the number of samples with cancer was very small, there was a certain amount of information that could be obtained. Of the two samples with pathologies in the cancer class, category 1 features were present in 100% (2 of 2) of cases and category 2 features were present in 50% (1 of 2) of cases. There were no observable category 3 features present, however this does not exclude the possibility of their presence in other samples. Of the two samples in the cancer class, two categories of features were present in 50% (1 of 2) of cases, specifically, two categories of pathological features were seen in the sample with brain cancer, while only category 1 features were present in the patient with lung cancer. Due to the small sample size and the lack of information regarding the stage and progression of the disease, more research will be needed to draw meaningful conclusions.

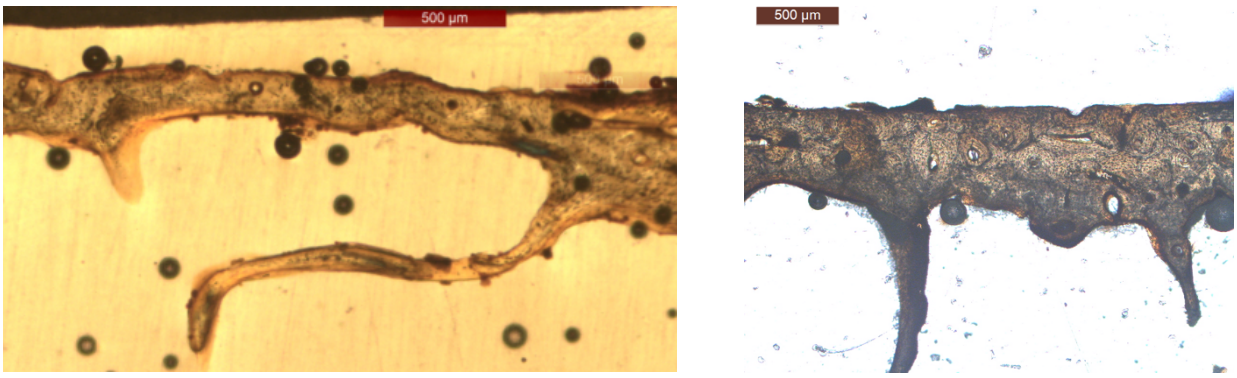

Figure 5.9: Left – Close-up of the interior surface of sample CC45, from a 64-year-old female suffering from lung cancer (image of sample CC45 courtesy of Julieta Garcia-Donas); Right – Close-up of the interior surface of sample CY198, from a 65-year old healthy female, 100x magnification.

5.1.2.1.3 Pathological features in the Cardiovascular class

The cardiovascular class consisted of ten samples. These samples include those patients with coronary artery disease (CAD), including atherosclerosis and myocardial infarction,

hypertension, cerebral haemorrhage, and endocarditis. Amongst these conditions, CAD was the most common. As the heart is adjacent to the ribs, it is possible for periosteal lesions to appear on the bones adjacent to the diseased heart, namely ribs and thoracic vertebrae (Schultz, 2001). Recently, it has also been discussed that there is a possibility of correlation between heart disease and osteoporosis (Sprini, et al., 2014; Bagger, et al., 2007; Magnus & Broussard, 2005).

The cardiovascular class was one of the larger disease sample sizes at ten samples. This sample size, however, is still relatively small, and any conclusions drawn from these results would require further enquiry. Of the ten samples with pathologies in the cardiovascular class, category 1 features were present in 90% (9 of 10) of cases, and category 2 features were present in 40% (4 of 10) of cases. There were no observable category 3 features, however this does not exclude the possibility of these features appearing in other samples. Of the ten samples in the cardiovascular class, two categories of features were present in 30% (3 of 10) of cases. All three cases with two categories of features present suffered from CAD and myocardial infarctions.

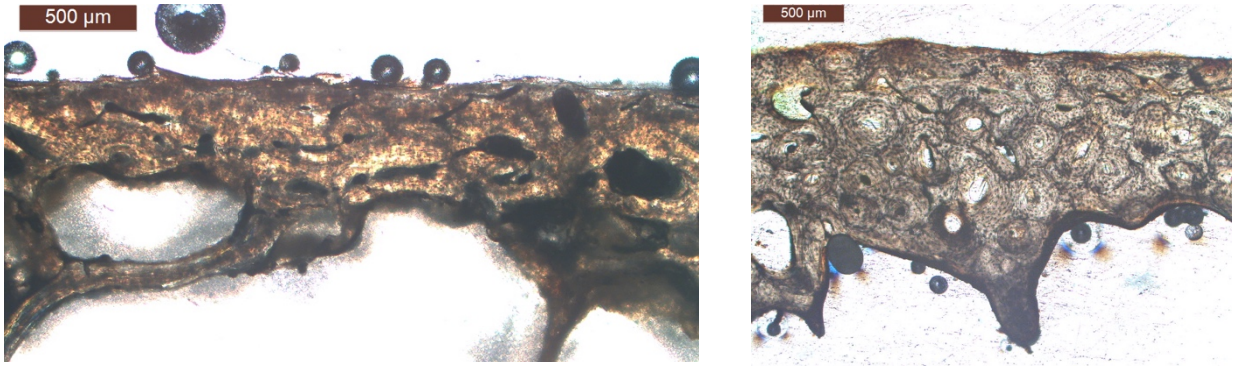

Figure 5.10: Left – Close-up of the exterior surface of sample FC18, a 57-year-old male with a myocardial infarction, CAD, and generalised atherosclerosis, 100x magnification; Right – Close-up of the interior surface of sample CY190, a healthy 57-year-old male, 100x magnification.

5.1.2.1.4 Pathological features in the Diabetes class

The diabetes class consisted of only one sample. It is unknown which type of diabetes the patient suffered from. As diabetes is a metabolic disorder, it likewise can influence the metabolism of other tissues in the body, including bone (Vestergaard, 2007; de Liefde, et al., 2005). As the sample size is incredibly small for this disease class, it is more useful to regard this sample as a case study, and to put off drawing any specific conclusions until further research has been conducted. In the single case of diabetes, both category 1 and category 2 features were present.

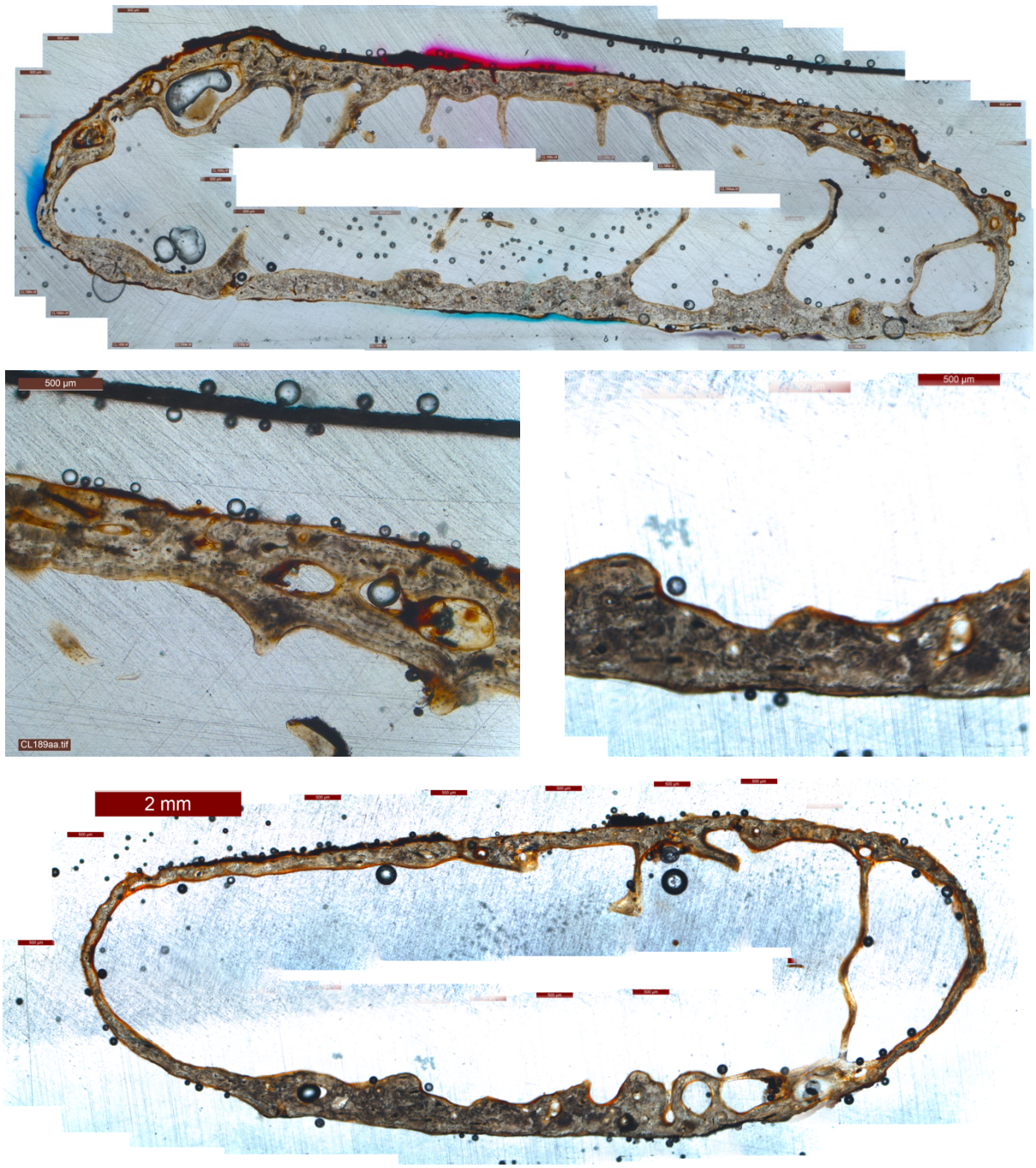

Figure 5.11: Top – Full cross-section of sample CC189, a 94-year-old male with diabetes; Middle Left – Close-up of sample CC189 exterior surface, 100x magnification; Middle Right – Close-up of sample CC83 exterior surface, a healthy 90-year-old female, 100x magnification; Bottom – full cross-section of sample CC83. (Pictures of CC83 courtesy of Julieta Garcia-Donas)

5.1.2.1.5 Pathological features in the Hepatic class

The hepatic class was the largest of the disease classes, consisting of sixteen samples. This is due in part to the fact that the project initially intended to only analyse individuals with

hepatic disease. While with sixteen cases the hepatic class is the largest disease sample size, it is still a relatively small sample size, and further research would be needed to draw specific conclusions from these results. The hepatic class included individuals with liver cirrhosis, hepatomegaly, possible hepatitis, and fatty liver. There has long been an acknowledged connection between chronic hepatic disease and disruptions to bone metabolism, especially as it relates to chronic alcohol abuse (George, et al., 2009; Diamond, et al., 1990; Bikle, et al., 1985; Schnitzler & Soloman, 1985; Verbanck, et al., 1976; Gonzalez-Calvin, et al., 1993; Spencer, et al., 1986; Lindsell, et al., 1982). Often this takes the form of osteoporosis and osteopenia, leading to a thinning and weakening of the bone inconsistent with the age of the individual.

Of all the disease classes, the hepatic class's larger sample size provides the best opportunity for analysis. Of the sixteen samples with pathologies in the hepatic class, category 1 features were present in 81.25% (13 of 16) of cases, and category 2 features were present in 18.75% (3 of 16) of cases. Category 3 features were the rarest of three types of features seen in the pathological group. They were present in only the hepatic class of the six pathology classes. Of the sixteen samples in the hepatic class, category 3 features were present in only 6.25% (1 of 16) of cases. The single case of category 3 features occurred in an individual suffering from liver cirrhosis. Of the sixteen samples in the hepatic class, two categories of features were present in 18.75% (3 of 16) of cases. These included one sample with category 1 and 3 features, and two samples with category 1 and 2 features. The samples with category 1 and 2 features suffered from fatty accumulation.

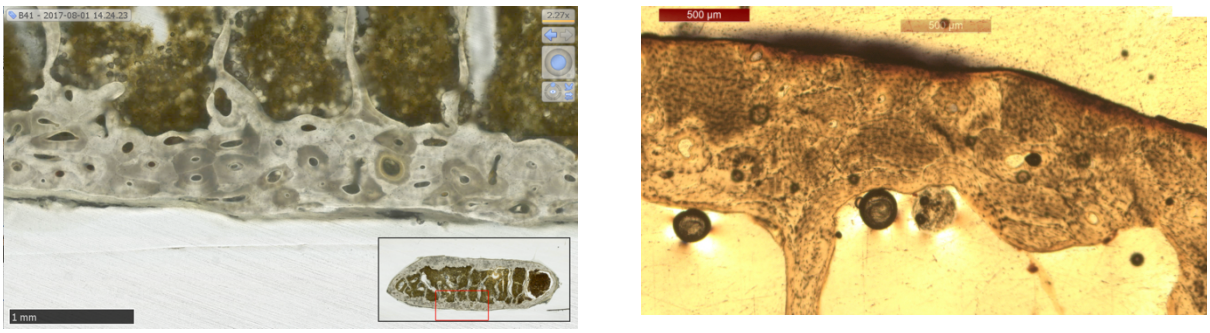

Figure 5.12: Left – Close-up of the exterior surface of sample B41 exterior surface, a 53-year-old male with generalised fatty liver; Right – Close-up of the interior surface of sample CY61 interior surface, a healthy 51-year-old female, 100x magnification. (image of sample CY61 courtesy of Julieta Garcia-Donas)

5.1.2.1.6 Pathological features in the Pulmonary class

The pulmonary class consisted of two samples, one with COPD (chronic obstructive pulmonary disorder), and one with chronic bronchopneumonia. From the literature, it is known that pulmonary conditions can affect the ribs due to their proximity to the site of primary disease (Schultz, 2012). In addition, it is possible for osteoporosis to occur alongside chronic pulmonary diseases, such as COPD (Jørgensen, et al., 2007; Cavaillès, et al., 2013; Chatila, et al., 2008).

As there are only two samples in this disease class, more research would be needed to connect any category of features definitively to pulmonary disease, however the following do have value and can be seen as case studies. Of the two samples with pathologies in the pulmonary class, category 1 features are present in 100% of cases, and category 2 features were also present in 100% of cases. This means that of the two samples in the pulmonary class, two categories of features were present in both cases. There were no cases showing category 3 features, however this does not exclude them from appearing in other samples.

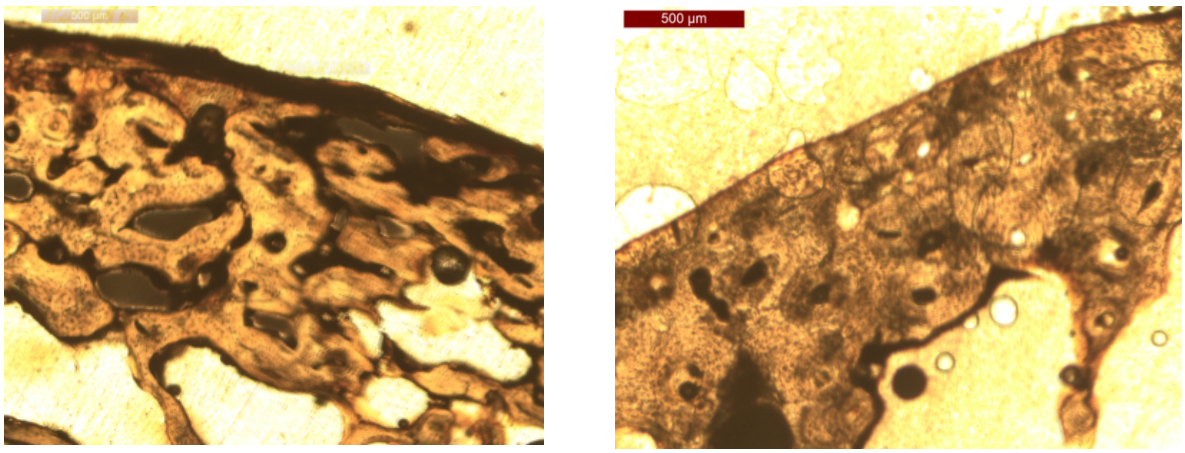

Figure 5.13: Left – Close-up of the exterior surface of sample CC203, an 85-year-old male with COPD, 100x magnification; Right – Close-up of the interior surface of sample CC187, a healthy 81-year-old male, 100x magnification. (Both images courtesy of Julieta Garcia-Donas)

5.1.2.1.7 Pathological features in the Renal class

Like the diabetes class of disease, the renal class consisted of only one case. In this case, the individual suffered from uraemia, indicating possible kidney failure (Cotran, et al., 1999). In many patients with chronic kidney disease, there is a marked development of bone abnormalities, especially as it pertains to mineral metabolism (Williams, 2009; Ott, 2009; Leonard, 2009; Miller, 2005). Like some of the other disease classes with very few samples, it would be best to treat this disease class as a case study, rather than to extrapolate from its results. Category 1 features were present in the single sample, but there were no indications of features from category 2 or 3. Likewise, there was not a case with multiple categories of features present. While these categories were not present in this sample, it is possible that these features could appear in another sample with renal pathology. Further research into the microstructure of ribs in cases with renal pathology must be made to further understand the significance of the features seen in this sample.

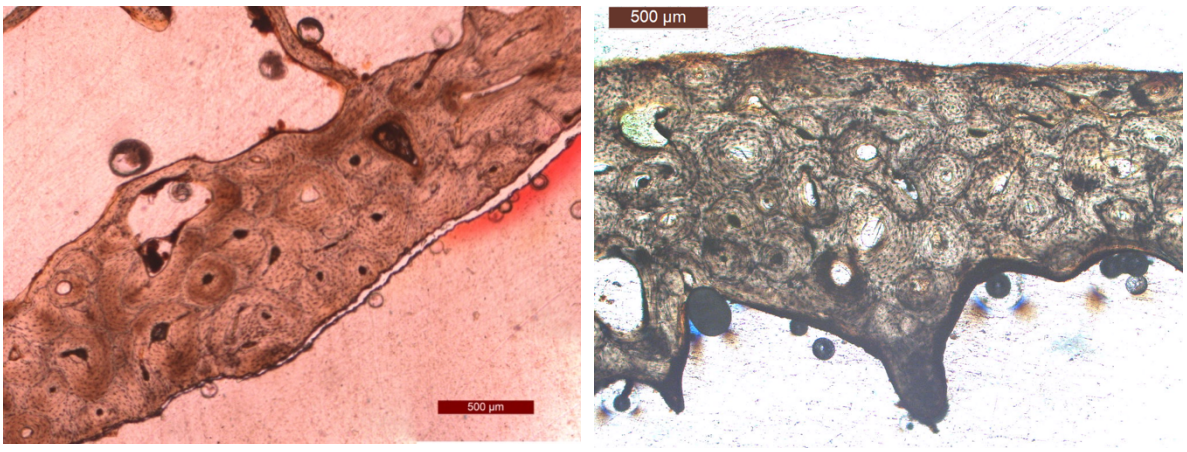

Figure 5.14: Left – Close-up of the exterior surface of sample CC6, a 58-year-old female with uraemia, 100x magnification; Right – Close-up of the interior surface of sample CY190, a 57-year-old healthy male, 100x magnification.

5.1.2.1.8 Pathological features in the Multiple class group

In addition to the samples with pathologies related to only one class of disease, there were eight samples with multiple pathologies belonging to more than one class of disease. These ranged from samples with disease in two classes, to a sample with disease in five different classes. For example, sample A10 came from an individual suffering from hypertension, diabetes, heart ischemia, left ventricular hypertrophy, hepatic steatosis, pyelonephritis, and bronchopneumonia. These conditions would fall in to multiple classes, in this case cardiovascular, diabetes, hepatic, renal and pulmonary. These samples were separated out from the samples with conditions that fell within only one disease class, as it was not possible to account for interactions between the diseases, or to know which condition or combination of conditions could have caused the changes to the bone microstructure. All the conditions involved in the multiple class group were also represented by single samples in the above sections, there were no disease classes that were present in the multiple class group that did not also appear in the rest of the pathological sample.

The multiple class category was one of the larger sample sizes available, with eight cases. In samples with multiple classes, category 1 features were present in 100% (8 of 8) of cases, and category 2 features were present in 25% (2 of 8) of cases. There were no samples with evidence of category 3 features, but it is possible for these features to appear in other samples. More research is needed. Of the samples with pathologies in multiple classes, features from two categories were present in 25% (2 of 8) of cases.

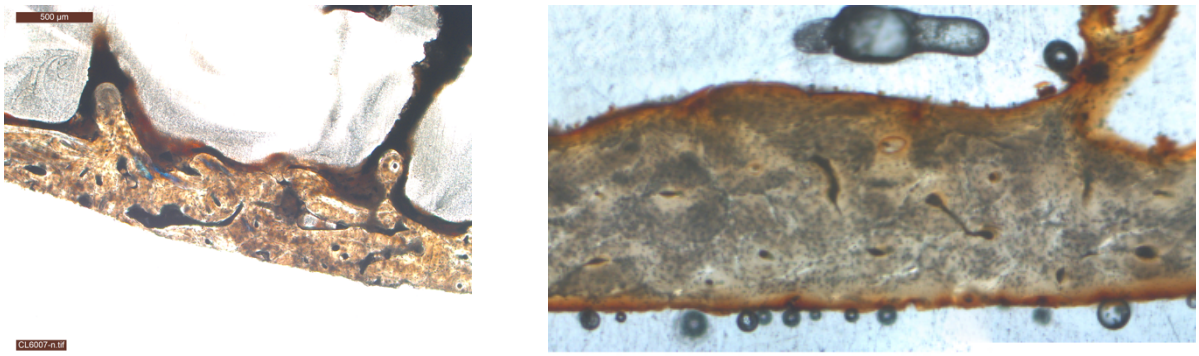

Figure 5.15: Left - Close-up of the interior surface of sample FC13 (52-year-old male), from an individual suffering from hypertension, coronary disease, and pulmonary complications of chronic heavy smoking, showing signs of category 2 features. (100x magnification); Right - Close-up of the interior surface of sample CY191, (48-year-old male) healthy control. (100x magnification) (image of sample CY191 courtesy of Julieta Garcia-Donas).

5.1.2.1.9 Analysis of Pathological Categories

Once each sample had been observed and evaluated, several chi squared tests were carried out to examine the relationships between the various disease classes and age groups with the different categories of pathological features. In all cases, a chi squared test for independence was used. This tests the null hypothesis that the variables are independent of each other. This is done by comparing expected values with the observed values. First, the expected values were calculated using the totals from each tested group. Then the chi squared test was performed on three tables of data and a *p*-value was returned. This *p*-value would then indicate whether the variables were independent or not.

The first to be tested were the healthy samples tested against their age group. This test was simpler than the others as there were very few samples with any sign of pathology, and all that did exhibit pathological features were exclusively in the first category, therefore only the first column of the table was able to be tested. The chi squared test returned a *p*-value of 0.9225, indicating that there is almost no chance that the variables of category 1 pathological features and age are independent of each other.

The next to be tested were the pathological samples tested against their age groups. Unlike the first-test conducted with the healthy samples, this test was carried out across the entire table, as all three categories of pathological features were represented, as well as by individual age group. The chi-squared test for the entire table returned a *p*-value of 0.7770, which while also indicating a very strong relationship between the pathological features and age, is slightly less than the results of the same test on the healthy samples. Below is a table of the results returned per age group.

Table 5.4: Table of chi squared test results comparing categories of pathological features between the pathological and healthy control groups, further separated by age group

Age Group	*p*-value
Less than 20 years old	0.4872
21-30 years old	0.8348
31-40 years old	0.5364
41-50 years old	0.6165
51-60 years old	0.8417
Greater than 60 years old	0.3527

The final variables to be tested were the disease classes. Again, as all categories of pathological features were represented, the chi squared test was carried out across the entire table, as well as for each individual disease class. The test for the entire table returned a *p*-

value of 0.6202, indicating a strong relationship between the categories of pathological features, and the different classes of disease. Below is a table of the results returned per disease class.

Table 5.5: Table of chi squared test results comparing categories of pathological features with disease classes

Disease Class	*p*-value
Cancer	0.8588
Cardiovascular	0.9138
Diabetes	0.2972
Hepatic	0.5286
Pulmonary	0.0608
Renal	0.8939
Multiple Groups	0.9345

5.2 Quantitative Analysis

Quantitative analysis for this study was separated into two groups. The first involved the standard histological practices for bone as developed by Stout and Paine (1992), and Cho and colleagues (2002). This involves the measurement of the cortical area, quantifying the number of secondary osteons in the cross-section (both complete and fragmented), and then calculating for osteon population density (OPD). These metrics can then be used in any age estimation formula previously developed, and then compared. It would also allow the study to compare age with cortical area and OPD, as previous studies have noted a significant relationship between age and these two variables (Stout & Paine, 1992; Stout, et al., 1996; Cho, et al., 2002). With these variables, it was possible to use previously developed age estimation, however since these formulae were not developed for this population, and had a very high level of inaccuracy, it was determined that directly comparing actual age to cortical area and OPD through correlation and regression would be more informative and beneficial.

The second group of data this study employed for the purposes of Quantitative analysis are the osteon specific data. These were measurements taken of individual osteons and canals from four sampled areas within each cross-section. These metrics were created for this study with the purpose of quantifying some observable changes in bone microstructure, such as the increased cortical bone porosity seen in osteoporosis and osteopenia. These are non-standard measurements, and therefore no outside comparisons can be drawn. The metrics chosen for this study include maximum and minimum osteon diameter, osteon circumference, osteon total area, canal area, osteon actual area (minus the canal area), osteon circularity, maximum and minimum canal diameter, and canal circularity.

5.2.1 Standard Bone Histology

The first section of the Quantitative Analysis section is the Standard Bone Histology. This includes the tried and tested measurements and quantifications that have been used as a standard for rib histology as first described by Stout and Paine (1992). Using this data, it was then possible to run statistics using the R statistical package. For this data, the statistical analysis was concentrated on correlations, regression analysis, inter-observer, and bootstrapping. All of these statistics were done on the pathological samples, the healthy samples, and then again on all the samples together. This is because previous studies have not separated out pathological samples, and it was the aim of this study to prove that removing pathological samples would lead to better, more accurate results when implementing population appropriate age-estimation formulae.

5.2.1.1 Inter-observer Error

The error rates for the standard histological analysis were conducted using inter-observer, to test the accuracy of quantification between two readers. Inter-observer error was done by each reader quantifying the same slide separately, and then comparing. By doing these tests, the accuracy of the quantifications can be determined.

Inter-observer errors for standard histology were conducted in conjunction with another study being undertaken at the University of Edinburgh. These tests were done using samples from the pooled collection of histological samples including both pathological and healthy individuals from Crete and Cyprus. There were two readers involved in the error testing, the author of this study, and Julieta Garcia-Donas. The quantifications from the other reader were not viewed until after all quantifications had been made, to decrease the incidence of bias. These quantifications were then subjected to a paired t-test to test for statistically significant differences between the two readers.

The first variable to be tested was the number of intact osteons per cross-section. The same 22 slides were examined by each reader, and the intact osteons quantified. A paired t-test was then performed. The t-value for these sets of data was calculated as 1.7091. The *p*-value was quantified as 0.1022. The 95% confidence interval was between -0.5912 and 6.04570. Lastly, the mean of the differences was 2.7273.

The next variable to be tested was the number of fragmented osteons per cross-section. The t-value for these sets of data was calculated as 3.6023. The *p*-value was calculated as 0.0017. The 95% confidence interval was between -19.788 and -5.3029. Lastly, the mean of the differences was -12.5455.

Finally, the last variable to be tested was the number of intact osteons per cross-section. The t-value for these sets of data was calculated as -2.1879. The *p*-value was calculated as 0.0401. The 95% confidence interval was between -19.1503 and -0.4861. Lastly, the mean of the differences was -9.8182.

These same sets of data were also assessed using TEM, *r*TEM, and associate R values by Julieta Garcia-Donas. Overall, these tests showed high repeatability, with most variables not exceeding the 5% acceptance threshold, with the exception of the number of fragmented osteons which was shown to have a 12% variance due to measurement error between observers (Garcia-Donas, 2017).

5.2.1.2 Correlations

For the purposes of this study, correlations were done using Spearman's r correlations. These were then converted to give *p*-values for significance. Full tables of both Spearman's r correlations and converted *p*-value correlations are available in the Appendix. While correlation does not equal causation, they provide a starting point from which to explore further, for example with regression analysis.

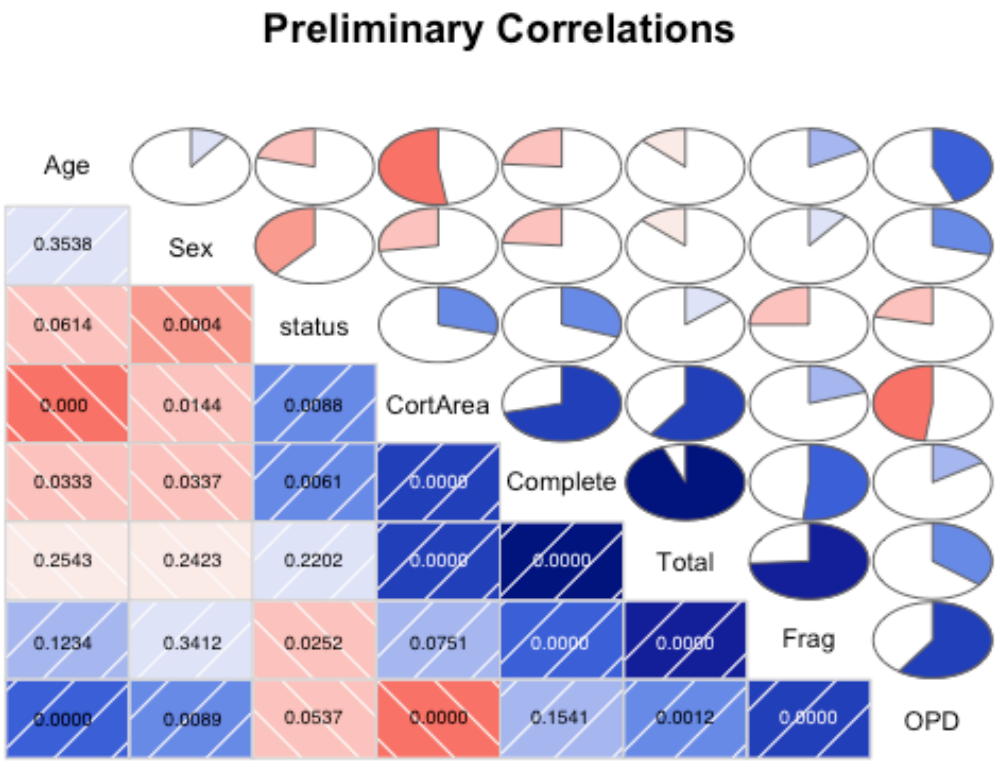

Figure 5.16: Heat map of Spearman's correlations using the entire sample, and the converted p-values

The above image is a heat map showing correlations between different factors, including Age, Sex, Status, Complete Osteons, Fragmented Osteons, Total Osteons, Cortical Area, and OPD. On the one side, colours and shades indicate positive correlation (blue) and negative correlation (red). The darker the shade, the stronger the correlation. On the other half, a pie chart for each factor intersection gives the strength of the correlation. Some correlations, including Age Estimation and OPD, and Complete or Fragmented Osteons and Total Osteons have strong correlations because one of the factors is a part of the other one. For example, Complete and Fragmented Osteons are added together to get Total Osteons. For the purposes of this study, the most important correlations to consider are those factors with strong correlations to Age. In this case, the strongest correlated factors with Age are Cortical Area, and OPD. Using Spearman's r, Age and Cortical Area correlation was valued at -0.51 (*p*-

value <0.0001). Using Spearman's r, Age and OPD correlation was valued at 0.47 (*p*-value <0.0001). All of these correlations, however, include both healthy and pathological samples.

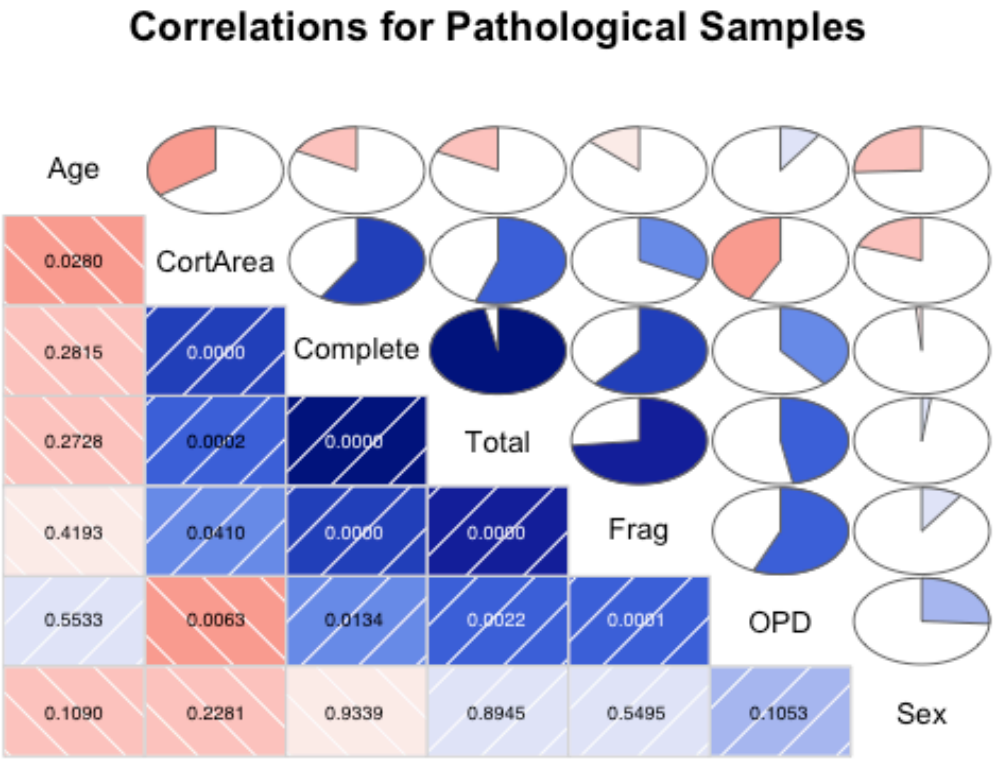

Figure 5.17: Heat map showing Spearman's correlations for only pathological samples, and converted p-values

The above image is a heat map showing correlations between the different factors, this time using only the pathological samples. Overall, the heat map appears much lighter, indicating that the strength of correlations is much weaker. This is again reinforced by the pie charts on the right of the image. Again, some correlations, such as Age Estimation and OPD, and Complete and Fragmented Osteons and Total Osteons, are strongly correlated due to a functional relationship. These correlations can then be excluded. Those factors that were strongly correlated with Age in the previous image are now far weaker. Using Spearman's r, Age and Cortical Area are now correlated at -0.35 (*p*-value 0.28), and Age and OPD are now correlated at 0.10 (*p*-value 0.5533).

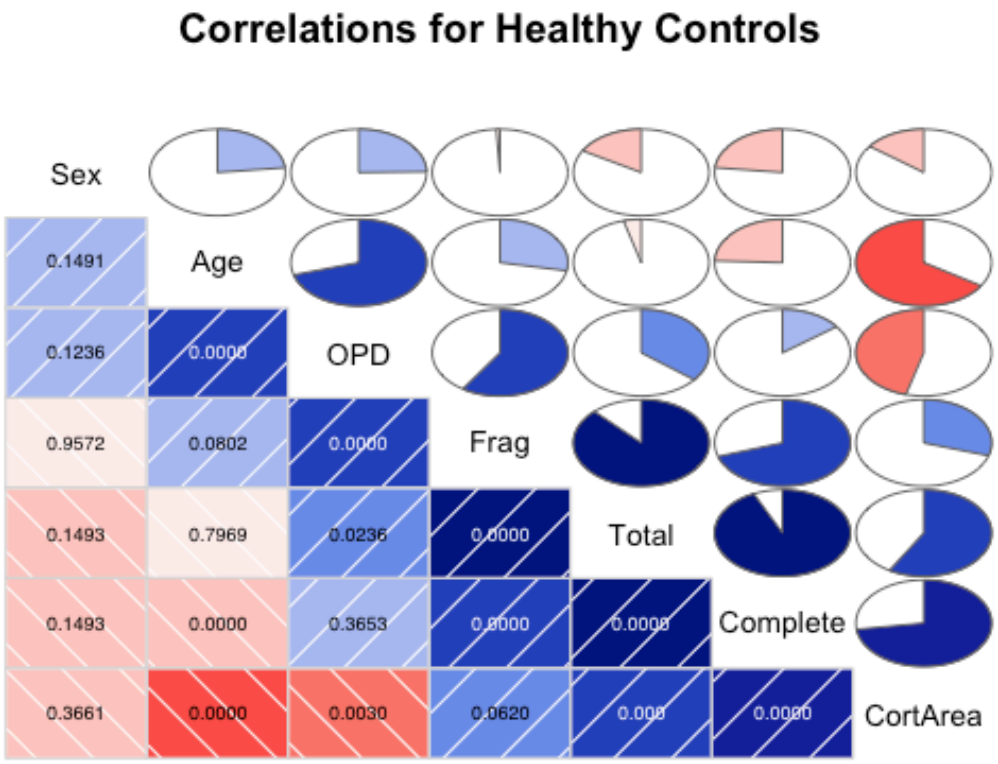

Figure 5.18: Heat map showing Spearman's correlations using only Healthy Samples, and converted p-values

The above image is a heat map showing correlations between different factors using only the healthy control samples. This map appears much brighter than the previous map showing the results of calculations using only the pathological samples. Looking at the pie charts to the left of the image, Age is shown to be very strongly correlated to OPD and Cortical Area. Using Spearman's r, Age and Cortical Area are now correlated at -0.66 (*p*-value <0.0001), and Age and OPD are now correlated at 0.70 (*p*-value <0.0001). These are not only stronger correlations than the pathological samples, but also stronger than the mixed correlations.

5.2.1.3 Regression Analysis

Building on the correlations between Age and Cortical Area, and Age and OPD, regression analysis was done on both the pathological and healthy samples and plotted to show the distributions and lines of regression for each. Full regression outputs can be found in the Appendix.

Included in the results from this calculation were coefficients, residual standard error, multiple R-squared, adjusted R-square, and *p*-value. As with the correlations, regressions were calculated first with all samples, and then separated into pathological and healthy control samples.

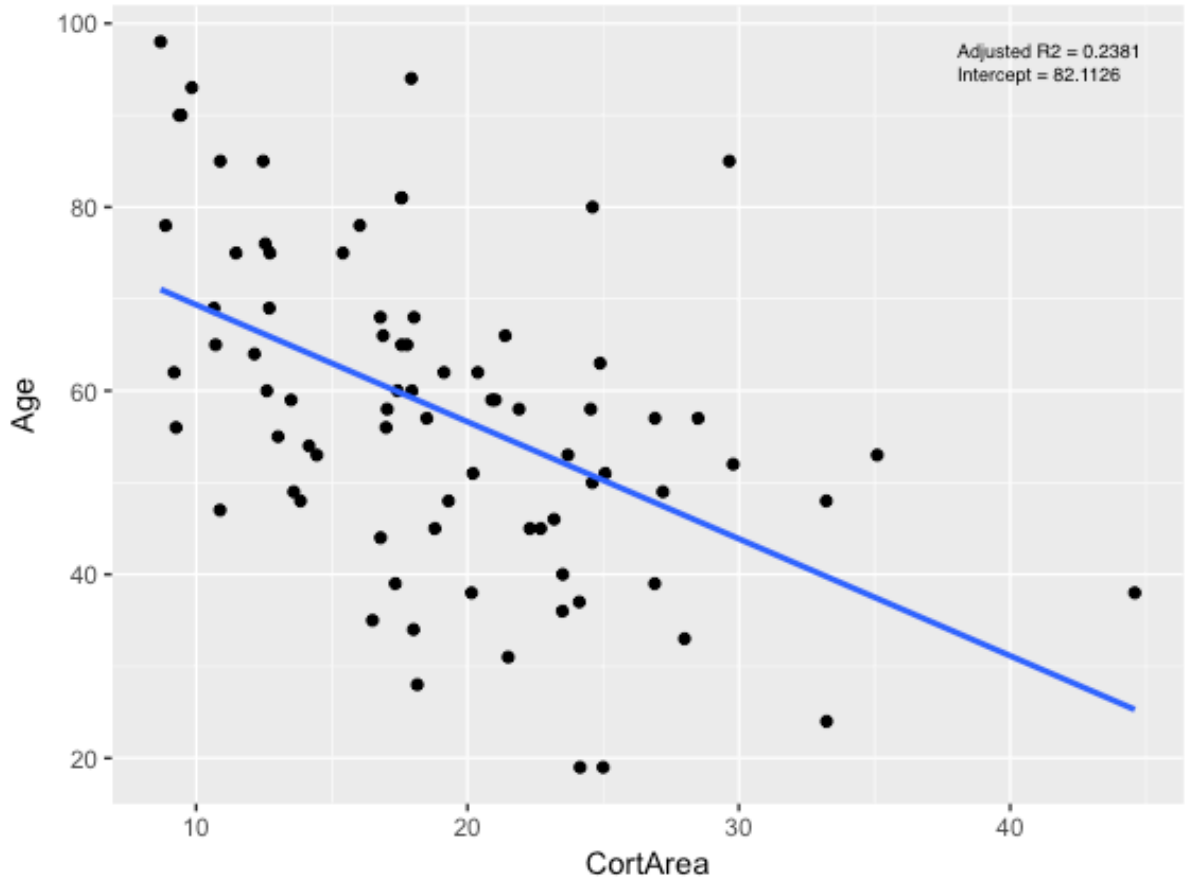

Figure 5.19: Scatterplot of Age compared to Cortical Area for the entire sample with the line of regression

First, regression was calculated using all samples. This would reflect previous research in the field, where pathological samples were not separated out. First, coefficients were calculated.

The Estimate coefficient was calculated as intercept 82.1126 and slope -1.2744. The Standard Error coefficient was calculated as from the intercept 5.1013 and from the slope 0.2514. Multiple R-squared was calculated as 0.2477, and Adjusted R-squared was calculated as 0.2381. Finally, *p*-value was calculated as <0.0001.

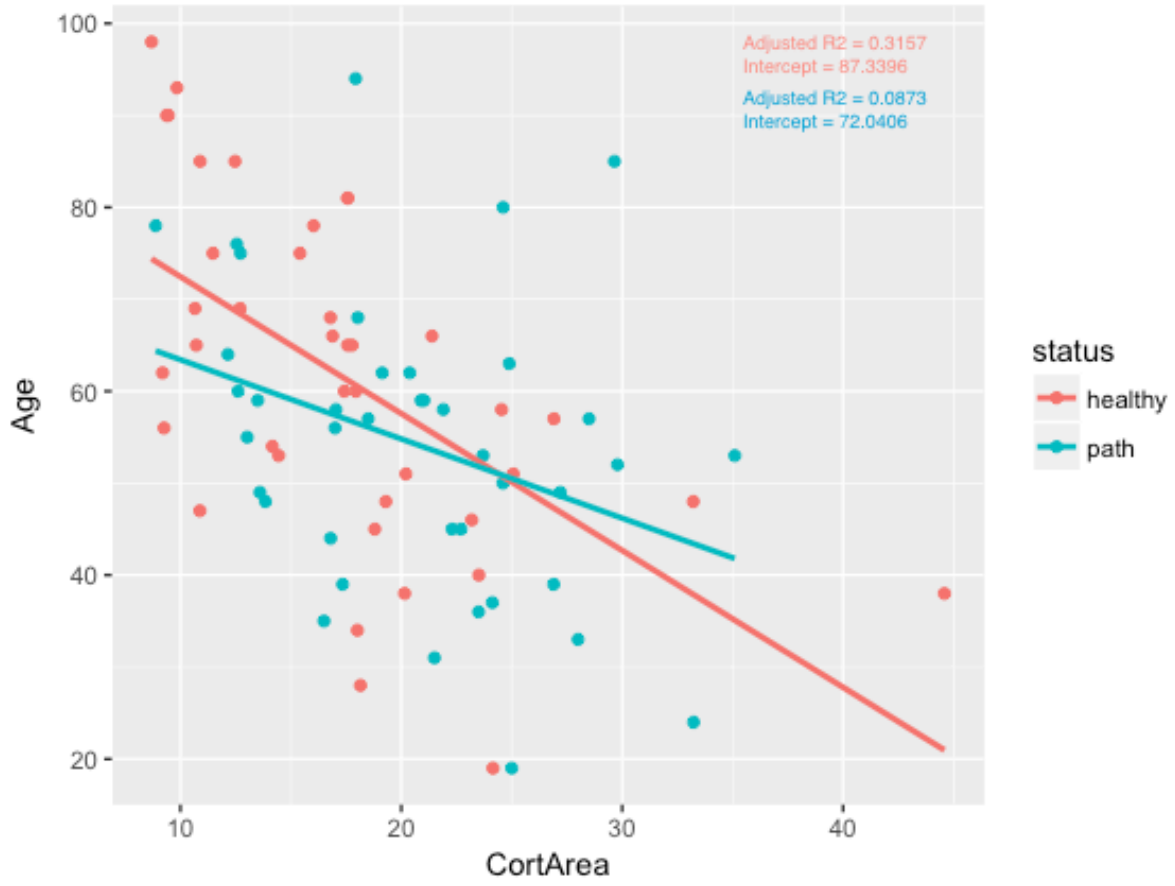

Figure 5.20: Scatterplot of Age compared to Cortical Area, separated by health status, with lines of regression

The above image is a scatterplot showing the distribution of both healthy and pathological samples with regard to the Age and Cortical Area factors. The downward slant of the regression lines shows the negative correlation between Age and Cortical Area. This also shows the red regression line (healthy) as a better fit to the line of regression than the blue regression line (blue).

Next, regression was calculated using only the pathological samples. The Estimate coefficient was calculated as intercept 72.0406 and slope -0.8615. The Standard Error coefficient was calculated as from the intercept 8.5843, and from the slope 0.3961. Multiple R-squared was calculated as 0.1107 and Adjusted R-squared was calculated as 0.0873. Lastly, *p*-value was calculated as 0.03593.

Lastly, regression was calculated for only the healthy control samples. First, the coefficients were calculated. The Estimate coefficient was calculated as intercept 87.3396 and slope -1.4886. The Standard Error coefficient was calculated as 13.598 from the intercept, and 0.3416 from the slope. Multiple R-squared was calculated as 0.3333 and Adjusted R-squared was calculated as 0.3157. Finally, *p*-value was calculated as <0.0001.

The results included in this calculation are the same as those for the Age and Cortical Area regression. As with the regressions for Age and Cortical Area, regressions were calculated first with all samples, and then separated into pathological and healthy control samples.

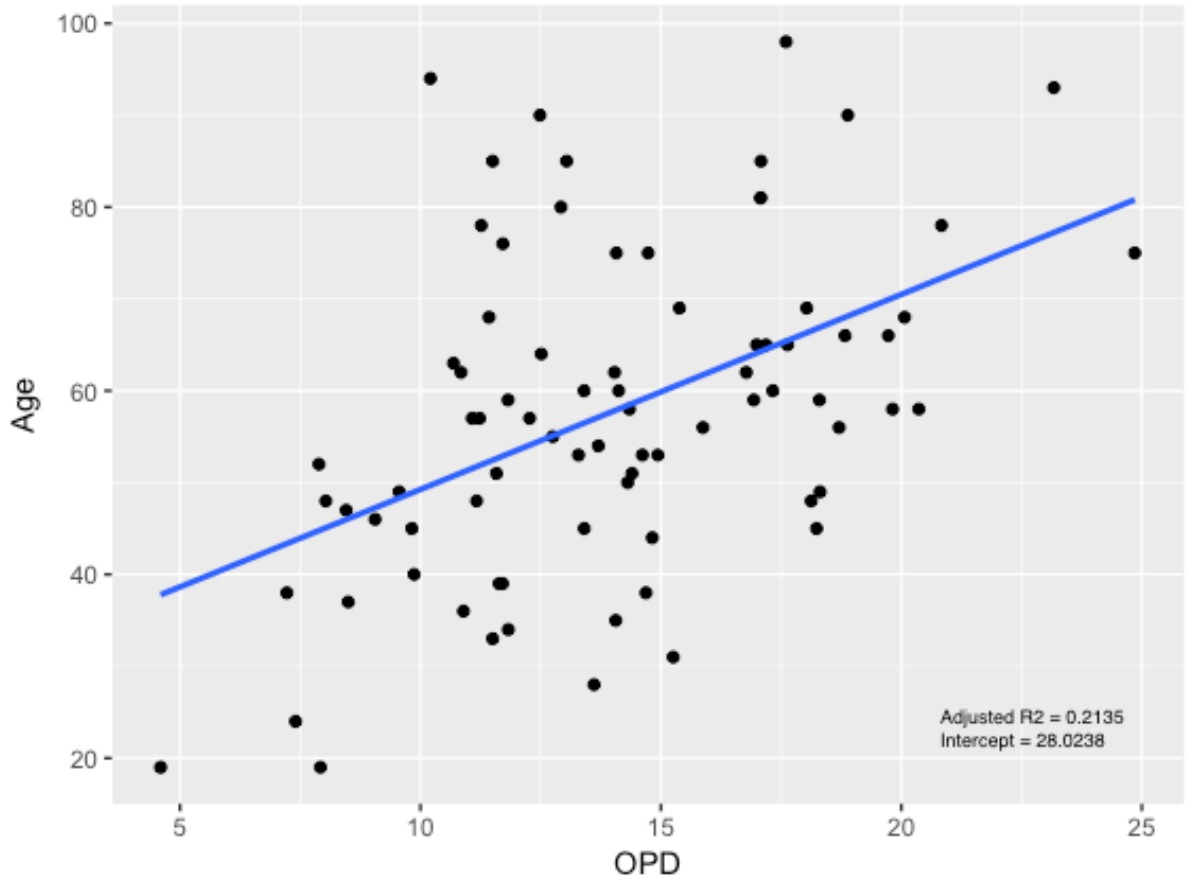

Figure 5.21: Scatterplot of Age compared to OPD for the entire sample with the line of regression

The above image is a scatterplot showing the distribution of the entire sample with regard to the Age and OPD factors. The upward slant of the regression lines shows the positive correlation between Age and OPD.

Regression was calculated for all samples. First the coefficients were calculated. The Estimate coefficient was calculated as intercept 28.0238 and slope 2.1234. The Standard Error coefficient was calculated as 6.5226 from the intercept and 0.4481 from the slope. Multiple R-squared was calculated as 0.2235 and Adjusted R-squared as 0.2135. Finally, the *p*-value was calculated as <0.0001.

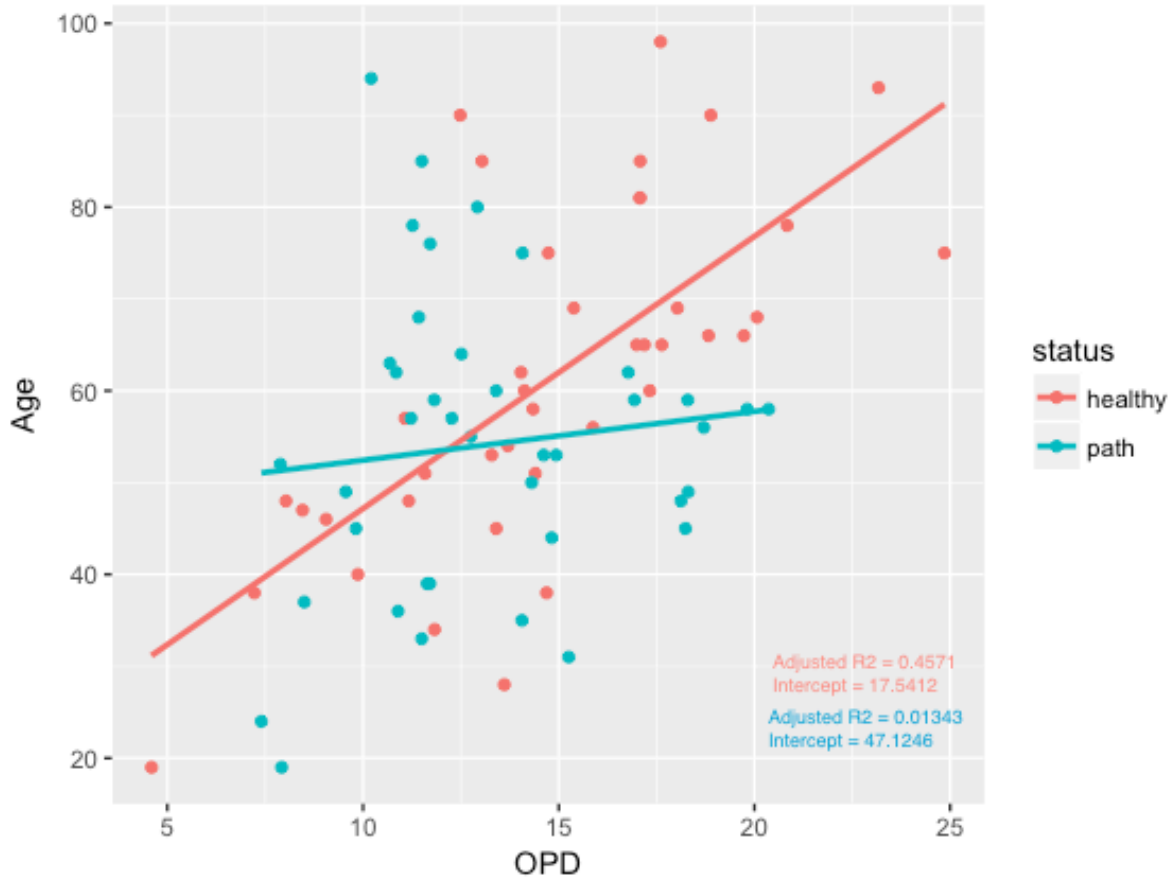

Figure 5.22: Scatterplot of Age compared to OPD, separated by health status, with lines of regression

The above image is a scatterplot showing the distribution of both healthy and pathological samples with regard to the Age and OPD factors. The upward slant of the regression lines shows the positive correlation between Age and OPD. This also shows the red regression line (healthy) as a better fit to the line of regression than the blue regression line (blue).

First, regression was calculated for only the pathological samples. First the residuals were calculated. The Estimate coefficient was calculated as intercept 47.1246 and slope 0.5312. The Standard Error coefficient was calculated as 10.4336 from the intercept and 0.7643 from the slope. Multiple R-squared was calculated as 0.01255 and Adjusted R-squared was calculated as -0.01343. Lastly, the *p*-value was calculated as 0.4913.

Finally, regression was calculated for only the healthy samples. First, the coefficients were calculated. The Estimate coefficient was calculated as intercept 17.5412 and slope 2.9633. The Standard Error coefficient was calculated as 7.8482 from the intercept and 0.5095 from the slope. The Multiple R-squared was calculated as 0.471, and the Adjusted R-squared was calculated as 0.4571. Lastly, the *p*-value was calculated as <0.0001.

5.2.1.4 Standard Errors

For the standard bone histology data, standard errors were calculated for each of the linear regression models. The standard error used in this section is the standard error of the estimate, or SEE, which measures the accuracy of predictions made with the regression line. For the SEE, a value closer to zero indicates a more accurate result. SEE was then calculated for the regression models comparing cortical area and age, and OPD and age.

Table 5.6: Table of SEE calculations for linear regression comparing cortical area and age, and OPD and age

Standard Error	Complete Data	Pathological Data	Healthy Data
SEE -Cortical Area	15.46	15.52	15.36
SEE-OPD	15.71	16.36	13.68

These standard errors give an indication of the accuracy of the regression predictions, which can then be compared with the standard errors of other studies that use cortical area and OPD as predictors of age.

5.2.1.5 Bootstrapping

For the purposes of this study, bootstrapping was used as a sampling and replacement method. Bootstrapping allows for assigning measurements of accuracy to the statistical estimates made earlier in the chapter. Specifically, bootstrapping was used to test the R-squared statistic for the regression analysis done in section 5.2.1.3. As in the regression section, resampling was applied to the R-squared statistic using the regression formula for each group comparing Age and Cortical Area, and Age and OPD. The standard for each resampling was 1000 replications. These were then plotted, and 95% confidence intervals calculated.

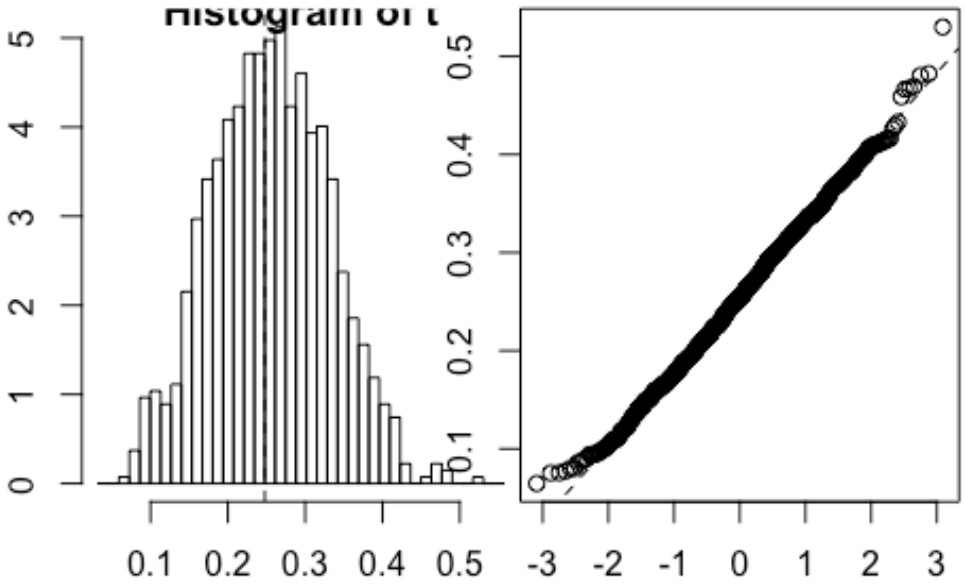

Figure 5.23: Plot of R-squared of Age and Cortical Area regression bootstrapping using All Samples

Using the complete set of sampled data, bootstrapping was applied to the Age and Cortical Area regression. The original R-squared, as reported in the above regression section was 0.2477. The bias was calculated as 0.0073. The standard error was calculated as 0.0760. Next,

95% confidence intervals were calculated. The Normal confidence interval was calculated as between 0.0914 and 0.3894. The Basic confidence interval was calculated as between 0.0893 and 0.3884. The Percentile confidence interval was calculated as between 0.1071 and 0.4062. Finally, the BCa confidence interval was calculated as between 0.0946 and 0.3842.

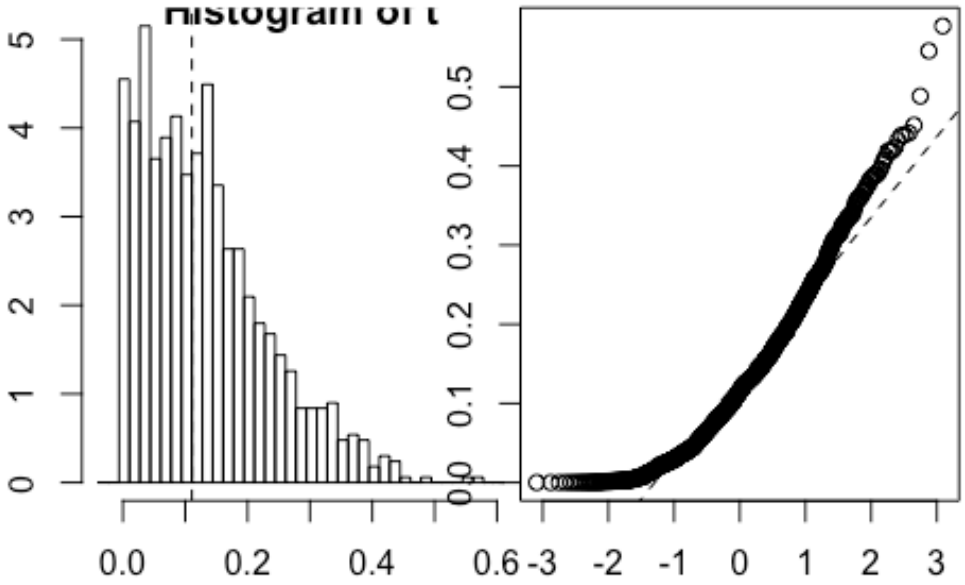

Figure 5.24: Plot of R-squared of Age and Cortical Area regression bootstrapping using only pathological samples

Next, using only the pathological samples, bootstrapping was applied to the Age and Cortical Area regression. The original R-squared, as reported above in the regression section, was calculated as 0.1107. The bias was calculated as 0.0212. the standard error was calculated as 0.1017. Following these bootstrap statistics, the 95% confidence intervals were calculated. The Normal confidence interval was calculated as between -0.1098 and 0.2889. The Basic confidence interval was calculated as between -0.1549 and 0.2198. The Percentile confidence interval was calculated as between 0.0016 and 0.3763. Finally, the BCa confidence interval was calculated as between 0.0007 and 0.3590.

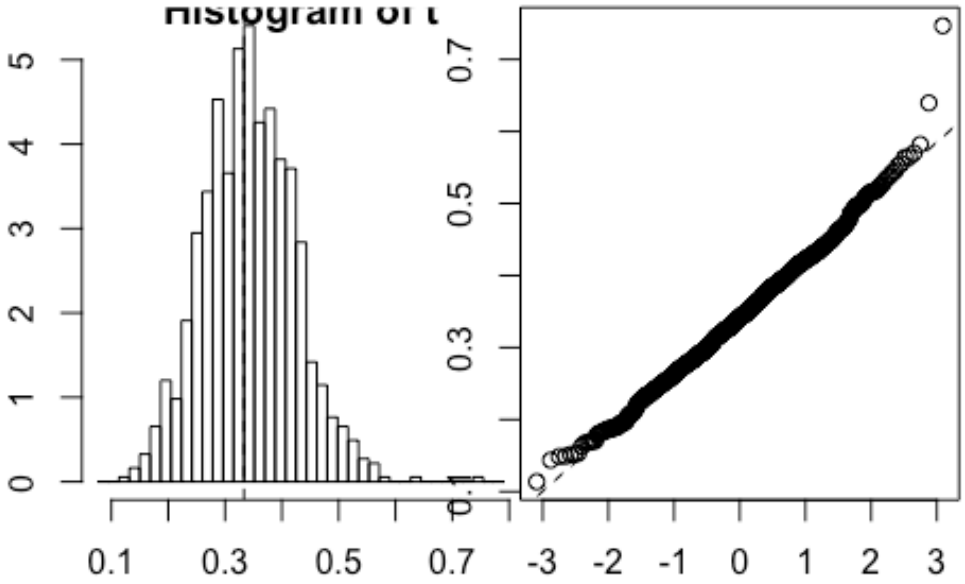

Figure 5.25: Plot of R-squared of Age and Cortical Area regression bootstrapping using only healthy control samples

Finally, bootstrapping was applied to the Age and Cortical Area regression using only the healthy control samples. The original R-squared, as reported above in the regression analysis section, was calculated as 0.3333. The bias was calculated as 0.0095. The standard error was calculated as 0.0807. Following these bootstrap statistics, 95% confidence intervals were calculated. The Normal confidence interval was calculated as between 0.1655 and 0.4820. The Basic confidence interval was calculated as between 0.1532 and 0.4790. The Percentile confidence interval was calculated as between 0.1875 and 0.5133. Lastly, the BCa confidence interval was calculated as 0.1704 and 0.4893.

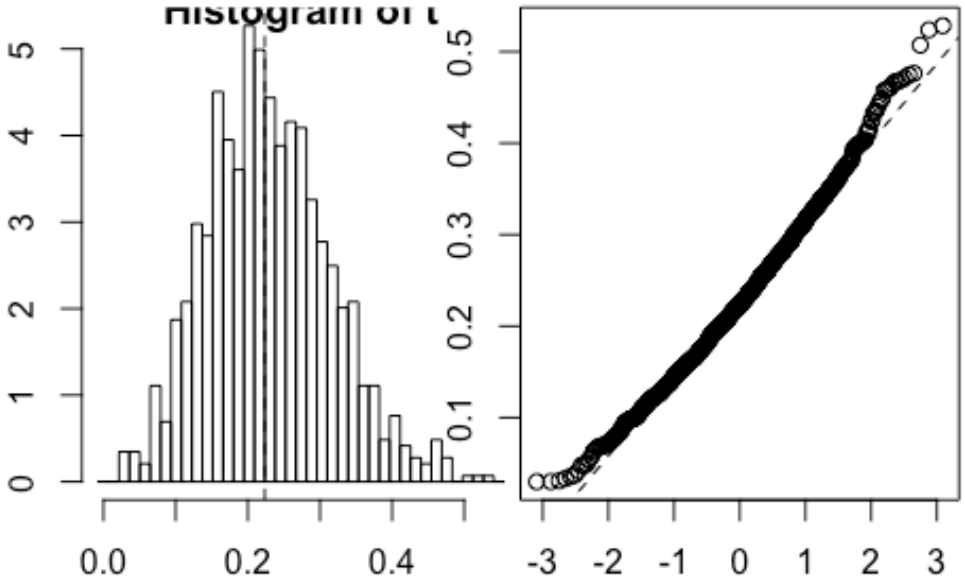

Figure 5.26: Plot of R-squared of Age and OPD regression bootstrapping using All Samples

After bootstrapping the regression for Age and Cortical area, bootstrapping was then applied to the R-squared statistic from the Age and OPD regression. As with the bootstrapping of the Age and Cortical Area regression, bootstrapping for the Age and OPD regression began with testing the R-squared statistic using all the sampled data. The original R-squared, as stated in the above regression analysis section, was calculated as 0.2235. The Bias was calculated as 0.006. The Standard Error was calculated as 0.0858. Following these bootstrap statistics, the 95% confidence intervals were calculated. The Normal confidence interval was calculated as between 0.0493 and 0.3855. The Basic confidence interval was calculated as between 0.0316 and 0.3717. The Percentile confidence interval was calculated as between 0.0753 and 0.4154. Lastly, the BCa confidence interval was calculated as between 0.0758 and 0.4157.

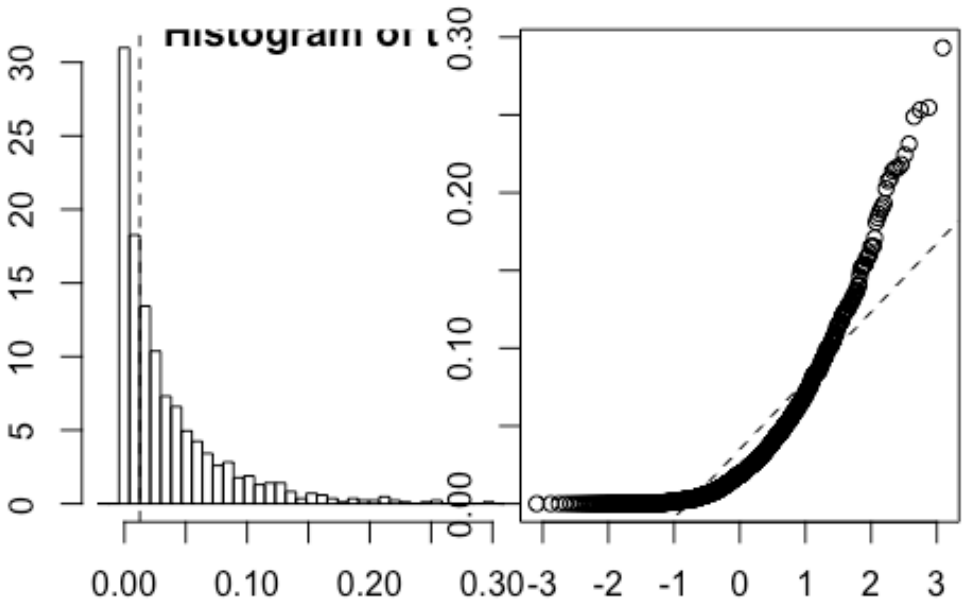

Figure 5.27: Plot of R-squared of Age and OPD regression bootstrapping using only pathological samples

Next, bootstrapping was applied to the R-squared statistic from the regression of Age and OPD using only the pathological samples. The original R-squared, as stated in the above regression analysis section was calculated as 0.0126. The bias was calculated as 0.0224. The standard error was calculated as 0.0442. Following these bootstrap statistics, the 95% confidence intervals were calculated. The Normal confidence interval was calculated as between -0.0964 and 0.0767. The Basic confidence interval was calculated as between -0.1338 and 0.0251. The Percentile confidence interval was calculated as between 0.0000 and 0.1589. Lastly, the BCa confidence interval was calculated as between 0.0000 and 0.1280.

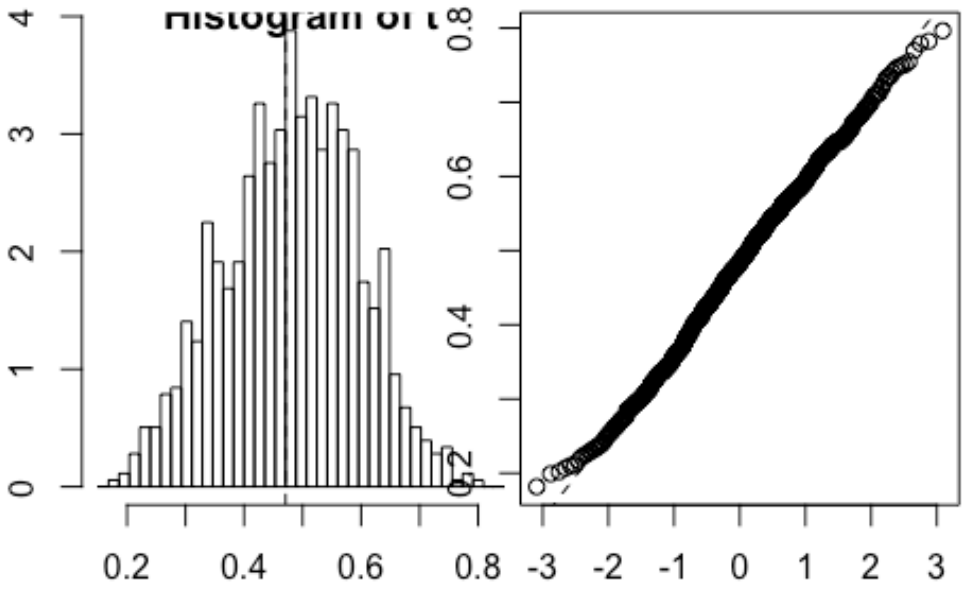

Figure 5.28: Plot of R-squared of Age and OPD regression bootstrapping using only healthy control samples

Finally, bootstrapping was applied to the R-squared statistic of the Age and OPD regression, this time only using the healthy control samples. The original statistic, as stated in the above regression analysis section, was calculated as 0.471. The bias was calculated as 0.0099. The standard error was calculated as 0.1142. Following these bootstrap statistics, the 95% confidence intervals were calculated. The Normal confidence interval was calculated as between 0.2373 and 0.6849. The Basic confidence interval was calculated as between 0.2451 and 0.6871. The Percentile confidence interval was calculated as between 0.2549 and 0.6969. Lastly, the BCa confidence interval was calculated as between 0.2295 and 0.6616.

5.2.2: Osteon Specific Metrics

Building upon the metrics and quantifications of the Standard Histology analysis, this study took the measurements further by taking metrics of individual osteons. The osteons were sampled from the entire cross-section, using four fields of view from the four cardinal points of the rib cross-section. Ten metrics were taken per osteon. These metrics include the maximum and minimum osteon length, the osteon perimeter, the total osteon area, the canal area, the osteon circularity, maximum and minimum canal length, and canal circularity. In the case of the total osteon area, this measurement has been defined as the area of the entire osteon, including the canal. The osteon area has been defined as the total osteon area minus the canal area. The circularity metrics measure how close the shape of the osteon or canal are to a perfect circle, a perfect circle being 1, and anything less than a perfect circle being between 1 and 0. A total of 52,700 measurements were taken. Inter and Intra-observer error were calculated for the micrometrics. The data was then analysed for correlation, for significance through the use of t-tests, by taking the mean value of each metric and comparing it to age divided by health status.

5.2.2.1 Inter and Intra-observer Error

5.2.2.1.1 Inter-observer Error

Inter-observer error for the osteon metric means was carried out by the author of this study, and an undergraduate volunteer. As this was carried out early in the process of gathering metric data, not all the metrics were accessed, specifically the osteon and canal circularity were not measured. In addition, the undergraduate volunteer only measured a small number of osteon perimeters, so this metric was excluded from the inter-observer analysis due to

insufficient data. Measurements were taken using the software ImageJ, and stitched photographs of the entire cross-section of the rib samples. The entire cross-section was used, as at the time of the inter-observer analysis, it had not yet been determined that sampled data would be a more efficient use of time and resources. It had also not yet been determined that the most accurate method for taking the measurements was with a stylus and tablet. In the future, the same measurement method and sampled data would be used by both observers, to yield more accurate results.

Table 5.7: Table showing results of independent t-test comparing two observers

Sample	OMaxL	OMinL	OTArea	CArea	OArea	CMaxL	CMinL
CC15	<0.0001	0.0009	0.5331	0.05114	0.301	0.0052	0.0077
CC169	<0.0001	0.569	0.0602	0.1108	0.0706	0.0063	0.2009
CC196	<0.0001	<0.0001	0.0386	0.5437	0.0137	0.1987	0.0458
FC2	0.03349	0.1724	0.5888	0.2348	0.7144	0.149	0.1217
FC3	0.0014	0.005	0.0164	0.2116	0.0117	0.0353	0.0701
FC6	<0.0001	<0.0001	<0.0001	0.0002	<0.0001	<0.0001	<0.0001
FC10	<0.0001	<0.0001	<0.0001	0.0495	<0.0001	0.009	0.0432
FC13	0.0250	0.0921	0.9357	0.6701	0.8818	0.1617	0.0094

Above is a table showing the *p*-value results of a Welch's independent t-test comparing the data from eight samples analysed by the two observers. Those *p*-values shown in red indicate a statistically significant difference between the metric data obtained by each observer. Those *p*-values shown in black indicate no statistically significant difference between the data obtained by the observers.

5.2.2.1.2 Intra-observer Error

Intra-observer error was conducted by the author. This was done to determine the consistency of the measurements. The original metrics were compared with a second set of

metrics taken several months later of the same slides. These were done using the sampled material, not the complete cross-sections, as was used in the inter-observer error section above. In addition, all variables were tested, as opposed to only some of the variables. This was possible as the second measurements were done after the first set of complete measurements was finished. A Welch's independent t-test was used to evaluate the data, as although the same slides were observed twice, there may be a small difference in the number of osteons measured per sample.

Table 5.8: Showing p-values results from the t-tests for intra-observer error

Sample	OMaxL	OMinL	OPeri	OTArea	CArea	OArea	OCirc	CMaxL	CMinL	CCirc
FC14	0.2819	0.057	0.1718	0.2065	0.7179	0.1213	0.1811	0.7883	0.8955	0.9368
CC203	0.0795	0.2613	0.2027	0.1857	0.7376	0.1395	0.6048	0.8117	0.5409	0.8078
CC45	0.8355	0.85	0.8203	0.6733	0.8939	0.5944	0.7898	0.7976	0.8382	0.2128
CC195	<0.0001	0.0004	<0.0001	0.0006	0.08274	0.0019	0.0002	0.0297	0.0248	0.3349
CY183	0.121	0.2495	0.137	0.2099	0.417	0.2177	0.0327	0.4035	0.3232	0.9721

Above is a table showing the *p*-value results of the Welch's independent t-tests. A t-test was run for each variable comparing the data for each slide's two sets of readings. The *p*-values shown in red indicate a statistically significant difference between the two sets of metrics taken by the observer. Those values shown in black indicate no statistically significant difference between data sets. With the exception of one slide, this difference is minimal, indicating consistent metric values.

5.2.2.2 Independent T-tests (Full Sample)

The ten osteon specific metrics were divided into pathological and healthy control groups. These groups were then compared to see if there was a statistically significant difference between the pathological and healthy control samples for any of the metric variables. This was done by using a Welch two sample independent t-test. A Welch two sample t-test was

used as there was unequal variance between the healthy set of metrics and the pathological set of metrics.

Table 5.9: Welch two sample t-test results comparing the complete healthy set with the complete pathological set

Results	OMaxL	OMinL	OPeri	OTArea	CArea	OArea	OCirc	CMaxL	CMinL	CCirc
t value	2.7563	0.18715	-0.90944	-0.39725	2.4604	-0.5317	-0.36434	2.7824	4.1266	5.2874
p-value	**0.0059**	0.8516	0.3632	0.6912	**0.0139**	0.595	0.7116	**0.0054**	**<0.0001**	**<0.0001**
95% confidence interval	2.5256 : 14.9694	-177.3952 : 214.8388	-526.4395 : 192.8515	-7911.636 : 5246.117	90.536 : 800.6157	-8322.864 : 4772.199	-0.0098 : 0.0067	1.3962 ; 8.0563	1.8828 : 5.2907	0.0123 : 0.0269
Healthy Sample Estimated Mean	245.9631	245.3245	656.1827	33484.14	4184.079	29303.06	0.8951	92.2381	53.2321	0.8332
Path Sample Estimated Mean	237.2156	226.6027	822.9777	34816.90	3738.503	31078.40	0.8967	87.5119	49.6454	0.8136

Of the ten variables tested, five exhibited a statistically significant difference between the healthy and pathological samples. These variables included osteon maximum length, canal area, canal maximum length, canal minimum length, and canal circularity.

5.2.2.3 Paired Independent T-tests (40 pairs, sex and age matched)

After all the metric variables were tested, 40 pairs of samples were compared. This was again done using an independent t-test, as due to the variability of the number of osteons per cross-section prevented a true paired t-test. Each of these pairs includes one pathological sample and one healthy control sample. These samples were paired based on age and sex, wherever possible. Some healthy controls were repeated, as the pairs were created based on the best match, rather than a one-to-one match across all samples. These samples were then further broken down into five age groups: under 30 years of age, ages 31-40, ages 41-50, ages 51-60, and over 60 years of age. Due to the distribution of the sample, there are fewer pairs in the

younger age groups, and more pairs in the older age groups. Note, when pairs are presented, the pathological sample appears first, followed by the healthy control sample.

Age Group 1: Under 30

Pair 1: A14 and CC53

The first pair to be compared was pathological sample A14, and healthy control CC53. A14 is from a male individual, aged 19. As there were no male healthy samples of analogous age to compare with, sample CC53 from a healthy 19-year-old female was selected. Below are the results of the comparative t-tests. There were no significant differences between the samples from the selected osteon metric variables.

Table 5.10: Pair 1 independent t-test results

Results	OMaxL	OMinL	OPeri	OTArea	CArea	OArea	OCirc	CMaxL	CMinL	CCirc
t value	0.47588	0.55034	0.77832	0.56846	0.22467	0.61669	-1.3531	0.96009	0.55515	-0.43465
p-value	0.6352	0.5832	0.4381	0.5709	0.8227	0.5387	0.1788	0.3393	0.58	0.6647
95% confidence interval	-21.2266: 34.6288	-13.2889: 23.5025	-42.9895: 98.5552	-5465.949: 9863.945	-1757.720: 2206.941	-4369.296: 8318.072	-0.0311: 0.0059	-12.3125: 35.4203	-7.0859: 12.5959	-0.0437: 0.028
A14 Sample Estimated Mean	244.9071	176.6064	671.0616	34934.56	3933.582	31000.98	0.9091	96.7470	52.7502	0.8306
CC53 Sample Estimated Mean	238.2060	171.4996	643.2787	32735.57	3708.972	29026.59	0.9218	85.1931	49.9952	0.8385

Pair 2: B1 and FC3

The next pair to be compared was pathological sample B1, and healthy control FC3. B1 is from a male individual, aged 24. Sample FC3 is from a healthy 28-year-old male. Below are the results of the comparative t-tests. Only the variable canal circularity (CCirc) showed a statistically significant difference between the samples.

Table 5.11: Pair 2 independent t-test results

Results	OMaxL	OMinL	OPeri	OTArea	CArea	OArea	OCirc	CMaxL	CMinL	CCirc
t value	0.02668	-0.2725	-0.0552	-1.1176	-1.3068	-0.8135	-0.7794	-0.8775	-1.3501	-2.0434
p-value	0.9788	0.7866	0.9562	0.2708	0.2002	0.4208	0.4393	0.3857	0.1854	**0.045**
95% confidence interval	-48.3283: 49.6262	-31.6503: 24.1259	-122.8233 : 116.2284	-24397.043 : 7046.559	-9673.271 : 2104.914	-17047.442 : 7265.316	-0.0521 : 0.023	-46.8937: 18.5319	-32.0039 : 6.4241	-0.11: -0.0001
B1 Sample Estimated Mean	276.9649	172.3393	725.5301	38072.36	3799.874	34272.49	0.8676	93.3316	49.0506	0.7891
FC3 Sample Estimated Mean	276.3160	176.1015	728.8025	46747.61	7584.052	39163.55	0.8822	107.5125	61.8405	0.8448

Age Group 2: 31-40

Pair 3: B12 and CC7

The third pair to be compared was pathological sample B12, and healthy control CC7. Sample B12 is from a female individual, aged 31. Sample CC7 is from a healthy 38-year-old female. Below are the results of the comparative t-tests. There were statistically significant results from six of the ten variables, including osteon max length (OMaxL), osteon perimeter (OPeri), canal area (CArea), osteon circularity (OCirc), canal minimum length (CMinL), and canal circularity (CCirc).

Table 5.12: Pair 3 independent t-test results

Results	OMaxL	OMinL	OPeri	OTArea	CArea	OArea	OCirc	CMaxL	CMinL	CCirc
t value	2.4317	0.9657	2.1068	0.5394	2.7176	0.13177	-2.383	1.7571	2.6105	-2.3691
p-value	**0.0160**	0.3353	**0.0364**	0.5901	**0.0077**	0.8953	**0.0184**	0.0807	**0.0103**	**0.0191**
95% confidence interval	4.5285: 43.5266	-5.8788: 17.1643	3.2323: 98.1398	-3894.568: 6830.325	306.3229: 1961.2318	-4661.581: 5329.784	-0.0423: -0.004	-1.2799: 21.9843	1.7194: 12.5456	-0.069: -0.0062
B12 Sample Estimated Mean	249.5261	166.7488	662.5972	32732.22	3323.239	29408.98	0.8918	82.9633	49.1482	0.8181
CC7 Sample Estimated Mean	225.4986	161.1061	611.9112	31264.34	2189.462	29074.88	0.9149	72.6111	42.0157	0.8557

Pair 4: B20 and CC152

The next pair to be compared was pathological sample B20, and healthy control CC152. Sample B20 is from a male individual, aged 33. Sample CC152 is from a healthy 34-year-old male. Below are the results of the comparative t-tests. There were no statistically significant differences between the two samples from the selected osteon metric variables.

Table 5.13: Pair 4 independent t-test results

Results	OMaxL	OMinL	OPeri	OTArea	CArea	OArea	OCirc	CMaxL	CMinL	CCirc
t value	-0.212	-0.1385	-0.0796	-0.3518	-0.4129	-0.279	-1.527	-0.0879	-0.7434	-1.0712
p-value	0.8325	0.8901	0.9367	0.7255	0.6804	0.7807	0.1292	0.9301	0.4586	0.286
95% confidence interval	-31.5034: 75.4092	-18.6554: 16.2142	-72.9472: 67.3034	-9798.983 : 6840.36	-2922.309 : 1913.069	-7888.421 : 5939.038	-0.0331 : 0.0043	-20.8118: 19.0416	-11.9936 : 5.4424	-0.0772 : 0.023
B20 Sample Estimated Mean	271.4267	187.3663	732.2250	40867.21	4376.37	36490.84	0.9055	102.5896	51.2810	0.7769
CC152 Sample Estimated Mean	274.4738	188.5868	735.0468	42346.52	4880.99	37465.53	0.9199	54.5567	54.5567	0.8041

Pair 5: A11 and CC7

The fifth pair to be compared was pathological sample A11, and healthy control CC7. Sample A11 is from a female individual, aged 35. Sample CC7 is from a healthy 38-year-old female. Below are the results of the comparative t-tests. There were three variables that showed statistically significant differences between the samples, including canal area (CArea), canal maximum length (CMaxL), and canal minimum length (CMinL).

Table 5.14: Pair 5 independent t-test results

Results	OMaxL	OMinL	OPeri	OTArea	CArea	OArea	OCirc	CMaxL	CMinL	CCirc
t value	2.8079	2.9752	2.4376	2.0035	1.4606	1.8683	-0.5927	0.7783	1.3035	-2.8289
p-value	**0.0057**	**0.0035**	**0.0167**	**0.0467**	0.1477	0.0633	0.5541	0.4374	0.1955	**0.0055**
95% confidence interval	8.8276: 50.7935	7.2815: 36.1536	20.6658 : 202.2483	93.9217: 12507.2214	-235.7814: 1543.5089	-316.8733: 11610.2888	-0.0205: 0.011	-6.3778: 14.6819	-1.9376: 9.353	-0.0818: -0.0145
A11 Sample Estimated Mean	255.3091	182.8236	723.3682	37564.91	2843.325	34721.59	0.9102	76.7632	45.7234	0.8075

CC7 Sample Estimated Mean	225.4986	161.1061	611.9112	31264.34	2189.462	29074.88	0.9149	72.61101	42.0157	0.8557

Pair 6: B31 and CC100

The sixth pair to be compared was pathological sample B31, and healthy control CC100. Sample B31 is from a male individual, aged 36. Sample CC100 is from a healthy 38-year-old male. Below are the results of the comparative t-tests. There were three variables that showed statistically significant differences between the samples, including osteon maximum length (OMaxL), osteon total area (OTArea), and osteon area (OArea).

Table 5.15: Pair 6 independent t-test results

Results	OMaxL	OMinL	OPeri	OTArea	CArea	OArea	OCirc	CMaxL	CMinL	CCirc
t value	-1.9913	-1.0095	-2.1383	-1.7633	1.6246	-2.9989	1.0547	0.3537	0.7819	1.8199
p-value	**0.049**	0.3152	**0.0349**	**0.0809**	0.109	**0.0033**	0.2932	0.7242	0.4359	0.0713
95% confidence interval	-55.5003: -0.1201	-6247.948 : 2034.022	-144.4918 : -5.4382	-14587.5469 : 858.5062	-472.1018: 4601.5127	-14961.856 : -3063.819	-0.0117 : 0.0385	-18.0453: 25.8787	-6.7735: 15.6056	-0.0038 : 0.0896
B31 Sample Estimated Mean	243.8297	167.674	655.2794	33372.14	6287.109	27085.03	0.9061	110.1242	60.773	0.8247
CC100 Sample Estimated Mean	271.6399	2274.637	730.2444	40236.66	4222.404	36097.87	0.8927	106.2074	56.3569	0.7818

Pair 7: B7 and CC7

The next pair to be compared was pathological sample B7, and healthy control CC7. Sample B7 is from a female individual, aged 37. Sample CC7 is from a healthy 38-year-old female. Below are the results of the comparative t-tests. Two of the variables returned statistically significant differences, including osteon circularity (OCirc) and canal circularity (CCirc).

Table 5.16: Pair 7 independent t-test results

Results	OMaxL	OMinL	OPeri	OTArea	CArea	OArea	OCirc	CMaxL	CMinL	CCirc
t value	1.7456	-0.6172	1.2804	-0.30282	0.56952	-0.3536	-3.3903	0.59782	-0.6097	-3.6355
p-value	0.08346	0.5381	0.2026	0.7624	0.5699	0.724	**0.0009978**	0.5508	0.5432	**0.000468**
95% confiden	-2.503509:	-15.68078	-17.85677:	-6396.113:	-289.3747:	-6369.896:	-0.05857776: -	-6.782382:	-4.824579:	-0.11109248 -

ce interval	39.777194	8: 8.217084	83.39838	4694.228	523.6005	4433.786	0.01533141	12.673190	2.553292	0.03255972
B7 Sample Estimated Mean	244.1354	157.3742	644.6820	30413.40	2306.575	28106.82	0.8779508	75.55649	40.88007	0.7838361
CC7 Sample Estimated Mean	225.4986	161.1061	611.9112	31264.34	2189.462	29074.88	0.9149054	72.61109	42.01571	0.8556622

Pair 8: FC14 and CC100

The eighth pair to be compared was pathological sample FC14, and healthy control CC100. Sample FC14 is from a male individual, aged 39. Sample CC100 is from a healthy 38-year-old-male. Below are the results of the comparative t-tests. Four of the variables returned statistically significant difference, including osteon perimeter (OPeri), osteon total area (OTArea), osteon area (OArea), and canal maximum length (CMaxL).

Table 5.17: Pair 8 independent t-test results

Results	OMaxL	OMinL	OPeri	OTArea	CArea	OArea	OCirc	CMaxL	CMinL	CCirc
t value	1.8162	1.0105	2.0447	2.3155	1.5696	2.3026	0.2437	2.5184	1.7507	1.4946
p-value	0.0733	0.3147	**0.0444**	**0.023**	0.1208	**0.0236**	0.808	**0.0137**	0.0831	0.14
95% confidence interval	-2.2768: 49.4626	-2031.782: 6250.183	1.7074: 131.9475	1067.18: 14027.80	-273.9705: 2305.3934	907.0753: 12323.7061	-0.033: 0.0258	4.9475: 42.147	-1.1316: 18.1153	-0.0951 : 0.0137
CC100 Sample Estimated Mean	271.6399	2274.6370	730.2444	40236.66	4222.404	36097.87	0.8927	106.2074	56.3569	0.7818
FC14 Sample Estimated Mean	248.047	165.4365	663.4170	32689.17	3206.692	29482.48	0.8963	82.6602	47.8651	0.8225

Pair 9: A2 and FC6

The next pair to be compared was pathological sample A2, and healthy control FC6. Sample A2 is from a female individual, aged 39. Sample FC6 is from a healthy 40-year-old female. Below are the results of the comparative t-tests. There were three variables that showed statistically significant differences between the samples, including canal area (CArea), canal maximum length (CMaxL), and canal minimum length (CMinL).

Table 5.18: Pair 9 independent t-test results

Results	OMaxL	OMinL	OPeri	OTArea	CArea	OArea	OCirc	CMaxL	CMinL	CCirc
t value	0.3822	0.1808	0.2855	0.4317	6.1083	-0.3008	-1.8515	4.5347	7.8382	0.3463
p-value	0.7029	0.8567	0.7757	0.6668	**<0.0001**	0.764	0.0662	**<0.0001**	**0.0001**	0.7296
95% confidence interval	-23.5185: 34.7875	-15.5676: 18.7035	-61.4024: 82.1277	-6182.364 : 9630.163	1926.001 : 3784.014	-8571.807 : 6309.591	-0.0461 : 0.0015	22.2885: 56.8776	16.7495 : 28.0802	-0.0412 : 0.0586
A2 Sample Estimated Mean	270.0996	178.5553	726.7970	39337.19	4754.209	34582.98	0.874	111.2070	60.0007	0.7971
FC6 Sample Estimated Mean	264.4651	176.9874	706.4343	37613.29	1899.202	35714.09	0.8964	71.634	37.5859	0.7884

Age Group 3: 41-50

Pair 10: B16 and CC184

The tenth pair to be compared is pathological sample B16 and healthy control CC184. B16 is from a male individual, aged 44. Sample CC184 is from a healthy 45-year-old male. Below are the results of the comparative t-tests. Only one of the variables returned a statistically significant result, for osteon maximum length (OMaxL).

Table 5.19: Pair 10 independent t-test results

Results	OMaxL	OMinL	OPeri	OTArea	CArea	OArea	OCirc	CMaxL	CMinL	CCirc
t value	1.9815	1.6775	1.6189	1.8294	1.3989	1.7239	1.6907	-0.1618	1.8647	1.701
p-value	**0.0497**	0.0955	0.1075	0.0693	0.1649	0.0868	0.093	0.8717	0.0645	0.0911
95% confidence interval	0.0442: 56.4974	-2.3493: 28.7843	-10.4686: 105.482	-441.8466: 11465.9901	-320.9356: 1856.9406	-692.8577: 10180.9962	-0.0035 : 0.0444	-12.0482 : 10.2249	-0.3482: 11.7968	-0.0065 : 0.0869
B16 Sample Estimated Mean	265.7569	176.3461	686.3228	35888.82	3455.861	32432.96	0.8955	82.8044	48.7217	0.8248
CC184 Sample Estimated Mean	237.4861	163.1286	638.8161	30376.75	2687.859	27688.89	0.875	83.716	42.9974	0.7846

Pair 11: A1 and CC184

The next pair to be compared was pathological sample A1, and healthy control CC184. Sample A1 is from a male individual, aged 45. Sample CC184 is from a healthy 45-year-old male. Below

are the results of the comparative t-tests. There were four variables that returned statistically significant differences between the samples. These included osteon maximum length (OMaxL), osteon minimum length (OMinL), osteon perimeter (OPeri), and osteon circularity (OCirc).

Table 5.20: Pair 11 independent t-test results

Results	OMaxL	OMinL	OPeri	OTArea	CArea	OArea	OCirc	CMaxL	CMinL	CCirc
t value	-2.9695	-2.449	-2.8675	-1.797	0.0902	-1.9556	2.9178	-1.7373	-0.3188	0.7126
p-value	**0.0035**	**0.0155**	**0.0048**	0.0744	0.9283	0.0524	**0.0042**	0.0844	0.7504	0.4774
95% confidence interval	-48.5345: -9.746	-31.1639: -3.328	-125.8012 : -23.1439	-9967.8001 : 472.7168	-901.5387 : 987.4340	-9631.3708 : 50.3922	0.0101 : 0.0527	-18.938: 1.2171	-6.7779: 4.8966	-0.0179 : 0.0594
A1 Sample Estimated Mean	208.3459	145.8827	564.3436	25629.21	2730.806	22898.40	0.9064	74.8556	42.0567	0.8004
CC184 Sample Estimated Mean	237.4861	163.1286	638.8161	30376.75	2687.859	27688.89	0.875	83.7161	42.9974	0.7846

Pair 12: B40 and CC184

The twelfth pair to be compared was pathological sample B40, and healthy control CC184. Sample B40 is from a male individual, aged 45. Sample CC184 is from a healthy 45-year-old male. Below are the results of the comparative t-tests. Six of the variables returned statistically significant results. These include osteon minimum length (OMinL), osteon perimeter (OPeri), osteon area (OArea), canal minimum length (CMinL), and canal circularity (CCirc).

Table 5.21: Pair 12 independent t-test results

Results	OMaxL	OMinL	OPeri	OTArea	CArea	OArea	OCirc	CMaxL	CMinL	CCirc
t value	-0.3393	-2.0747	-2.6815	-1.9155	1.4084	-2.7971	4.9311	-0.8857	2.0269	4.6773
p-value	0.7352	**0.0398**	**0.0082**	0.0574	0.1628	**0.0059**	**<0.0001**	0.3776	**0.0452**	**<0.0001**
95% confidence interval	-56.3536: 39.9181	-29.3834: -0.7132	-133.4806 : -20.2104	-10634.1170 : 165.8879	-490.5489: 2868.0637	-10963.572 : -1882.172	0.0324: 0.0759	-19.2736 : 7.3603	0.1644: 14.8448	0.0578: 0.1462
B40 Sample Estimated Mean	229.2684	148.0803	561.9706	25142.64	3876.616	21266.02	0.9292	77.7594	50.502	0.8848
CC184 Sample Estimated Mean	237.4861	163.1286	638.8161	30376.75	2687.859	27688.89	0.875	83.7161	42.9974	0.7846

Pair 13: A10 and CC194

The next pair to be compared was pathological sample A10, and healthy control CC194. Sample A10 is from a female individual, aged 49. Sample CC194 is from a healthy 46-year-old female. Below are the results of the comparative t-tests. All ten variables return statistically significant differences.

Table 5.22: Pair 13 independent t-test results

Results	OMaxL	OMinL	OPeri	OTArea	CArea	OArea	OCirc	CMaxL	CMinL	CCirc
t value	-5.2336	-7.5475	-6.0805	-6.0899	-4.5625	-5.8646	-4.4539	-4.3523	-6.9617	-3.1404
p-value	**<0.0001**	**<0.0001**	**<0.0001**	**<0.0001**	**<0.0001**	**<0.0001**	**<0.0001**	**<0.0001**	**<0.0001**	**0.0023**
95% confidence interval	-101.5433 : -45.8372	-93.9215: -54.9198	-296.1803 : -150.7805	-33612.12 : -17131.97	-8112.418 : -3205.593	-26361.81 : -13064.27	-0.082: -0.0315	-66.2108: -24.8175	-46.6906 : -26.03	-0.1369 : -0.0308
A10 Sample Estimated Mean	221.0757	136.2049	576.4706	24853.56	3312.407	21541.16	0.8515	90.7935	42.5459	0.7378
CC194 Sample Estimated Mean	294.7660	210.6255	799.9510	50225.61	8971.413	41254.2	0.9082	136.3076	78.9062	0.8217

Pair 14: A15 and CY191

The next pair to be compared was pathological sample A15, and healthy control CY191. Sample A15 is from a male individual, aged 49. Sample CY191 is from a healthy 48-year-old male. Below are the results of the comparative t-test. Eight of the ten variables returned statistically significant differences. These included osteon maximum length (OMaxL), osteon minimum length (OMinL), osteon perimeter (OPeri), osteon total area (OTArea), canal area (CArea), canal maximum length (CMaxL), and canal minimum length (CMinL).

Table 5.23: Pair 14 independent t-test results

Results	OMaxL	OMinL	OPeri	OTArea	CArea	OArea	OCirc	CMaxL	CMinL	CCirc
t value	-7.0264	-8.5783	-7.8562	-7.3257	-2.2442	-7.7105	0.4175	-3.5852	-2.9378	0.5182
p-value	**<0.0001**	**<0.0001**	**<0.0001**	**<0.0001**	**0.0262**	**<0.0001**	0.6769	**0.0005**	**0.0038**	0.6051

95% confidence interval	-117.0493 : -65.6809	-77.2641: -48.3509	-308.7989 : -184.735	-32489.64 : -18690.35	-3073.0611 : -195.8222	-30093.69 : -17817.41	-0.0144 : 0.0221	-49.61308 : -14.32959	-19.4257 : -3.8032	-0.0317 : 0.0542
A15 Sample Estimated Mean	222.6759	158.1452	604.2167	28726.46	2780.948	25945.51	0.9131	73.6687	44.2989	0.8402
CY191 Sample Estimated Mean	314.0410	220.9527	850.9878	54316.45	4415.390	49901.06	0.9092	105.64	55.9134	0.8289

Pair 15: B28 and CY191

The fifteenth pair to be compared was pathological sample B28, and healthy control CY191. B28 is from a male individual, aged 50. Sample CY191 is form a healthy 48-year-old male. Below are the results of the comparative t-test. Five of the variables returned statistically significant differences. These include osteon maximum length (OMaxL), osteon minimum length (OMinL), osteon perimeter (OPeri), osteon total area (OTArea), and osteon area (OArea).

Table 5.24: Pair 15 independent t-test results

Results	OMaxL	OMinL	OPeri	OTArea	CArea	OArea	OCirc	CMaxL	CMinL	CCirc
t value	-4.5805	-4.6543	-4.9018	-4.7632	0.1923	-5.3449	0.9147	-1.4302	0.1154	0.9358
p-value	**<0.0001**	**<0.0001**	**<0.0001**	**<0.0001**	0.8478	**<0.0001**	0.3618	0.1548	0.9083	0.351
95% confidence interval	-84.6366: -33.6278	-51.1783: -20.6839	-215.3601 : -91.6541	-23545.990 : -9740.847	-1641.553 : 1995.464	-23037.76 : -10602.99	-0.01: 0.0272	-31.8222 : 5.1042	-8.3894: 9.4304	-0.0219 : 0.0614
Sample Estimated Mean	254.9088	185.0217	697.4808	37673.03	4592.346	33080.69	0.9178	92.281	56.4339	0.8486
Sample Estimated Mean	314.0410	220.9527	850.9878	54316.45	4415.390	49901.06	0.9092	105.640	55.9134	0.8289

Age Group 4: 51-60

Pair 16: FC13 and CC87

The next pair to be compared was pathological sample FC13, and healthy control CC87. Sample FC13 is from a male individual, aged 52. Sample CC82 is from a healthy 53-year-old

male. Below are the results from the comparative t-test. Nine of the ten variables returned statistically significant differences. The only variable without a statistically significant difference between the samples was osteon circularity (OCirc).

Table 5.25: Pair 16 independent t-test results

Results	OMaxL	OMinL	OPeri	OTArea	CArea	OArea	OCirc	CMaxL	CMinL	CCirc
t value	3.3421	3.072	3.0146	2.7764	2.0833	2.4564	-0.3074	2.9756	2.6267	2.4914
p-value	**0.0016**	**0.0034**	**0.004**	**0.0083**	**0.0457**	**0.017**	0.7598	**0.0051**	**0.0133**	**0.0149**
95% confidence interval	24.7016: 99.0161	14.7658: 70.4858	52.1166: 260.2943	4733.44: 30030.74	157.985: 15393.277	1779.989: 17432.933	-0.0279 : 0.0205	15.4364: 81.3229	14.9313: 118.8974	0.0113 : 0.1017
CC87 Sample Estimated Mean	267.7133	189.2502	717.9651	42622.11	10109.163	32512.95	0.9094	117.9576	106.8015	0.8839
FC13 Sample Estimated Mean	205.8544	146.6244	561.7596	25240.02	2333.532	22906.48	0.9131	69.5779	39.8871	0.8274

Pair 17: B29 and CC87

The next pair to be compared was pathological sample B29 and healthy control CC87. Sample B29 is from a male individual, aged 53. Sample CC87 is from a healthy 53-year-old male. Below are the results of the comparative t-test. Only one of the variables returned a statistically significant result. This variable was canal circularity (CCirc).

Table 5.26: Pair 17 independent t-test results

Results	OMaxL	OMinL	OPeri	OTArea	CArea	OArea	OCirc	CMaxL	CMinL	CCirc
t value	-0.7841	-0.8334	-0.8102	-0.98	-1.5335	-0.07698	1.0691	-1.2117	-2.0915	-4.249
p-value	0.437	0.4094	0.4223	0.3332	0.1352	0.9389	0.2898	0.2335	0.0448	**<0.0001**
95% confidence interval	-49.8053: 21.8802	-37.0971: 15.4181	-139.338: 59.4735	-18512.395 : 6432.378	-13407.427 : 1897.538	-7715.145 : 7145.016	-0.0113 : 0.037	-52.2152: 13.1597	-105.3842 : -1.3078	-0.1249: -0.0455
B29 Sample Estimated Mean	253.7507	178.4107	678.0328	36582.10	4354.219	32227.88	0.9222	98.4299	53.4555	0.7986
SCC87 ample Estimated Mean	267.7133	189.2502	717.9651	42622.11	10109.163	32512.95	0.9094	117.9576	106.8015	0.8839

Pair 18: B41 and CC87

The next pair to be compared was pathological sample B41, and healthy control CC87. Sample B41 is from a male individual, aged 53. Sample CC87 is from a healthy 53-year-old male. Below are the results of the comparative t-test. Three of the results returned statistically significant differences. These include osteon area (OArea), osteon circularity (OCirc), and canal circularity (CCirc).

Table 5.27: Pair 18 independent t-test results

Results	OMaxL	OMinL	OPeri	OTArea	CArea	OArea	OCirc	CMaxL	CMinL	CCirc
t value	1.9603	0.8359	1.8087	1.1898	-1.3338	2.9625	2.1291	-0.8018	-1.827	-3.4945
p-value	0.0551	0.4075	0.0769	0.2401	0.192	**0.0041**	**0.0364**	0.4281	0.0774	**0.0007**
95% confidence interval	-0.8354: 74.1503	-15.7802: 38.1974	-10.2896: 193.8894	-5357.518: 20865.660	-12636.055: 2644.233	4180.704: 21319.260	-0.0575: -0.0019	-45.4106: 19.6925	-98.613: 5.4388	-0.0984: -0.0271
B41 Sample Estimated Mean	304.3707	200.4588	809.7650	50376.18	5113.252	45262.93	0.8797	105.0986	60.2143	0.8211
CC87 Sample Estimated Mean	267.7133	189.2502	717.9651	42622.11	10109.163	32512.95	0.9094	117.9576	106.8015	0.8839

Pair 19: CC22 and CC202

The next pair to be compared was pathological sample CC22, and healthy control CC202. Sample CC22 is from a male individual, aged 55. Sample CC202 is from a healthy 56-year-old male. Below are the results of the comparative t-test. Seven of the ten variables returned statistically significant differences. These include osteon maximum length (OMaxL), osteon minimum length (OMinL), canal area (CArea), osteon area (OArea), canal maximum length (CMaxL), and canal minimum length (CMinL).

Table 5.28: Pair 19 independent t-test results

Results	OMaxL	OMinL	OPeri	OTArea	CArea	OArea	OCirc	CMaxL	CMinL	CCirc
t value	2.0129	1.9993	-0.9944	1.4942	-2.7104	3.8832	1.0798	-2.7207	-3.0237	2.2836
p-value	**0.0473**	**0.0497**	0.326	0.1387	**0.0089**	**0.0002**	0.2829	**0.0085**	**0.0038**	**0.0252**
95% confidence interval	0.2817: 46.3072	0.0281: 36.8841	-32094.10: 10927.09	-1412.892: 9971.122	-5522.5217: -828.9733	3646.609: 11263.116	-0.0095: 0.0321	-40.1404: -6.1201	-35.5085: -7.1961	0.0043: 0.0636
CC22 Sample	204.4657	148.8354	558.4359	24004.08	2932.577	21071.51	0.9131	72.1645	47.5852	0.8994

Estimated Mean										
CC202 Sample Estimated Mean	181.1712	130.3793	11141.9410	19724.97	6108.324	13616.64	0.9018	95.2948	68.9375	0.8655

Pair 20: B33 and CY121

The twentieth pair to be compared was pathological sample B33, and healthy control CY121. Sample B33 is from a female individual, aged 56. Sample CY121 is from a 60-year-old female. Below are the results from the comparative t-tests. None of the variables tested returned statistically significant differences.

Table 5.29: Pair 20 independent t-test results

Results	OMaxL	OMinL	OPeri	OTArea	CArea	OArea	OCirc	CMaxL	CMinL	CCirc
t value	-0.8946	-0.7394	0.274	0.5224	-0.0178	0.5654	-1.2125	1.7253	0.394	-1.0477
p-value	0.3732	0.4607	0.7844	0.6022	0.9858	0.5728	0.227	0.0868	0.6941	0.2962
95% confidence interval	-182.4129: 69.064	-18.071: 8.2229	-41.1207: 54.3773	-5853.134: 10061.328	-1389.672: 1364.850	-5287.420: 9520.435	-0.0269: 0.0064	-1.8912: 27.7405	-5.3831: 8.0667	-0.0591: 0.0181
Sample Estimated Mean	236.3056	161.7866	630.3899	32995.44	3284.874	29710.57	0.9117	88.999	50.4624	0.8433
Sample Estimated Mean	292.9801	166.7107	623.7616	30891.35	3297.285	27594.06	0.9219	76.0744	49.1206	0.8638

Pair 21: FC18 and CY190

The next pair to be compared was pathological sample FC18, and healthy control CY190. Sample FC18 is from a male individual, aged 57. Sample CY190 is from a healthy 57-year-old male. Below are the results from the comparative t-tests. Six of the ten variables returned statistically significant differences, including osteon maximum length (OMaxL), osteon minimum length (OMinL), osteon perimeter (OPeri), osteon total area (OTArea), osteon area (OArea), and canal circularity (CCirc).

Table 5.30: Pair 21 independent t-test results

Results	OMaxL	OMinL	OPeri	OTArea	CArea	OArea	OCirc	CMaxL	CMinL	CCirc
t value	2.3045	3.4296	2.372	2.7488	0.94505	2.9642	1.2894	1.0456	1.5155	2.3071
p-value	**0.0228**	**0.0008**	**0.0191**	**0.0068**	0.3467	**0.0036**	0.2	0.2986	0.132	**0.0231**

95% confidence interval	4.0574: 53.2823	11.0273: 41.0752	12.4569: 137.4678	2614.031: 16035.645	-1422.241 : 4016.275	2669.542: 13386.100	-0.0078 : 0.0369	-27.4016: 88.2518	-2.3772: 17.9595	0.0081 : 0.1071
CY190 Sample Estimated Mean	279.2856	191.8360	738.5316	42278.99	6325.056	35953.93	0.9127	139.8149	65.4978	0.8483
FC18 Sample Estimated Mean	250.6157	165.7847	663.5692	32954.15	5028.040	27926.11	0.8981	109.3897	57.7066	0.7907

Pair 22: A13 and CY190

The next pair to be compared was pathological sample A13, and healthy control CY190. Sample A13 is from a male individual, aged 57. Sample CY190 is from a healthy 57-year-old male. Below are the results of the comparative t-test. Eight of the ten variables returned statistically significant differences. These include osteon maximum length (OMaxL), osteon minimum length (OMinL), osteon perimeter (OPeri), osteon total area (OTArea), canal area (CArea), osteon area (OArea), canal minimum length (CMinL), and canal circularity (CCirc).

Table 5.31: Pair 22 independent t-test results

Results	OMaxL	OMinL	OPeri	OTArea	CArea	OArea	OCirc	CMaxL	CMinL	CCirc
t value	-5.2773	-5.0951	-4.8561	-5.0655	-2.3576	-4.9379	-1.5979	-1.8362	-3.2431	-1.9985
p-value	**<0.0001**	**<0.0001**	**<0.0001**	**<0.0001**	**0.0206**	**<0.0001**	0.1135	0.0699	**0.0015**	**0.0484**
95% confidence interval	-86.7612: -39.4457	-59.1123: -26.0395	-217.1718: -91.4445	-23269.11: -10195.22	-5492.2833: -467.9264	-19261.900: -8242.221	-0.0443: 0.0048	-109.4765: 4.374	-24.4772: -5.9215	-0.0954: -0.0003
Sample Estimated Mean	216.1822	149.2601	584.2235	25546.82	3344.952	22201.87	0.8929	87.2636	50.2984	0.8004
Sample Estimated Mean	279.2856	191.8360	738.5316	42278.99	6325.056	35953.93	0.9127	139.8149	65.4978	0.8483

Pair 23: B27 and CC89

The next pair to be compared was pathological sample B27 and healthy control sample CC89. Sample B27 is from a male individual, aged 58. Sample B27 is from a healthy 58-year-old male. Below are the results of the comparative t-test. Seven of the ten variables returned

statistically significant differences. These include osteon maximum length (OMaxL), osteon minimum length (OMinL), osteon perimeter (OPeri), osteon total area (OTArea), osteon area (OArea), canal maximum length (CMaxL), and canal minimum length (CMinL).

Table 5.32: Pair 23 independent t-test results

Results	OMaxL	OMinL	OPeri	OTArea	CArea	OArea	OCirc	CMaxL	CMinL	CCirc
t value	-4.4392	-4.8237	-4.5334	-3.1229	-1.814	-3.4535	-0.5878	-3.2467	-2.5389	0.7871
p-value	**<0.0001**	**<0.0001**	**<0.0001**	**0.0023**	0.0734	**0.0007**	0.5574	**0.0015**	**0.0128**	0.4324
95% confidence interval	-76.7173: -29.4492	-56.2115: -23.4939	-210.1513: -82.4773	-25299.005: -5652.606	-7780.0319: 359.2088	-18501.104: -5029.683	-0.0233: 0.0126	-44.8081: -10.8868	-25.507: -3.1122	-0.0273: 0.0636
B27 Sample Estimated Mean	210.6399	145.0057	566.9143	25673.57	2768.685	22904.89	0.8989	80.5288	44.1058	0.8132
CC89 Sample Estimated Mean	263.7231	184.8584	713.2286	41149.38	6479.097	34670.28	0.9042	108.3763	58.4154	0.7951

Pair 24: FC15 and CC89

The next pair to be compared was pathological sample FC15 and healthy control sample CC89. Sample FC15 is from a male individual, aged 59. Sample CC89 is from a healthy 58-year-old male. Below are the results from the comparative t-test. Seven of the variables returned statistically significant differences. These include osteon maximum length (OMaxL), osteon minimum length (OMinL), osteon perimeter (OPeri), osteon total area (OTArea), osteon area (OArea), canal maximum length (CMaxL), and canal minimum length (CMinL).

Table 5.33: Pair 24 independent t-test results

Results	OMaxL	OMinL	OPeri	OTArea	CArea	OArea	OCirc	CMaxL	CMinL	CCirc
t value	2.5062	2.9847	2.7241	2.4636	1.76	2.5527	0.0809	3.0352	2.4225	-0.0564
p-value	**0.0135**	**0.0034**	**0.0073**	**0.0154**	0.0821	**0.0119**	0.9357	**0.0029**	**0.0172**	0.9551
95% confidence interval	6.7027: 56.9717	9.2275: 45.5212	25.3618: 159.9999	2352.527: 21789.858	-470.9129: 7709.1480	1896.715: 15007.436	-0.0208: 0.0226	8.9708: 42.6143	2.5684: 25.7906	-0.0518: 0.0489
CC89 Sample Estimated Mean	263.7231	184.8584	713.2286	41149.38	6479.097	34670.28	0.9042	108.3763	58.4154	0.7951
FC15 Sample	231.8859	157.4840	620.5478	29078.19	2859.979	26218.21	0.9034	82.5837	44.2359	0.7965

Estimated Mean										

Pair 25: FC16 and CC173

The next pair to be compared was pathological sample FC16, and healthy control sample CC173. Sample FC16 is from a male individual, aged 59. Sample CC173 is from a healthy 60-year-old male. Below are the results from the comparative t-test. Only one of the variables returned statistically significant differences, this variable was osteon minimum length (OMinL).

Table 5.34: Pair 25 independent t-test results

Results	OMaxL	OMinL	OPeri	OTArea	CArea	OArea	OCirc	CMaxL	CMinL	CCirc
t value	0.79329	2.013	1.1355	0.8034	0.3141	0.9775	0.4737	0.2605	0.8129	1.5393
p-value	0.4293	**0.0465**	0.2586	0.4235	0.7541	0.3305	0.6367	0.795	0.4181	0.1267
95% confidence interval	-18.8634: 44.049	0.3282: 41.6656	-33.9308: 125.0117	-6086.963: 14387.862	-4043.128 : 5563.945	-3483.467: 10263.550	-0.0199 : 0.0323	-21.7304: 28.3029	-8.57531 : 20.4931	-0.0114 : 0.0909
FC16 Sample Estimated Mean	262.7835	171.6636	698.3296	37991.05	6103.700	31887.35	0.8927	110.2789	59.3084	0.7845
CC173 Sample Estimated Mean	275.3764	192.6605	743.8701	42141.50	6864.108	35277.39	0.8989	113.5652	65.2673	0.8243

Pair 26: B24 and CC173

The next pair to be compared was pathological sample B24, and healthy control CC173. Sample B24 is from a male individual, aged 59. Sample CC173 is from a healthy 60-year-old male. Below are the results from the comparative t-test. Seven of the ten variables returned statistically significant differences. These include osteon maximum length (OMaxL), osteon minimum length (OMinL), osteon perimeter (OPeri), osteon total area (OTArea), osteon area (OArea), canal maximum length (CMaxL), and canal minimum length (CMinL).

Table 5.35: Pair 26 independent t-test results

Results	OMaxL	OMinL	OPeri	OTArea	CArea	OArea	OCirc	CMaxL	CMinL	CCirc
t value	2.6978	-3.8555	-3.1224	-2.7989	-1.4867	-3.0344	-0.6721	-2.6354	-2.2228	0.8929

p-value	**0.0083**	**0.0002**	**0.0024**	**0.0062**	0.1414	**0.0031**	0.5031	**0.0098**	**0.0287**	0.3741
95% confidence interval	-77.7592: -11.8255	-59.1221: -18.9369	-210.977: -46.9576	-22053.173 : -3749.701	-7403.647 : 1077.713	-16109.091 : -3367.849	-0.0335 : 0.0165	-58.5719: -8.2439	-29.165: -1.6399	-0.029: 0.0765
B24 Sample Estimated Mean	230.5840	153.6310	614.9028	29240.06	3701.141	25538.92	0.8904	80.1572	49.8649	0.848
CC173 Sample Estimated Mean	275.3764	192.6605	743.8701	42141.50	6864.108	35277.39	0.8989	113.5652	65.2673	0.8243

Pair 27: CC17 and CC173

The next pair to be compared was pathological sample CC17, and healthy control CC173. Sample CC17 is from a male individual, aged 60. Sample CC173 is from a healthy 60-year-old male. Below are the results of the comparative t-test. None of the variables returned statistically significant differences between the samples.

Table 5.36: Pair 27 independent t-test results

Results	OMaxL	OMinL	OPeri	OTArea	CArea	OArea	OCirc	CMaxL	CMinL	CCirc
t value	-0.3324	0.9938	-0.7733	0.9516	-1.0942	0.9673	-0.9059	-0.3237	-1.5898	0.0207
p-value	0.7403	0.3251	0.4413	0.3459	0.2772	0.338	0.3672	0.747	0.1152	0.9835
95% confidence interval	-41.7123: 29.7459	-3095.861: 9159.974	-127.4331 : 55.9967	-162679.8 : 455643.0	-6756.151 : 1963.071	-160250.5: 458006.7	-0.039: 0.0145	-40.2291: 28.9593	-24.8182 : 2.7458	-0.0511 : 0.0522
CC17 Sample Estimated Mean	269.3932	3224.7167	708.1519	188623.1	4467.568	184155.54	0.8867	107.9303	54.2311	0.8248
CC173 Sample Estimated Mean	275.3764	192.6605	743.8701	42141.5	6864.108	35277.39	0.8989	113.5652	65.2673	0.8243

Pair 28: CC6 and CY121

The next pair to be compared was pathological sample CC6, and healthy control CY121. Sample CC6 is from a female individual, aged 58. Sample CY121 is from a healthy 60-year-old female. Below are the results of the comparative t-test. Two of the variables returned

statistically significant differences. These were osteon circularity (OCirc), and canal circularity (CCirc).

Table 5.37: Pair 28 independent t-test results

Results	OMaxL	OMinL	OPeri	OTArea	CArea	OArea	OCirc	CMaxL	CMinL	CCirc
t value	-0.7878	0.7704	1.4858	0.8271	0.3306	0.8636	-2.4825	1.8094	0.2919	-2.7535
p-value	0.4327	0.442	0.139	0.4092	0.7413	0.3889	**0.0139**	0.072	0.7707	**0.0065**
95% confidence interval	-175.8281: 75.9031	-8.6903: 19.8281	-12.6959: 90.2273	-3377.039: 8252.607	-1277.061: 1790.862	-2800.334: 7162.100	-0.0338: -0.0039	-0.9569: 22.1277	-6.1781: 8.3238	-0.0898: -0.0148
CC6 Sample Estimated Mean	243.0176	172.2796	662.5273	33329.13	3554.186	29774.94	0.9031	86.6598	50.1935	0.8115
CY121 Sample Estimated Mean	292.9801	166.7107	623.7616	30891.35	3297.285	27594.06	0.9219	76.0744	49.1206	0.8638

Age Group 5: Over 60

Pair 29: CC193 and CC173

The twenty-eighth pair to be compared was pathological sample CC193, and healthy control CC173. Sample CC193 is from a male individual, aged 62. Sample CC173 is from a healthy 60-year-old male. Below are the results from the comparative t-test. Two of the ten variables returned statistically significant differences, including canal maximum length (CMaxL), and canal minimum length (CMinL).

Table 5.38: Pair 29 independent t-test results

Results	OMaxL	OMinL	OPeri	OTArea	CArea	OArea	OCirc	CMaxL	CMinL	CCirc
t value	1.5547	1.2544	1.4516	1.3981	1.7944	0.7842	0.3782	2.8101	2.854	-0.2331
p-value	0.1232	0.2124	0.1496	0.1657	0.0783	0.4345	0.7061	**0.0064**	**0.0058**	0.8162
95% confidence interval	-5.7051: 46.989	-6.517: 28.979	-17.9845: 116.2351	-2450.504: 14059.724	-410.9949: 7446.1500	-3486.553 : 8060.618	-0.0175 : 0.0257	8.6404: 50.885	5.1118: 28.9155	-0.0501 : 0.0396
CC193 Sample Estimated Mean	254.7344	181.4295	694.7448	36336.89	3346.531	32990.36	0.8948	83.8025	48.2536	0.8295
CC173 Sample Estimated Mean	275.3764	192.6605	743.8701	42141.50	6864.108	35277.39	0.8989	113.5652	65.2673	0.8243

Pair 30: FC9 and CC173

The next pair to be compared was pathological sample FC9 and healthy control sample CC173. Sample FC9 is from a male individual, aged 62. Sample CC173 is from a healthy 60-year-old male. Below are the results from the comparative t-test. Eight of the ten variables returned statistically significant differences. These include osteon maximum length (OMaxL), osteon minimum length (OMinL), osteon perimeter (OPeri), osteon total area (OTArea), canal area (CArea), osteon area (OArea), canal maximum length (OMaxL), and canal minimum length (CMinL).

Table 5.39: Pair 30 independent t-test results

Results	OMaxL	OMinL	OPeri	OTArea	CArea	OArea	OCirc	CMaxL	CMinL	CCirc
t value	4.2187	6.3949	5.0971	4.6029	2.4432	5.0715	0.9285	3.2733	4.8398	1.0453
p-value	**<0.0001**	**<0.0001**	**<0.0001**	**<0.0001**	**0.0179**	**<0.0001**	0.355	**0.0015**	**<0.0001**	0.2979
95% confidence interval	31.7447: 88.0053	36.2181: 68.9212	106.3132 : 241.7834	10282.32 : 26001.79	851.1979: 8652.5824	8146.418: 18633.910	-0.0136 : 0.0377	14.5956: 59.7266	16.3518 : 39.4168	-0.0268 : 0.0869
FC9 Sample Estimated Mean	215.5014	140.0908	569.8218	23999.45	2112.218	21887.23	0.8869	76.4041	37.383	0.7942
CC173 Sample Estimated Mean	275.3764	192.6605	743.8701	42141.50	6864.108	35277.39	0.8989	113.5652	65.2673	0.8243

Pair 31: CC15 and CY202

The thirtieth pair to compared was pathological sample CC15, and healthy control CY202. Sample CC15 is from a male individual, aged 63. Sample CY202 is from a healthy 68-year-old male. Below are the results of the comparative t-test. Four of the variables returned statistically significant differences, including osteon perimeter (OPeri), osteon total area (OTArea), osteon area (OArea), and canal minimum length (CMinL).

Table 5.40: Pair 31 independent t-test results

Results	OMaxL	OMinL	OPeri	OTArea	CArea	OArea	OCirc	CMaxL	CMinL	CCirc
t value	1.6238	-0.2369	2.421	2.0158	-1.133	2.3783	1.3022	-1.9209	-2.4207	-0.2266

p-value	0.1084	0.813	**0.0176**	**0.0468**	0.2589	**0.0197**	0.1984	0.0575	**0.0168**	0.8211
95% confidence interval	-4.4644 44.0047	-31.3621: 24.6382	13.4749: 137.4604	81.4475: 11329.5888	-1170.8235 : 317.0373	1003.566: 11261.256	-0.1101 : 0.5176	-22.425: 0.3581	-10.1985 : -1.0272	-0.0359 : 0.0285
Sample Estimated Mean	211.9880	144.1163	597.5261	26328.27	2391.094	23937.18	1.0806	65.8109	39.5474	0.8558
Sample Estimated Mean	192.2178	147.4782	522.0585	20622.76	2817.987	17804.77	0.8768	76.8444	45.1602	0.8595

Pair 32: CC45 and CC86

The next pair to be compared was pathological sample CC45, and healthy control sample CC86. Sample CC45 is from a female individual, aged 64. Sample CC86 is from a healthy 65-year-old female. Below are the results from the comparative t-test. Six of the ten variables returned statistically significant differences. These include osteon minimum length (OMinL), osteon perimeter (OPeri), osteon total area (OTArea), canal area (CArea), osteon area (OArea), and canal minimum length (CMinL).

Table 5.41: Pair 32 independent t-test results

Results	OMaxL	OMinL	OPeri	OTArea	CArea	OArea	OCirc	CMaxL	CMinL	CCirc
t value	1.7291	2.6214	2.1505	2.6088	2.182	2.5785	1.4407	1.756	2.3156	-0.2744
p-value	0.08993	**0.0115**	**0.0365**	**0.0123**	**0.035**	**0.0131**	0.154	0.0863	**0.0253**	0.7847
95% confidence interval	-6.0736: 81.2968	6.306: 47.5719	7.0297: 207.3902	3093.074: 24067.953	282.7964: 7342.1783	2150.193 17385.860	-0.0087 : 0.054	-4.0784: 58.844	2.0346: 29.3486	-0.0547 : 0.0415
CC45 Sample Estimated Mean	260.8061	177.2105	698.3643	39091.85	6938.500	32153.35	0.9101	109.3567	63.5639	0.8374
CC86 Sample Estimated Mean	223.1944	150.2715	591.1543	25511.34	3126.013	22385.32	0.8875	81.9739	47.8723	0.844

Pair 33: FC2 and CY202

The next pair to be compared was pathological sample FC2, and healthy control sample CY202. Sample FC2 is from a male individual, aged 68. Sample CY202 is from a healthy 68-year-old male. Below are the results from the independent t-test. Only two of the variables

returned statistically significant differences. These are osteon area (OArea), and canal circularity (CCirc).

Table 5.42: Pair 33 independent t-test results

Results	OMaxL	OMinL	OPeri	OTArea	CArea	OArea	OCirc	CMaxL	CMinL	CCirc
t value	-1.7559	-0.0676	-1.7682	-1.828	1.5412	-2.2611	-1.6759	1.1105	0.7941	2.072
p-value	0.0825	0.9462	0.0805	0.0707	0.1256	**0.0263**	0.0966	0.2698	0.4297	**0.0409**
95% confidence interval	-37.5693: 2.3184	-28.6021: 26.7071	-105.2404 : 6.1493	-9537.8863 : 392.5443	-178.227: 1437.181	-9775.4687 : -628.8274	-0.0411 : 0.0034	-5.3825: 19.0169	-4.1356: 9.6169	0.0017 : 0.0783
FC2 Sample Estimated Mean	209.8433	147.4782	522.0585	20622.76	2817.987	17804.77	0.8768	76.8444	45.1602	0.8595
CY202 Sample Estimated Mean	192.2178	148.4257	571.6040	25195.43	2188.510	23006.92	0.8957	70.0271	42.4196	0.8195

Pair 34: CC27 and CY39

The next pair to be compared was pathological sample CC27, and healthy control CY39. Sample CC27 is from a male individual, aged 75. Sample CY39 is from a healthy 75-year-old male. Below are the results from the comparative t-test. None of the variables returned a statistically significant difference.

Table 5.43: Pair 34 independent t-test results

Results	OMaxL	OMinL	OPeri	OTArea	CArea	OArea	OCirc	CMaxL	CMinL	CCirc
t value	-0.4969	-1.1645	-0.5264	-0.5384	-1.3243	-0.3178	-1.7958	-1.4738	-1.4231	-1.5171
p-value	0.6207	0.248	0.6002	0.5918	0.1883	0.7515	0.077	0.1444	0.1583	0.1324
95% confidence interval	-32.9775: 19.8142	-28.6055: 7.5042	-85.243: 49.6184	-8016.651: 4603.430	-1968.598: 392.215	-6677.259: 4840.422	-0.0425: 0.0022	-22.583: 3.3615	-13.5918: 2.2492	-0.0625: 0.0083
CC27 Sample Estimated Mean	227.4267	156.1222	609.5986	28638.66	3198.885	25439.78	0.8937	80.2929	49.4599	0.8471
CY39 Sample Estimated Mean	234.0084	166.6728	627.4110	30345.27	3987.076	26358.20	0.9138	89.9037	55.1312	0.8742

Pair 35: CC196 and CY39

The next pair to be compared was pathological sample CC196, and healthy control sample CY39. Sample CC196 is from a male individual, aged 76. Sample CY39 is from a healthy 75-year-old male. Below are the results from the comparative t-test. All ten variables returned statistically significant differences between the samples.

Table 5.44: Pair 35 independent t-test results

Results	OMaxL	OMinL	OPeri	OTArea	CArea	OArea	OCirc	CMaxL	CMinL	CCirc
t value	-5.1968	-5.8727	-4.5092	-4.7211	-5.3999	-4.095	-5.8153	-7.4022	-6.9713	-4.0135
p-value	**<0.0001**	**<0.0001**	**<0.0001**	**<0.0001**	**<0.0001**	**<0.0001**	**<0.0001**	**<0.0001**	**<0.0001**	**0.0001**
95% confidence interval	-72.077: -32.325	-60.7111: -30.0823	-171.1416: -66.7353	-16015.009: -6558.044	-3160.927: -1462.410	-13311.287: -4638.429	-0.1586: -0.0775	-42.9290: -24.8232	-26.4856: -14.7776	-0.1466: -0.0495
CC196 Sample Estimated Mean	181.8074	121.2761	508.4725	19058.75	1675.408	17383.34	0.7958	56.0276	34.4996	0.7761
CY39 Sample Estimated Mean	234.0084	166.6728	627.4110	30345.27	3987.076	26358.20	0.9138	89.9037	55.1312	0.8742

Pair 36: CC169 and CY39

The thirty-fifth pair to be compared was pathological sample CC169 and healthy control CY39. Sample CC169 is from a male individual, aged 78. Sample CY39 is from a healthy 75-year-old male. Below are the results from the comparative t-test. Eight of the ten variables returned statistically significant differences. These include osteon maximum length (OMaxL), osteon minimum length (OMinL), osteon perimeter (OPeri), osteon total area (OTArea), osteon area (OArea), canal maximum length (CMaxL), and canal minimum length (CMinL).

Table 5.45: Pair 36 independent t-test results

Results	OMaxL	OMinL	OPeri	OTArea	CArea	OArea	OCirc	CMaxL	CMinL	CCirc
t value	-4.3902	-6.2825	-3.5233	-4.3876	-3.2566	-4.1827	0.81767	-4.1749	-4.612	-1.852
p-value	**<0.0001**	**<0.0001**	**0.0007**	**<0.0001**	**0.0015**	**<0.0001**	0.4162	**<0.0001**	**<0.0001**	0.0682
95% confidence interval	-70.8063: -26.6297	-59.1918: -30.7422	-160.0334: -44.4524	-15467.426: -5835.257	-2448.8864: -596.4327	-13461.722: -4795.641	-0.0107: 0.0256	-33.678: -11.9642	-21.7361: -8.6618	-0.0773: 0.0029

CC169 Sample Estimated Mean	185.2904	121.7059	525.1681	19693.93	2464.417	17229.51	0.9213	67.0825	39.9322	0.8369
CY39 Sample Estimated Mean	234.0084	166.6728	627.4110	30345.27	3987.076	26358.20	0.9138	89.9037	55.1312	0.8742

Pair 37: CC23 and CC187

The next pair to be compared was pathological sample CC23, and healthy control CC187. Sample CC23 is from a male individual, aged 80. Sample CC187 is from a healthy 81-year-old male. Below are the results from the comparative t-test. Only two of the variables returned statistically significant differences, including canal area (CArea), and canal maximum length (CMaxL).

Table 5.46: Pair 37 independent t-test results

Results	OMaxL	OMinL	OPeri	OTArea	CArea	OArea	OCirc	CMaxL	CMinL	CCirc
t value	1.2604	1.8963	-0.45	0.4543	-2.4059	1.3455	1.3394	-2.0419	-1.5053	1.1583
p-value	0.209	0.0594	0.6535	0.6502	**0.0173**	0.18	0.1817	**0.0426**	0.1338	0.2479
95% confidence interval	-6.1753: 28.0621	-0.4418: 22.5249	-157.3897 : 99.0796	-3423.175 : 5470.709	-2661.3906 : -261.4309	-1157.134 : 6127.490	-0.0047 : 0.0244	-23.1028 : -0.3982	-10.9127 : 1.4633	-0.0117 : 0.045
CC23 Sample Estimated Mean	211.5538	151.3811	635.3844	27034.30	4566.804	22467.49	0.9149	92.6854	54.0697	0.8281
CC187 Sample Estimated Mean	222.4972	162.4226	606.2294	28058.06	3105.394	24952.67	0.9248	80.935	49.3449	0.8448

Pair 38: CC203 and CC12

The next pair to be compared was pathological sample CC203, and healthy control sample CC12. Sample CC203 is from a male individual, aged 85. Sample CC12 is from a healthy 80-year-old male. Below are the results from the comparative t-test. Only one of the variables returned a statistically significant difference. This was the osteon circularity (OCirc).

Table 5.47: Pair 38 independent t-test results

Results	OMaxL	OMinL	OPeri	OTArea	CArea	OArea	OCirc	CMaxL	CMinL	CCirc

t value	0.4811	-1.6139	0.0372	-0.9119	-0.7491	-0.8536	-2.4431	0.1723	-1.8953	-0.9616
p-value	0.6318	0.1104	0.9704	0.3645	0.4559	0.3958	**0.01741**	0.8638	0.06165	0.3395
95% confidence interval	-31.2988: 51.2381	-43.367: 4.5158	-100.2494 : 104.0671	-15513.011 : 5760.307	-3882.385 : 1758.322	-12703.734 : 5075.094	-0.0814: -0.0081	-25.5958: 30.4195	-21.8668 : 0.5327	-0.0841 : 0.0294
CC203 Sample Estimated Mean	282.7163	198.4736	753.7134	45850.74	6656.782	39193.95	0.9054	113.8621	70.1197	0.8334
CC12 Sample Estimated Mean	292.6859	179.0480	755.6223	40974.38	5594.750	35379.63	0.8606	116.2740	59.4526	0.806

Pair 39: CC189 and CC195

The next pair to be compared was pathological sample CC189, and healthy control sample CC195. Sample CC189 is from a male individual, aged 94. Sample CC195 is from a healthy 98-year-old female. Below are the results from the comparative t-test. Only two of the ten variables returned statistically significant differences. These include osteon circularity (OCirc), and canal minimum length (CMinL).

Table 5.48: Pair 39 independent t-test results

Results	OMaxL	OMinL	OPeri	OTArea	CArea	OArea	OCirc	CMaxL	CMinL	CCirc
t value	-0.7645	-1.7343	0.1669	0.5695	-1.0786	0.9155	-10.58	-1.8948	-3.4828	0.9857
p-value	0.4462	0.0859	0.8678	0.5702	0.2834	0.362	**<0.0001**	0.0608	**0.0008**	0.3279
95% confidence interval	-28.3396: 12.5634	-24.9479: 1.675	-48.4575: 57.3677	-3052.419 : 5512.946	-1714.8346 : 507.0524	-2137.051 : 5805.360	-0.2249: -0.1537	-23.6821 : 0.5334	-20.995: -5.7312	-13.2153 : 38.9719
CC189 Sample Estimated Mean	188.4756	129.3649	537.7561	21991.60	2323.625	19667.97	0.7245	61.5343	36.4399	13.7443
CC195 Sample Estimated Mean	196.3637	141.0013	533.3010	20761.33	2927.516	17833.82	0.9139	73.1086	49.803	0.866

Pair 40: CC45 and CY194

The final pair to be compared was pathological sample CC45, and healthy control CY194. Sample CC45 is from a female individual, aged 64. Sample CY194 is from a healthy 65-year-old female. Below are the results from the comparative t-test. All but two of the variables

returned statistically significant differences. These included osteon maximum length (OMaxL), osteon minimum length (OMinL), osteon perimeter (OPeri), osteon total area (OTArea), canal area (CArea), osteon area (OArea), osteon circularity (OCirc), and canal minimum length (CMinL).

Table 5.49: Pair 40 independent t-test results

Results	OMaxL	OMinL	OPeri	OTArea	CArea	OArea	OCirc	CMaxL	CMinL	CCirc
t value	2.1897	2.6971	2.4545	2.8354	2.3613	2.8114	2.3974	1.9052	2.2588	-0.1401
p-value	**0.0344**	**0.0098**	**0.0184**	**0.0071**	**0.0234**	**0.0074**	**0.0195**	0.064	**0.0288**	0.8891
95% confidence interval	3.4831: 86.4745	6.7633: 46.6918	20.728: 212.9475	4142.75: 24671.71	583.1881: 7564.8706	2919.359: 17747.046	0.0059 : 0.0648	-1.7827: 60.2219	1.6721: 29.1494	-0.0483 : 0.042
CC45 Sample Estimated Mean	260.8061	177.2105	698.3643	39091.85	6938.500	32153.35	0.9101	109.3567	63.5639	0.8374
CY194 Sample Estimated Mean	215.8273	150.4830	581.5266	24684.62	2864.471	21820.15	0.8748	80.1371	48.1532	0.8406

5.2.2.4 Metric Mean Values vs Age

Once the osteon metrics were tested for significance between pathological and healthy controls using complete sets of data, the metrics were further evaluated using mean values. Mean values were calculated by averaging all the measurements of each metric. This was done for each sample. From there, the metric means were evaluated for correlations, as well as through regression analysis. Both types of analyses were done separately for the pathological samples, and the healthy controls, to show the changes in correlation and significance between groups. For both the correlation and regression analysis the primary comparative factor was age.

5.2.2.4.1 Correlations

As for the standard histological analysis, correlations were done using Spearman's r correlations. These were then converted to give *p*-values for significance. Full tables of both Spearman's r correlations and converted *p*-value correlations are available in the Appendix.

Again, while correlation does not equal causation, it provides a starting point from which to further analyse the data, such as with Regression Analysis.

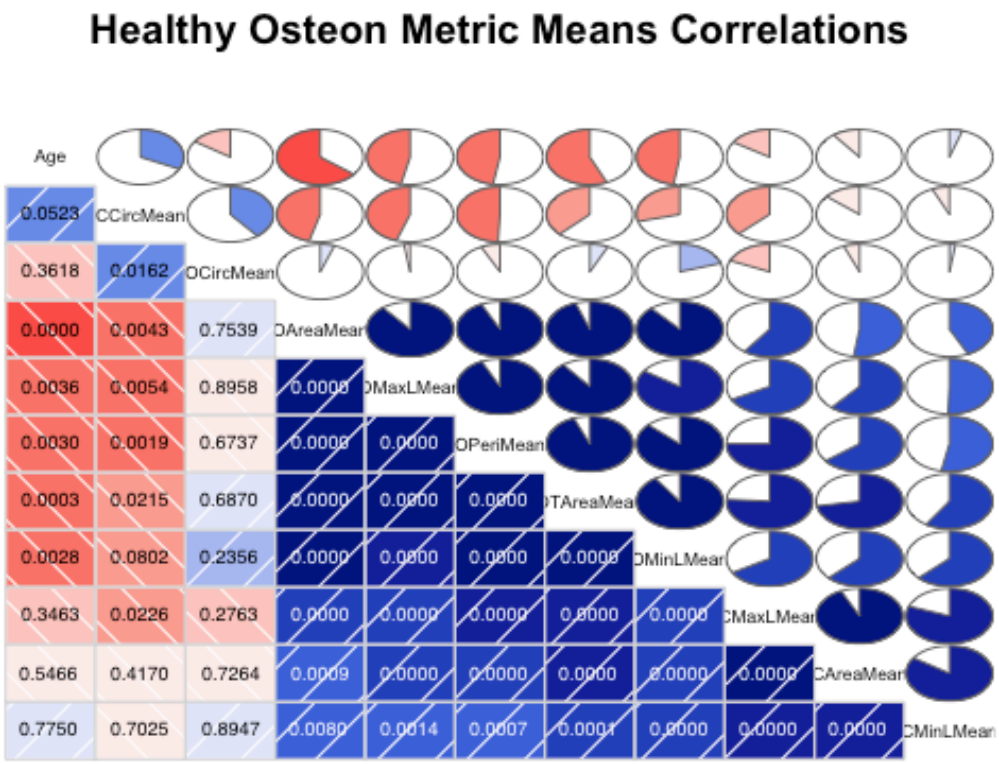

Figure 5.29: Heat map showing p-value correlations between Age and osteon metric means for healthy control samples

As in the section on correlations for the standard histological analysis, a heat map with integrated pie charts was used to illustrate the correlations between age and the various osteon metric means. While there are some very interesting correlations between the various osteon metrics, of primary interest for the purposes of this study are the correlations with age. The strongest correlations with age were (in order) osteon area, osteon total area, osteon minimum length, osteon perimeter, and osteon maximum length. All of these correlations happened to be negative, as indicated by the red colour on the heat map. Using Spearman's r, osteon area had a correlation of -0.64 (*p*-value <0.0001) with age, osteon total area had a correlation of -0.56 (*p*-value 0.0003), osteon minimum length had a correlation of

-0.48 (*p*-value of 0.0028), osteon perimeter had a correlation of -0.47 (*p*-value of 0.003), and osteon maximum length also had a correlation of -0.47 (*p*-value of 0.0036). All other correlations with age were not statistically significant.

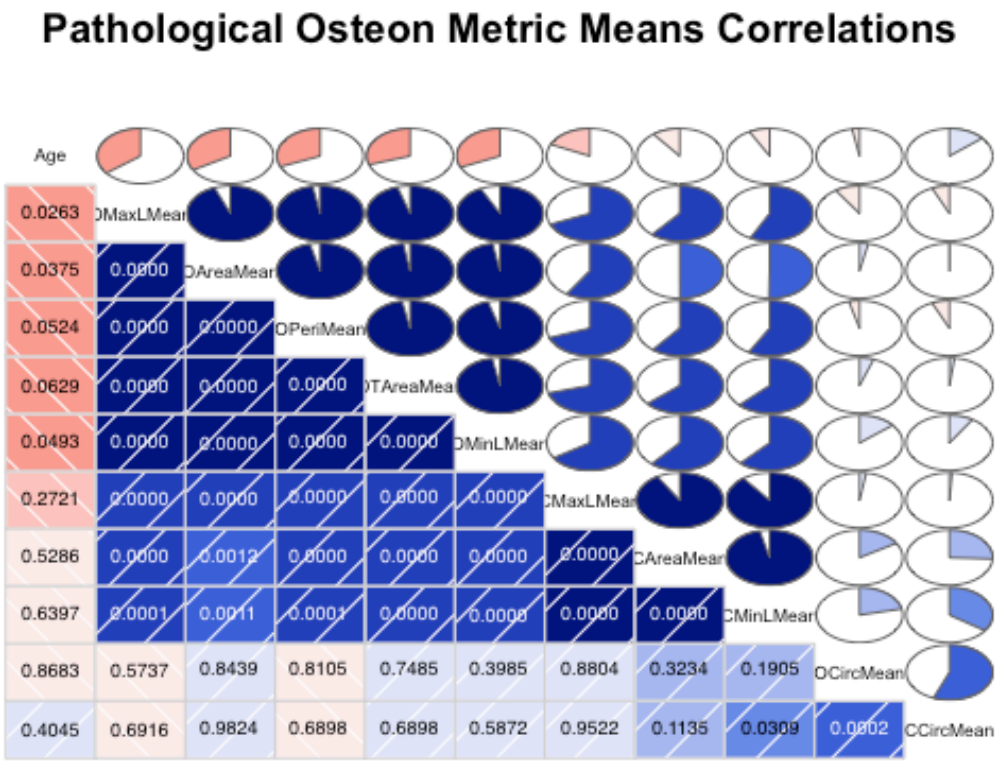

Figure 5.30: Heat map showing p-value correlations between Age and osteon metric means for pathological samples

As in the previous image, a heat map was used to illustrate the correlations between age and the various osteon metric means of the pathological samples. Once again, there are some interesting correlations between osteon metrics means, but for the purposes of this study, correlations with age were the main focus. Unlike the healthy control samples, the pathological samples appear to have much weaker correlations with age. Only three of the ten osteon metrics had a statistically significant correlation with age. These were (in order) osteon maximum length, osteon area, and osteon minimum length. Again, all of these correlations were negative, as shown by the colour of the heat map. Using Spearman's r

osteon maximum length had a correlation of -0.36 (*p*-value 0.0263) with age, osteon area had a correlation of -0.33 (*p*-value 0.0375), and osteon minimum length had a correlation of -0.32 (*p*-value 0.0493). All other correlations with age were not statistically significant.

5.2.2.4.2 Regression Analysis

Building on the correlations between age and the five statistically significant osteon metrics from the correlations. Regression analysis was done on both the pathological and healthy samples and plotted to show the distributions and lines of regression for each. Full regression outputs can be found in the Appendix.

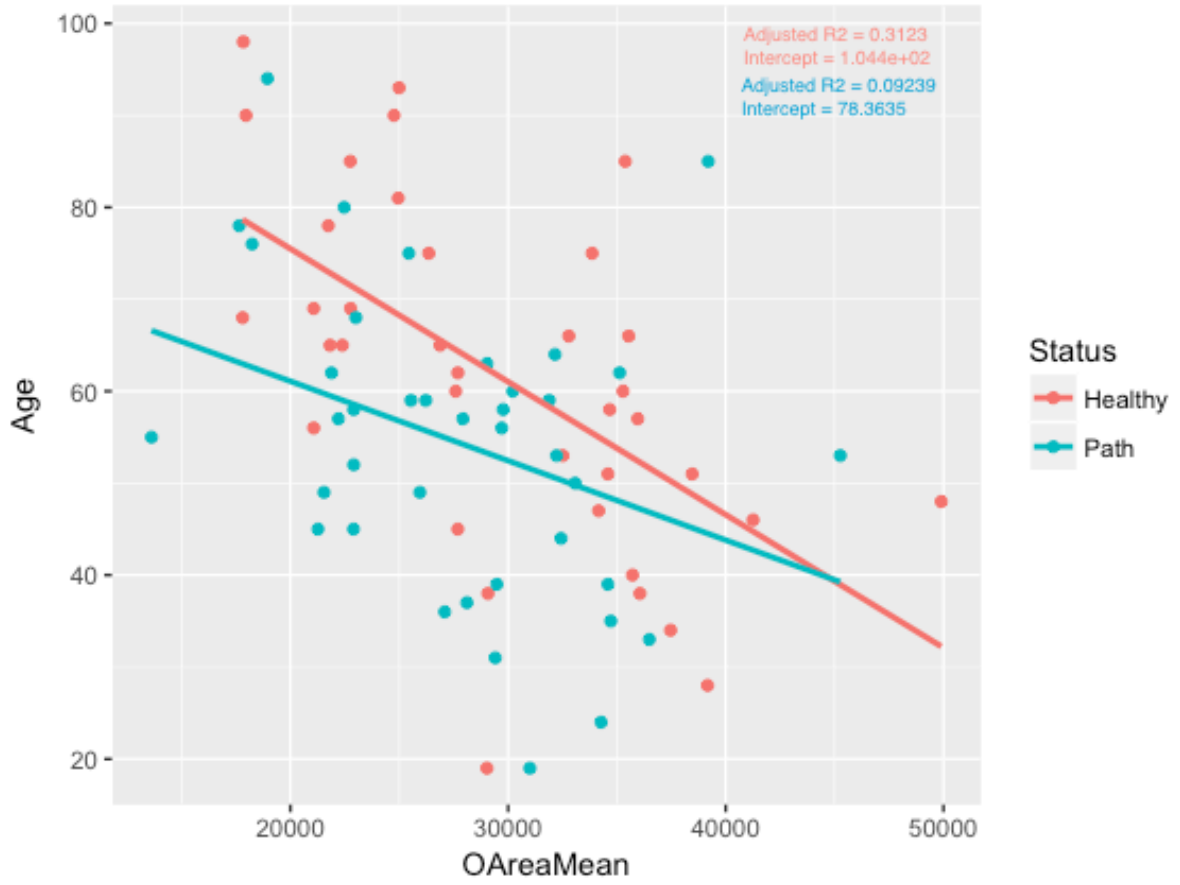

Figure 5.31: Scatterplot showing the distribution and lines of regression of osteon area metric means compared with Age

The above image is a scatterplot showing the distribution of both healthy and pathological samples with regard to the Age and osteon area metric means. The downward slant of the

regression lines shows the negative correlation between age and osteon area. This also shows the red regression line (healthy) as a better fit to the line of regression than the blue regression line (blue). Included in the results from this calculation were, coefficients, residual standard error, multiple R-squared, adjusted R-square, and *p*-value.

First, regression for the healthy control samples was calculated. The Estimate coefficient was calculated as intercept 104.4 and slope -1.446e-03. The Standard Error coefficient was calculated as from the intercept 10.63 and from the slope 3.473e-04. Following the coefficients, Residual Standard Error was calculated as 15.65. Multiple R-squared was calculated as 0.3314, and Adjusted R-squared was calculated as 0.3123. Finally, *p*-value was calculated as 0.0002.

Next, regression for the pathological samples was calculated. First, coefficients were calculated. The Estimate coefficient was calculated as intercept 78.3635 and slope -0.0009. The Standard Error coefficient was calculated as 11.1873 from the intercept, and 0.0003916 from the slope. Following the coefficients, Residual Standard Error was calculated as 15.65. Multiple R-squared was calculated as 0.1163, and Adjusted R-squared was calculated as 0.0924. Finally, the *p*-value was calculated as 0.0337.

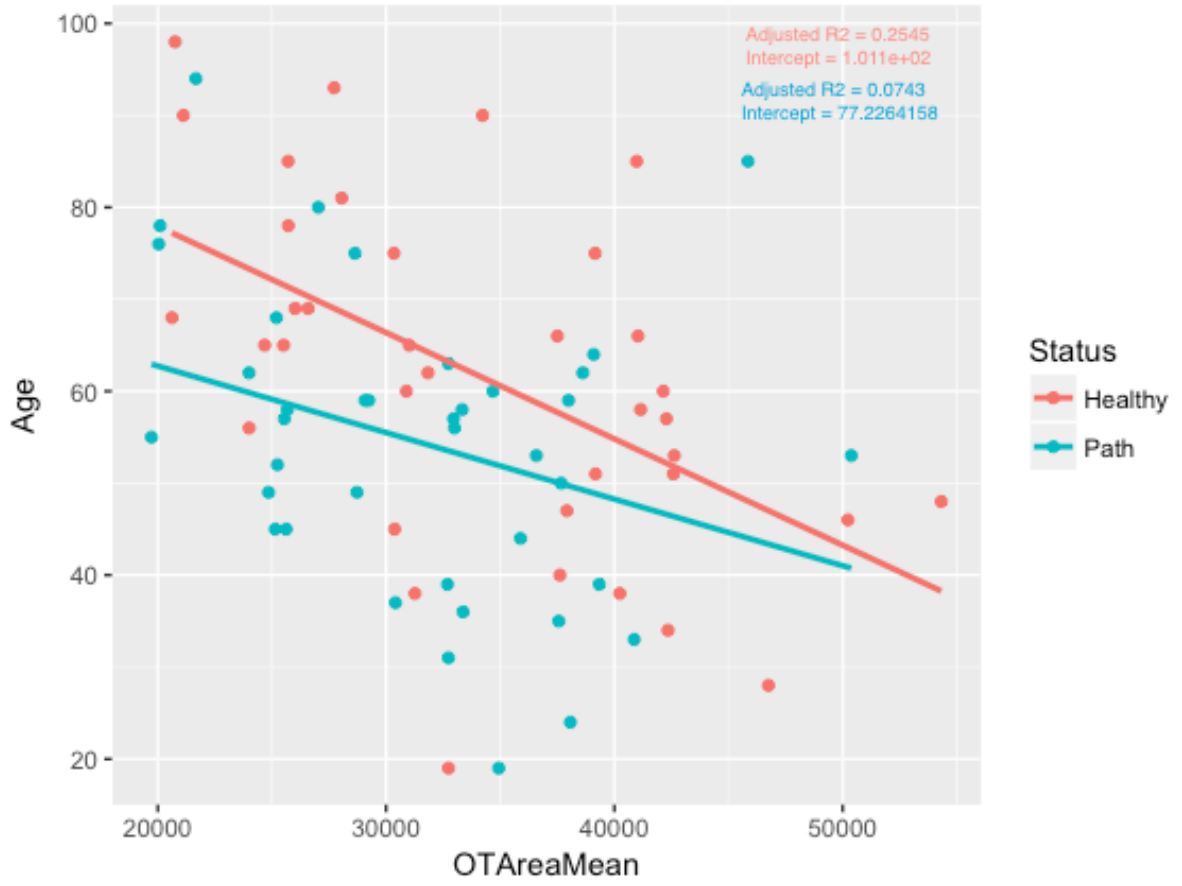

Figure 5.32: Scatterplot showing the distribution and lines of regression of osteon total area metric means compared with Age

The above image is a scatterplot showing the distribution of both healthy and pathological samples with regard to the age and osteon total area metric means. This shows the red regression line (healthy) as a better fit to the line of regression than the blue regression line (pathological). As with the regressions for age and osteon area metric means, regression for healthy control samples were calculated first, and then calculated for the pathological samples.

Regression for the healthy control samples was calculated. First, the coefficients were calculated. The Estimate coefficient was calculated as intercept 1.011e+02 and slope -1.156e-03. The Standard Error coefficient was calculated as from the intercept 1.119e+01 and from the slope 3.172e-04. Following the coefficients, Residual Standard Error was calculated as

16.29. Multiple R-squared was calculated as 0.2752, and Adjusted R-squared was calculated as 0.2545. Finally, *p*-value was calculated as 0.0009.

Next, regression for the pathological samples was calculated. First, four coefficients were calculated. The Estimate coefficient was calculated as intercept 77.2264 and slope -0.0007. The Standard Error coefficient was calculated as 11.6661 from the intercept, and 0.0004 from the slope. Following the coefficients, Residual Standard Error was calculated as 15.81. Multiple R-squared was calculated as 0.0987, and Adjusted R-squared was calculated as 0.0743. Finally, the *p*-value was calculated as 0.0515.

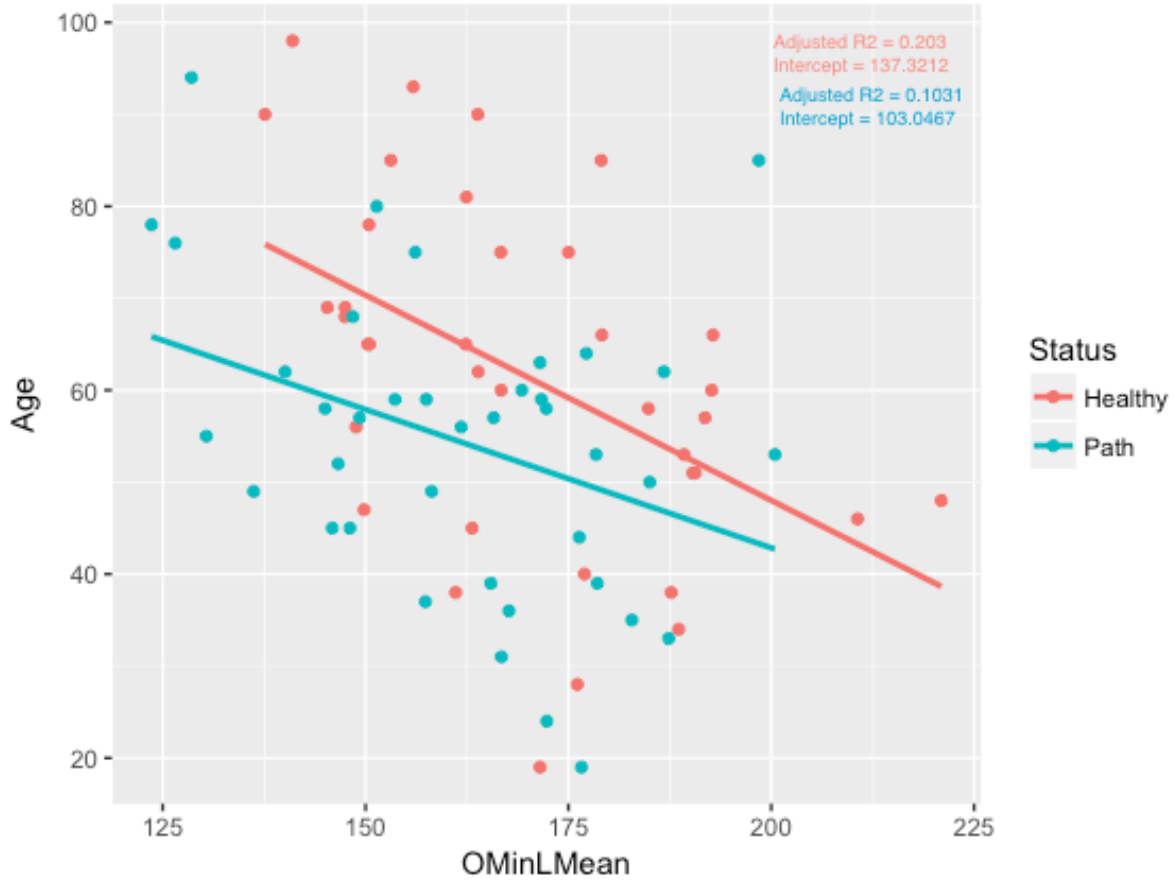

Figure 5.33: Scatterplot showing the distribution and lines of regression of osteon minimum length metric means compared with Age

The above image is a scatterplot showing the distribution of both healthy and pathological samples with regard to the age and osteon minimum length metric means. This shows the red regression line (healthy) as a better fit to the line of regression than the blue regression line (pathological). As with the previous regressions, regression for healthy control samples were calculated first, and then calculated for the pathological samples.

Regression for the healthy control samples was calculated. First, coefficients were calculated. The Estimate coefficient was calculated as intercept 137.3212 and slope -0.446. The Standard Error coefficient was calculated as from the intercept 23.9512 and from the slope 0.1400. Following the coefficients, Residual Standard Error was calculated as 16.85. Multiple R-squared was calculated as 0.2251, and Adjusted R-squared was calculated as 0.203. Finally, *p*-value was calculated as 0.003.

Next, regression for the pathological samples was calculated. First, the coefficients were calculated. The Estimate coefficient was calculated as intercept 103.0467 and slope -0.3010. The Standard Error coefficient was calculated as 21.1816 from the intercept, and 0.1299 from the slope. Following the coefficients, Residual Standard Error was calculated as 15.56. Multiple R-squared was calculated as 0.1267, and Adjusted R-squared was calculated as 0.1031. Finally, the *p*-value was calculated as 0.0261.

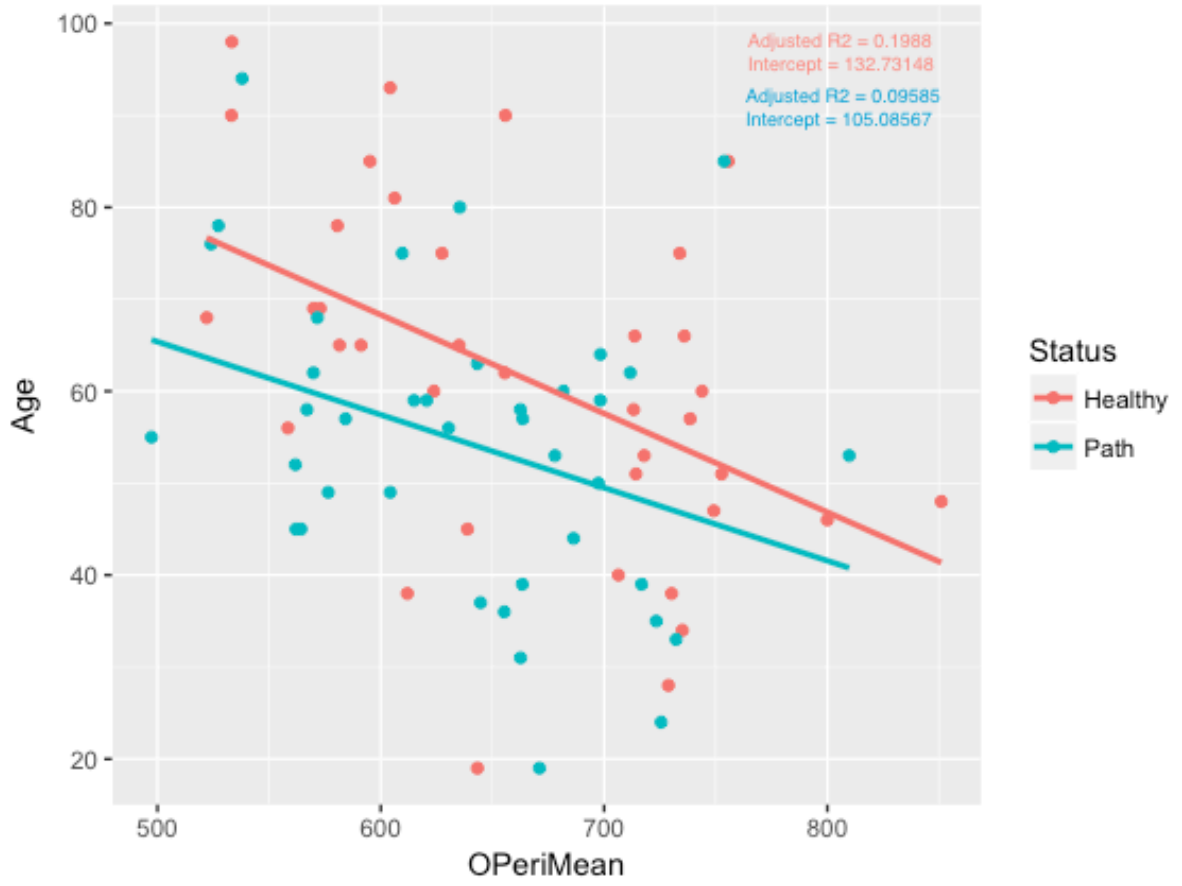

Figure 5.34: Scatterplot showing the distribution and lines of regression of osteon perimeter metric means compared with Age

The above image is a scatterplot showing the distribution of both healthy and pathological samples with regard to the age and osteon perimeter metric means. As with the previous scatterplots, the red regression line (healthy) as a better fit to the line of regression than the blue regression line (pathological). Again, regression for healthy control samples were calculated first, and then calculated for the pathological samples.

Regression for the healthy control samples was calculated. First, the coefficients were calculated. The Estimate coefficient was calculated as intercept 132.7315 and slope -0.1074. The Standard Error coefficient was calculated as from the intercept 22.7861 and from the slope 0.0341. Following the coefficients, Residual Standard Error was calculated as 16.89.

Multiple R-squared was calculated as 0.221, and Adjusted R-squared was calculated as 0.1988. Finally, *p*-value was calculated as 0.0033.

Next, regression for the pathological samples was calculated. First, the coefficients were calculated. The Estimate coefficient was calculated as intercept 105.0857 and slope --0.0794. The Standard Error coefficient was calculated as 22.7821 from the intercept, and 0.0354 from the slope. Following the coefficients, Residual Standard Error was calculated as 15.62. Multiple R-squared was calculated as 0.1196, and Adjusted R-squared was calculated as 0.0959. Finally, the *p*-value was calculated as 0.031.

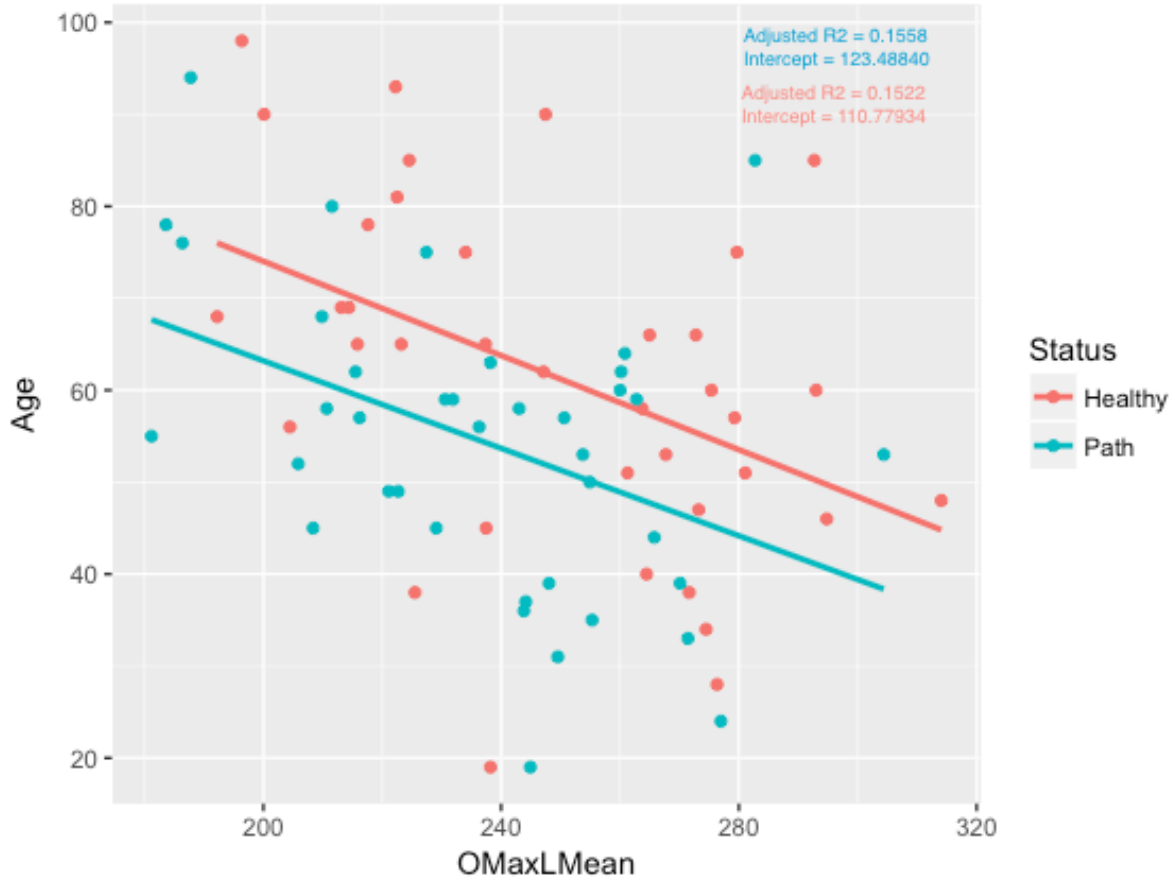

Figure 5.35: Scatterplot showing the distribution and lines of regression of osteon maximum length metric means compared with Age

The above image is a scatterplot showing the distribution of both healthy and pathological samples with regard to the age and osteon maximum length metric means. This shows the red regression line (healthy) as a better fit to the line of regression than the blue regression line (pathological). As with the previous regressions, regression for healthy control samples were calculated first, and then calculated for the pathological samples.

Regression for the healthy control samples was calculated. First, the coefficients were calculated. The Estimate coefficient was calculated as intercept 123.4884 and slope -0.2509. The Standard Error coefficient was calculated as from the intercept 22.4824 and from the slope 0.0897. Following the coefficients, Residual Standard Error was calculated as 17.24. Multiple R-squared was calculated as 0.1786, and Adjusted R-squared was calculated as 0.1558. Finally, *p*-value was calculated as 0.0082.

Next, regression for the pathological samples was calculated. First, the coefficients were calculated. The Estimate coefficient was calculated as intercept 110.7793 and slope -0.2379. The Standard Error coefficient was calculated as 20.3362 from the intercept, and 0.0851 from the slope. Following the coefficients, Residual Standard Error was calculated as 15.13. Multiple R-squared was calculated as 0.1745, and Adjusted R-squared was calculated as 0.1522. Finally, the *p*-value was calculated as 0.0081.

6. Limitations

The current research project, regardless of the amount of planning put into it at the beginning, was faced with certain limitations. These limitations have been divided into three sections: Research limitations, methodological limitations, and personal limitations.

6.1. Research Limitations

Bone histomorphometry is a destructive technique that requires specialised equipment and knowledge to be applied. In addition, it is time-consuming and observer and experience dependent. The development of research methodologies based on destructive techniques is often criticized due to ethical guidelines set out by different professional bodies and academic institutions. The current research was conducted in a country that has strict regulations for the use of human tissue in research that made the collection of samples practically impossible from local sources in the timeframe of the PhD project. More specifically, due to the regulations laid out in the Human Tissue (Scotland) Act of 2006 it was easier to obtain samples from countries outside of the UK. For this reason, samples were collected from forensic departments and modern skeletal collections in Crete, Albania, and Cyprus. These countries were chosen in part for their connections to the project's supervisor, Dr Elena Kranioti. While these samples were more easily obtained and provided the quantity and type of samples required for this research, certain limitations accompanied these relationships. These included short, translated records of pathology and cause of death. As further information was not available, or was difficult to obtain, the records was assumed to be accurate. Research would have been improved by a more open relationship with the forensic departments, and more in-depth medical and autopsy records.

Originally, in the project proposal, it was intended that all pathological samples would be taken from individuals with liver disease associated with chronic alcohol abuse. This would have allowed for a more specific study of a particular system, in this case the hepatic system, and its relationship and effect on the skeletal system. This, however, turned out to be impractical due to a number of factors such as lack of detailed medical history, different degrees of decomposition and problems with importing samples in the course of the study. Consequently, the criteria for inclusion of samples in the study was expanded to include individuals with a history of any chronic pathology, to increase the number of samples to a statistically relevant number for the proposed project. Even with these expanded criteria, the collection of these samples took the greater part of three years. As the samples were imported from three different countries, which created several problems and delays with regard to the selection of the samples, the collection of ante-mortem information, and transportation depending on each country's legislation.

As discussed in the literature review, the way that bone remodels as a tissue, is in itself a constraint, especially as it pertains to the observation of changes caused by disease. As osseous tissue has a very slow turnover rate, only a chronic disease would have the necessary time and ability to have a pathological effect on the tissue's microstructure. Especially in the case of a disease that does not target bone directly, as in the case of an infection, the disease would need time to permeate and disrupt the metabolism of the entire body in order to have any measurable effect on the bone. Even then, the effect on the bone is fundamentally restricted to a single reaction with one of two effects: creating imbalance in the remodelling process, and either causing greater osteoclast (destructive) or osteoblast (prolific) activity. This in turn could result in lesions, both lytic and prolific, osteopenia and/or osteoporosis.

Due to the restriction in the ways bone tissue can react, it is very difficult, if not impossible to reverse engineer a diagnosis of a specific disease from observation of the bone microstructure. Once this limitation has been understood, it is possible to proceed, and try to understand what can be observed about pathology from the microstructure of bone. It is also impossible to differentiate between certain changes that occur as part of the natural aging or postmenopausal processes, although these changes occur at much higher rates in individuals with chronic disease.

One of the most difficult limitations of the project was that of current software and technology, specifically in the case of taking the osteon specific metrics. There is currently no software available for the automation of quantification of osteons, osteon fragments, or measuring of Haversian systems. If such a software did exist, it would be possible to assess many more samples much more quickly with increased accuracy. At this point in time, however, it is not yet possible to automate these measurements, forcing researchers to quantify and measure features by hand. This adds a certain amount of human error to the process and is why inter and intra-observer error calculations and researcher experience are so important in these studies. In the future, it might be possible to mitigate these limitations by using software capable of measuring Haversian Systems. One such software is QuPath, a quantitative pathology and BioImage analysis software currently being developed by the University of Edinburgh Division of Pathology (University of Edinburgh, Division of Pathology, 2017). If such future software is capable of delivering accurate measurements of Haversian Systems, this research would be improved both in practicality and accuracy.

Finally, the protocols themselves provide a certain amount of limitation. Certain aspects of this thesis project required the creation of new criteria, categories of features, and metric measurements. As with all excursions into the frontier, it is not possible to compare these variables with existing data. In the future more comparative data should be generated in order to verify or reject the observations of the current work.

6.2 Practical Limitations

There were also some limitations that occurred in the lab during the course of this project. The first of these is the protocol for thin sectioning and creating the slides. The protocol evolved over the course of the project, and in some cases were forced to change due to change in facilities or the needs of fellow researchers in the laboratory. At the start of the project, the protocol set out by Paine (2007) was followed, which included the boiling and macerating of the bone, in the case of any remaining soft-tissue existing on the bone. This process occurred in the Edinburgh City morgue. The samples were then taken back to the histology lab at the University, and following Paine's instructions, embedded in epoxy resin, thin sectioned, and adhered to glass slides for reading. This protocol was amended, however, after experiments done in the lab by Julieta Garcia-Donas discovered that after embedding the slides, cleaner and clearer slides were produced by cutting the embedded sample in half, polishing the area, adhering it to the slide with resin, and then cutting the thin-section using a slide-holder chuck for the IsoMet^{TM} saw. The full details of this revised method can be read in Garcia-Donas and colleagues (2017).

Protocol was further amended after the addition of another project to the lab involving bio-mechanical analysis of bone. Due to the scarcity and difficulty in obtaining samples, these autopsy samples were often shared amongst multiple projects. With the addition of the biomechanics project, the maceration process had to be changed, as boiling would change the integrity of the bone and render it unusable for biomechanical experiments. For this reason, going forward bones were defleshed by hand with a scalpel instead of boiled and macerated. This caused several changes to the thin sectioning process. Bone samples now had to be kept in refrigerated or freezing temperatures until embedding in resin to limit spread of bacteria. The remaining tissues, as well as the remaining bacteria in the trabeculae caused the thin sections to be less clear in some circumstances. In future, bone samples that are unable to be boiled could be defleshed by hand and then soaked in acetone to help remove additional flesh and kill any bacteria that might obscure the slide.

Although a more consistent protocol would have been better for the control of the project, the length of time over which the samples were prepared, and the change in adjacent projects and facilities meant that the protocol had no choice but to be amended to fit the circumstances. Ultimately, the slides were legible, and the analysis of the slides was able to be carried out, regardless of the method used to prepare them.

6.2.1 Slide analysis

For the standard histological analysis, photographs were not necessary for the quantification of the microstructural elements. The features of complete and fragmented osteons were possible to quantify with a transmitted light microscope fitted with a polarised filter.

Calculating cortical area, however, required either a stitched image created by seaming multiple photographs of the slide together to create a complete cross-section in software attached to the microscope, or for the cross-section to be photographed using a handheld microscope camera, like a Dino-Lite digital microscope. Preferably, if everything had gone according to plan, full stitched cross-sections would have been taken of each slide, but as this was not always possible, a compromise was devised, and a solution was implemented. In the case of several samples, the Leica software attached to the photographing microscope was unable to stitch a cross-section together. This may have been related to a glitch in the software, or possibly the clarity of the slide. These slides were then photographed using the Dino-Lite to calculate cortical area, and four individual field of view photographs were taken for use in the osteon specific metrics. Any slides that were unable to meet the criteria for data of the standard histological analysis were excluded from the study.

The majority of the slides used as healthy controls were obtained from another study being conducted in tandem with this project. In the case of these slides, another researcher, with very similar results in quantification of histological features, provided the quantifications for standard histology, as they had already been quantified for other research. The same was true for the other study, with this researcher contributing data for some slides used in that study. While this saved time, these numbers would ideally have all been re-quantified by the researcher conducting this study. In the case of two slides used as healthy controls for the standard histological analysis, photographs were unavailable and were therefore excluded from the osteon specific metrics analysis.

In the case of the osteon specific metrics, the original protocol, as designed, called for measurements of every complete osteon in the cross-section. After several months of attempts, it was determined that measuring the entire cross-section was extremely time-consuming and impractical for the purposes of useful research. Several of the slides were reassessed using one field of view from each cardinal point of the rib. These were then compared to the data gathered from the measurements of the complete cross-section and subjected to a comparative t-test. It was found that there was no statistically significant difference between the two sets of data, and therefore it was determined that sampling of the cross-section would be the protocol going forward. Although a complete cross-section and additional data would always be worth having for analysis, the impracticalities of obtaining said data forced the change to the study protocol.

6.3 Problems in infrastructure

The current project is a lab-based project requiring specific equipment and facilities to accommodate work on modern bone tissue as appropriate for the development of any forensic methodology. Although the PhD proposal was approved by the University of Edinburgh, and a functioning histology lab already existed within the confines of the School of History, Classics and Archaeology (HCA), due to governmental and University regulations it was not possible to work with modern samples obtained from autopsy in this lab. This was revealed to both the researcher and the supervisor of this project after the beginning of the PhD project and naturally led to negotiations on how to resolve the issue. To solve the problem HCA has negotiated a lab space for those students undertaking research in forensic anthropology using modern samples in the Anatomy building next to the HCA building. In

addition to this move, new equipment for creating histological bone samples was ordered for the new histology laboratory. By the time the use of this new lab had been finalised, and the necessary equipment obtained and set up, it was six months into the beginning of this project, adding to the delay in sample preparation.

Work continued in this lab for about two years, with samples being processed and thin sectioned as they arrived. In September of 2016, for unknown reasons to the researcher it was decided by the anatomy department that it was no longer acceptable for the bone histology lab to remain there. In addition, for reasons unknown to the histology lab users, including the researcher of this project and the supervisor, HCA started an investigation regarding the appropriate permissions for conducting modern histology work in the lab. This lead to a six-month stall in the project as the laboratory was closed overnight, and without notice, and the samples that had been collected were confiscated and locked away pending an inquiry by the National Health Service (NHS). Ultimately, it was discovered that all the necessary paperwork had been filed, the projects being undertaken by the student at the bone histology lab were all in accordance with established regulations, and that a mistake had been made on the part of the University. By the time this was discovered, however, six months had passed, causing a long interruption in studies as well as large amount of anxiety and upset on the part of the students working in the histology laboratory. A new lab facility was finally found in March of 2017, when the department was offered bench space in the pathology lab at Western General Hospital, in Edinburgh. The final preparations and analysis were then undertaken at the hospital.

In addition to these limitations caused by accessibility to samples and facilities, there were personal limitations on the part of the researcher, most notably stress and anxiety caused by turbulent circumstances during their thesis project. The disturbance in lab facilities, as well as the enquiry by the NHS caused a large amount of stress and anxiety for the student undertaking this project. In addition to these normal stress responses, additional stress and loss of time were caused when the student, who was studying internationally, had to apply for a visa extension to finish their studies from their home country, due to the disruption in lab facilities. This process ultimately took longer than anticipated, resulting in the student being forced to stay in their home country for a month and a half while the visa extension was sorted out between the Home Office, and the University. Finally, in March of 2018, a nationwide strike by University staff limited the amount of interaction between the student and their supervisor during the writing up period.

7. Discussion

Forensic anthropology is a discipline often faced with the challenges of analysing fragmented remains with the aim of creating a biological profile that will lead to forensic identification of the deceased. Although complete skeletons can be assessed for biological characteristics using a variety of techniques, these have a limited value in the case of extreme fragmentation. In that event, microscopic methods such as bone histomorphometry are the most plausible option for continued analysis.

Bone histomorphometry in particular, has been used for estimating age based on the predicted remodelling patterns of bone tissue for many decades. Early research includes the pioneering work of Kerley (1965) on the femur, and later Stout and Paine's (1992) work on the rib and clavicle. These methods have been expanded and improved over the years by the addition of validation studies such as Ahlqvist and Damsten (1969), population studies (Cho & al., 2002; Bednarek, et al., 2009; Lee, et al., 2014; Garcia-Donas, 2017), sexual dimorphism (Cho, et al., 2006), age (Goliath, et al., 2016), dietary deficiencies (Paine & Brenton, 2006), and paleopathology (Schultz, 2001). Different bones present different variation in the histomorphometric variables, but the correlation with age is present in all cases at least until the asymptote is reached.

Several researchers have investigated the relationship between histomorphometric variables and sex claiming that sexual dimorphism exists (Ericksen, 1991; Cho, et al., 2006) while others reported the opposite (Kerley, 1965; Pfeiffer, 1998). The degree of correlation with age is affected by several factors such as genetics, diet and activity, although these factors are most

apparent in the weight-baring bones. The ribs are considered an excellent material for histomorphometry as they are not affected by mechanical loading, making it the most popular bone for integration in histomorphometric studies. It is for this reason that the rib was chosen as the subject for the current study.

The purpose of this study was to investigate the effect of systemic metabolic disease on bone metabolism as reflected in the bone microstructure. To best assess the changes to the bone microstructure, a number of qualitative and quantitative variables were selected and tested on a group of subjects suffering from metabolic disease. These were then compared to a group of healthy controls. The results are discussed in relation to the impact of pathology in bone microstructure as an age indicator and as a general health indicator.

The study employed two sets of variables, qualitative and quantitative, that will be analysed separately.

7.1 Qualitative Interpretations and Explanations

7.1.1 Category 1 Features

The most common qualitative features encountered in this study are those features belonging to category 1. This category includes the subtler, abnormally shaped osteons and canals. This means that the Haversian system is complete and intact, but the shape and size of the osteon and/or its canal is outside the realm of normal. Features in this category include changes in the circularity of both the osteon and canal, as well as disproportionate sizing of the osteon and canal. These features are often accompanied by the thinning of cortical bone. This can be

observed, for example, in those patients with osteoporosis (Parfitt, 1984). Their bones are unusually porous, and this has been seen and identified by the enlarged canals visible in the cross-section. Category 1 pathological features are caused by an imbalance in the bone metabolism in favour of the osteoclasts. This causes the destruction of bone cells to outweigh the construction of new bone, resulting in increased porosity, and sometimes cortical bone thinning.

A combination of abnormally sized and shaped osteons, and slight to moderate cortical thinning was described in all but one of the pathological cases in this study (97.5%) and in four of the healthy controls (10.8%). These features represent evident signs of the disruption of the normal remodelling process. This level of metabolic disturbance does not prevent the bone from forming complete Haversian systems, but it contributes to the overall increase in bone porosity. These features seem to increase with age especially for individuals over 30 years old. In the younger age groups, it is not possible to confirm the trend as the number of cases is too small to make any statistically relevant conclusions. The healthy controls that present category 1 features are all over 41, suggesting that age is a factor in their appearance. Age-related bone loss has been associated with an increase in the number and the size of Haversian canals (Thompson, 1980; Brockstedt, et al., 1993; Brockstedt, et al., 1995; Bell, et al., 1997). Category 1 features in pathological samples seem to manifest earlier than the expected age-related changes. This suggests that the underlying pathology accelerates remodelling disturbance and bone loss. As category 1 features appeared in the higher age groups of both the pathological and healthy control groups, these features could also be attributed to pathology, the aging process or a combination of the two, as suggested by the trends of the older age brackets of pathological group. At this time, from the samples

analysed for this study, it is not possible to differentiate between category 1 features caused by pathology and those caused by aging or a combination of the two. Further research is needed.

Cortical thinning and bone loss have been described in cases of menopausal females as a result of oestrogen deficiency (Kaptoge, et al., 2003). It does however also occur in males at a slower rate (Frost, 2003). The clear majority of the pathological sample was male, and therefore no meaningful comparison can be made between the sex groups. It is worth noting that from the five females that presented category 1 features in the study four were in menopause and all presented cortical thinning as would have been anticipated (Kaptoge, et al., 2003). Yet, almost all samples with recorded pathologies, the vast majority of which were men, were associated with features of category 1 and showed cortical thinning. The same is observed for four healthy controls. Therefore, the underlying mechanism of normal remodelling disruption cannot be attributed solely to hormonal changes. As with the older age groups, however, it is not currently possible to differentiate between the category 1 features caused by postmenopausal hormonal changes, and those caused by pathology. Again, further research is needed.

Low bone mass in patients has been found to be a risk factor for cardiac episode or death compared to subjects with normal bone mass (Sprini, et al., 2014; Bagger, et al., 2007; Magnus & Broussard, 2005; Farhat, et al., 2006). Marcovitz and colleagues (2005) were able to use low BMD as a predictor of CAD, connecting osteoporosis with heart disease predominantly in postmenopausal women. This is in line with the results of this study, which show that 90%

patients in the cardiovascular group have type 1 features correlated with abnormal osteons and bone thinning. The results further suggest that menopause is not the only factor linking bone metabolism and CAD as the majority of individuals in the current study were male. This is, however, expected as CAD is more frequent in males than females (Fabian Sanchis-Gomar et al., 2016). In addition, most subjects with CAD were diagnosed with diabetes, alcoholism or were heavy smokers, which suggest a multifactorial effect on bone metabolism.

Decreased bone density has also been connected to chronic alcoholism (Bikle, et al., 1985; Feitelberg, et al., 1987), with alcoholic liver disease (ALD) being named as a possible cause of increased incidence of osteoporosis and osteopenia in patients who abuse alcohol (Long, et al., 1978; Spencer, et al., 1986; Labib, et al., 1989). It is likely that conditions often associated with ALD, such as vitamin D deficiency and hypogonadism, are connected to the systemic metabolic disturbances that eventually reach the skeletal system, causing the stimulation of osteoclasts, and resulting in osteoporosis (George, et al., 2009). The current study showed that 81.25% of patients with hepatic disease presented signs of category 1 features associated with abnormal osteons and cortical thinning. The majority of the subjects were males (6 of 7) while all subjects but one had a history of alcoholism. The medical data did not include further information on the time of alcohol abuse, or the daily consumption of alcohol and the histological examination of the liver thin sections showed slight to moderate fatty accumulation, which indicates a similar level of alcohol abuse in all cases associated with type 1 features. Age for these subjects ranged from 50 to 59 and showed no positive correlation with the degree of fatty accumulation. The most severe case of hepatic disease, which resulted in liver cirrhosis showed category 3 features.

Cancer (Greenspan & Remagen, 1998; Drake, 2013), diabetes (Bouillon, 1991), pulmonary disease (Jørgensen, et al., 2007; Cavaillès, et al., 2013), and renal disease (Malluche & Faugere, 1990; Ott, 2009; Williams, 2009) all have documented connections to osteoporosis and osteopenia. Yet, the sample sizes for each of these disease classes was too small to make any significant inferences. While meaningful conclusions cannot be drawn from these categories, it is worth noting that all the samples in each of these classes had category 1 features, consistent with previous studies connecting these diseases and the abnormal osteons and cortical thinning associated with osteoporosis (Drake, 2013; Choi & Chung, 2016; Cavaillès, et al., 2013; Ott, 2009).

Each of the diseases encountered during this study can manifest systemically, causing consequences in multiple systems (Magnus & Broussard, 2005; Pérez-Castrillón, et al., 2004; Spencer, et al., 1986; Kuller, et al., 2000; Jørgensen, et al., 2007; Webster, et al., 2017). It is therefore unsurprising that several of the individuals sampled had multiple conditions affecting different systems. Likewise, it is consistent with the findings of this study that all the samples from the multiple class group had category 1 features present. Due to the varied nature of this group, it is not possible to insinuate which disease contributed to the skeletal manifestation of pathology, and in fact the pathological features of the bone may have been caused by the presence of more than one systemic pathology. Another important factor to take under consideration is the fact that although subjects were diagnosed with these conditions it is not known whether there were receiving treatment at the time of death and for how long. This is very difficult to track due to the nature of the collected sample. One could speculate differences in the manifestation of metabolic disease in the skeletal system between untreated subjects and subjects under medication.

7.1.2 Category 2 Features

This category of features contains the deranged Haversian systems, or Swiss Cheese Effect. While similar in some ways to the category 1 features, in that they display an increase in bone porosity, the features seen in the deranged, or incomplete, Haversian systems of category 2 are much more evident and clearly distinguished from normal bone formation. While category 2 features can appear on their own, they can also appear in conjunction with category 1 and 3 features. Like the category 1 features, category 2 features can also appear either on their own, or with thinning of the cortical bone. Category 2 features can appear as single focci in the compact bone or can affect the entire cross-section.

These features can be thought of as a possible extension of the features seen in category 1, and can also be associated with osteoporosis, as they are contributing to the unusual and extreme porosity, or even trabecularisation, of the cortical bone, both features of advanced osteoporosis (Parfitt, 1984). Therefore category 2 features are more advanced signs of imbalance in the bone metabolism favouring the destructive osteoclasts. Again, this causes the destruction to outpace the reconstruction of bone, but in a more dramatic fashion, resulting in the extreme porosity, incomplete Haversian systems, and deranged canals associated with category 2.

Category 2 features were present in 32.5% (12/40) of the pathological cases, and in none of the healthy controls. In all cases category 1 features coexisted with category 2 features, which may further suggest that they are different stages of the same metabolic disruption. The

presence of category 2 features seems to increase with age, with four cases appearing under the age of 40, and nine appearing later. This figure however, may be skewed by the age distribution of the samples, as the sample size for younger individuals was very small. In addition, since these features do not appear in any of the healthy controls one can exclude the possibility of representing age-related changes. The higher frequency with which they appear with increasing age can simply be an association with the severity of the disease with progressing age and not the age itself.

Although bone loss has been described in both post-menopausal females (Kaptoge, et al., 2003) and in older individuals of both sexes (Frost, 2003; Goliath, et al., 2016), as discussed for category 1 features, the presence of category 2 features seemed to fall outside the range of normal for bone porosity. All but two of the samples with category 2 features present were males, and the two females with category 2 features were both under the age of 40. Therefore, these changes cannot be associated with hormonal changes based on the existing data.

The higher risk of bone loss in cardiovascular disease (Sprini, et al., 2014; Bagger, et al., 2007; Magnus & Broussard, 2005; Farhat, et al., 2006) is consistent with the fact that 40% of the cardiovascular cases, namely the ones associated with generalised atherosclerosis and myocardial infarction presented with category 2 features. With many cardiovascular conditions beginning in childhood and manifest in adulthood (Theise, 2015), there is ample time for some cases to develop into more pronounced cases of osteoporosis.

Likewise, in the case of hepatic disease, chronic disease of the liver is associated with bone loss (Bikle, et al., 1985; Spencer, et al., 1986; Feitelberg, et al., 1987; George, et al., 2009). The effect of chronic liver disease, as is that case with ALD, on bone depends heavily on the severity and progression of the disease, inferring that some cases of bone loss associated with liver disease (hepatic osteodystrophy) would be more pronounced than others (George, et al., 2009). In the current study 18.75% one (3 of 7) of the samples from the hepatic class presented with category 2 features, correlated with dramatic porosity of the cortical bone.

Samples from the cancer class (1 of 2), diabetes class (1 of 1), and pulmonary class (2 of 2) had category 2 features present, consistent with previous studies (Greenspan & Remagen, 1998; Drake, 2013; Bouillon, 1991; Jørgensen, et al., 2007; Cavaillès, et al., 2013) connecting these diseases and the cortical porosity. The renal class, which consisted of only one sample, did not show any signs of category 2 features, however the connection between chronic kidney disease and renal osteodystrophy (Ott, 2009) suggests that it is possible that more dramatic forms of osteoporosis may exist in other CKD patients.

As the diseases used in this study manifest systemically (Magnus & Broussard, 2005; Pérez-Castrillón, et al., 2004; Spencer, et al., 1986; Kuller, et al., 2000; Jørgensen, et al., 2007; Webster, et al., 2017), it is expected that several of the individuals with multiple conditions affecting different systems would also have more pronounced bone loss. It is therefore consistent with the findings of this study that 25% the samples from the multiple class group had category 2 features present. Again, as this group is varied, with different combinations of diseases, it is not possible to indicate which disease caused the pathological bone response, or whether the response was caused by multiple conditions.

Diabetes in particular is reported in the medical history of four subjects, three of whom had multiple diagnoses involving other disease classes, without further information on whether it was type 1 or 2, under treatment or not. Type 2 diabetes has two characteristics a) high serum insulin levels and b) tissue insulin resistance (Choi & Chung, 2016) These features have been associated with low bone mass and "deteriorated bone strength" (Choi, et al., 2014; Choi, et al., 2014). It has been widely accepted that type 2 diabetes is associated with higher bone porosity and fracture risk in subjects over 50(Choi & Chung, 2016). Similarly, type 1 diabetes presents higher risk of fractures due to porosity even when scaled for factors such as age, sex, duration and complications of the disease and when compared to type 2 (Shah, et al., 2015). The difference would probably be in the earlier appearance of signs of metabolic disturbance in type 1, which is inherited, compared to type 2. From the four subjects suffering from diabetes, three had multiple pathological conditions, and one only reported diabetes (age 94 years old). It is very likely that this individual also had asymptomatic or undiagnosed CAD, of which diabetes is the primary cause, that could have been the cause of death. This information unfortunately is not included in the Census office archives. Interestingly, this is the only individual that presented category 2 features of the diabetic subjects, but also the oldest individual in the group. Of the remaining three individuals, the youngest and only female was 49 years old and suffered from several conditions (Hypertension, Diabetes, Heart ischemia, left ventricular hypertrophy, hepatic steatosis, pyelonefritis, bronchopneumonia) according to her medical records.

7.1.3 Category 3 Features

The last, and least common category of features encountered in this study was category 3 features. Unlike the previous two categories, this category of features is characterised by prolific bone formation, as opposed to a loss of bone. The striated bone deposited near the periosteum is very different from the previous two categories and should immediately be evident to the observer. Category 3 features can also appear alongside category 1 and 2 features, as well as thinning cortical bone. This is possibly due to the misdirection of bone building osteoblasts and destroying osteoclasts, as opposed to a complete and overall imbalance (Ortner, 2003). Similar to category 2 features, category 3 features are more likely to appear in part of the cross-section, and most likely near the periosteum, than over the entire cross-section.

The rapid deposition of striations of bone was described in only one case in this study. As such, it is not possible to make any inferences from the results of this category, however it may be useful to treat this one sample as a case study. The case occurred in a 62-year-old male with liver cirrhosis, the most progressed hepatic disease in the whole group, leaving open the possibility of associations between age and disease with the presence of category 3 features.

This kind of rapid bone deposition has been described in several other studies referencing extraspinal hyperostosis related to DISH (Lill, 2013), and several cases of lesions as a response to chronic infection (Schultz, 2012; Schultz, 2001). While this type of pathological feature is clearly the work of constructive osteoblasts, the aetiology of these kinds of prolific lesions in hepatic disease patients is unknown. Further study, with a larger sample size, is necessary to understand whether the presence of this category of feature is related to hepatic disease, or

possibly to another unidentified underlying condition, and whether they have any connection to aging process.

In summary, category 1 and 2 features are indicators of different degrees of cortical porosity due to disruption of bone metabolism with increased osteoclast activity with category 2 features being the more severe indicators. It seems that the majority of conditions can cause category 1 features as early signs of disease, appearing earlier when compared with the similar age-related changes in healthy subjects. Category 2 features appear in cases of longer duration of more severe manifestation of the disease, and they are not compatible with age-related changes as they do not appear in any of the healthy subjects. The relatively small number of females in the study does not allow for testing the influence of menopause on the degree of porosity that has been previously reported in the literature (Kaptoge, et al., 2003; McCarthy, 2010; Riggs, et al., 1998; Brickley & Ives, 2008). Yet it seems that more than one underlying mechanism exists for the metabolic disruption associated with both category 1 and 2 features. Category 3 features appeared only in one case of liver cirrhosis but as form of rapid bone deposition that suggests a different mechanism compared to the other two categories.

7.2 Quantitative Interpretations and Explanations

As in the previous results chapter, quantitative analysis and discussion has been separated into two sections, one for standard bone histology and one for osteon specific metrics. Again, the first section involves the standard histological metrics and quantifications as developed by Stout and Paine (1992). These include the quantification of osteons, both complete

secondary and fragmented osteons, measurements, such as cortical area, and calculated values, in this case OPD. These are the metrics used in most age estimation methods focusing on rib cross-sections, as developed by Stout and Paine (1992), and Cho and colleagues (2002). While these particular age estimation methods were not used in this study, as they proved ineffective for the study population (Garcia-Donas, 2017), they could be used to develop a population-specific age estimation formula. Even without a formula for age estimation, significant connections remain between cortical area and OPD, and age. This is then important when comparing the correlations and regressions of cortical area and OPD versus age between the healthy control group and the pathological group.

The second section discusses the results of the osteon specific metrics and deals with the new metric measurements and statistics developed for this study. The purpose of these measurements was to quantify changes in the bone microstructure. In the previous section of this chapter qualitative changes were noted from visual analysis, in this section the measurements provide quantifiable data to apply to the observations made in the qualitative analysis. In this chapter, the results given in the previous chapter will be discussed, as well as any implications or possible future used for these metrics, and the consequences of including or excluding pathological individuals from the sample.

7.2.1 Standard Bone Histology

The standard bone histology section of the results chapter dealt with, as previous described, the standard quantifications and measurements as set out by (Stout & Paine, 1992). Once this data had been collected, it was subjected to several forms of statistical analysis. These

analyses included inter-observer error, correlations, regressions, standard errors, and bootstrapping. The correlations and regressions were all applied first to the complete set of data, to simulate previous collections used in the creation of age estimation techniques. Afterwards, the data was split into two groups, healthy controls and pathological samples, and applied to the statistical models again, to see if there was any significant difference between the two groups, or indeed between the two groups and the complete sample. The results of these statistical analyses will now be discussed in the following sections.

7.2.1.1 Inter-observer Error

Inter-observer error was calculated for the standard histology variables, number of intact osteons, number of fragmented osteons, and total number of osteons. For this study, each variable was analysed using a paired t-test to compare the values of both observers. In addition, the other observer, Julieta G. Garcia-Donas, analysed these variables using TEM, relative TEM (rTEM), and associate R values for a related study done in conjunction with this one (Garcia-Donas, 2017).

The first variable to be tested was the number of intact osteons. From the values returned by the paired t-test, it is possible to conclude that within a 95% confidence interval that there was no statistically significant difference between the two observers. These results are consistent with the results of the TEM and rTEM conducted on the same population by Garcia-Donas (2017) and represent a high degree of repeatability between observers and with other histological studies (Keough, et al., 2009). Contrary to this, for fragmented osteons statistically significant differences were found between the two observers. This is consistent with the results from Garcia-Donas (2017), as well as other histological studies (Lynnerup, et

al., 1998; Crowder, 2005) and it suggests that the classification of fragmented osteons is more subjective. Fragmented osteons are defined as osteons where at least 10% of their Haversian canal has been remodelled by the next generation of osteons. This includes the remnants of osteons in which the entirety of their canal has been obscured (Stout & Crowder, 2012). As this classification relies upon the observers' judgement as to what constitutes at least 10% of the canal, it follows that the number of fragmented osteons quantified by each observer would be inconsistent.

The last variable to be tested was the total number of osteons in the cross-section. From the values returned by the paired t-test it is possible to conclude that within a 95% confidence interval that there was a statistically significant difference between the two observers. The difference, however, is relatively small, and likely due to the difference in the previous variable. When tested by Garcia-Donas using TEM and rTEM, it was concluded that less than 3% of the variance was due to measurement error, and that the rTEM was below the 5% acceptance threshold (Garcia-Donas, 2017). While this variable meets the standards for acceptable levels of inter-observer error seen in other studies (Keough, et al., 2009; Crowder, 2005), it would be advised to be cautious of overly inconsistent fragmented osteon quantifications, as this can in turn effect the repeatability of other important variables, such as OPD, where the number of total osteons is a factor in calculating the OPD variable (Crowder, 2005).

From the results of these paired t-tests, and the TEM testing by Garcia-Donas (2017), the observations of the two observers were relatively consistent, and demonstrate a degree of repeatability within acceptable levels. It is advised, however, for further studies to take inter-

observer error into account when quantifying the number of fragmented and total osteons, as these variables are the most likely to suffer from higher inter-observer error.

7.2.1.3 Correlations

The first set of correlations was calculated using the complete data set, including information from both the healthy control and pathological groups. This mirrored the samples used by Stout and Paine to create their 1992 formula. While correlations between all variables were calculated, those correlations of primary interest were those most strongly correlated with age. As expected, the strongest correlations with age were cortical area and OPD, with cortical area presenting a strong negative correlation with age, and OPD presenting a strong positive correlation with age. While these results are consistent with the findings of Stout and Paine (1992), as well as subsequent studies using cortical area and OPD as variables for age estimation (Cho & al., 2002; Bednarek, et al., 2009; Lee, et al., 2014), it was the aim of this research to assess if better results could be obtained by separating out the pathological cases.

The next correlations were calculated using only the pathological samples. In the case of the pathological samples, none of the expected correlations existed to the extent that was expected. While cortical area was still significantly correlated with age, this correlation was much weaker than the correlation between these two variables in the complete set of data. When comparing OPD and age the correlation was even weaker, as there was no significant correlation between these variables in the pathological sample. The only consistency between the complete data and the pathological group was the direction of the correlations, with cortical area and age remaining a negative correlation, and OPD and age remaining a positive correlation.

These results are inconsistent with most previous research using cortical area and OPD for age estimation (Stout & Paine, 1992; Stout & Paine, 1994; Cho & al., 2002; Cho, et al., 2006; Bednarek, et al., 2009; Lee, et al., 2014). Instead, the results of these correlations are consistent with research done using individuals with bone affected by malnutrition (Paine & Brenton, 2006). The significance, or lack thereof, of these correlations in the pathological group would indicate that pathological bone, like the pellagra cases, could negatively impact the significance of the correlations between cortical area and OPD, and age in the complete set of data.

The final correlations were calculated using only the healthy control samples. For the healthy samples, age was once again strongly correlated with cortical area and OPD. While these findings are consistent with the correlations found and used for age estimation in previous studies (Stout & Paine, 1992; Cho & al., 2002), the improvement upon removing the pathological samples from the data set is notable. The correlation values for the healthy data set demonstrate that the correlations between age, and cortical area and OPD are stronger and more significant when the pathological samples are removed.

Although it is important to note that correlation does not equal causation, the correlations found between the variables of cortical area and OPD, and age provide evidence that supports the hypothesis of this study, which suggests pathologically affected bone has the potential to negatively affect the results of histological age estimation. Even though the complete data set returned reasonably sound results, confirming the results of past studies (Stout & Paine, 1992; Cho & al., 2002), the marked improvement of correlations for the healthy data set, and

the decreased correlation for the pathological data set support the expectations of this study. From the results of these correlations, regression models can then be created to test the significance of the relationships between the variables and age, which then provide a basis for histological age estimation formulae.

7.2.1.4 Regression Analysis

Following the results of correlations, these regression models were also divided into the same three groups and focused on the relationships between age and cortical area, and age and OPD. Regression analysis is particularly important in terms of bone histology, as it is regression models that form the basis of all histological age estimation formulae, following the original model set out by Kerley (1965) for his equation using the femur. These regression equations were then continued into further methods using other bones, like the Stout and Paine method (1992), which popularised the use of ribs for age estimation, and any improved methods created since (Cho & al., 2002; Bednarek, et al., 2009; Goliath, et al., 2016). Since previous studies have reported R^2, both multiple and adjusted, as the most significant indicators of model fit, these were the statistics focused on for this study (Han, et al., 2009; Goliath, et al., 2016; Maat, et al., 2006). Likewise, R^2 has been presented as a percentage, for better comparison.

The first regression model was the model for the complete sample group comparing cortical area and age. As with the correlations, this group was analysed to simulate the sample data used to develop previous age estimation formulae, such as Stout and Paine (1992) and Cho (2002). For the complete data set, a multiple R^2 of 24.77% and an adjusted R^2 of 23.81% were reported. These represent the amount of age variance that could be attributed to cortical

area. While cortical area has been demonstrated as having a strong relationship with age, consistent with the Stout and Paine (1992) formula, cortical area alone would not be a good predictor of age. It could, however, as in other age estimation formulae (Stout & Paine, 1992; Cho & al., 2002; Lee, et al., 2014), be combined with another variable, in a multiple linear regression, for greater predictive abilities.

After the regression analysis for the complete group, the same variables were analysed using only the pathological data. While there does appear to be a relationship between age and cortical area for the pathological group, the relationship was much weaker than the corresponding values from the complete data set, and the fit of the model was not as good as the previous model. As for the first regression, R^2 was used as an indicator of fit. For the pathological data set, a multiple R^2 of 11.07% and an adjusted R^2 of 8.73% were reported. These results are an indicator of the poor fit of the model between cortical area and age, a reflection of the weak correlation between the variables seen in the previous section. Even if cortical area was included in a multiple linear regression formula such as the Stout and Paine (1992) formula, the performance of the equation would most likely be too poor for forensic standards (Christensen & Crowder, 2009; Scientific Working Group for Forensic Anthropology (SWGANTH), 2013). The next step was to compare the results of the healthy control group, and to see if the regression model improved once the pathological samples were removed.

Finally, the healthy data set was analysed using linear regression, comparing cortical area and age. The results given for this regression model show an improved outcome from the first regression model, which included the pathological data. The healthy data set reported a multiple R^2 of 33.33% and an adjusted R^2 of 31.57%, a nearly 6% improvement from the model

using the complete data set. This data proves that equations which utilise cortical area as a variable, such as Stout and Paine (1992) or Cho and colleagues (2002) would yield more accurate results if pathological data were to be excluded.

Once regression models had been completed for the variables cortical area and age, regression models were created to analyse the relationship between OPD and age. As with the previous models, the complete data set was analysed first. The resulting regression model shows a significant relationship between the variables; however, it is slightly weaker than the cortical area regression results. With a multiple R^2 of 22.35% and an adjusted R^2 of 21.35%, indicating the percentage of variance in age attributed to OPD, the model fits, but would be a poor predictor of age alone. As OPD is usually the most significant variable used in histological age estimation techniques (Stout & Paine, 1992; Cho & al., 2002; Garcia-Donas, 2017), it is unusual to have a lower R^2 for OPD than for cortical area. This is possibly caused by the inclusion of the pathological data in the model.

Next, a regression model was created to analyse the relationship between OPD and age using only the pathological data. The regression model for this data set show no significant relationship between OPD and age, a reflection of the correlation results discussed above. With a multiple R^2 of 1.26% and an adjusted R^2 of 1.34%, only a very small percentage of the variance in age could be attributed to OPD. This is inconsistent with the findings of most histological age estimation studies, as typically, OPD is one of the strongest variables for age prediction (Stout & Paine, 1992; Cho & al., 2002; Garcia-Donas, 2017; Goliath, et al., 2016). Not only is OPD a poor predictor of age for the pathological group, but it is likely that the

underperformance of OPD as a predictor for the complete group is due to the inclusion of the pathological samples in the data set.

Finally, to test if age prediction improves when the pathological data was excluded, a regression model was created using only the healthy data set. The regression model for this data set showed a significant relationship between OPD and age. A multiple R^2 of 47.1% and an adjusted R^2 of 45.71% were reported, increasing the strength of OPD as a predictor of age by over 24% when compared with the complete data set. These results are consistent with the Garcia-Donas study on the same population (2017), as well as other histological age estimation studies giving OPD as a significant predictor of age (Stout & Paine, 1992; Cho & al., 2002; Goliath, et al., 2016). This proves that pathology has a clear effect on the strength of OPD as an age predictor, and that pathological data should be excluded to ensure accurate histological age estimation.

Overall, the results of the regression models comparing cortical area and age, and OPD and age, were consistent with the expectations of this study. As bone microstructure is affected by pathology, it is unlikely that the metrics and variables typically used in histological age estimation techniques would continue to have the same relationships with age. This is particularly true of OPD as a variable, and any study incorporating a histological age estimation method in which OPD is a factor should exclude any pathological samples from the data to avoid inaccurate results. These findings are also consistent with the results of Paine and Brenton (Paine & Brenton, 2006) which note similar inaccuracies in a population with dietary deficiencies and malnutrition.

7.2.1.5 Standard Errors

While R^2 statistics are useful in evaluating the strength of a variable as a predictor as they are given as a percentage and are easily understood, often the standard error is a better indicator of the usefulness of a regression model. As the standard error of the estimates (SEE) measures the accuracy of prediction made with the regression model, with better accuracy yielding a SEE closer to zero, these numbers can easily be compared and analysed as part of the development of an age estimation formula. For this reason, many previous studies have included SEE as well as R^2 statistics when describing new regression equations for age estimation (Stout & Paine, 1992; Crowder, 2005; Keough, et al., 2009; Goliath, et al., 2016). The results of the SEE calculations for the cortical area and OPD regression models can then be compared for accuracy with the results of previous studies.

First, standard errors were calculated for the cortical area and age regression model. Overall, the results were very similar, with the pathological data set performing slightly worse than the complete data set, and the healthy data set performing slight better than the other two data sets. All three data sets yielded standard errors between 15.36-15.52, meaning there was only a difference of 0.16 between the best performing and the worst performing regression models. These standard errors are slightly higher than the standard errors reported by Cho and colleagues (2002) and Garcia-Donas (2017) for cortical area, and much higher than the standard errors reported by Pfeiffer (2016).

Standard errors were then calculated for the OPD and age regression model. These results were more variable than the standard errors for the cortical area regression model. Like the results from the cortical area regressions, the pathological data set performed the worst of

the three regression models, and the healthy data performed the best of all three models. For the OPD regression models there was a difference of 2.68 between the highest and lowest scoring models, a much larger difference than seen in the cortical area models. The standard error for the healthy data set is slightly higher than the standard error reported by Garcia-Donas (2017), and generally higher than the standard errors reported in other studies (Cho & al., 2002; Pfeiffer, et al., 2016). As most studies use OPD as part of a multiple linear regression-based model, the standard errors reported for these models are generally better than the errors returned from this study. If OPD were to be included in a multiple regression model, it is speculated that the standard error would improve with the fit of the model.

Overall, the results of the SEE calculations were consistent, if slightly higher than the standard errors reported by other studies. As many of these studies incorporated multiple linear regressions, it is speculated that if cortical area and OPD were combined in an equation, like those developed by Stout and Paine (1992) or Cho and colleagues (2002), the error rates would improve. In both the case of the cortical area regression model and the OPD regression model, the pathological data set performed poorly, and appeared to have an impact on the accuracy of the complete data set regression models. The healthy data set performed best, supporting the notion that pathological data should be excluded from use in histological age estimation methods.

7.2.1.6 Bootstrapping

The last statistical analysis used for the standard histology was bootstrapping. By using a sampling and replacement method, it was possible to simulate the results of the true population, by resampling from the relatively small sample size used for this study. For the

purposes of this study, bootstrapping was used to test the multiple R-squared statistic, resulting from the earlier regression analysis. The bootstrapping was used to confirm the results of the regressions from the previous section, focusing on the regressions comparing age and cortical area, and age and OPD. By using bootstrapping, this study could better compare its results with those of studies with larger samples sizes (Cho & al., 2002; Pfeiffer, et al., 2016).

Beginning with the cortical area and age regression model, bootstrapping was applied first to the entire sample, and then separately to the pathological and healthy control groups. From the results of the bootstrapping the differences between the pathological group and the other two groups become apparent. The bootstrapping mimics a larger population, theoretically improving the results of the regression, as well as testing the accuracy of the linear regression models. The bias and the standard error both indicate a good fit for the model, with the healthy data set performing best, followed by the complete data set, and then the pathological data set last, performing poorer than the others and by a larger increment. The BCa 95% confidence interval indicates that the pathological data set has a much larger range included in the confidence interval than the other data sets. These statistics prove the validity of the above calculated linear regression models, as well as displaying the deviance of the pathological samples from the normal healthy samples. This also has implications for the creation and application of histological age estimation formulae for this population, as the healthy group exhibits a good fit relationship between the variables of age and cortical area. As demonstrated by the results of the study, the inclusion of pathological samples could, however, have a negative effect on these estimations.

Following the bootstrapping for cortical area and age, bootstrapping was applied to the regression model comparing OPD and age. Again, it is evident that the results from the pathological samples are different from those of the healthy and complete data sets. From the bias results, it is evident that the healthy and complete data sets have lower results relative to the pathological data set, indicating a better fit to the regression model. This reflects expectations and the results from the previous regression section. The standard errors for the groups are low, indicating a good fit for the regression models, however inverse to the results from the cortical area regression model, the pathological group has the lowest standard error of the three groups tested. As for the cortical area results, the BCa 95% confidence interval indicates that the pathological data set has a much larger range included in the confidence interval than the other data sets. This reflects the fit of the linear regression model, and the bootstrapping implies that while the healthy regression model is a good fit, the pathological data set is not a good fit for the regression model. This could have potential implications for histological age estimation methods and supports the concept of excluding pathological samples from the creation of such formulae, as well as indicating the relative effectiveness of implementing such a formula when attempting to estimate the age of an individual with a pathology.

Overall, the results of the bootstrapping analysis corroborated the results of the regression analysis, confirming the accuracy of the R^2 statistic. This supports the previous comparisons with other studies (Stout & Paine, 1992; Cho & al., 2002; Goliath, et al., 2016; Pfeiffer, et al., 2016), as well as the implications of including pathological samples when using histological age estimation formulae.

7.2.2 Osteon Specific Metrics

Once the effects of pathology on the standard building blocks of histological age estimation had been thoroughly examined, the study continued on to analyse osteon specific metrics. These metrics were designed for this study and do not reflect any previous research, although several of the metrics appear individually in other studies (Keough, et al., 2009; Goliath, et al., 2016). These metrics were done to better quantify the observations made in the qualitative section, as the appearance of unusual or enlarged canals does not necessarily mean that they are metrically unusual upon measurement. In addition, these metrics could then be compared to age, to see if there are any correlations that might be useful in further histological research. Ten measurements were taken per Haversian system, with a total of 52,700 measurements taken in total. Inter and intra-observer error were calculated to test the reliability of the metrics. Welch's t-tests were then done to compare the healthy and pathological groups, first as a complete data set, and then as 40 individual pairs. The metric variables were then analysed through means, for correlations with age, and linear regression analysis with age.

7.2.2.1 Inter-observer Error

Inter-observer error was done by this researcher and an undergraduate volunteer. As it was carried out early in the process, not all the variables had been finalised, and the sampling technique has not yet been adopted. For these reasons, only seven of the ten osteon specific metrics were tested, but they were tested across the entire cross-section, as opposed to the four fields of view sampling methods.

Overall, the inter-observer error was not successful. While certain measurements, like the cortical area were statistically similar, most of the other variables were not as effective. There

were statistically similar measurements in all but one of the metrics, osteon maximum length, which had no statistically similar measurements. This is not necessarily uncommon, as other studies also reported high variability between observers (Keough, et al., 2009; Crowder, 2005).

There are several possible explanations for the marked difference between observers. The undergraduate volunteer was relatively new to bone histology, and therefore part of the dissimilarities could be due to experience level (Crowder, 2005), especially when considering the irregular Haversian system formations found in this study. Another possible explanation could be the method for measuring each osteon. Eventually, each osteon was measured by tracing the cement line of osteon and the canal. From this measurement, the maximum and minimum length, as well as perimeter and area could be taken. If, however, the observer had tried to measure maximum and minimum length by eye, the measurement would be less accurate, and less reliable. Method of tracing, for example using a mouse, or a stylus, could also influence the accuracy of the results. It is recommended that further testing be done in conditions that control for measurement method and experience, on all ten variables, perhaps with a sample only containing healthy individuals, to confirm these osteon specific metrics.

7.2.2.2 Intra-observer Error

Intra-observer error was done by one observer, the author, to determine the consistency of the measurements. Metrics were conducted on thin sections from five samples, using the final ten metrics, and sampling method. Each set of measurements were taken several

months apart, to avoid bias. As for the intra-observer error conducted on the standard histological variables, independent t-tests were used to evaluate the measurements.

Overall, the results for the intra-observer error were successful. Three of the five samples had all statistically similar results, and one had only one statistically different metric. One sample, CC195, had only two statistically similar variables. Two variables, canal area and canal circularity had statically similar results across all five samples, and one metric, osteon circularity, had three statistically similar results. The rest of the metric variables had four of five statistically similar results.

A possible explanation for the majority statistically different results for sample CC195, is the timing of the measurements. CC195 was one of the first slides measured, and as for the inter-observer error, may have suffered from similar problems. The more accurate stylus method of taking measurements had not yet been developed, and length measurements may have been taken separately from the area and perimeter measurements, again, possibly affecting the accuracy of the results.

While the intra-observer results suggest a reasonable amount of reliability and repeatability, similar to other studies incorporating intra-observer error for osteon specific metrics (Pfeiffer, et al., 2016; Goliath, et al., 2016), it is important to use a consistent technique to avoid varying results. It is recommended that a validation study be conducted in the future to confirm the osteon specific metrics, using a larger sample size and a consistent measurement technique.

7.2.2.3 Independent T-Tests (Full Sample)

The first comparative tests run on the osteon specific metrics were a set of ten independent t-tests on the complete sets of data to determine whether the health status of the individual had an influence on the metrics of osteons and canals. These variables could be tied to the observations made in the qualitative analysis section about osteon and canal size and shape. A Welch's independent t-test was used to analyse the samples due to the unequal variance between the pathological and healthy sets of variables.

From the results of the t-tests, five of the metrics taken had statistically significant differences between the healthy and the pathological data sets. The samples estimated means for osteon maximum length indicate that overall, osteon maximum length is smaller in the pathological samples. Canal area was significantly larger in healthy control group. This is not consistent with expectations (Brickley & Ives, 2008; Parfitt, 1984; Cho, et al., 2006), and whether this is consistent throughout the various age groups will be evaluated in the next section. For canal maximum length, the healthy samples were statistically larger than the pathological samples. Likewise, for canal minimum length, the healthy samples were statistically larger than the pathological samples. The final significant variable was canal circularity, with the sample means indicating that the healthy samples had greater circularity than the pathological samples.

From these results, several useful conclusions can be made. Overall, canals are larger in the healthy control set. It is possible that the larger canals observed in the qualitative section merely appear larger in comparison with the thinning cortical area often seen in the

pathological samples, meaning that canals occupy a larger portion of the section compared to osteons. This observation implies that qualitative assessment of bone thin section contains the same level of subjectivity as any other non-metric visual method (Nakhaeizadeh, et al., 2014; Todd, 1920; Işcan, et al., 1984; Phenice, 1969; Buikstra & Ubelaker, 1994), and quantification is necessary in order to draw useful and reliable conclusions. Another useful conclusion is the significant difference in circularity found in the canals (Ortner & Turner-Walker, 2003). This confirms the observations made earlier, as the pathological samples appear to be far less circular and consistent in shape, than the healthy controls. This supports the hypothesis that chronic pathology can have a significant effect on the metabolism of bone, similar to post-menopausal or age-related osteoporosis (Parfitt, 1984; Brickley & Ives, 2008; Cho, et al., 2006), which in turn will significantly change the bone's microstructure.

7.2.2.4 Paired Independent T-Tests

After tests had been run on the complete data set, the samples were divided into 40 pairs of one pathological and one healthy sample, matched by age, and sex if available, and tested against each other. This was done using a Welch's two sample t-test to account for the variance between samples. These samples were then further divided into five age groups, to assess any age-related connections to the metric variables.

While it is important to note that there were more samples in the older age groups on average, the older age groups also appeared to have more statistically significant differences between the healthy and the pathological samples. Overall, of 400 t-tests run for this section, approximately 42% (169 of 400) showed statistically significant differences between the

pathological sample and its healthy control samples. Of the five age groups, the group with the proportionally largest disparity between the healthy and pathological samples was age group 3 (41-50 years) with 57% (34 of 60) of metric variables returning statistically significant differences between pairs. Next was age group 4 (51-60 years) with 45% (58 of 130) and age group 5 with 43% (52 of 120). Age groups 2 and 1 had notably weaker results, with 34% (24 of 70) and 5% (1 of 20) respectively. This reflects the earlier conclusion from the qualitative section implying that age is a contributing factor in the appearance of pathological changes to bone microstructure. The fact remains that the highest percentage of differences between pathological and healthy controls was from the middle age group. One interpretation of this data may be that the period between ages 40 and 50 there is enough time for chronic disease to develop and affect the bone, while healthy bone has usually yet to be affected by age (Ortner, 2003). This may account for the 12% difference between age group 3 (41-50 years) and the next highest percentage group. It may also be connected to the OPD asymptote, the point where OPD no longer reflects age (Stout & Paine, 1994; Stout & Crowder, 2012).

Age Group 1: Under 30

Age group 1 only included two pairs, the first were both 19-years-old, and the second were 24 and 28-years-old. Of the ten variables tested, only the canal circularity metric from the second pair showed a statistically significant difference between the healthy and pathological samples. From the sample estimated means shown in the previous chapter, it is evident that on average the canals of the pathological sample were less circular than the healthy samples. This is consistent with previous findings in this study that show osteon shape irregularity in the pathological samples, as well as general expectations of bone metabolism related to osteoporosis (Ortner & Turner-Walker, 2003; Wu, et al., 2009). In the case of this age group,

the one statistically significant result came from the older of the two pairs, which included an individual with hypertension.

Age Group 2: 31-40

Age group 2 consisted of seven age-matched pairs. Of the ten osteon specific metrics tested, osteon perimeter had the most statistically significant differences between the pathological and healthy, with four of the seven pairs, followed by osteon maximum length, osteon total area, and canal circularity, which were present in three pairs of samples. Overall, there is a marked increase in statistically significant differences, jumping from 5% significant differences in the first age group, to 34% in the second. The trend in osteon metrics, rather than canal metrics is worth noting, as osteon dimensions appear to be more varied, while canal dimensions appear to remain similar regardless of health status. Canal circularity is also significant as it appeared in the previous age group as well and is consistent with expectations from previous studies (Ortner & Turner-Walker, 2003; Wu, et al., 2009).

Of the pairs included in this age group, the pair that returned the most statistically significant results was pair 3, which included the pathological sample B12 from an individual with generalised hepatic steatosis. While four other pathological samples in this age group had disease in the hepatic class, all were less advanced cases of hepatic steatosis, reflected in the fewer statistically significant results for those pairs. Two pairs from this age group included individuals who presented with atherosclerosis and returned four and three statistically significant results respectively.

Age Group 3: 41-50

The third age group consisted of six pairs. Of the ten osteon specific metrics, three had the most statistically significant differences appearing in five of the six pairs, including osteon maximum length, osteon minimum length, and osteon perimeter, followed by osteon area, which appeared in four of the six pairs. Of the six pairs, pair 13 had the most statistically significant differences, with differences present for all ten metric variables. Again, osteon dimensions seem to be the most varied, while canal dimensions appear to remain similar regardless of health status. Of all the age groups, age group 3 had the largest proportion of statistically significant differences between pathological and healthy samples, with 57% (34 of 60) of comparative tests returning statistically significant *p*-values. This could be an indication of a 'sweet spot' between chronic pathology development, and age-related bone microstructural changes (Stout & Paine, 1994; Stout & Crowder, 2012).

Of the pairs included in this age group, the pair that returned the most statistically significant results was pair 13, which included an individual with multi-system pathology, including hypertension, heart ischemia, left ventricular hypertrophy, diabetes, hepatic steatosis, pyelonephritis, and bronchopneumonia. This pair had statistically significant results for all ten variables, although due to the extent of the disease and the systemic involvement, it is not possible to know which condition provoked the skeletal response, or if the response was provoked by multiple conditions. The next most significant results came from pair 14, which included an individual with atherosclerosis, left ventricular hypertrophy, and hepatomegaly, with eight of ten variables returning significant results. The remaining pairs in this group came back with at least four significant results, with the exception of pair 10, which included an individual with hepatic steatosis. Although other pairs from this group included individuals with hepatic steatosis, it is possible those cases were more advanced, resulting in more

statistically significant results for those pairs. More research into pathology and this age group is recommended.

Age Group 4: 51-60

The next group, age group 4, consisted of thirteen pairs. Of the ten variables, two variables, osteon minimum length and osteon area, had statistically significant differences present in the most pairs, appearing in eight of the thirteen pairs, followed by osteon maximum length, and canal circularity that had statistically significant differences in seven of the thirteen pairs. Again, osteon dimensions, with the exception of canal circularity appear to be the main point of difference between the healthy and pathological samples. Of the thirteen pairs, pair 16 had the most statistically significant differences, with p-values <0.05 for nine of the ten variables. Approximately 45% (58 of 130) of the paired tests returned statistically significant results, a 12% decrease from the previous age group. As the groups are of unequal sample sizes, it is difficult to determine whether this difference is significant, however, it may be due to the increase in age, as relatively healthy bone can begin to show age-related osteoporosis (Parfitt, 1984; Ortner, 2003; Cho, et al., 2006; Stout & Crowder, 2012).

Of the pairs included in age group 4 (51-60 years), the pair that returned the most statistically significant results was pair 16, which included an individual with CAD and hypertension, as well as complications from heavy smoking, with nine statistically significant results. Pair 22, which included an individual with CAD and chronic hepatitis, had eight statistically significant results. There were four other pairs that returned seven statistically significant results, one with cancer, one with CAD and a myocardial infarction, and two with hepatic steatosis.

Overall, the results from the pairs in this age group were higher scoring, perhaps due to their age as well as the duration of their disease. Age group 4 did, however, include several lower scoring pairs, including two with hepatic steatosis, possibly indicating a less severe or shorter duration of disease in those individuals.

Age Group 5: Over 60

The last group, age group 5, consisted of twelve pairs. The metric with the highest number of significant differences was canal minimum length, with *p*-values <0.05 for eight of twelve pairs, followed by osteon area, which had statistically significant differences for seven of twelve pairs. This is inconsistent with the statistical differences seen in the previous age groups, which favoured osteon dimensions and canal circularity as the main points of difference between pathological and healthy samples. This may be due to the age of the healthy samples, as healthy individuals can show signs of age-related osteoporosis (Parfitt, 1984; Brickley & Ives, 2008), minimising the differences between the pathologically affected samples and the healthy samples. The pair with the most significant differences was pair 35, with statistically significant differences <0.0001 for all ten variables. In contrast, pair 34 showed no significant differences for any of the ten variables. There was only a slight difference between the prevalence of statistically significant differences of this age group and the previous age group, decreasing to 43% (52 of 120). While still significant, the decrease in prevalence for this age group may be due to the overlap with age-related osteoporosis and the OPD asymptote (Parfitt, 1984; Ortner, 2003; Cho, et al., 2006; Stout & Crowder, 2012), rather than a decrease in pathologically significant features.

Of the pairs included in the final group, pair 35, which included and individual with diabetes, CAD and brain ischemia, had the most statistically significant results, with all ten variables returning significant results. Three other pairs returned eight statistically significant results, including one with cancer, and two with multi-systemic diagnoses. Overall, this group had more lower scoring pairs than the previous two groups, but that may be due to age-related bone loss, as opposed to less significant disease.

Overall, the metric variables which seemed to differ the most significantly between healthy and pathological groups were those related to osteon dimensions. While this seems incongruous with previous research (Jowsey, 1963; Ortner, 1975), stating that canal dimensions change with osteoporosis, they may only appear to change. Meaning, as the dimensions of the osteon change around the Haversian canal, the canal dimensions only appear to change in relation to the surrounding osteon. The one exception appears to be osteon circularity, which was found significantly different in most of the above age groups. This implies that the metabolic changes caused by the presence of systemic pathology can affect the shape of canals, supporting the observations made in the qualitative analysis section, as well as other studies involving the histopathology of bone (Ortner & Turner-Walker, 2003; Cho, et al., 2006; Paine & Brenton, 2006). The exception to these results is the oldest age group, however due to the inherent changes present in aging bone, the possible presence of age-related osteoporosis, and the crossing of the OPD asymptote (Stout & Paine, 1994; Stout & Crowder, 2012), it is not possible to gauge which of these histomorphometric changes are related or age or pathology. As the type and severity of disease was extremely

varied, it is recommended that this testing be verified using more consistent pathological samples.

7.2.2.5 Metric Mean Values vs. Age

After statistics had been run using the complete data sets, means for each metric in each sample were calculated. These metric means were then used for correlations and linear regression models. As there is no previous research using these ten variables to test against, unlike the standard histological analysis done earlier, samples were split into pathological and healthy controls only. As age is the most significant comparative factor, the five variables observed to have a strong correlation with age were then compared with age using linear regression models to evaluate their ability to predict age, and the influence pathology would have on the metric variable's ability to predict age.

7.2.2.5.1 Correlations

To create a baseline for the new osteon specific metrics, correlations were run for the ten osteon metric means, and age. Of primary interest to this study, however, were the correlations with age. Potential age correlations may support the observations made in the qualitative section, as well as previous observations of histological bone that had not yet been quantified (Parfitt, 1984; Ortner & Turner-Walker, 2003). In addition, correlations were used as a starting point from which to begin linear regression analysis.

In the healthy group 50% (5 of 10) of the osteon specific metrics had statistically significant correlations with age. All other variables were not significantly correlated. This is consistent with Keough and colleagues (2009), who found no correlation between canal diameter and age. The variables significantly correlated with age were osteon area, osteon total area, osteon minimum length, osteon perimeter, and osteon maximum length. The correlation of osteon area with age is consistent with the findings of Goliath and colleagues (2016), however that study also found a relationship between osteon shape and age that was not reflected here for the osteon circularity variable. All five variables were negatively correlated with age.

The negative correlation implies that as age increases, the value of the variable decreases. As all the significantly correlated variables were related to osteon dimensions, this suggests that as an individual ages, the overall size of the osteons shrink, however, as there is no statistically significant correlation with age for any of the canal metrics, it appears that the canal size generally stays the same. It would then appear to the observer that the canal size had increased, as noted in the qualitative section. This observation is consistent with the findings of the 40 paired t-tests.

In connection with the standard histological correlations, it is evident that there is a negative correlation between age and cortical area. Therefore, if the average area of the cortical bone and the osteons decrease, but the area of the canals stay the same, this would contribute to the increased porosity seen in age-related osteoporosis, as observed in the qualitative section, and in previous studies (Parfitt, 1984; Paine & Brenton, 2006; Brickley & Ives, 2008). These results are consistent with expectations and provide a baseline for the correlation

analysis of the pathological samples, as well as linear regression to test the predictive abilities of the metric variables.

In the case of the pathological group as with the healthy samples, relationship to age was the primary focus of the correlation analysis. In the pathological correlations, 30% (3 of 10) of the osteon specific metrics had statistically significant correlations with age, however these correlations were much weaker than those seen in the healthy group. All other variables were not significantly correlated. The lack of correlation with the canal dimensions is consistent with the results from the healthy group and further support the findings of Keough and colleagues (2009). The variables that showed statistically significant correlation with age were osteon maximum length, osteon area, and osteon minimum length. As with the healthy controls, the significance of osteon area agrees with the findings of Goliath and colleagues (2016), despite the weaker results from the pathological group. All three variables showed a negative correlation with age which, means a decrease of osteon size with progressing age.

As with the healthy samples, negative correlations between the variables and age imply an inverse relationship. It is important to note, however, the strength of these relationships declines considerably between the healthy and the pathological samples. Osteon maximum length, the strongest correlation in the pathological group, returned a *p*-value of 0.0263, and the other two variables with significant correlations, osteon area and osteon minimum length were closer to 0.05. In comparison with the healthy group, osteon total area and osteon perimeter do not have a statistically significant relationship with age in the pathological group, implying that pathology could influence these values. This corroborates observations

made earlier in this study, and from previous studies on histopathology (Schultz, 2001; Paine & Brenton, 2006; Schultz, 2012), that pathology can have a significant effect on the histomorphometrics of bone. While this was suggested by the results of the standard histological analysis, by measuring the dimensions of the osteons, it is now possible to quantify which specific features are most affected by the pathological interruption of normal bone metabolism.

7.2.2.5.2 Regression Analysis

After the correlations for both the healthy and pathological groups, the results of these correlations were then used to inform linear regression models to test the predictive value of the relationships. As the five metric variables, osteon area, osteon total area, osteon minimum length, osteon perimeter, and osteon maximum length, were all significantly correlated with age for the healthy controls, these were the variables selected for regression analysis.

The most promising of the healthy variables was osteon area, with an adjusted R^2 of 0.3123, suggests approximately 31% of the age variance can be attributed to osteon area. Osteon total area was also promising with an adjusted R^2 of 0.2545, or approximately 25% of the age variance attributable to osteon total area. This is consistent with the findings of Goliath and colleagues (2016), which found that osteon area combined with osteon circularity in a multiple linear regression equation using the femur, produced an accurate formula (within roughly 5.9 years) for histological age estimation. Osteon minimum length and osteon perimeter were less promising, with adjusted R^2 of 0.203 and 0.1988 respectively, or

approximately 20% of the age variance attributable to the variables. This does not show a strong enough relationship with age to be useful in the context of histological age estimation, although it does provide a contrast for comparison with the results of the pathological group regressions. The final healthy variable, osteon maximum length, had the weakest result, with an adjusted R^2 of 0.1558, or approximately 16% of the age variance attributable to osteon maximum length. While the last three variables are most likely not useful in terms of histological age estimation methods, they do provide a platform for comparison with the regression analysis from the pathological group.

The pathological variables were compared with age using linear regression models in the same order as the healthy controls. The results of these models take almost reverse order to the healthy controls, the osteon total area variable being the weakest, with an adjusted R^2 of 0.0743 or approximately 7% of the age variance attributable to the variable. Osteon area was only slightly better, with an adjusted R^2 of only 0.0924, or approximately 9% of the age variance attributable to osteon area. While the healthy group returned good results for possible histological age estimation, it is clear that these variables would only work for a healthy population, and any method containing these variables, such as Goliath and colleagues (2016), would not be advised for use on individuals suffering from pathology. The variables osteon minimum length and osteon perimeter also returned low adjusted R^2, 0.1031 and 0.0959 respectively, or approximately 10% of the age variance attributable to age. These also show a clear difference between the healthy and pathological groups, regarding the variables' relationship with age, although there is less of a difference for osteon minimum length and osteon perimeter than for osteon area and osteon total area. The final variable, osteon maximum length, returned an adjusted R^2 of 0.1522, or approximately 15% of the age

variance attributable to the variable. This is very close to the R^2 returned by this variable in the healthy group, inferring that there is little difference between the healthy and the pathological groups with relationship to age for this variable. Although these results could be good for potential age estimation, as the regression models for this variable show that it is too weak to be useful as a predictor for histological age estimation.

Overall, of the regressions models created for the five most promising osteon metric means, the variable with the strongest correlation was the best for predictive purposes, although with an adjusted R-squared value of only 0.3123 it would not be recommended to use on its own, but rather as part of a multiple linear regression equation, possibly with the standard histological variables of OPD or cortical area. Although each metric variable was not valuable on its own for their predictive abilities with relation to age, the comparison of the healthy and pathological metric means was valuable, illustrating how the changes to the pathological microstructure negatively influence the correlations between the histomorphometrics and age. This clarifies the observations made from the standard histological regressions, and confirms the results of other studies that tested pathological or osteoporotic samples (Paine & Brenton, 2006; Cho, et al., 2006; Goliath, et al., 2016).

From these results, a better indication is given of the changes that might be influencing the bone remodelling process in pathological individuals, as osteon area and osteon total area, which were the most effective models for age prediction in the healthy group, were the weakest models for prediction in the pathological group. As for the standard histology variable regression models, these results indicate a change in the osteon area caused by the pathological imbalance in the bone metabolism. These fundamental changes to the bone

microstructure therefore must be taken into account when developing, or using, histological age estimation methods, such as Stout and Paine (1992) or Cho and colleagues (2002).

The variables tested between healthy and pathological samples clearly illustrate that changes in the microstructure of pathological bone reduce the correlation with age and negatively influence age estimation formulae. This is an important outcome as several studies, some of which have very limited sample sizes (e.g. Goliath et al., 2016), include pathological cases in the sample that is used to produce age estimation formulae without any control for the effect that this may have in the reliability of such formulae. Paine and Brenton (2006) have proven the relationship between pathology and bone microstructure in the case of pellagra and showed its negative influence in age prediction equations. The current study corroborates this evidence but larger samples for each pathology are needed in order to better describe in detail the associated changes in bone microstructure. As to the purposes of the current research it is evident that the inclusion pf pathological samples cannot be recommended when age estimation methods are developed for forensic purposes.

8: Conclusions

Modern disease is a challenge for the biological anthropologist and pathologist. For years, as archaeological and forensic based biological anthropology are inextricably linked, focus has been drawn by diseases of the past. Infections and vitamin deficiencies that, for the most part, are gone from the modern world. In their place, new monsters, of our own making, are rising from the shadows. Metabolic and lifestyle diseases have existed well before the twentieth century, but as infections and deficiencies have receded to the background, non-communicable diseases have been allowed to come to the fore. In today's world, it is non-communicable lifestyle diseases that kill humans by the millions. If biological anthropologists wish to apply their knowledge of the human skeleton to these problems, they must adapt to these new diseases, and learn to see the marks they leave on the bone.

Bone histology can, and should, be a part of this adaptation. As many of these diseases affect bone on a metabolic level, macro assessment of the bones can only tell us so much. By examining the bone histologically, we are better able to see and understand the changes to the bone on a micro level, to see the imbalance of the bone metabolism as it wreaks havoc on the microstructure of the skeleton. Once these changes to the microstructure are identified and classified, they can be applied to modern material, as well as historical. As histological age estimation methods have been developed and improved over the past 50 years, acknowledging these changes becomes even more important, especially when it comes to the application of forensics.

While accuracy is important in the application of methods to archaeological material, it is even more vital in the context of forensic applications. An accurate age estimation allows forensic anthropologists to help in the identification of deceased individuals, something that is becoming ever more significant in light of current world events. With the prevalence of these non-communicable diseases in the developing as well as the developed world, it is important to consider them when attempting to estimate the age of an individual.

With these considerations in mind, the following are the conclusions drawn from this research.

With regards to the qualitative analysis, three categories of micro-morphological features of pathological bone were defined. These correspond to three different responses of bone metabolism to pathological stimuli. By categorising these pathological features, it will be easier for other pathologists to recognise and replicate the results of this study. It also makes it easier to compare the pathological features of different conditions.

The sample sizes of the disease classes make it difficult to assess the connection between any particular class and any category of pathological feature. That being said category 1 features were overwhelmingly present in most pathological cases. Category 2 features were the second most common. Category 3 features, unlike the first two categories, represent a rapid deposit of bone and were only present in one case, being the least common of the pathological features. While it is unlikely that these categories could be used for diagnostic purposes due to the broad definitions and the commonality between disease classes, further study into the applications of this categorisation with larger sample sizes could yield more

informative results. Expanding into other populations and doing more disease specific studies could also enhance our understanding of pathological changes to bone microstructure.

It was also observed that age group had an effect on the appearance of pathological features, although this only included category 1 features, and only in the oldest three age groups. This skew towards the older age groups does not appear to be as present in the pathological data, but as the study included more samples in the older age groups, it would be beneficial for further studies to compare across a more even distribution of sample ages, to better understand the connection between age and the appearance of pathological features in the bone microstructure.

Quantitative analysis served a dual purpose. The first involved the analysis of the data using the standard histological variables used for histological age estimation formulae using the rib. For the complete set of data, a significant relationship was proven to exist, using correlation and regression statistics, between cortical area and age, and OPD and age. These are the same statistics Stout and Paine (1992) originally used to create the histological age estimation formulae. There was, however, a significant improvement in the relationship between cortical area and age, and OPD and age, in the healthy control group. The pathological group had very weak relationships, and poor fitting regression regarding the two variables and age. This suggests that pathology does have a significant effect on the accuracy of histological age estimation techniques. Bootstrapping confirms the fit of the models, alleviating some of the pitfalls associated with relatively small sample size. The strength of the relationships between the healthy samples and age, and the weakness of the relationships between the pathological samples and age, should not only be considered when creating new formulae for new

populations, but also for the application of these techniques on potentially pathological individuals. Further study involving other populations to investigate whether these differences in accuracy exist in them as well should be done to confirm this research.

The second part of the quantitative analysis involved the osteon specific metrics. Welch's two sample t-tests, both for the complete set of data as well as the 40 test pairs proved that there was a significant difference between the metrics of the pathological group and the healthy control group. While not every metric was significant, the canal dimensions proved to be significantly different between the groups. For the paired data, divided into age groups, age was proved to be a factor in the number of significantly different metrics, with differences peaking in the 41-50 age group at 57%. This is likely due to the fact that by this age, chronic conditions have had the time to dramatically affect the bone, but normal changes due to aging have not yet begun. These changes should be considered when attempting to estimate age for any individuals in these age groups who potentially have pathologically affected bone, as the aging affects could obscure the results. These results should also be considered when selecting metrics for use in age estimation regression equations.

The metric means of the osteon specific metrics were analysed to assess the potential relationships that might exist between any metric and age. Correlation statistics found negative relationships between the osteon metric means and age in the healthy control group, suggesting osteon dimensions shrink with age, while canal dimensions, which showed no correlation with age, would stay the same. These relationships weakened noticeably in the pathological group, suggesting pathology has a significant effect on the normal dimensions of osteons. While the regressions of these significant relationships were not particularly strong,

on their own, they could be useful if incorporated with another variable, such as OPD or cortical area, in a multiple linear regression equation. They also proved valuable when comparing the relationships of the healthy control groups with the pathological groups, giving further evidence of the microstructural differences between pathological and healthy bone. As these measurements are new to being used for histological assessment, it is recommended that further validation studies, especially on other populations, be undertaken to test the accuracy of these assessments. It is also recommended that further inter-observer studies be undertaken, to test the repeatability of the method and measurements.

Overall this study succeeded in proving the connection between chronic pathologies with the ability to affect the metabolism, and bone microstructure. If there are suspected pathological features present when samples are histologically examined, it is suggested that this be considered when attempting to estimate age, as this study has proven pathology to affect the microstructure of bone. Further studies into specific pathologies, different populations, as well as validations of the novel research undertaken in this study are recommended.

Bibliography

Ahlqvist, J. & Damsten, O., 1969. A modification of Kerleýs Method for the microscopic determination of age in human bone. *Journal of Forensic Sciences,* 14(2), pp. 205-212.

Arnaud, S., 1982. 25- Hydroxyvitamin D3 treatment of bone disease in primary biliary cirrhosis. *Gastroenterology,* 83(1), pp. 137-149.

Augat, P. & Schorlemmer, S., 2006. The role of cortical bone and its microstructure in bone strength. *Age and Ageing,* 35(S2), pp. ii27-ii31.

Bagger, Y. Z. et al., 2007. Links between cardiovascular disease and osteoporosis in postmenopausal women: serum lipids or atherosclerosis per se?. *Osteoporosis International,* Volume 18, pp. 505-512.

Baran, D. et al., 1980. Effect of alcohol ingestion on bone and mineral metabolism in rats. *American Journal of Physiology-Endocrinology and Metabolism,* 238(6), pp. E507-E510.

Bednarek, J., Awska, E. B., Engelgardt, P. & Wolska, E., 2009. Validity of histomorphometric rib assessment for age at death prediction. *Problems of Forensic Sciences,* Volume LXXX, pp. 403-410.

Bellido, T., Plotkin, L. I. & Bruzzaniti, A., 2013. Bone Cells. In: D. Burr & M. Allen, eds. *Basic and Applied Bone Biology.* London: Academic Press, pp. 27-45.

Bell, K. et al., 1997. Cortical Remodeling Following Suppression of Endogenous Estrogen with Analogs of Gonadotrophin Releasing Hormone. 12(8), pp. 1231-1240.

Bell, L. S., 2012. Histotaphonomy. In: C. Crowder & S. Stout, eds. *Bone Histology: An Anthropological Persepctive.* Boca Raton(FL): CRC Press.

Bikle, D. et al., 1985. Bone Disease in Alcohol Abuse. *Annals of Internal Medicine,* Volume 103, pp. 42-48.

Bouillon, R., 1991. Diabetic Bone Disease. *Calcified Tissue International,* Volume 49, pp. 155-160.

Brickley, M. & Ives, R., 2008. *The Bioarchaeology of Metabolic Bone Disease.* 1st Edition ed. London: Acadmic Press.

Brockstedt, H., Christiansen, P., Mosekilde, L. & Melsen, F., 1995. Reconstruction of cortical bone remodeling in untreated primary hyperparathyroidism and following surgery. *Bone,* 16(1), pp. 109-117.

Brockstedt, H. et al., 1993. Age-and sex-related changes in iliac cortical bone mass and remodeling. *Bone,* 14(4), pp. 681-691.

Buikstra, J. & Ubelaker, D., 1994. *Standards for Data Collection from Human Skeletal Remains.* 1st Edition ed. Fayetteville(AK): Arkansas Archaeological Survey.

Burr, D. & Akkus, O., 2013. Bone Morphology and Organization. In: D. Burr & M. Allen, eds. *Basic and Applied Bone Biology.* San Diego(CA): Academic Press, pp. 3-25.

Cavaillès, A. et al., 2013. Comorbidities of COPD. *European Respiratory Review,* Volume 22, pp. 454-475.

Chatila, W. et al., 2008. Comorbidities in Chronic Obstructive Pulmonary Disease. *Proceedings of the American Thoracic Society,* Volume 5, pp. 549-555.

Cho, H. & al., e., 2002. Population-Specific Histological Age-Estimating Method: A Model for Known African-American and European-American Skeletal Remains. *Journal of Forensic Sciences,* 47(1), pp. 12-18.

Cho, H., Stout, S. & Bishop, T., 2006. Cortical Bone Remodeling Rates in a Sample of African American and European American Descent Groups from the American Midwest: Comparisons of Age and Sex in Ribs. *American Journal of Physical Anthropology,* 130(2), pp. 214-226..

Cho, H., Stout, S., Madsen, R. W. & Streeter, M. A., 2002. Population-Specific Histological Age-Estimating Method: A Model for Known African-American and European-American Skeletal Remains. *Journal of Forensic Sciences,* 47(1), pp. 12-18.

Choi, Y. & Chung, Y., 2016. Type 2 diabetes mellitus and bone fragility: special focus on bone imaging. *Osteoporosis and Sarcopenia,* 2(1), pp. 20-24.

Choi, Y., Kim, D., Lee, Y. & Chung, Y., 2014. Insulin is inversely associated with bone mass especially in the insulin-resistant population: the Korea and US National Health and Nutrition Examination Surveys. *The Journal of Clinical Endocrinology & Metabolism,* 99(4), pp. 1433-1441.

Christensen, A. M. & Crowder, C. M., 2009. Evidentiary Standards for Forensic Anthropology. *Journal of Forensic Science,* 54(6), pp. 1211-1216.

Christensen, A. M., Passalaqua, V., N. & Bartelink, E. J., 2014. Age Estimation. In: A. M. Christensen, Passalaqua, N. V. & E. J. Bartelink, eds. *Forensic Anthropology: Current Methods and Practice.* Oxford: Academic Press, pp. 243-284.

Clarke, B., 2008. Normal Bone Anatomy and Physiology. *Clinical Journal of the American Society of Nephrology,* 3(S3), pp. S131-139.

Cotran, R., Kumar, V. & Collins, T., 1999. Neoplasia. In: R. Contran, V. Kumar & T. Collins, eds. *Robbins Pathologic Basis of Disease.* 6th Edition ed. Philadelphia(PA): W. B. Saunders Company, pp. 260-328.

Cotran, R., Kumar, V. & Collins, T., 1999. *Robbins Pathologic Basis of Disease.* Sixth Edition ed. Philadelphia(PA): W. B. Saunders Company.

Cotran, R., Kumar, V. & Collins, T., 1999. The Kidney. In: *Pathologic Basis of Disease.* 6th Edition ed. Philadelphia: W. B. Saunders Company, pp. 930-996.

Crawford, J., 1999. The Liver and Biliary Tract. In: R. Cotran, V. Kumar & T. Collins, eds. *Robbins Pathologic Basis of Disease.* Sixth Edition ed. San Diego(CA): W. B. Saunders Company, pp. 845-901.

Crawford, J. & Cotran, R., 1999. The Pancreas. In: R. Cotran, V. Kumar & T. Collins, eds. *Pathologic Basis of Disease.* 6th Edition ed. Philadelphia(PA): W. B. Saunders Company, pp. 902-929.

Crowder, C., 2005. *Evaluating the use of quantitative bone histology to estimate adult age at death.* s.l.:University of Toronto.

Crowder, C., Heinrich, J. & Stout, S., 2012. Rib Histomorphometry for Adult Age Estimation. In: L. S. Bell, ed. *Foresic Microscopy for Skeletal Tissues.* Totowa(NJ): Humana Press, pp. 109-127.

Crowder, C. & Rosella, L., 2007. Assessment of Intra- and Intercostal Variation in Rib Histomorphometry: Its Impact on Evidentiary Examination. *Journal of Forensic Sciences,* 52(2), pp. 271-276.

Currey, J. D., 2003. The many adaptations of bone. *Journal of Biomechanics,* 36(10), pp. 1487-1495.

de Liefde, I. I. et al., 2005. Bone mineral density and fracture risk in type-2 diabetes mellitus: the Rotterdam Study.. *Osteoporosis International,* Volume 16, pp. 1713-1720.

Diamond, T. et al., 1990. Osteoporosis and skeletal fractures in chronic liverdisease. *Gut,* Volume 31, pp. 82-87.

Dorfman, H. & Czerniak, B., 1998. Metastatic tumors in bone. In: H. Dorfman & B. Czerniak, eds. *Bone Tumors.* St Louis(MO): Mosby, pp. 1009-1040.

Drake, M. T., 2013. Osteoporosis and Cancer. *Current Osteoporosis Reports,* Volume 11, pp. 163-170.

Ericksen, M. F., 1991. Histologic Estimation of Age at Death Using the Anterior Cortex of the Femur. *American Journal of Physical Anthropology,* 84(2), pp. 171-179.
Fabbri, L. M., Luppi, F., Beghé, B. & Rabe, K. F., 2008. Complex chronic comorbidities of COPD. *European Respiratory Journal,* 31(1), pp. 204-212.

Farhat, G. N. et al., 2006. Volumetric and Areal Bone Mineral Density Measures Are Associated with Cardiovascular Disease in Older Men and Women: The Health, Aging, and Body Composition Study. *Calcified Tissue International,* 79(2), pp. 102-111.

Feitelberg, S., Epstein, S., Ismail, F. & D'Amanda, C., 1987. Deranged Bone Mineral Metabolism in Chronic Alcoholism. *Metabolism,* 36(4), pp. 322-326.

Fenton, T. W., Birkby, W. H. & Cornelison, J., 2003. A fast and safe non-bleaching method for forensic skeletal preparation. *Journal of Forensic Sciences,* 48(2), pp. 274-276.

Frost, H. M., 1966. *The bone dynamics in osteoporosis and osteomalacia.* s.l.:CC Thomas.

Frost, H. M., 1969. Tetracycline-basedHistological Analysis of Bone Remodeling. *Calcified Tissue International,* Volume 3, pp. 211-237.

Frost, H. M., 2001. From Wolff's Law to the Utah Paradigm: Insights About Bone Physiology and Its Clinical Applications. *The Anatomical Record: An Official Publication of the American Association of Anatomists,* 262(4), pp. 398-419.

Frost, H. M., 2003. Bone's mechanostat: a 2003 update. *The anatomical record part A: discoveries in molecular, cellular, and evolutionary biology,* 275(2), pp. 1081-1101.

Garcia-Donas, J., 2017. *Age estimation on two Mediterranean samples using rib histomorphometry.* Edinburgh: University of Edinburgh.

Garcia-Donas, J. & al., e., 2017. A revised method for the preparation of dry bone samples used in histological examination: Five simple steps. *Journal of Comparative Human Biology,* Volume 68, pp. 283-288.

Garcia-Donas, J. e. a., 2015. Accuracy and sampling error of two age estimation techniques using rib histomorphometry on a modern sample. *Journal of Forensic and Legal Medicine,* Volume 38, pp. 28-35.

George, J. et al., 2009. Bone mineral density and disorders of mineral metabolism in chronic liver disease. *World Journal of Gastroenterology,* 15(28), pp. 3516-3522.

Giraud-Guille, M. M., 1988. Twisted Plywood Architecture of Collagen Fibrils in Human Compact Bone Osteons. *Calcified Tissue International,* 42(3), pp. 167-180.

Goliath, J., Stewart, M. & Stout, S., 2016. Variation in osteon histomorphometrics and their impact on age-at-death estimation in older individuals. *Forensic Science International,* Volume 262, pp. 282-e1.

Gonzalez-Calvin, J. et al., 1993. Mineral Metabolism, Osteoblastic Function and Bone Mass in Chronic Alcoholism. *Alcohol and Alcoholism,* 28(5), pp. 571-579.

Gray, H., 2010. General Anatomy or Histology. In: T. Pickering Pick & R. Howden, eds. *Gray's Anatomy.* 15th Edition ed. New York(NY): Barnes and Noble.

Greenspan, A. & Remagen, W., 1998. Metasteses. In: A. Greenspan & W. Remagen, eds. *Differential Diagnosis of Tumors and Tumor-like Lesions of Bones and Joints.* Philadelphia(PA): Lippincott-Raven, pp. 367-387.

Guise, T. & Mundy, G., 1998. Cancer and Bone. *Endocrine Reviews,* 19(1), pp. 18-54.
Han, S. H. et al., 2009. Microscopic age estimation from the anterior cortex of the femur in Korean adults. *Journal of Forensic Sciences,* 54(3), pp. 519-522.

Healey, J., 1999. The epidemic of chemotherapy-related osteoporosis. *Current Opinion in Orthopaedics,* 10(5), pp. 331-333.

Herlong, H. F., Recker, R. R. & Maddrey, W. C., 1982. Bone disease in primary biliary cirrhosis: Histologic features and response to 25- hydroxyvitamin D. *Gastroenterology,* 83(1), pp. 103-108.

Hirbe, A., Morgan, E., Uluçkan, Ö. & Weilbaecher, K., 2006. Skeletal Complications of Breast Cancer Therapies. *Clinical Cancer Research,* 12(S20), pp. 6309-6314.

Hofbauer, L., Brueck, C., Singh, S. & Dobnig, H., 2007. Osteoporosis in Patients With Diabetes Mellitus. *Journal of Bone and Mineral Research,* 22(9), pp. 1317-1328.

Horvai, A., 2015. Bones, Joints, and Soft Tissue Tumors. In: V. Kumar, A. K. Abbas & J. C. Aster, eds. *Robbins & Cotran Pathologic Basis od Disease: Ninth Edition.* Philadelphia: Elsevier, pp. 1179-1226.

Işcan, M., Loth, S. & Wright, R., 1984. Metamorphosis at the sternal rib end: a new method to estimate age at death in white males. *American Journal of Physical Anthropology,* 65(2), pp. 147-156.

Imel, E., DiMeglio, L. & Burr, D., 2014. Metabolic Bone Diseases. In: D. Burr & M. Allen, eds. *Basic and Applied Bone Biology.* London: Acadmic Press, pp. 317-344.
Jørgensena, N. R. et al., 2007. The prevalence of osteoporosis in patients with chronic obstructive pulmonary disease—A cross sectional study. *Respiratory Medicine,* Volume 101, pp. 177-185.

Jørgensen, N. R. et al., 2007. The prevalence of osteoporosis in patients with chronic obstructive pulmonary disease—A cross sectional study. *Respiratory Medicine,* Volume 101, pp. 177-185.

Jähn, K. & Bonewald, L. F., 2012. Bone Cell Biology: Osteoclasts, Osteoblasts, Osteocytes. In: F. Glorieux, J. Pettifor & H. Jüppner, eds. *Paediatric Bone Biology and Diseases.* London: Academic Press, pp. 1-8.

Jowsey, J., 1960. Age Changes in Human Bone. *Clinical Orthopaedics,* Volume 17, pp. 210-218.

Jowsey, J., 1963. Microradiography of bone resorption. In: R. Sognnaes, ed. *Mechanisms of Hard Tissue Destruction.* Washington DC: American Association for the Advancement of Science, pp. 447-469.

Kaptoge, S. et al., 2003. Effects of gender, anthropometric variables, and aging on the evolution of hip strength in men and women aged over 65. *Bone,* 32(5), pp. 561-570.

Keough, N., L'Abbé, E. & Steyn, M., 2009. The evaluation of age-related histomorphometric variables in a cadaver sample of lower socioeconomic status: implications for estimating age at death. *Forensic Science International,* 191(1-3), pp. 114-e1.

Kerley, E., 1965. The Microscopic Determination of Age in Human Bone. *American Journal of Physical Anthropology,* 23(2), pp. 149-164.

Kerley, E. & Ubelaker, D., 1978. Revisions in the Microscopic Method of Estimating Age at Death in Human Cortical Bone. *American Journal of Physical Anthropology,* 49(4), pp. 545-546.

Kobzik, L., 1999. The Lungs. In: R. Cotran, V. Kumar & T. Collins, eds. *Robbins Pathologic Basis of Disease.* Sixth Edition ed. Philadelphia(PA): W. B. Saunders Company, pp. 697-755.
Kontopoulos, I., Nystrom, P. & White, L., 2016. Experimental taphonomy: post-mortem microstructural modifications in Sus scrofa domesticus bone. *Forensic Science International,* Volume 266, pp. 320-328.

Kranioti, E. F. et al., 2017. Sexual dimorphism of the tibia in contemporary Greek-Cypriots and Cretans: Forensic applications. *Forensic Science International,* Volume 271, pp. 129.e1-129.e7.

Kranioti, E. F., Işcan, M. Y. & Michalodimitrakis, M., 2008. Craniometric analysis of the modern Cretan population. *Forensic Science International,* Volume 180, pp. 1-5.

Kuller, L. H., Matthews, K. A. & Meilahn, E. N., 2000. Estrogens and women's health: interrelation of coronary heart disease, breast cancer and osteoporosis. *Journal of Steriod Biochemistry and Molecular Biology,* 74(5), pp. 297-309.

Kusinitz, M., 2014. Metabolism. In: K. L. Lerner & B. W. Lerner, eds. *The Gale Encyclopedia of Science.* 5th ed. Farmington Hills(MI): Gale.

Labib, M. et al., 1989. Bone disease in chronic alcoholism: the value of plasma osteocalcin measurement. *Alcohol and alcoholism,* 24(2), pp. 141-144.
Lalor, B. et al., 1986. Bone and mineral metabolism and chronic alcohol abuse. *QJM: An International Journal of Medicine,* 59(2), pp. 497-511.

Lee, U. Y., Jung, G. U., Choi, S. G. & Kim, Y. S., 2014. Anthropological age estimation with bone histomorphometry from the human clavicle. *The Anthropologist,* 17(3), pp. 929-936.

Leonard, M., 2009. A Structural Approach to Skeletal Fragility in Chronic Kidney Disease. *Seminars in Nephrology,* 29(2), pp. 133-143.

Levey, A. S. & Coresh, J., 2012. Chronic kidney disease. *The Lancet,* 379(9811), pp. 165-180.

Lill, C., 2013. *A Histological Study of Extra-spinal Hyperostosis related to Diffuse Idiopathic Skeletal Hyperostosis (DISH): A Comparison of Two Case Studies.* Edinburgh: University of Edinburgh.

Lindsell, D., Wilson, A. & Maxwell, J. D., 1982. Fractures on the chest radiograph in detection of alcoholic liver disease. *British Medical Journal,* Volume 285, pp. 597-599.

Long, R. et al., 1978. Clinical, biochemical, and histological studies of osteomalacia, osteoporosis, and parathyroid function in chronic liver disease. *Gut,* 19(2), pp. 85-90.

Lynnerup, N., Frohlich, B. & Thomsen, J. L., 2006. Assessment of age at death by microscopy: Unbiased quantification of secondary osteons in femoral cross sections. *Forensic Science International,* 159(S15), pp. S100-103.

Lynnerup, N., Thomsen, J. & Frohlich, B., 1998. Intra-and inter-observer variation in histological criteria used in age at death determination based on femoral cortical bone. *Forensic Science International,* 91(3), pp. 219-230.

Maat, G. J. R., Maes, A., Aarents, M. J. & Nagelkerke, N. J. D., 2006. Histological age prediction from the femur in a contemporary Dutch sample: The decrease of nonremodeled bone in the anterior cortex. *Journal of Forensic Sciences,* 51(2), pp. 230-237.

Maat, G., Maes, A., M.J., A. & Nagelkerke, N., 2006. Histological Age Prediction from the Femur in aContemporary Dutch Sample* The decrease of nonremodeled bone in theanterior cortex. *Journal of Forensic Sciences,* 51(2), pp. 230-237.

Maggiano, C. M., 2012. Making the Mold: A Microstructural Persepctive on Bone Modelling during Growth and Mechanical Adaptation. In: C. Crowder & S. Stout, eds. *Bone Histology: an anthropological persepctive.* Boca Raton(FL): CRC Press, pp. 45-90.

Maggi, S. et al., 2009. Osteoporosis Risk in Patients With Chronic Obstructive Pulmonary Disease: The EOLO Study. *Journal of Densitometry,* 12(3), pp. 345-352.

Magnus, J. & Broussard, D., 2005. Relationship between bone mineral density and myocardial infarction in US adults. *Osteoporosis International,* Volume 16, pp. 2053-2062.
Malluche, H. H. & Faugere, M.-C., 1990. Renalbonedisease190:Anunmetchalenge forthenephrologis. *Kidney International,* 38(2), pp. 193-211.

Marcovitz, P. et al., 2005. Usefulness of Bone Mineral Density to Predict Significant Coronary Artery Disease. *The American Journal of Cardiology,* 96(8), pp. 1059-1063.

Martin, D. L., 1983. *Paleophysiological aspects of bone remodeling in the Meroitic, X-Group and Christian populations from Sudanese Nubia.* s.l.:University of Massachusetts.

Martin, E., ed., 2010. *Oxford Colour Concise Medical Dictionary.* 5th Edition ed. Oxford: Oxford University Press.

McCarthy, E., 2010. Metabolic Bone Disorders. In: J. Khurana, E. McCarthy & P. Zhang, eds. *Essentials in Bone and Soft Tissue Pathology.* New York(NY): Springer, pp. 61-68.

Miller, P., 2005. Treatment of Osteoporosis in Chronic Kidney Disease and End-stage Renal Disease. *Current Osteoporosis Reports,* 3(1), pp. 5-12.

Mineo, T. et al., 2005. Bone mineral density improvement after lung volume reduction surgery for severe emphysema. *Chest,* 127(6), pp. 1960-1966.

Mobarhan, S. et al., 1984. Metabolic Bone Disease in Alcoholic Cirrhosis: A Comparison of the Effect of Vitamin D2 25-Hydroxyvitamin D, or Supportive Treatment. *Hepatology,* 4(2), pp. 266-273.

Morrison, L. B. & Bogan, I. K., 1927. Bone development in diabetic children: a roentgen study. *American Journal of Medical Science,* Volume 174, pp. 313-319.

Mulhern, D. & Ubelaker, D., 2012. Differetiating Human from Nonhuman Bone Microstructure. In: C. Crowder & S. Stout, eds. *Bone Histology: An Anthropological Persepctive.* Boca Raton(FL): CRC Press, pp. 109-134.

Mulhern, D. & Van Gerven, D., 1997. Patterns of Femoral Bone Remodeling Dynamicsin a Medieval Nubian Population. *American Journal of Physical Anthropology,* 104(1), pp. 133-146.

Mussolino, M. E., Madans, J. H. & Gillum, R. F., 2003. Bone mineral density and mortality in women and men: the NHANES I Epidemiologic Follow-up Study.. *Annals of Epidemiology,* 13(10), pp. 692-697.

Nakhaeizadeh, S., Dror, I. & Morgan, R., 2014. Cognitive bias in forensic anthropology: visual assessment of skeletal remains is susceptible to confirmation bias. *Science and Justice,* 54(3), pp. 208-214.

Nor, F. M., Pastor, R. F. & Schutkowski, H., 2014. Age at death estimation from bone histology in Malaysian males. *Medicine, Science, and the Law,* 54(4), pp. 203-208.
Olszta, M. J. et al., 2007. Bone structure and formation: A new perspective. *Materials Science and Engineering R Reports,* 58(3), pp. 77-116.

Ortner, D. J., 2003. Methods Used in the Analysis of Skeletal Lesions. In: D. Ortner, ed. *Identification of Pathological Conditions in Human Skeletal Remains.* San Diego: Academic Press, pp. 45-64.

Ortner, D. J., 2003. Osteoarthritis and Diffuse Idiopathic Skeletal Hyperostosis. In: D. Ortner, ed. *Identification of Pathological Conditions in Human Skeletal Remains.* San Diego(CA): Academic Press, pp. 545-560.

Ortner, D. J., 2003. Theoretical Issues in Paleopathology. In: *Identification of Pathological Conditions in Human Skeletal Remains.* 2nd Edition ed. San Diego(CA): Academic Press, pp. 109-118.

Ortner, D. J., 1975. Aging effects on osteon remodelling. *Calcified Tissue Research,* 18(1), pp. 27-36.

Ortner, D. J., 2003. Metabolic Disorders. In: D. J. Ortner, ed. *Identification of Pathological Conditions in Human Skeletal Remains.* 2nd ed. San Diego(CA): Academic Press, pp. 383-418.

Ortner, D. J., 2003. Theoretical Issues in Paleopathology. In: D. J. Ortner, ed. *Identification of Pathological Conditions in Human Skeletal Remains.* 2nd Edition ed. San Diego(CA): Academic Press, pp. 109-118.

Ortner, D. J., 2003. Tumors and Tumor-like Lesions of Bone. In: D. J. Ortner, ed. *Identification of Pathological Conditions in Human Skeletal Remains.* 2nd Edition ed. San Diego: Academic Press, pp. 503-544.

Ortner, D. J. & Turner-Walker, G., 2003. The Biology of Skeletal Tissues. In: D. J. Ortner, ed. *Identification of Pathological Conditions in Human Skeletal Remains.* 2nd Edition ed. San Diego: Academic Press.

Ott, S., 2009. Bone Histomorphometry in Renal Osteodystrophy. *Seminars in Nephrology,* 29(2), pp. 122-132.

Paine, R., 2007. Do it yourself How to equip a basic histological lab for the anthropological assessment of human bone and teeth. *Journal of Anthropological Sciences,* Volume 85, pp. 213-219.

Paine, R. & Brenton, B., 2006. Dietary Health Does Affect Histological Age Assessment: An Evaluation of the Stout and Paine (1992) Age Estimation Equation Using Secondary Osteons from the Rib. *Journal of Forensic Science,* 51(3), pp. 489-492.

Parfitt, A. M., 1984. Age-Related Structural Changes in Trabecular and Cortical Bone: Cellular Mechanisms and Biomechanical Consequences. *Calcified Tissue International,* 36(S1), pp. 123-128.

Pérez-Castrillón, J.-L.et al., 2004. Non-insulin-dependent diabetes, bone mineral density, and cardiovascular risk factors. *Journal of Diabetes and its Complications,* 18(6), pp. 317-321.

Peris, P. et al., 1992. Reduced spinal and femoral bone mass and deranged bone mineral metabolism in chronic alcoholics. *Alcohol and alcoholism,* 27(6), pp. 619-625.

Pfeiffer, S., 1998. Variability in osteon size in recent human populations. *American Journal of Physical Anthropology,* 106(2), pp. 219-227.

Pfeiffer, S., Heinrich, J., Beresheim, A. & Alblas, M., 2016. Cortical Bone Histomorphology of Known-Age Skeletons From the Kirsten Collection, Stellenbosch University, South Africa. *American Journal of Physical Anthropology,* 160(1), pp. 137-147.

Pfeiffer, S. & Zehr, M., 1996. A morphological and histological study of the human humerus from Border Cave. *Journal of Human Evolution,* Volume 31, pp. 49-59.

Phenice, T., 1969. A newly developed visual method of sexing the os pubis. *American Journal of Physical Anthropology,* Volume 30, pp. 297-301.

Rey, C., Combes, C., Drouet, C. & Glimcher, M. J., 2009. Bone mineral: update on chemical composition and structure. *Osteoporosis International,* 20(6), pp. 1013-1021.

Reznikov, N., Shahar, R. & Weiner, S., 2014. Three-dimensional structure of human lamellar bone: The presence of two different materials and new insights into the hierarchical organization. *Bone,* Volume 59, pp. 93-104.

Riggs, B. L., Khosla, S. & Melton, L. J., 1998. A Unitary Model for Involutional Osteoporosis: Estrogen Deficiency Causes Both Type I and Type II Osteoporosis in Postmenopausal Women and Contributes to Bone Loss in Aging Men. *Journal of Bone and Mineral Research,* 13(5), pp. 763-773.

Rosenberg, A., 1999. Bones, Joints, and Soft Tissue Tumors. In: R. Cotran, V. Kumar & T. Collins, eds. *Robbins Pathologic Basis of Disease.* Sixth Edition ed. Philadelphia: W. B. Saunders Company, pp. 1215-1268.

Ruff, C. B., Larsen, C. S. & Hayes, W. C., 1984. Structural changes in the femur with the transition to agriculture on the Georgia coast. *American Journal of Physical Anthropology,* 64(2), pp. 125-136.

Samson, D. & Branigan, K., 1987. A new method of estimating age at death from fragmentary and weathered bone. In: A. Bodington, A. Garland & R. Janaway, eds. *Death, decay, and reconstruction: approaches to archaeology and forensic science.* Manchester: Machester University Press.

Scheuer, L. & Black, S., 2004. *The Juvenile Skeleton.* 1st Edition ed. London: Elsevier.
Schnitzler, C. & Soloman, L., 1985. Bone changes after alcohol abuse. *South African Medical Journal,* Volume 66, pp. 730-734.

Schoen, F. & Cotran, R., 1999. Blood Vessels. In: R. Cotran, V. Kumar & T. Collins, eds. *Pathologic Basis of Disease.* 6th Edition ed. Philadelphia(PA): W. B. Saunders Company, pp. 493-542.

Schoen, F. J., 1999. The Heart. In: R. Cotran, V. Kumar & T. Collins, eds. *Pathologic Basis of Disease.* 6th Edition ed. Philadelphia: W. B. Saunders Company, pp. 543-600.

Schultz, M., 2001. Paleohistopathology of Bone: A New Approach to the Study of Ancient Diseases. *Yearbook of Physical Anthropology,* Volume 44, pp. 106-147.

Schultz, M., 2012. Light Microscopic Analysis of Macerated Pathologically Changed Bones. In: C. Crowder & S. Stout, eds. *Bone Histology: an Anthropologyical Perspective.* Boca Raton(FL): CRC Press, pp. 153-220.

Schultz, M., 2012. Light Microscopic Anlaysis of Macerated Pathologically Changed Bones. In: C. Crowder & S. Stout, eds. *Bone Histology: An Anthropological Perspective.* Boca Raton(FL): CRC Press, pp. 253-296.

Scientific Working Group for Forensic Anthropology (SWGANTH), 2013. *Age Estimation.* [Online]
Available at:
https://www.nist.gov/sites/default/files/documents/2018/03/13/swganth_age_estimation.pdf
[Accessed 10 May 2019].

Seeman, E., 2008. Modeling and Remodeling: The Cellular Machinery Responsible for the Gain and Loss of Bone's Material and Structural Strength. In: T. J. Martin, L. G. Raisz & J. P. Bilezikian, eds. *Principles of Bone Biology.* 3rd Edition ed. London: Acadmic Press, pp. 3-28.

Shah, V., Shah, C. & Snell-Bergeon, J., 2015. Type 1 diabetes and risk of fracture: meta-analysis and review of the literature. *Diabetic Medicine,* 32(9), pp. 1134-1142.

Shulman, G. & Peterson, K. F., 2017. Metabolism. In: W. Boron & E. Boulpaep, eds. *Medical Physiology.* 3rd Edition ed. Philadelphia(PA): Elsevier.

Smith, M., 2006. Treatment-Related Osteoporosis in Men with Prostate Cancer. *Clinical Cancer Research,* 12(S20), pp. 6315-6319.

Spencer, H. et al., 1986. Chronic Alcoholism: Frequently Overlooked Cause of Osteoporosis in Men. *The AMerican Journal of Medicine,* Volume 80, pp. 393-397.

Sprini, D. et al., 2014. Correlation between osteoporosis and cardiovascular disease. *Clinical Cases in Mineral and Bone Metabolism,* 11(2), pp. 117-119.

Stein, E. et al., 2011. Vitamin D deficiency influences histomorphometric features of bone in primary hyperparathyroidism. *Bone,* 48(3), pp. 557-561.

Stout, S., 1986. The use of bone histomorphometry in skeletal identification: the case of Francisco Pizarro. *Journal of Forensic Science,* 31(1), pp. 296-300.

Stout, S. & Crowder, C., 2012. Bone Remodelling, Histomorphology, and Histomorphometry. In: C. Crowder & S. Stout, eds. *Bone Histology: An Anthropological Perspective.* Boca Raton(FL): CRC Press, pp. 1-22.

Stout, S. & Gehlert, S., 1982. Effects of Field Size When Using Kerley's Histological Method for Determination of Age at Death. *American Journal of Physical Anthropology,* 58(2), pp. 123-125.

Stout, S. & Paine, R., 1992. Brief Communication: Histological Age Estimation Using Rib and Clavicle. *American Journal of Physical Anthropology,* Volume 87, pp. 111-115.

Stout, S. & Paine, R., 1994. Brief Communication: Bone Remodeling Rates: A Test of an Algorithm for Estimating Missing Osteons. *American Journal of Physical Anthropology,* Volume 93, pp. 123-129.

Stout, S., Porro, M. & Perotti, B., 1996. Brief Communication: A Test and Correction of the Clavicle Method of Stout and Paine for Histological Age Estimation of Skeletal Remains. *American Journal of Physical Anthropology,* Volume 100, pp. 139-142.

Streeter, M., 2012. Histological Age-at-Death Estimation. In: C. Crowder & S. Stout, eds. *Bone Histology: an anthropological perspective.* Boca Raton(FL): CRC Press, pp. 135-152.

Theise, N. D., 2015. Liver and Gallbladder. In: V. Kumar, A. K. Abbas & J. C. Aster, eds. *Robbins and Cotran Pathologic Basis of Disease.* 9th Edition ed. Philadelphia: W. B. Saunders Company, pp. 821-881.

Thompson, D., 1980. Age changes in bone mineralization, cortical thickness, and haversian canal area. *Calcified Tissue International,* 31(1), pp. 5-11.

Thompson, D. D., 1979. The Core Technique in the Determination of Age at Death in Skeletons. *Journal of Forensic Sciences,* 24(4), pp. 902-915.

Thompson, D. D. & Galvin, C. A., 1983. Estimation of Age At Death By Tibial Osteon Remodeling in an Autopsy Series. *Forensic Science International,* 22(2-3), pp. 203-211.

Todd, T., 1920. Age changes in the pubic bone. *American Journal of Physical Anthropology,* Volume 3, pp. 467-470.

Trivedi, D. P. & Khaw, K. T., 2001. Bone mineral density at the hip predicts mortality in elderly men. *Osteoporosis International,* 12(4), pp. 259-265.

Turner, R., Greene, V. & Bell, N., 1987. Demonstration that ethanol inhibits bone matrix synthesis and mineralization in the rat. *Journal of Bone and Mineral Research,* 2(1), pp. 61-66.

Ulijaszek, S. J. & Kerr, D. A., 1999. Anthropometric measurement error and the assessment of nutritional status. *British Journal of Nutrition,* Volume 82, pp. 165-177.

University of Edinburgh, Division of Pathology, 2017. *QuPath.* [Online]
Available at: https://qupath.github.io
[Accessed 27 April 2019].

Uytterschaut, H. T., 1985. Determination of skeletal age by histological methods. *Zeitschrift für Morphologie und Anthropologie,* Volume 75, pp. 331-340.

Väänänen, H. K., Zhao, H., Mulari, M. & Halleen, J. M., 2000. The cell biology of osteoclast function. *Journal of Cell Science,* 113(3), pp. 377-381.

Van Daele, P. et al., 1995. Bone Density in Non-Insulin-Dependent Diabetes Mellitus The Rotterdam Study. *Annals of Internal Medicine,* 122(6), pp. 409-414.

Van Der Klift, M. et al., 2002. Bone mineral density and mortality in elderly men and women: the Rotterdam Study.. *Bone,* 30(4), pp. 643-648.

Van der Merwe, A. E., Maat, G. J. R. & Steyn, M., 2010. Ossified Haematomas and Infectious Bone Changes on the Anterior Tibia: Histomorphological Features as an Aid for Accurate Diagnosis. *Internaitonal Journal of Osteoarchaeology,* 20(2), pp. 227-239.

Verbanck, M., Verbanck, J., Brauman, J. & P., M. J., 1976. Bone Histology and 25-OH Vitamin D Plasma Levels in Alcoholics without Cirrhosis. *Calcified Tissue Research,* Volume 22, pp. 538-541.

Vestergaard, P., 2007. Discrepancies in bone mineral density and fracture risk in patients with type 1 and type 2 diabetes—a meta-analysis. *Osteoporosis International,* Volume 18, pp. 427-444.

Viguet-Carrin, S., Garnero, P. & Delmas, P. D., 2006. The role of collagen in bone strength. *Osteoporosis International,* 17(3), pp. 319-336.

Webster, A. C., Nagler, E. V., Morton, R. L. & Masson, P., 2017. Chronic kidney disease. *The Lancet,* 389(10075), pp. 1238-1252.

White, T. & Folkens, P., 2005. *The Human Bone Manuel.* 1 ed. Burlington(MA): Elsevier Academic Press.

Williams, M., 2009. Chronic Kidney Disease/Bone and Mineral Metabolism: The Imperfect Storm. *Seminars in Nephrology,* 29(2), pp. 97-104.

World Health Organisation, 2017. *Chronic obstructive pulmonary disease (COPD).* [Online]
Available at: http://www.who.int/en/news-room/fact-sheets/detail/chronic-obstructive-pulmonary-disease-(copd)
[Accessed 18 September 2018].

World Health Organisation, 2018. *Chronic Respiratory Diseases.* [Online]
Available at: http://www.who.int/respiratory/en/
[Accessed 18 September 2018].

World Health Organization, 2017. *Cardiovascular diseases (CVD's).* [Online]
Available at: http://www.who.int/en/news-room/fact-sheets/detail/cardiovascular-diseases-(cvds)
[Accessed 17 September 2018].

World Health Organization, 2017. *Diabetes.* [Online]
Available at: http://www.who.int/en/news-room/fact-sheets/detail/diabetes
[Accessed 18 September 2018].

World Health Organization, 2018. *Alcohol.* [Online]
Available at: http://www.who.int/en/news-room/fact-sheets/detail/alcohol
[Accessed 19 September 2018].

World Health Organization, 2018. *Noncommunicable Diseases.* [Online]
Available at: http://www.who.int/news-room/fact-sheets/detail/noncommunicable-diseases
[Accessed 21 September 2018].

Wu, Y. et al., 2009. Cortical bone mineralization differences between hip-fractured females and controls. A microradiographic study.. *Bone,* 45(2), pp. 207-212.

Yoshino, M., Imaizumi, K., Miyasaka, S. & Seta, S., 1994. Histological estimation of age at death using microradiographs of humeral compact bone. *Forensic Science International,* 64(2-3), pp. 191-198.

Appendix

A. 1: Spearman's R and Converted *p*-values for Standard Histology

A.1.1 Complete Sample

	Age	Sex	status	Complete	Frag	Total	CortArea	OPD
Age	1.00	0.11	-0.21	-0.24	0.17	-0.13	-0.52	0.44
Sex	0.11	1.00	-0.38	-0.24	0.11	-0.13	-0.27	0.29
status	-0.21	-0.38	1.00	0.30	-0.25	0.14	0.29	-0.22
Complete	-0.24	-0.24	0.30	1.00	0.52	0.94	0.71	0.16
Frag	0.17	0.11	-0.25	0.52	1.00	0.74	0.20	0.60
Total	-0.13	-0.13	0.14	0.94	0.74	1.00	0.60	0.36
CortArea	-0.52	-0.27	0.29	0.71	0.20	0.60	1.00	-0.48
OPD	0.44	0.29	-0.22	0.16	0.60	0.36	-0.48	1.00

n= 80

P

	Age	Sex	status	Complete	Frag	Total	CortArea	OPD
Age		0.3538	0.0614	0.0333	0.1234	0.2543	0.0000	0.0000
Sex	0.3538		0.0004	0.0337	0.3412	0.2423	0.0144	0.0089
status	0.0614	0.0004		0.0061	0.0252	0.2202	0.0088	0.0537
Complete	0.0333	0.0337	0.0061		0.0000	0.0000	0.0000	0.1541
Frag	0.1234	0.3412	0.0252	0.0000		0.0000	0.0751	0.0000
Total	0.2543	0.2423	0.2202	0.0000	0.0000		0.0000	0.0012
CortArea	0.0000	0.0144	0.0088	0.0000	0.0751	0.0000		0.0000
OPD	0.0000	0.0089	0.0537	0.1541	0.0000	0.0012	0.0000	

A.1.2 Pathological Sample

	Origin	Age	Sex	Complete	Frag	Total	CortArea	OPD	AgeEst
Origin	1.00	0.71	-0.25	-0.34	-0.27	-0.33	-0.31	-0.10	-0.10
Age	0.71	1.00	-0.26	-0.17	-0.13	-0.18	-0.35	0.10	0.10
Sex	-0.25	-0.26	1.00	-0.01	0.10	0.02	-0.19	0.26	0.26
Complete	-0.34	-0.17	-0.01	1.00	0.61	0.97	0.59	0.39	0.39
Frag	-0.27	-0.13	0.10	0.61	1.00	0.73	0.32	0.57	0.57
Total	-0.33	-0.18	0.02	0.97	0.73	1.00	0.55	0.47	0.47
CortArea	-0.31	-0.35	-0.19	0.59	0.32	0.55	1.00	-0.42	-0.42
OPD	-0.10	0.10	0.26	0.39	0.57	0.47	-0.42	1.00	1.00
AgeEst	-0.10	0.10	0.26	0.39	0.57	0.47	-0.42	1.00	1.00

n= 40

P

	Origin	Age	Sex	Complete	Frag	Total	CortArea	OPD	AgeEst
Origin		0.0000	0.1198	0.0329	0.0909	0.0354	0.0501	0.5232	0.5232
Age	0.0000		0.1090	0.2815	0.4193	0.2728	0.0280	0.5533	0.5533
Sex	0.1198	0.1090		0.9339	0.5495	0.8945	0.2281	0.1053	0.1053
Complete	0.0329	0.2815	0.9339		0.0000	0.0000	0.0000	0.0134	0.0134
Frag	0.0909	0.4193	0.5495	0.0000		0.0000	0.0410	0.0001	0.0001
Total	0.0354	0.2728	0.8945	0.0000	0.0000		0.0002	0.0022	0.0022
CortArea	0.0501	0.0280	0.2281	0.0000	0.0410	0.0002		0.0063	0.0063
OPD	0.5232	0.5533	0.1053	0.0134	0.0001	0.0022	0.0063		0.0000
AgeEst	0.5232	0.5533	0.1053	0.0134	0.0001	0.0022	0.0063	0.0000	

A.1.3. Healthy Sample

	Origin	Age	Sex	Complete	Frag	Total	CortArea	OPD	AgeEst
Origin	1.00	0.18	0.19	0.28	0.53	0.42	0.12	0.34	0.34
Age	0.18	1.00	0.23	-0.24	0.28	-0.04	-0.66	0.70	0.70
Sex	0.19	0.23	1.00	-0.23	-0.01	-0.17	-0.15	0.25	0.25
Complete	0.28	-0.24	-0.23	1.00	0.70	0.93	0.73	0.15	0.15
Frag	0.53	0.28	-0.01	0.70	1.00	0.88	0.30	0.59	0.59
Total	0.42	-0.04	-0.17	0.93	0.88	1.00	0.58	0.36	0.36
CortArea	0.12	-0.66	-0.15	0.73	0.30	0.58	1.00	-0.46	-0.46
OPD	0.34	0.70	0.25	0.15	0.59	0.36	-0.46	1.00	1.00
AgeEst	0.34	0.70	0.25	0.15	0.59	0.36	-0.46	1.00	1.00

n= 40

P

	Origin	Age	Sex	Complete	Frag	Total	CortArea	OPD	AgeEst
Origin		0.2568	0.2510	0.0793	0.0005	0.0063	0.4632	0.0293	0.0293
Age	0.2568		0.1491	0.1301	0.0802	0.7969	0.0000	0.0000	0.0000
Sex	0.2510	0.1491		0.1493	0.9572	0.3045	0.3661	0.1236	0.1236
Complete	0.0793	0.1301	0.1493		0.0000	0.0000	0.0000	0.3653	0.3653
Frag	0.0005	0.0802	0.9572	0.0000		0.0000	0.0620	0.0000	0.0000
Total	0.0063	0.7969	0.3045	0.0000	0.0000		0.0000	0.0236	0.0236
CortArea	0.4632	0.0000	0.3661	0.0000	0.0620	0.0000		0.0030	0.0030
OPD	0.0293	0.0000	0.1236	0.3653	0.0000	0.0236	0.0030		0.0000
AgeEst	0.0293	0.0000	0.1236	0.3653	0.0000	0.0236	0.0030	0.0000	

A.2 Regression Outputs for Standard Histology

A.2.1 Complete Sample Regression Model Output: Cortical Area and Age

```
Residuals:
  Min      1Q  Median      3Q     Max
-32.336 -10.564   0.799   9.118  40.673

Coefficients:
  Estimate Std. Error t value Pr(>|t|)
(Intercept)  82.1126     5.1013  16.097  < 2e-16 ***
  CortArea     -1.2744     0.2514  -5.068 2.63e-06 ***
  ---
  Signif. codes:  0 ‘***’ 0.001 ‘**’ 0.01 ‘*’ 0.05 ‘.’ 0.1 ‘ ’ 1

Residual standard error: 15.46 on 78 degrees of freedom
Multiple R-squared:  0.2477,  Adjusted R-squared:  0.2381
F-statistic: 25.69 on 1 and 78 DF,  p-value: 2.633e-06
```

A.2.2 Pathological Sample Regression Model Output: Cortical Area and Age

```
Residuals:
   Min      1Q  Median      3Q     Max
-31.502 -11.520   0.516   8.016  38.504

Coefficients:
         Estimate Std. Error t value Pr(>|t|)
(Intercept)  72.0406     8.5843   8.392 3.51e-10 ***
CortArea     -0.8615     0.3961  -2.175   0.0359 *
---
Signif. codes:  0 ‘***’ 0.001 ‘**’ 0.01 ‘*’ 0.05 ‘.’ 0.1 ‘ ’ 1

Residual standard error: 15.52 on 38 degrees of freedom
Multiple R-squared:  0.1107,  Adjusted R-squared:  0.0873
F-statistic:  4.73 on 1 and 38 DF,  p-value: 0.03593
```

A.2.3 Healthy Sample Regression Model Output: Cortical Area and Age

```
Residuals:
   Min     1Q Median     3Q    Max
-32.39 -11.81   2.39  11.42  23.60

Coefficients:
         Estimate Std. Error t value Pr(>|t|)
(Intercept)  87.3396     6.4228  13.598 3.54e-16 ***
CortArea     -1.4886     0.3416  -4.358 9.63e-05 ***
---
```

```
Signif. codes:  0 ‘***’ 0.001 ‘**’ 0.01 ‘*’ 0.05 ‘.’ 0.1 ‘ ’ 1

Residual standard error: 15.36 on 38 degrees of freedom
Multiple R-squared:  0.3333,  Adjusted R-squared:  0.3157
F-statistic: 18.99 on 1 and 38 DF,  p-value: 9.625e-05
```

A.2.4 Complete Sample Regression Model Output: OPD and Age

```
Residuals:
  Min      1Q  Median      3Q     Max
-29.418  -9.674  -1.630   7.496  44.304

Coefficients:
  Estimate Std. Error t value Pr(>|t|)
(Intercept)  28.0238     6.5226   4.296 4.96e-05 ***
  OPD          2.1234     0.4481   4.738 9.51e-06 ***
  ---
  Signif. codes:  0 ‘***’ 0.001 ‘**’ 0.01 ‘*’ 0.05 ‘.’ 0.1 ‘ ’ 1

Residual standard error: 15.71 on 78 degrees of freedom
Multiple R-squared:  0.2235,  Adjusted R-squared:  0.2135
F-statistic: 22.45 on 1 and 78 DF,  p-value: 9.511e-06
```

A.2.5 Pathological Sample Regression Model Output: OPD and Age

```
Residuals:
   Min      1Q  Median      3Q     Max
-32.332 -11.202   0.203   6.752  41.454

Coefficients:
          Estimate Std. Error t value Pr(>|t|)
(Intercept)  47.1246    10.4336   4.517 5.93e-05 ***
OPD          0.5312     0.7643   0.695    0.491
---
Signif. codes:  0 ‘***’ 0.001 ‘**’ 0.01 ‘*’ 0.05 ‘.’ 0.1 ‘ ’ 1

Residual standard error: 16.36 on 38 degrees of freedom
Multiple R-squared:  0.01255,           Adjusted R-squared:  -0.01343
F-statistic: 0.4831 on 1 and 38 DF,  p-value: 0.4913
```

A.2.6 Healthy Sample Regression Model Output: OPD and Age

```
Residuals:
   Min      1Q  Median      3Q     Max
```

```
-29.869  -8.658  -2.011   6.647  35.464

Coefficients:
            Estimate Std. Error t value Pr(>|t|)
(Intercept)  17.5412     7.8482   2.235   0.0314 *
OPD           2.9633     0.5095   5.817 1.02e-06 ***
---
Signif. codes:  0 ‘***’ 0.001 ‘**’ 0.01 ‘*’ 0.05 ‘.’ 0.1 ‘ ’ 1

Residual standard error: 13.68 on 38 degrees of freedom
Multiple R-squared:  0.471,    Adjusted R-squared:  0.4571
F-statistic: 33.83 on 1 and 38 DF,  p-value: 1.016e-06
```

A.3 Osteon Specific Metrics Correlations

A.3.1 Spearman's R Healthy Osteon Specific Metrics Correlations

	Age	OMaxLMean	OMinLMean	OPeriMean	OTAreaMean	CAreaMean	OAreaMean	OCircMean	CMaxLMean	CMinLMean	CCircMean
Age	1	-0.47	-0.48	-0.47	-0.56	-0.1	-0.64	-0.15	-0.16	0.05	0.32
OMaxLMean	-0.47	1	0.85	0.93	0.89	0.61	0.89	-0.02	0.67	0.5	-0.45
OMinLMean	-0.48	0.85	1	0.87	0.9	0.63	0.89	0.2	0.66	0.63	-0.29
OPeriMean	-0.47	0.93	0.87	1	0.94	0.64	0.93	-0.07	0.75	0.53	-0.49
OTAreaMean	-0.56	0.89	0.9	0.94	1	0.72	0.95	0.07	0.76	0.59	-0.38
CAreaMean	-0.1	0.61	0.63	0.64	0.72	1	0.52	-0.06	0.93	0.84	-0.14
OAreaMean	-0.64	0.89	0.89	0.93	0.95	0.52	1	0.05	0.6	0.43	-0.46
OCircMean	-0.15	-0.02	0.2	-0.07	0.07	-0.06	0.05	1	-0.18	0.02	0.39
CMaxLMean	-0.16	0.67	0.66	0.75	0.76	0.93	0.6	-0.18	1	0.81	-0.37
CMinLMean	0.05	0.5	0.63	0.53	0.59	0.84	0.43	0.02	0.81	1	-0.06
CCircMean	0.32	-0.45	-0.29	-0.49	-0.38	-0.14	-0.46	0.39	-0.37	-0.06	1

A.3.2 Converted *p*-value Healthy Osteon Specific Metrics Correlations

	Age	OMaxLMean	OMinLMean	OPeriMean	OTAreaMean	CAreaMean	OAreaMean	OCircMean	CMaxLMean	CMinLMean	CCircMean
Age		0.0036	0.0028	0.003	0.0003	0.5466	0	0.3618	0.3463	0.775	0.0523
OMaxLMean	0.0036		0	0	0	0	0	0.8958	0	0.0014	0.0054
OMinLMean	0.0028	0		0	0	0	0	0.2356	0	0	0.0802
OPeriMean	0.003	0	0		0	0	0	0.6737	0	0.0007	0.0019
OTAreaMean	0.0003	0	0	0		0	0	0.687	0	0.0001	0.0215
CAreaMean	0.5466	0	0	0	0		0.0009	0.7264	0	0	0.417
OAreaMean	0	0	0	0	0	0.0009		0.7539	0	0.008	0.0043
OCircMean	0.3618	0.8958	0.2356	0.6737	0.687	0.7264	0.7539		0.2763	0.8947	0.0162
CMaxLMean	0.3463	0	0	0	0	0	0	0.2763		0	0.0226
CMinLMean	0.775	0.0014	0	0.0007	0.0001	0	0.008	0.8947	0		0.7025
CCircMean	0.0523	0.0054	0.0802	0.0019	0.0215	0.417	0.0043	0.0162	0.0226	0.7025	

A.3.3 Spearman's R Pathological Osteon Specific Metrics Correlations

	Age	OMaxLMean	OMinLMean	OPeriMean	OTAreaMean	CAreaMean	OAreaMean	OCircMean	CMaxLMean	CMinLMean	CCircMean
Age	1	-0.36	-0.32	-0.31	-0.3	-0.1	-0.33	-0.03	-0.18	-0.08	0.14
OMaxLMean	-0.36	1	0.93	0.97	0.95	0.61	0.94	-0.09	0.68	0.57	-0.07
OMinLMean	-0.32	0.93	1	0.95	0.97	0.61	0.97	0.14	0.66	0.62	0.09
OPeriMean	-0.31	0.97	0.95	1	0.97	0.61	0.96	-0.04	0.69	0.58	-0.07
OTAreaMean	-0.3	0.95	0.97	0.97	1	0.63	0.97	0.05	0.71	0.62	0.02
CAreaMean	-0.1	0.61	0.61	0.61	0.63	1	0.5	0.16	0.91	0.96	0.26
OAreaMean	-0.33	0.94	0.97	0.96	0.97	0.5	1	0.03	0.59	0.5	0
OCircMean	-0.03	-0.09	0.14	-0.04	0.05	0.16	0.03	1	0.02	0.21	0.56
CMaxLMean	-0.18	0.68	0.66	0.69	0.71	0.91	0.59	0.02	1	0.9	0.01
CMinLMean	-0.08	0.57	0.62	0.58	0.62	0.96	0.5	0.21	0.9	1	0.35
CCircMean	0.14	-0.07	0.09	-0.07	0.02	0.26	0	0.56	0.01	0.35	1

A.3.4 Converted *p*-values Pathological Osteon Specific Metrics Correlations

	Age	OMaxLMean	OMinLMean	OPeriMean	OTAreaMean	CAreaMean	OAreaMean	OCircMean	CMaxLMean	CMinLMean	CCircMean
Age		0.0263	0.0493	0.0524	0.0629	0.5286	0.0375	0.8683	0.2721	0.6397	0.4045
OMaxLMean	0.0263		0	0	0	0	0	0.5737	0	0.0001	0.6916
OMinLMean	0.0493	0		0	0	0	0	0.3985	0	0	0.5872
OPeriMean	0.0524	0	0		0	0	0	0.8105	0	0.0001	0.6898
OTAreaMean	0.0629	0	0	0		0	0	0.7485	0	0	0.9085
CAreaMean	0.5286	0	0	0	0		0.0012	0.3234	0	0	0.1135
OAreaMean	0.0375	0	0	0	0	0.0012		0.8439	0	0.0011	0.9824
OCircMean	0.8683	0.5737	0.3985	0.8105	0.7485	0.3234	0.8439		0.8804	0.1905	0.0002
CMaxLMean	0.2721	0	0	0	0	0	0	0.8804		0	0.9522
CMinLMean	0.6397	0.0001	0	0.0001	0	0	0.0011	0.1905	0		0.0309
CCircMean	0.4045	0.6916	0.5872	0.6898	0.9085	0.1135	0.9824	0.0002	0.9522	0.0309	

A.4 Osteon Specific Metrics Regression Outputs

A.4.1 Healthy Regression Model Osteon Area

```
Residuals:
   Min     1Q  Median     3Q    Max
-43.436  -8.011  -0.546  11.557  31.753

Coefficients:
             Estimate Std. Error t value Pr(>|t|)
(Intercept)  1.044e+02  1.063e+01   9.823 1.35e-11 ***
OAreaMean   -1.446e-03  3.473e-04  -4.165 0.000193 ***
---
Signif. codes:  0 ‘***’ 0.001 ‘**’ 0.01 ‘*’ 0.05 ‘.’ 0.1 ‘ ’ 1

Residual standard error: 15.65 on 35 degrees of freedom
Multiple R-squared:  0.3314,  Adjusted R-squared:  0.3123
F-statistic: 17.35 on 1 and 35 DF,  p-value: 0.0001931
```

A.4.2 Pathological Regression Model Osteon Area

```
Residuals:
   Min     1Q  Median     3Q    Max
-32.578 -12.481   2.482   9.615  40.501

Coefficients:
             Estimate Std. Error t value Pr(>|t|)
(Intercept) 78.3634634 11.1873066   7.005 2.79e-08 ***
OAreaMean   -0.0008640  0.0003916  -2.206   0.0336 *
---
Signif. codes:  0 ‘***’ 0.001 ‘**’ 0.01 ‘*’ 0.05 ‘.’ 0.1 ‘ ’ 1

Residual standard error: 15.65 on 37 degrees of freedom
Multiple R-squared:  0.1163,  Adjusted R-squared:  0.09239
F-statistic: 4.868 on 1 and 37 DF,  p-value: 0.03365
```

A.4.3 Healthy Regression Model Osteon Total Area

```
Residuals:
   Min     1Q  Median     3Q    Max
-44.210  -9.214  -0.199   9.741  31.316

Coefficients:
             Estimate Std. Error t value Pr(>|t|)
(Intercept)  1.011e+02  1.119e+01   9.033 1.13e-10 ***
OTAreaMean  -1.156e-03  3.172e-04  -3.645 0.000859 ***
```

```
---
Signif. codes:  0 ‘***’ 0.001 ‘**’ 0.01 ‘*’ 0.05 ‘.’ 0.1 ‘ ’ 1

Residual standard error: 16.29 on 35 degrees of freedom
Multiple R-squared:  0.2752,  Adjusted R-squared:  0.2545
F-statistic: 13.29 on 1 and 35 DF,  p-value: 0.0008589
```

A.4.4 Pathological Regression Model Osteon Total Area

```
Residuals:
   Min     1Q  Median     3Q    Max
-32.928 -11.947   2.153   9.383  40.977

Coefficients:
             Estimate Std. Error t value Pr(>|t|)
(Intercept) 77.2264158 11.6661447   6.620 9.15e-08 ***
OTAreaMean  -0.0007242  0.0003598  -2.012   0.0515 .
---
Signif. codes:  0 ‘***’ 0.001 ‘**’ 0.01 ‘*’ 0.05 ‘.’ 0.1 ‘ ’ 1

Residual standard error: 15.81 on 37 degrees of freedom
Multiple R-squared:  0.09866,           Adjusted R-squared:  0.0743
F-statistic:  4.05 on 1 and 37 DF,  p-value: 0.05149
```

A.4.5 Healthy Regression Model Osteon Minimum Length

```
Residuals:
   Min     1Q  Median     3Q    Max
-41.739  -5.218   0.181  12.106  27.632

Coefficients:
            Estimate Std. Error t value Pr(>|t|)
(Intercept) 137.3212    23.9512   5.733 1.73e-06 ***
OMinLMean    -0.4465     0.1400  -3.189  0.00301 **
---
Signif. codes:  0 ‘***’ 0.001 ‘**’ 0.01 ‘*’ 0.05 ‘.’ 0.1 ‘ ’ 1

Residual standard error: 16.85 on 35 degrees of freedom
Multiple R-squared:  0.2251,  Adjusted R-squared:  0.203
F-statistic: 10.17 on 1 and 35 DF,  p-value: 0.003008
```

A.4.6 Pathological Regression Model Osteon Minimum Length

```
Residuals:
   Min     1Q  Median     3Q    Max
-30.891 -13.035   1.649   9.958  41.691
```

```
Coefficients:
             Estimate Std. Error t value Pr(>|t|)
(Intercept) 103.0467    21.1816   4.865 2.14e-05 ***
OMinLMean    -0.3010     0.1299  -2.317   0.0261 *
---
Signif. codes:  0 ‘***’ 0.001 ‘**’ 0.01 ‘*’ 0.05 ‘.’ 0.1 ‘ ’ 1

Residual standard error: 15.56 on 37 degrees of freedom
Multiple R-squared:  0.1267,  Adjusted R-squared:  0.1031
F-statistic: 5.369 on 1 and 37 DF,  p-value: 0.02614
```

A.4.7 Healthy Regression Model Osteon Perimeter

```
Residuals:
   Min     1Q  Median     3Q    Max
-44.663  -5.758  -0.841   9.904  33.400

Coefficients:
             Estimate Std. Error t value Pr(>|t|)
(Intercept) 132.73148   22.78609   5.825 1.31e-06 ***
OPeriMean    -0.10737    0.03407  -3.151  0.00332 **
---
Signif. codes:  0 ‘***’ 0.001 ‘**’ 0.01 ‘*’ 0.05 ‘.’ 0.1 ‘ ’ 1

Residual standard error: 16.89 on 35 degrees of freedom
Multiple R-squared:  0.221,    Adjusted R-squared:  0.1988
F-statistic: 9.931 on 1 and 35 DF,  p-value: 0.003323
```

A.4.8 Pathological Regression Model Osteon Perimeter

```
Residuals:
   Min     1Q  Median     3Q    Max
-32.797 -11.619   0.973   9.210  39.766

Coefficients:
             Estimate Std. Error t value Pr(>|t|)
(Intercept) 105.08567   22.78209   4.613 4.64e-05 ***
OPeriMean    -0.07941    0.03541  -2.242    0.031 *
---
Signif. codes:  0 ‘***’ 0.001 ‘**’ 0.01 ‘*’ 0.05 ‘.’ 0.1 ‘ ’ 1

Residual standard error: 15.62 on 37 degrees of freedom
Multiple R-squared:  0.1196,  Adjusted R-squared:  0.09585
F-statistic: 5.028 on 1 and 37 DF,  p-value: 0.03101
```

A.4.9 Healthy Regression Model Osteon Maximum Length

```
Residuals:
   Min     1Q  Median     3Q    Max
-44.719  -7.764  -0.088  10.177  34.950

Coefficients:
            Estimate Std. Error t value Pr(>|t|)
(Intercept) 123.48840   22.48244   5.493 3.31e-06 ***
OMaxLMean    -0.25091    0.08969  -2.798  0.00821 **
---
Signif. codes:  0 ‘***’ 0.001 ‘**’ 0.01 ‘*’ 0.05 ‘.’ 0.1 ‘ ’ 1

Residual standard error: 17.24 on 36 degrees of freedom
Multiple R-squared:  0.1786,  Adjusted R-squared:  0.1558
F-statistic: 7.827 on 1 and 36 DF,  p-value: 0.008214
```

A.4.10 Pathological Regression Model Osteon Maximum Length

```
Residuals:
   Min     1Q Median     3Q    Max
-33.51 -11.98   1.44  10.15  41.48

Coefficients:
            Estimate Std. Error t value Pr(>|t|)
(Intercept) 110.77934   20.33621   5.447 3.52e-06 ***
OMaxLMean    -0.23791    0.08506  -2.797  0.00814 **
---
Signif. codes:  0 ‘***’ 0.001 ‘**’ 0.01 ‘*’ 0.05 ‘.’ 0.1 ‘ ’ 1

Residual standard error: 15.13 on 37 degrees of freedom
Multiple R-squared:  0.1745,  Adjusted R-squared:  0.1522
F-statistic: 7.822 on 1 and 37 DF,  p-value: 0.00814
```

A.5 Conferences and Contributions

Lill, C.; Garcia-Donas, J. G.; Paine, R. R.; Xhemali, B.; Kranioti, E. F. (2018, April) *The effect of pathology on bone microstructure: implications for histological age estimation.* Poster presented at 86th Annual Meeting of the American Association for Physical Anthropology, New Orleans, LA.

Lill, C. (2016, April) *The effect of pathology on bone histomorphometric variables for age estimation: A Pilot Study.* Oral presentation given at 3rd Annual Scottish Students Forensic Research Symposium, Glasgow.